UNIVERSITAT POLITÈCNICA DE VALÈNCIA

Escuela Técnica Superior de Ingeniería de Caminos Canales y Puertos

Departamento de Ingeniería de la Construcción
Y
Proyectos de la Ingeniería Civil

TESIS DOCTORAL

HORMIGONES ECO-CELULARES "ONE-PART" (ECC-OP) BASADOS 100% EN MATERIALES RESIDUALES

Por

ALBA FONT PÉREZ

Directores

JORDI PAYÁ BERNABEU

LOURDES SORIANO MARTÍNEZ

Valencia, invierno 2019

Nina…

A ti, que siempre sonreíste cuando yo reía y que siempre lloraste cuando yo estaba en un mal momento.

A ti, a tu amor y confianza que son los que me guían, me han dado siempre las alas y a la vez el hacha.

No te cambio por nada ni nadie…

A ti, con la que empecé a caminar, hablar, razonar y soñar.

Siento orgullo, lealtad, ganas de luchar, de sembrar, de seguir, de resistir, de resurgir…de vivir.

A ti, la mujer de mi vida

Conclusión: Hoy estoy aquí.

A la memoria de Menchu

AGRADECIMIENTOS

Es imposible enfrentarte, en solitario, a una travesía, en la que se combina la carrera de fondo con los esprints más intensos, y en la que se cruzan un sinfín de mareas cambiantes. Durante estos tres años he compartido, amenizado y sufrido con personas a las que quiero dedicar las primeras líneas del documento que plasma todo este periodo y pone fin a una importante etapa de mi vida.

En primer lugar, mi corazón me pide a gritos dedicar esta Tesis a mi directora, compañera y sobre todo AMIGA: Lourdes Soriano Martínez. Sin ella esto no hubiese funcionado. Ha sido esa persona que me ha entendido en todo momento, ha sabido escucharme, responderme, animarme, hablarme y también callarme. Además, me ha aguantado todos y cada uno de los días, desde el primero en que entré por la puerta del laboratorio, para bien o para mal, siempre con la mejor de las actitudes. Ese "cero dramas" que junto a ella y "Joado" adoptamos como lema ha sido de las lecciones mas importantes que he aprendido en la vida. ¡Gracias Lur! (Además, se que es la parte de las Tesis que a ella mas le gusta cotillear, así que…doble finalidad porque así le hago llorar).

Mi segundo agradecimiento es para mi director de Tesis: Jordi Payá Bernabeu. Sin duda, la persona que desde el principio me ha inspirado, tan inteligente y perseverante como humilde y dedicado a los demás. Siempre he dicho que trabajar junto a él es un agotamiento mental, pero a la vez gratificante cuando asimilas todo lo que aprendes.

Los dos han sido los mejores directores que he podido tener, han logrado sacar lo mejor de mi durante todos estos años; me han ofrecido toda su dedicación y exigencias.

A Viki con mucho cariño. A la que considero una gran científica, una gran investigadora, una gran docente, una maravillosa persona y buena; pero sobre todo, una gran MADRE, incluso de aquellos que no son sus hijos. Dedicada al 100 % a los demás, se ha preocupado desde el primer momento por mi, me ha ayudado y apoyado. Además, ha sido un eslabón activo durante todas las etapas de esta Tesis Doctoral.

A Pepe, Ana y Merche, por su apoyo, sus consejos, sus aportes y sobre todo por el cariño que me han brindado en todo momento.

A Mauro esa persona con un corazón gigante siempre dispuesta a ayudar, a colaborar y a pelear lo que se nos resiste para que podamos progresar. Siempre bromeamos: ¡este chico no duerme! pero es verdad…en cualquier momento del día en que le necesitamos él esta ahí. Me ha dado valiosos y sabios consejos a lo largo de la investigación.

Quiero hacer un agradecimiento especial a dos compañeros y amigos: Joado y Manolo Paredes. Con ellos he pasado, sin duda, los momentos mas bonitos, divertidos y memorables de mis andanzas en el laboratorio. He aprendido mucho, tanto en lo profesional como en lo personal, me han ayudado incondicionalmente y en los momentos mas complicados se han desvivido por sacarme una sonrisa. ¡Gracias!

En general quiero extender mi agradecimiento, a todos y cada uno de mis compañeros del grupo GIQUIMA, los que están y los que han estado. Con los que he compartido vivencias y he trabajado en las distintas etapas de esta andanza. Cada uno de ellos ha aportado un pequeño granito en el desarrollo de esta Tesis.

También, al resto de compañeros de ICITECH y a todos los técnicos que no han dudado en echarme una mano siempre que lo he necesitado. Extiendo este agradecimiento a Manolo, Merche, Alicia, Chimo y José Luis, técnicos del servicio de microscopía electrónica de la UPV.

A mi "GymUPVteam", con los que cada mañana he sufrido cada entrene y cargaba las pilas para emprender las jornadas de experimental y/o de escritura. Sobre todo, a Rober, Carlos, Jordi, America, Javi, Paco, Elo, Juan Manuel, David, Fede …y con especial cariño a mis dos chicas del "Café de los Lunes": Mi Mari Paz de las mañanas y Ana. Otros much@s, no se ni el nombre…pero se les agradezco de todo corazón a tod@s el pequeño o pequeños momentos que me han dedicado.

A mis amigos, mi gente, aquellos con los que he coincidido en algún momento de mi vida y que se han quedado para siempre: Víctor Starlich, Kike, Anna, Anafe, Charlypep y Marta. A mis mallorquines Noguera, Pere y Marga. A mi "paella tots junts": Kiko, Yle, Wencho, Mir, Paco y Roberto. Y por supuesto a mis medias naranjas: Sara y Zazu.

Además, hoy 15 de octubre de 2019, me he sentado a escribir esta parte tan importante del documento y ha ocurrido algo muy bonito: Ha nacido la sobrina de mi mejor amiga Sara. Quiero dar un pedacito de esto a ella, Alma, y a su mama, Esther, que han luchado mucho y se lo merecen.

En general, ya que no hay cabida para nombrar por partes y uno a uno a todos, quiero agradecer a todas las personas que de un modo u otro han colaborado en hacerme dar un pasito mas cada día hacia mis objetivos, todos aquellos que han dedicado un poquito de su tiempo en mi.

A Menchu, Baltasar, Balta y Ulises, sin duda las personas mas bondadosas, positivas y humildes que he conocido. Me siento muy afortunada. Y a Inés, en muy poco tiempo hemos compartido momentos tan intensos que me han permitido ver su bonito interior y su gran corazón. Gracias por cuidarme y apoyarme tanto.

A los que desde que tengo uso de razón siempre han estado ahí luchando por mi y viendo como evolucionaba: mi tía Momo, mi tío Arturo, mi tía Merche y la *Wilita* guapa de mis amores. Una pequeña parte de mi son ellos.

A mis primos Paula y Junior las personitas mas importantes, y de las que me enorgullezco cada día más. Gracias por tomarme como un ejemplo y motivarme para seguir trabajando para ser cada vez mejor persona.

A mis padres Nina y Punti, que han sido, son y serán mis pies y mis manos cuando de repente se me olvida andar y se me escapan las cosas que intento agarrar.

Por último, quiero dedicar cada momento de este gran logro al amor de mi vida: Vladi. Por él podría escribir miles de Tesis y ninguna estaría a la altura de expresar lo que me aporta.

¡Gracias a todos de corazón!

AGRAÏMENTS

És impossible enfrontar-se, en solitari, a una travessia, en la que es combina la carrera de fons amb els esprints més intensos, i en la que s'encreuen una infinitat de marees canviants. Durant estos tres anys he compartit, amenitzat i patit amb persones a qui vull dedicar les primeres línies del document que plasma tot este període i posa fi a una important etapa de la meua vida.

En primer lloc, el meu cor em demana a crits dedicar esta Tesi a la meua directora, companya i sobretot AMIGA: Lourdes Soriano Martínez. Sense ella açò no haguera funcionat. Ella es la persona que m´ha entès en tot moment, ha sabut escoltar-me, respondre'm, animar-me, parlar-me i també callar-me. A més, m'ha aguantat tots i cada un dels dies, des del primer en que vaig entrar per la porta del laboratori, per a bé o per a mal, sempre amb la millor de les actituds. Eixe "zero drames" que junt amb ella i "Joado" adoptarem com a lema ha sigut una de les lliçons més importants que he aprés. Gràcies Lur! (A més a més, aquesta es la part de les Tesis que mes li agrada xafardejar, així que...doble finalitat perquè així li faig plorar).

En segon lloc, el meu agraïment és per al meu director de Tesi: Jordi Payá Bernabeu. Sense cap dubte la persona que des del principi m´ha inspirat, tan intel·ligent i perseverant com humil i dedicat als altres. Sempre he dit que treballar amb ell és un esgotament mental, però al mateix temps gratificant quan assimiles tot el que aprens.

Els dos han sigut els millors directors que he pogut tindre, han aconseguit traure'm el millor durant tots estos anys; m'han oferit tota la seua dedicació i exigències.

A Viki amb molt afecte. A la que considere una gran científica, una gran investigadora, una gran docent, una meravellosa persona i bona; però sobre tot una gran MARE, inclús d'aquells que no són el seus fills. Dedicada al 100 % als altres, s'ha preocupat des del primer moment de mi, m'ha ajudat i recolzat. Amés, ha sigut una peça clau durant totes les etapes d'esta Tesi Doctoral.

A Pepe, Ana i Merche, pel seu suport, els seus consells i aportacions i sobretot per l'afecte que m´han brindat en tot moment.

A Mauro, eixa persona amb un cor gegant sempre disposada a ajudar, a col·laborar i a barallar el que se'ns resistix per poder progressar. Sempre bromegem: este xic no dorm! Però és veritat...en qualsevol moment del dia en què el necessitem ell esta al 100 %. M'ha donat valuosos i savis consells al llarg de la investigació.

Vull fer un agraïment especial a dos companys i amics: Joado y Manolo Paredes. Amb ells he passat, sense cap dubte, els moments mes bonics,

divertits i memorables dels meus recorreguts en el laboratori. He aprés molt, tant professionalment com personalment, m´han ajudat incondicionalment i en els moments més complicats s´han desviscut per traure'm un somriure. Gràcies!

En general vull estendre el meu agraïment, a tots i cadascun dels meus companys del grup GIQUIMA. Els que estan i els que han estat. Amb els que he compartit vivències i he treballat en les distintes etapes d'este recorregut. Cada un d'ells ha aportat un xicotet gra en aquesta Tesi.

També, a la resta de companys d'ICITECH i a tots els tècnics que no han dubtat a tirar-me una mà sempre que ho he necessitat. Estenc aquest agraïment a Manolo, Merche, Ali, Ximo i Jose Luis, tècnics del servici de microscòpia electrònica a la UPV.

Als meus companys de "GymUPVteam" amb els que cada matí he patit els entrenes i carregava les piles per a mamprendre les jornades d'experimental i/o escriptura. Sobretot, a Rober, Carlos, Jordi, America, Javi, Paco, Elo, Juan Manuel, David, Fede...i amb especial afecte a les meues dos xiques del "cafè de dilluns" Mari Paz dels matins i Ana. Altres molts no se ni el nom...però he de agrair els moments que m'han dedicat.

Als meus amics, la meua gent, aquells amb els qui he coincidit en algun moment de la meua vida i que s'han quedat per sempre: Victor Starlich, Kike, Anna, Anafe, Charlypep i Marta. Als meus mallorquins Noguera, Pere i Marga. A "paella tots junts": Kiko, Yle, Wencho, Mir, Paco i Roberto. I per descomptat a les meues mitges taronges: Sara i Zazu.

A més, hui es 15 d'octubre de 2019, m'he sensat a escriure aquesta part tan important del document i ha ocorregut quelcom molt bonic: a nascut la neboda de la meua millor amiga Sara. Vull dedicar una miqueta d'açò a ella, Alma, i a la seua mare, Esther, que han lluitat molt i se'l mereixen.

En general, ja que no hi ha cabuda per a anomenar per parts i un a un a tots, vull agrair a totes les persones que d'una o altra manera han col·laborat a fer-me donar cada pas als meus objectius. Tots aquells que han dedicat un poquet del seu tems en mi.

A Menchu, Baltasar, Baltasar (fill) i Ulises: les persones mes bondadoses, positives i humils que he conegut. Em sent molt afortunada. I a Inés, que en molt poc de temps he compartit amb ella moments molt intensos i m'han permès veure el seu bonic interior i el seu gran cor. Gràcies per cuidar-me i recolzar-me tant.

Als que des que tinc ús de raó sempre han estat ací, lluitant per mi i veient com evolucionava: la meua tia Momo, el meu tio Arturo, la meua tia Merche i la Wilita dels meus amors. Una xicoteta part de mi són ells.

Als meus cosins Paula i Junior les personetes més importants, i de les que m'enorgullisc cada dia més. Gràcies per prendre'm com un exemple i motivar-me a continuar treballant per a ser poc a poc millor persona.

Als meus pares Nina i Punti, que han sigut, són i seran els meus peus i les meues mans quan de sobte m'oblide de caminar i se m'escapen les coses que vull agafar.

Finalment, vull dedicar cada moment d'este gran èxit a l'amor de la meua vida: Vladi. Per ell podria escriure milers de Tesis i cap estaria a l'altura d'expressar el que m'aporta.

Gràcies a tots de cor!

RESUMEN

El mundo actual es claramente insostenible, a consecuencia del consumismo indiscriminado y la mentalidad humana de considerar los recursos inagotables. Por ello, se esta iniciando una época que puede ser definida como "de transición", en la que el horizonte a alcanzar es un estilo de vida sostenible, respetuoso y eficiente. El desarrollo de políticas, que integran los conceptos de sociedad, economía y medioambiente, para conseguir "un mundo mejor", se ha convertido en una tendencia estrictamente necesaria a lo largo de la última década: a nivel global, se plantea una relación recíproca entre los Objetivos de Desarrollo Sostenible (ODS) y la Economía Circular (EC), dando lugar a un nuevo concepto de Economía Inteligente.

La eminente influencia del sector de la construcción, en este periodo de transición, hace necesario adoptar un nuevo concepto de "ECODISEÑO" en torno a todas las etapas relacionadas con las actividades y los materiales involucrados. Concretamente, la industria de los prefabricados se presenta con un elevado potencial para implantar la circularidad económica en el sector.

En este sentido, el empleo del **hormigón celular tradicional (TCC)** en los prefabricados está siendo cada vez más estudiado, por su sencillez de fabricación, la ergonomía y manejabilidad de las piezas (baja densidad y resistencia mecánica moderada) y sus excelentes propiedades aislantes. Se trata de un material compuesto por cemento Portland y agua que adquiere una estructura alveolar interna al adicionarse polvo de aluminio que reacciona liberando gas hidrógeno, y que requiere de un tratamiento de curado en autoclave para alcanzar las características físico-mecánicas requeridas.

El presente trabajo de investigación presenta un nuevo concepto de hormigón celular basado en el consumo minimizado de recursos y casi nulo de energías, durante la fase de producción del material como a lo largo de la vida útil de las edificaciones: los nuevos **hormigones eco-celulares "one-part" (ECC-OP)**. Se lleva a cavo el desarrollo, caracterización y evaluación medioambiental del material. Para ello, se a llevado a cabo un plan de trabajo distribuido en pasos paulatinos de mejora centradas por una parte en los materiales constituyentes y por otra en el procedimiento de fabricación.

En la primera etapa de trabajo, se introducen e investigan los nuevos **hormigones celulares geopoliméricos (GCC) y hormigones celulares de activación alcalina (AACC)** en los que el cemento Portland, conocido por su uso indiscriminado a nivel mundial y su gran impacto ambiental y económico, se sustituye por el catalizador gastado de craqueo catalítico (FCC) y la escoria de alto horno (BFS) respectivamente. A partir de la concepción de estos nuevos materiales se va introduciendo variables de mejora: i) empleo de agentes aireantes alternativos: papel de aluminio reciclado, agua oxigenada y sub-productos del tratamiento de escorias salinas; ii) desarrollo del concepto

de co-molienda entre los precursores y los aireantes alternativos; iii) combinación de aireación mecánica y química de las matrices mediante polvo de aluminio y un espumante, el lauril sulfato de sodio; y vi) estudio del comportamiento frente a tratamientos de curado alternativos al autoclave. Los materiales se estudian y comparan microestructuralmente, se ensayan sus características funcionales (densidad, resistencia mecánica a la compresión y conductividad térmica) y se evalúan medioambientalmente. Además, se caracteriza la matriz porosa resultante combinando técnicas microscópicas y de análisis de imagen, así como mediante ensayos hídricos.

Los nuevos GCC y AACC se obtienen a partir de la mezcla del precursor y el reactivo generador de gas (bien por separado, bien en co-molienda) con una disolución activadora de elevada alcalinidad, constituida por dos reactivos químicos con elevado impacto medioambiental: silicatos e hidróxidos alcalinos. Por todo ello, una vez concluida esta etapa de trabajo, la investigación se centra en la mejora de la eco-eficiencia de los GCC y AACC, sustituyendo los reactivos químicos por fuentes residuales alternativas.

En esta segunda etapa de trabajo, se introduce el concepto de **hormigón eco-celular (ECC)**, en el que los silicatos comerciales de la disolución activadora se sustituyen por una fuente alternativa de sílice procedente de un residuo agrícola: la ceniza de cáscara de arroz (RHA). Se desarrollan e investigan sistemas de ECCs con FCC y ECCs con BFS, en los que se emplea como agente aireante el papel de aluminio residual y se incorpora mediante el procedimiento de co-molienda con el precursor. Los ECCs se diseñan para obtener unas propiedades óptimas y se comparan con los TCC, GCC y AACC, tanto física y mecánicamente como medioambientalmente. Como resultado, se obtienen ECCs estables, con densidades inferiores a los 1000kg/cm^3 y con los que se consigue una reducción de las emisiones de CO_2 del 74 % en el caso de los constituidos con FCC y del 78 % para los constituidos con BFS, respecto a los sistemas tradicionales.

Finalmente, en la tercera etapa de trabajo se presenta la mayor innovación en cuanto a la ecoeficiencia y el objetivo de consumo nulo de recursos naturales planteados: el estudio de la ceniza de hueso de oliva (OBA) como fuente alcalina alternativa en la disolución activadora. La OBA es un residuo agrícola compuesto fundamentalmente de potasio y calcio, y se presenta como una alternativa potencial para la sustitución del hidróxido alcalino comúnmente empleado en la activación de la BFS. El empleo de la OBA se estudia inicialmente en sistemas de activación alcalina de BFS: se desarrollan, en primer lugar, sistemas binarios (**BAAM**) con OBA/BFS y a continuación se complementa el estudio combinando esta ceniza con la RHA constituyendo sistemas ternarios (**TAAM**) con OBA/BFS/RHA.

Una vez sentadas las bases previas, se desarrolla la cuarta etapa experimental en la que se aplica el empleo de OBA a la fabricación de ECCs de BFS y como culminación final del estudio, se aplica por primera vez la modalidad de fabricación “one-part”, que consiste en la co-molienda de todos los materiales sólidos de modo que únicamente se requiere de su mezcla con agua para la

producción del material final: los **nuevos ECC-OP**. Estos materiales son diseñados y analizados en torno a las características funcionales exigidas por la normativa europea para la industria de los prefabricados: densidad aparente, resistencia mecánica y conductividad térmica. Además, se evalúan medioambientalmente mediante un análisis del ciclo de vida limitado por la modalidad cradle-to-gate en el que se obtiene el Global Warming Potential para un periodo de 100 años (GWP-100).

Como conclusión final de la Tesis Doctoral se presentan los nuevos ECC-OP constituidos por un 100 % de residuos y fabricados mediante un proceso de consumo energético casi nulo. Los nuevos ECC-OP resultan óptimos para su aplicación en la fabricación industrial de piezas prefabricadas, con excelentes prestaciones funcionales que favorecen la concepción del ECODISEÑO en las edificaciones y con un GWP-100 de 19.2 $kgCO_2eq$ por metro cúbico de hormigón celular, lo que supone una reducción del 96 % respecto al GWP-100 de los sistemas tradicionales (TCC).

RESUM

A l'actualitat, el món es clarament insostenible, a conseqüència del consumisme indiscriminat i la mentalitat humana de considerar els recursos inesgotables. Per això, s'està iniciant una època que pot ser definida com "de transició" a la que l'horitzó a aconseguir és un estil de vida sostenible, respectuós i eficient. L'aparició de polítiques on els conceptes de societat, economia i medi ambient s'integren amb la finalitat d'aconseguir "un món millor" s'ha convertit en una tendència estrictament necessària al llarg de l'última dècada: a nivell global, es planteja una relació recíproca entre els Objectius de Desenvolupament sostenible (ODS) i l'Economia Circular, donant lloc a un nou concepte d'Economia Intel·ligent.

L'eminent influència del sector de la construcció en aquest període de transició, fa necessari adoptar un nou concepte de "ECODISENY" a totes les etapes relacionades amb les activitats i els materials involucrats en l'activitat. Concretament, la indústria dels prefabricats es presenta amb un elevat potencial per a implantar la circularitat econòmica en el sector.

En efecte, l'ús del **formigó cel·lular tradicional (TCC)** al sector dels prefabricats està sent cada vegada més estudiat per la facilitat de fabricació, l'ergonomia i manejabilitat de les peces (densitat baixa i resistència mecànica moderada), així com per les excel·lents propietats aïllants que presenten. El TCC es un material compost de ciment Pòrtland i aigua que adquirix una estructura alveolar interna característica degut a l'adició de alumini en pols que al reaccionar amb la basicitat del medi s'oxida alliberant hidrogen. Aquest material requerix d'un tractament de curat en autoclau per a aconseguir les característiques requerides.

El present treball d'investigació presenta un nou concepte de formigó cel·lular basat en un consum mínim de recursos i quasi nul d'energies durant la fase de producció del material així com durant la vida útil de les edificacions: els nous formigons eco-cel·lulars "one-part" (ECC-OP). Es desenvolupa, caracteritza i avalua mediambientalment el material mitjançant un pla de treball que s'ha distribuït en passos graduals de millora. Les etapes del treball han estat centrades d'una banda en els materials constituents i d'altra banda en el procediment de fabricació.

A la primera etapa de treball, s'introduïxen i investiguen els nous **formigons cel·lulars geopolimèrics (GCC) i formigons cel·lulars d'activació alcalina (AACC)** en els quals el ciment Pòrtland, conegut pel seu us indiscriminat i el seu gran impacte ambiental i econòmic, se substituïx per catalitzador gastat de craqueig catalític (FCC) i escòria d'alt forn (BFS) respectivament. A partir de la concepció d'estos nous materials es van introduint variables de millora: i) ús d'agents aireantes alternatius: paper d'alumini reciclat, aigua oxigenada i subproductes del tractament d'escòries salines; ii) desenvolupament del

concepte de co-mòlta entre els precursors i els reactius generadors de gas alternatius; iii) combinació de generació de porositats a les matrius per medi mecànic i químic utilitzant pols d'alumini i un tensioactiu, el lauril sulfat de sodi; i iv) estudi del comportament amb l'aplicació de tractaments de curat alternatius a l'autoclau. Els materials s'estudien i comparen micro-estructuralment, s'analitzen les propietats funcionals (densitat, resistència mecànica a la compressió i conductivitat tèrmica) i s'avaluen mediambientalment. A més, es caracteritza la matriu porosa resultant combinant tècniques microscòpiques i d'anàlisi d'imatge, així com per mitjà d'assajos hídrics.

Els nous GCC i AACC s'obtenen a partir de la mescla del precursor i el reactiu generador de gas (bé per separat, bé per co-mòlta) amb una dissolució activadora d'elevada alcalinitat, constituïda per dos reactius químics amb elevat impacte mediambiental: silicats i hidròxids alcalins. Per tot això, una vegada conclosa esta etapa de treball, la investigació se centra en la millora de l'eco- eficiència dels GCC i AACC, substituint els reactius químics per fonts residuals alternatives.

En esta segona etapa de treball, s'introduïx el concepte de **formigó eco-cel·lular (ECC)** , en el que els silicats comercials de la dissolució activadora se substituïxen per una font alternativa de sílice procedent d'un residu agrícola: la cendra de corfa d'arròs (RHA) . S' investiguen sistemes d'ECC amb FCC i sistemes d'ECC amb BFS, en els que s'empra com a agent generador de gas el paper d'alumini residual i s'incorpora per mitjà del procediment de co-mòlta amb el precursor. Els ECCs es dissenyen per a obtindre unes propietats òptimes i es comparen amb els TCC, GCC i AACC, tant física i mecànicament com mediambientalment. Com a resultat, s'obtenen ECCs estables, amb densitats inferiors als 1000kg/cm^3 i amb els que s'aconseguix una reducció de les emissions de CO_2 del 74 % en el cas dels constituïts amb FCC i del 78 % per als constituïts amb BFS, respecte als sistemes tradicionals.

Finalment, en la tercera etapa de treball es presenta la major innovació quant a l'eco-eficiència i l'objectiu de consum nul de recursos naturals: l'estudi de la cendra d'os d'oliva (OBA) com a font alcalina alternativa per a la fabricació de la dissolució activadora. L'OBA és un residu agrícola compost fonamentalment de potassi i calci, i es presenta com una alternativa potencial per a la substitució de l'hidròxid alcalí comunament empleat en l'activació de la BFS. L'ús de l'OBA s'estudia inicialment en sistemes d'activació alcalina de BFS: sistemes binaris (**BAAM**) amb OBA/BFS. A continuació, es complementa l'estudi que combina l'ús de l'OBA amb la RHA constituint sistemes ternaris (**TAAM**) formats per OBA/BFS/RHA. Es du a terme la caracterització de la cendra així com els estudis de dosificació de les mescles i metodologia de fabricació. Finalment, s'analitzen les propietats físiques i mecàniques de les provetes per a poder procedir a la seua aplicació en la tecnologia dels formigons cel·lulars.

Una vegada assentades les bases prèvies, es du a terme la quarta etapa experimental en què s'aplica la inclusió d'OBA a la fabricació d'ECC de BFS i

com a culminació final de l'estudi, s'aplica per primera vegada la modalitat de fabricació "one-part", que consistix en la co-mòlta de tots els materials sòlids de manera que únicament es requerix de la seua mescla amb aigua per a la producció del material final: els **nous ECC-OP**. Estos materials són dissenyats i analitzats segons les característiques funcionals exigides per la normativa europea per a la indústria dels prefabricats: densitat aparent, resistència mecànica i conductivitat tèrmica. A més, s'avaluen mediambientalment per mitjà d'una anàlisi del cicle de vida limitat per la modalitat cradle-to-gate en el que s'obté el Global Warming Potential per a un període de 100 anys (GWP-100).

Com a conclusió final de la Tesi Doctoral es presenten els nous ECC-OP constituïts per un 100 % de residus i fabricats per mitjà d'un procés de consum energètic quasi nul. Els nous ECC-OP resulten òptims per a la fabricació industrial de peces prefabricades, amb excel·lents prestacions funcionals que afavorixen la concepció de l'ECODISENY en les edificacions i amb un GWP-100 de 19.2 $kgCO_2eq$ per metre cúbic de formigó cel·lular, la qual cosa suposa una reducció del 96 % respecte al GWP-100 dels sistemes tradicionals (TCC).

ABSTRACT

Nowadays, the mindset of society is focused on the consumerism considering the unlimited natural resources, thus the world situation is becoming unsustainable. We are living in a transition era from the present linear economy to a new circular economy concept. The aim is to search an efficient and careful lifestyle with a political development in which society, economy and environment will be integrated. The relationship between the sustainable development goals (SDGs) and the circular economy (CE) is currently a growing trend has given way a new concept: The Smart Economy.

The construction sector has an eminent influence in the transition era; thus, a new concept implementation of "ECO-DESIGN" would be necessary in all stages of the activity. The precast industry is increasingly making headway by its high potential to the implementation of the circularity in the construction.

The **traditional cellular concrete (TCC)** is being studied to the precast units manufacture by its low density (piece handy and ergonomic), good mechanical behaviour and high insulating properties. The TCC is an Ordinary Portland Cement (OPC) - based material mixed with water in which aluminium powder (A) is added. The A reacts in the fresh OPC's basic medium and a stable alveolar structure is achieved when the material is hardening. To steadfast matrix development, an autoclave treatment (high pressure and temperature conditions) of the TCCs is required.

In this investigation, a new concept of cellular concrete had been developed based on both the low natural resources as well as nearly zero-energy consumptions: the new **one-part eco-cellular concrete (ECC-OP).** The development, the characterization and the environmental assessment of the material were carried out. A working plan has been broken down into progressive stages where the improvements were focused on the constitutive materials as well as on the manufacture procedures.

In the first working step, **the geopolymer cellular concretes (GCC) and the alkali-activated cellular concretes (AACC)** were investigated. The OPC worldwide known by its high economic costs, non-reasonable use and its environmental issues was replaced for the fluid catalytic cracking catalyst residue (FCC) and for the blast furnace slag (BFS) respectively. In the new GCC and AACC systems, steps of improvements were introduced progressively: i) the use of alternative aerating agents as the recycled aluminium foil, hydrogen peroxide and salt-slags recycled by-products; ii) a new concept of co-milling between precursors and the alternative aerating agents was introduced; iii) matrix aeration by the chemical and mechanical means where the aluminium powder was combined with the sodium lauryl sulphate (SLS), and vi) alternative curing treatments to the traditional autoclave. A microstructural and functional characterisation and an environmental assessment of the

materials were carried out. Furthermore, the air-void characterization was done by microscopic, image analysis and hydric tests means.

The GCC and AACC manufacture consist on the mixing the precursor and the aerating agent (singly or in co-milling) with a high alkalinity activation dissolution. The alkali-activated dissolution is based on chemical reagents with a high environmental and economic impact: alkali silicates and hydroxides. By this reason when the GCC and AACC were completely developed, the next investigation step was focused in the alternative cellular concretes eco-efficiency improvement: the search of chemical reagents replacement by residual alternatives.

In the second working step, the new **eco-cellular concretes (ECC)** were introduced and investigated. The silicates in the alkali-activated dissolution were replaced by an alternative silica sourced from an agricultural residue: the rice husk ash (RHA). The new systems were developed with the use of both the BFS and the FCC as precursors and the aerating agent was the recycled aluminium foils by the co-milling procedure. The optimal properties of the new ECC were investigated and a comparison with the TCC, GCC and AACC was done. The new ECCs yielded densities less than 1000kg/cm3 and, comparing with the TCC systems, the CO2 emissions were lower in 74 % when the FCC was employed and in 78 % when the BFS was employed.

Finally, in the third working step, the more highlighted novelty in the ecoefficiency and the objective of near cero natural resources consumption was presented: the study of the olive-stone biomass ash (OBA) as an alternative alkali source for the activating dissolution. The OBA is a farming waste mainly composed of potassium and calcium, thus, is a well alternative to the traditional potassium hydroxide employed for the BFS activation. The OBA was firstly introduced in binary systems (**BAAM**) composed by OBA/BFS mixed with water. Then, the OBA and RHA were combined to the BFS activation in the new ternary systems composed 100 % by residues (**TAAM**). A complete characterization of the OBA, as well as the mortars and pastes manufacture procedure investigations were carried out. The microstructural, physical and mechanical characterization of the new TAAM was done to its application in the cellular concrete technology.

The last working step of the present investigation consisted of the ECCs based on BFS activated with RHA and OBA. Furthermore, for the first time, the "one-part" manufacture procedure was applied to obtain the **new "one-part" eco-cellular concretes (ECC-OP)**. The "one-part" consist of the co-milling of all solid materials and their mix with water to obtain the cellular concrete (similar to the traditional OPC procedure). The materials were designed from scratch: dosages, characterization, comparisons with the TCC, AACC and ECC, European standards compliments. Furthermore, environmental issues of the ECC-OP through the cradle-to-gate modality of the life circle analysis (LCA) were evaluated obtaining their 100 years Global Warming Potential (GWP-100).

Concluding the present Thesis, the new ECC-OP 100 % waste – based are presented whose manufacture involves the nearly zero-energy consumption. An excellent functional behaviour of the ECC-OP for its application in the precast industry have proven, thus the concept of ECODESIGN can be effectively achieved. The GWP-100 per cubic meter of the new ECC-OP was 19.2 kgCO2eq which leads to a decrease of 96 % with respect to the GWP-100 of the TCC systems.

ORGANIZACIÓN DE LA TESIS

El documento que a continuación se presenta tiene como objetivo plasmar de manera ordenada y clara el recorrido experimental que ha supuesto la investigación llevada a cabo por Alba Font Pérez con el objeto de la obtención del título de Doctora. Para ello el texto se ha articulado en torno a 5 capítulos tal y como se resume a continuación:

CAPÍTULO 1: INTRODUCCIÓN

En el primer capítulo se sitúa la investigación dentro del contexto socio-económico actual. Se expone de manera escalonada los aspectos indirectos de mejora que se pretende abordar con la consecución de los objetivos de la Tesis Doctoral.

Además, se posiciona al lector en un punto de origen: se conceptualiza los hormigones celulares tradicionales y se da a conocer la problemática asociada y soluciones individuales propuestas por la comunidad científica. Estos puntos ofrecen progresivamente un "porque" de la investigación.

Finalmente se presentan los antecedentes experimentales que dan inicio a la presente investigación.

CAPÍTULO 2: ENFOQUE DE LA TESIS DOCTORAL

A continuación, en el capítulo 2 del documento, se da a conocer el objetivo general de la Tesis, seguido de los objetivos parciales cuyas conclusiones sirven como guía y precedente durante el plan de trabajo de la misma.

Al final del capítulo se presenta un esquema conceptual del desarrollo experimental y las publicaciones científicas que constituyen la columna vertebral de la Tesis Doctoral.

CAPÍTULO 3: TRABAJO EXPERIMENTAL

El tercer capítulo ofrece una visión general de las materias primas empleadas y procedimientos desarrollados a lo largo de la investigación. Se pretende que el lector tenga una visión esquemática y general del trabajo experimental que facilite la comprensión del capítulo 4.

CAPÍTULO 4: DESARROLLO DE NUEVOS HORMIGONES ECO-CELULARES "ONE-PART" (HEC-OP)

El capítulo 4 constituye la columna vertebral del presente trabajo de investigación, donde se presentan las publicaciones científicas que enmarcan la Tesis Doctoral.

El capítulo se ha estructurado mediante una exposición progresiva de acuerdo al desarrollo de los objetivos parciales y la consecución del objetivo general de la tesis, marcados en el plan de trabajo:

- Estudio "paso a paso" de la consecución de los objetivos parciales de la Tesis
    - Hormigones Celulares Geopoliméricos (GCC) y Hormigones Celulares de Activación Alcalina (AACC)
    - Hormigones Eco-celulares (ECC)
- Culminación del objetivo general de la Tesis
    - Desarrollo de materiales de activación alcalina binarios (BAAM) y ternarios (TAAM)
    - Hormigones Eco-celulares "one-part" (ECC-OP)

CAPÍTULO 5: CONCLUSIONES Y LINEAS DE INVESTIGACIÓN FUTURA

El cierre de la presente Tesis Doctoral se da con un último capítulo en el que se concentran los resultados emergidos más relevantes y se expone las conclusiones que emanan de la investigación. Además, se propone para futuras investigaciones una serie de aspectos que no han podido ser abordados o que surgen a raíz de resultados obtenidos en la presente.

ABREVIATURAS

Las abreviaciones empleadas para la redacción del presente documento se corresponden, en su mayoría, a las siglas en inglés del vocablo al que se refieren exceptuando algunas que hacen referencia a nombres de compuestos o productos químicos.

Se presenta una lista de las abreviaciones, clasificadas por tipología.

MATERIAS PRIMAS

Nomenclatura	Español	Inglés
OPC	Cemento portland ordinario	Ordinary Portland cement
BFS	Escoria de alto horno	Blast furnace slag
FCC	Catalizador gastado de craqueo catalítico	Fluid catalytic cracking catalyst residue
A	Polvo de aluminio comercial	Commercial aluminium powder
A_R	Papel de aluminio reciclado	Recycled aluminium foil
H_2O_2	Peróxido de hidrogeno (agua oxigenada)	Hydrogen peroxide
SLS	Lauril sulfato de sodio	Sodium lauril sulphate
PG	Sub-producto de escorias salinas (Paval granulado)	Salt-slags recycled by-products (Granulate Paval)
WG	Silicato sódico comercial	Commercial waterglass (sodium silicate)
NaOH	Hidróxido de sodio	Sodium hydroxide
KOH	Hidróxido de potasio	Potassium hydroxide
RHA	Ceniza de cáscara de arroz	Rice husk ash
OBA	Ceniza de biomasa de hueso de oliva	Olive-stone biomass ash
KPH	Kephalite	Kephalite

MATERIALES ESTUDIADOS

Con el fin de dar continuidad y coherencia al estudio evolutivo de la presente Tesis Doctoral, a efectos del presente documento, se ha renombrado los materiales. Por tanto, en algunos casos, la nomenclatura de los hormigones alternativos empleada en el documento no se corresponde con la que aparece en la publicación correspondiente.

A continuación, se citan las abreviaciones empleadas a lo largo de este documento para identificar los materiales estudiados:

Nomenclatura	Español	Inglés
TCC	Hormigón celular tradicional	Traditional cellular concrete
GCC	Hormigón celular geopolimérico	Geopolymer cellular concrete
AACC	Hormigón celular de activación alcalina	Alkali-activated cellular concrete
ECC	Hormigón eco-celular	Eco-cellular concrete
BAAM	Material binario de activación alcalina	Binary alkali-activated material
TAAM	Material ternario de activación alcalina	Ternary alkali-activated material
ECC-OP	Hormigón eco-celular “one-part”	One-part eco-cellular concrete

PROCEDIMIENTOS EXPERIMENTALES

Se presenta una relación de las abreviaciones y nomenclaturas empleadas para unificar los procedimientos experimentales de todas las publicaciones que comprenden la Tesis Doctoral. En el Capítulo 4 se detalla cada uno de ellos.

x. Fabricación de materiales (Capítulo 3 - sección 3.2)

Pre-tratamiento de materias primas (Capítulo 3 - sección 3.2 - punto 3.2.1)

Nomenclatura	Español	Inglés
Co-M	Co-molienda de materias primas	Co-milling
FCCRm	Co-molienda de FCC y A_R	FCC and A_R co-milled
BFSRm	Co-molienda de BFS y A_R	BFS and A_R co-milled
FCCPGm	Co-molienda de FCC y PG	FCC and PG co-milled
BFSPGm	Co-molienda de BFS y PG	BFS and PG co-milled
BRm-RO	Co-molienda de BFS/A_R/RHA/OBA	BFS/A_R/RHA/OBA co-milled

Procedimiento de amasado (Capítulo 3 - sección 3.2 - punto 3.2.2)

Nomenclatura	Español	Inglés
NM	Amasado con amasadora convencional	Normal mixer
PD	Amasado con mezcladora de pintura	Power drill

Procedimiento de curado (Capítulo 3 - sección 3.2 - punto 3.2.2)

Nomenclatura	Español	Inglés
TB	Baño térmico	Thermal bath
TA	Temperatura ambiente	Ambient temperature
CM	Combinación de TB y TA	TB with TA combination

xi. Ensayos de caracterización (Capítulo 3 - sección 3.3)

Nomenclatura	Español	Inglés
XRF	Fluorescencia de rayos-X	X-ray fluorescence
PSD	Análisis de partículas por difracción de rayos láser	Particle size distribution
FESEM	Microscopía electrónica de barrido de emisión de campo	Field emission scanning electron microscopy
EDS	Microanálisis por energía dispersiva de rayos-X	Energy dispersive X-ray spectroscopy
DRX	Difracción de rayos-X	X-ray diffraction
TGA	Análisis termogravimétricos	Thermogravimetric analysis
MIP	Porosimetría de intrusión de mercurio	Mercury intrusion porosimetry
OM	Microscopía óptica	Optical microscopy
LCA	Análisis del ciclo de vida	Life cycle analysis

xii. Propiedades de los materiales (Capítulo 3 - sección 3.3)

Nomenclatura	Español	Inglés
Rc	Resistencia a la compresión	Compressive strength
Rf	Resistencia a la flexión	Flexural strength
$\mathbf{D_N}$	Densidad natural	Natural density
$\mathbf{D_{AP}}$	Densidad aparente	Bulk density
ΦT	Porosidad total	Total porosity
Φa	Porosidad abierta	Open porosity
Φc	Porosidad cerrada	Close porosity
λ	Conductividad térmica	Thermal conductivity

ÍNDICE

CAPÍTULO I: INTRODUCIÓN

CONTENIDO

1 INTRODUCCIÓN

El propósito del presente capítulo es facilitar la lectura y permitir una correcta comprensión y asimilación de la Tesis Doctoral objeto del presente documento. Los siguientes aspectos previos permiten situar al lector en un entorno contextual adecuado y en un punto de "inicio" al desarrollo de la investigación.

1.1 CONTEXTO SOCIO-ECONÓMICO EN QUE SE ENMARCA EL DESARROLLO DE LA TESIS

A lo largo del siglo XX, se ha experimentado de manera creciente un estado generalizado de bienestar basado en el consumismo y en la filosofía de "usar y tirar". Se trata del tradicional **modelo económico lineal** (**EL**) basado en "tomar-fabricar-consumir y eliminar"(Servicio de Estudios del Parlamento Europeo (EPRS), 2015). Esta situación subyace a una dinámica de producción que está agotando los recursos naturales no renovables disponibles y además pone en peligro la reposición de aquellos que son renovables. A nivel mundial, nos encontramos en una situación insostenible desde el punto de vista medioambiental, económico y social, debido a estos tres aspectos fundamentales (Noticias-Parlamento Europeo, 2015).

- El aumento de la demanda de materias primas y la escasez de recursos. Gran parte de las materias primas cruciales son finitas y, como la población mundial crece, la demanda también aumenta.
- Dependencia de otros países: hoy en día la mayor parte de países depende de otros países para obtener sus materias primas, e inevitablemente esta dependencia se torna política, económica y social.
- Impacto en el cambio climático: La extracción, el tratamiento y uso de materias primas tienen importantes consecuencias medioambientes, aumenta el consumo de energía y las emisiones de gases de efecto invernadero.

Es por ello que, en la actualidad, la sociedad está experimentando un cambio de mentalidad generalizado enfocado en los conceptos de sostenibilidad y desarrollo sostenible.

Desde 2014 se viene desarrollando la estrategia económica estructural *Europa 2020* para generar un crecimiento inteligente, sostenible e integrador: actividades e iniciativas encaminadas a fomentar la **transición de una economía lineal a una economía circular (EC)** (ver Figura 1.1**)**. Esta estrategia está respaldada por el Parlamento Europeo y el Consejo Europeo, siendo uno de sus pilares básicos: "Avanzar hacia una Europa más eficiente en el uso de los recursos"(Comisión Europea, 2014). Con esta finalidad, en diciembre de 2015, la comisión europea adoptó un ambicioso *Plan de Acción para la Economía Circular* con diversos horizontes que incluye 54 medidas con las que pretende

dar respaldo, entre otras, a la estrategia *Europa 2020* (Comisión Europea - Medio Ambiente, 2015).

En la actualidad, el término *ECOINNOVACIÓN* se considera el lema fundamental en la toma de decisiones técnicas de carácter social, económico y medioambiental y en junio de 2019 se creó el Comité Técnico de Normalización de UNE sobre EC (*CTN 323 Economía Circular*) con perspectiva multisectorial (Comisión Europea - Medio Ambiente, 2019).

Contextualizando la situación, recientemente los ministerios de Agricultura y Pesca, Alimentación y Medioambiente y Economía de España, han lanzado el *Pacto por una **economía circular (EC)**: El compromiso de los agentes económicos y Sociales 2018-2020* (Ministerio de Agricultura y Alimentación Pesca y Medio Ambiente (MAPAMA) and Ministerio de Economía Industria y Competitividad (MINECO), 2018), enmarcado dentro del *Plan de Acción* de la Comisión Europea. Además, en el Foro Permanente de Economía Circular del Gabinete de Historia Natural se realiza anualmente una actualización del *Anuario de Economía Circular de España* (Alfonso et al., 2018).

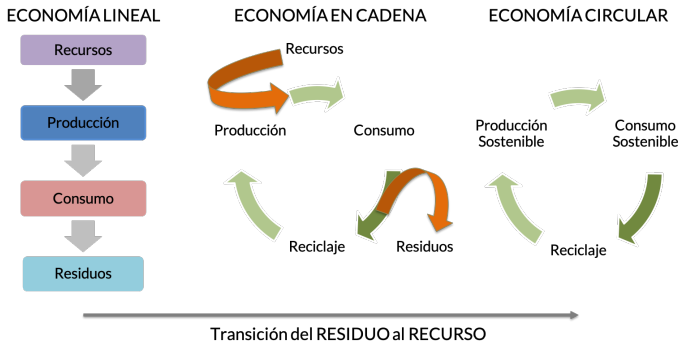

***Figura 1.1:** Transición del modelo de economía lineal a un nuevo modelo de energía circular ((Telos digital - Fundación Telefónica, 2018)- elaboración propia)*

El nuevo modelo de EC engloba 10 ejes fundamentales mediante los que se pretende "cerrar el círculo" de los ciclos de vida de los productos a través de un mayor reciclado y reutilización (Comisión Europea, 2014):

- **El residuo se convierte en recurso**: es la principal característica. Todo el material biodegradable vuelve a la naturaleza y el que no es biodegradable se reutiliza.
- El **segundo uso**: reintroducir en el circuito económico aquellos productos que ya no corresponden a las necesidades iniciales de los consumidores.
- La **reutilización**: reusar ciertos residuos o ciertas partes de los mismos, que todavía pueden funcionar para la elaboración de nuevos productos.

- La **reparación**: encontrar una segunda vida a los productos estropeados.
- El **reciclaje**: utilizar los materiales que se encuentran en los residuos.
- La **valorización**: aprovechar energéticamente los residuos que no se pueden reciclar.
- Economía de la **funcionalidad**: la economía circular propone eliminar la venta de productos en muchos casos para implantar un sistema de alquiler de bienes. Cuando el producto termina su función principal, vuelve a la empresa, que lo desmontará para reutilizar sus piezas válidas.
- **Energía de fuentes renovables**: eliminación de los combustibles fósiles para producir el producto, reutilizar y reciclar.
- La **eco-concepción**: considera los impactos medioambientales a lo largo del ciclo de vida de un producto y los integra desde su concepción.
- La **ecología industrial y territorial**: establecimiento de un modo de organización industrial en un mismo territorio caracterizado por una gestión optimizada de los stocks y de los flujos de materiales, energía y servicios.

Por otra parte, un aspecto con mayor trayectoria es la preocupación por los efectos de la **contaminación** que, en la actualidad, ya ha contribuido a la firma de tres acuerdos históricos: i) el *Acuerdo de París sobre el cambio climático* (Naciones Unidas, 2015a); ii) la *Agenda 2030* para alcanzar los Objetivos de Desarrollo Sostenible (ODS)(Naciones Unidas, 2015b); y iii) la Declaración ministerial de la Asamblea de las Naciones Unidas sobre el Medio Ambiente: *Hacia un planeta sin contaminación* (Naciones Unidas, 2018).

Llegados a este punto se plantea:

> Economía y medioambiente se presentan como dos términos conceptualmente muy alejados, sin embargo, relacionar las acciones, encaminadas a la mejora, del contexto económico con el medioambiental puede resultar determinante para alcanzar la calidad de vida global.

ODS + EC = Economía inteligente

Precisamente, Schroeder et al. (Schroeder et al., 2018) han presentado recientemente los resultados de un estudio en el que se plantea la influencia de la adopción de la EC en la consecución de los ODS. En el análisis llevado a cabo se argumenta que las prácticas y principios de la EC son transversales y que su implementación es necesaria para lograr gran parte de las metas establecidas en distintos ODS. Teniendo en cuenta que los ODS constan de 17 objetivos y 169 metas, los autores afirman que el desarrollo de una EC permitiría alcanzar directamente 21 metas e indirectamente 28 metas.

Concretamente, enumeran la relación más directa con los siguientes objetivos: ODS6 (Agua limpia y saneamiento); ODS7 (Energía asequible y no contaminante), ODS8 (Trabajo decente y crecimiento económico), ODS12 (Producción y consumo responsables) y ODS15 (Vida de ecosistemas terrestres). Además, en el estudio se desvela el potencial que ofrecen los modelos circulares para generar sinergias entre los distintos ODS: i) entre los que promueven el crecimiento económico y la generación de empleo (ODS8, ODS1, ODS2); y ii) los que promueven la protección de la biodiversidad en los océanos y la tierra (ODS14 y ODS15). Por último, los autores afirman que progresar hacia los ODS puede ayudar a incentivar la transición hacia una EC.

En definitiva, la economía circular se ha convertido en una tendencia mundial irreversible necesaria para alcanzar un estado de bienestar social y en equilibrio con el medio ambiente. Su consecución supone un cambio sistémico, en el que la investigación y la innovación, tanto tecnológica como no tecnológica juegan un papel fundamental.

1.1.1 El sector de la construcción

El sector de la construcción es un sector clave para el desarrollo económico tanto por su propia actividad como por la que genera en otros ámbitos.

En España, la actividad de la edificación y construcción de infraestructuras representa el 40 % del consumo final de energías, el 35 % de las emisiones de gases de efecto invernadero, el 50 % de todos los materiales extraídos, el 30 % del consumo de agua y el 35 % del total de residuos generados (Green building council españa (GBCe), 2017). Además, el 54 % de los residuos de construcción y demolición (RCD) terminan en vertedero (frente al 6 % de cifra media en la UE) y de estos residuos el 71 % procede de la actividad de edificación y el 29 % restante de la obra civil.

Como indicador de la escasa o nula circularidad en el sector podemos recurrir a datos del pasado 2018 donde sólo el 40,9 % de los RCD declarados se valorizaron siendo el objetivo establecido a nivel europeo para 2020 de un 70 % (Funfación Conama - Grupo de trabajo GT-6, 2018).

Consecuentemente, es posible afirmar que el sector de la construcción representa un indiscutible desafío en la transición hacia el nuevo modelo de EC. En este sentido, la optimización del sector y un menor uso de recursos naturales implica no solo una importante disminución del impacto ambiental, si no también una oportunidad económica derivada de la ventaja competitiva. Además, si se desarrollan los procesos de restauración necesarios, se puede desarrollar una mejor restitución y regeneración del capital natural (Consejo Económico y Social (CES), 2016).

Para la implantación de un marco conceptual de EC en el sector de la construcción es necesario realizar un enfoque de ciclo de vida que tenga en cuenta toda la cadena de valor (procesos y agentes implicados):

- Agentes: Administraciones públicas, extractores de materias primas, fabricantes, empresas (constructoras, promotoras), usuarios, transportistas, investigadores, gestores de residuos, formadores.
- Procesos extrínsecos: extracción de materias primas, recogida de residuos, procesos de reciclaje, procesos de producción de materias primas secundarias, transporte.
- Procesos intrínsecos (ciclo de vida del sector en sí): Fase de planificación y diseño, fase de ejecución, fase de uso, mantenimiento y rehabilitación y, finalmente, fase de demolición al final de la vida útil.

La innovación de procesos y productos es la clave para la competitividad permanente en el sector de la construcción. Como punto de inicio, el grupo de trabajo "*Economía circular en el sector de la construcción*" (GT-6) (Funfación Conama - Grupo de trabajo GT-6, 2018) coordinado por el Green Building Council España (GBCe) y la Asociación Española de Reciclaje de Residuos de Construcción y Demolición (RCD Asociación), propone una serie de sinergias entre procesos y agentes, que constituyen tres ejes fundamentales de actuación hacia la implantación de la EC en el sector de la construcción:

- Por una parte, todos los agentes implicados deben de promover actividades y enfoques hacia la formación, captación y sensibilización que permitan adoptar nuevas prácticas y renovar conceptualmente el sector. La implantación del nuevo modelo económico circular en el sector requiere de un cambio de mentalidad generalizado que se inicie en los profesionales de todas las áreas implicadas.
- En segundo lugar, se recae en la industria extractiva (donde entran en juego los extractores como agentes implicados y varios procesos extrínsecos del sector) como el origen responsable de la extracción, gestión y transformación de los recursos naturales. La implantación de buenas prácticas en este momento del ciclo de vida (sistema de gestión minero-mineralúrgica-metalúrgica sostenible de acuerdo con la UNE-22480-2019(CTN 22 Minería y explosivos, 2019) permite la producción de materiales en su mayoría inertes, naturales, reutilizables y 100 % reciclables. Esto requiere de una sinergia directa con el final de vida de las construcciones, ya que en la etapa de deconstrucción y gestión se tienen que aplicar las técnicas adecuadas, que eviten su contaminación y permitan su reutilización(BOE-RD 105, 2008). En 2017 se consumieron en España 31.4 millones de toneladas de materias primas para la fabricación de cemento de las cuales únicamente 1.4 millones procedían de residuos o subproductos industriales.
- Finalmente, se otorga un papel fundamental a los fabricantes y asociaciones de fabricantes, éstos deben de encaminar sus prácticas hacia el nuevo concepto de *ECODISEÑO* donde además entran en juego las denominadas Declaraciones Ambientales de Producto (DAP o EPD en sus siglas en inglés), desarrolladas mediante un

análisis de ciclo de vida (ACV o LCA en sus siglas en inglés)[1] y que certifican el desempeño ambiental de productos y servicios de la construcción.

Aquí es donde se debe nombrar el desarrollo de la norma UNE 14006 "Sistemas de gestión ambiental", una serie de directrices para la incorporación del *ECODISEÑO*, llamada GESTIÓN DEL ECODISEÑO (AENOR, 2011):

ECODISEÑAR consiste en una primera fase en la que se identifican todos los impactos ambientales durante todas las etapas del Ciclo de Vida (realizar LCA), seguida de la evaluación, priorización y clasificación los impactos en sus diferentes etapas (transporte, consumo de energía…) para finalmente establecer objetivos de mejora individualizados: reducción de consumo de agua, mejora de embalajes, cambio en la formulación, entre otros. Mediante estas directrices se pretende identificar, controlar y mejorar de manera continua los aspectos medioambientales de los productos y/o servicios en todo su ciclo de vida para adaptarse progresivamente a los avances tecnológicos y a un modelo de desarrollo más sostenible.

Concretamente, en la actualidad, el sector de la construcción esta evolucionando no solo hacia técnicas que minimicen los consumos energéticos(Ministerio de Fomento - Gobierno de España, 2018), sino también, hacia el fomento de sistemas constructivos que representen un menor impacto ambiental. Precisamente, las técnicas de cálculo aplicables concretas para el sector de la construcción se recogen en la norma UNE-EN 15978 "Sostenibilidad en la construcción. Evaluación del comportamiento ambiental de los edificios. Métodos de cálculo"(AENOR, 2012).

1.1.2 Construcción modular y prefabricada

Respecto a la última sinergia planteada, para los fabricantes y asociaciones de fabricantes, la **construcción modular y prefabricada** se presenta como una alternativa interesante que puede contribuir a la adopción de una economía circular responsable con los materiales, el suelo, el agua, el aire limpio y la energía. Precisamente, la Asociación Nacional de la Industria del prefabricado de Hormigón (ANDECE), como representante de la industria española de fabricantes de elementos prefabricados de hormigón, ha firmado recientemente la adhesión al *Pacto por una **economía circular (EC)*** nombrado anteriormente (Ministerio de Agricultura y Alimentación Pesca y Medio

[1] Análisis del ciclo de vida (ACV o LCA):"Marco metodológico para estimar y evaluar los impactos medioambientales atribuibles a un producto o servicio durante todas las etapas de su vida ("de la cuna a la tumba") mediante la configuración de inventarios de entradas y salidas del sistema, evaluación de los impactos e interpretación de los resultados de las fases analizadas (extracción de materias primas, transporte, fabricación, distribución, uso y fin de vida (reutilización, reciclaje, valorización y eliminación/disposición de los residuos)" (Comité Técnico ISO/TC 207, Gestión ambiental, Subcomité SC 5, 2017).

Ambiente (MAPAMA) and Ministerio de Economía Industria y Competitividad (MINECO), 2018). El acuerdo recoge como medida fundamental el impulso del análisis del ciclo de vida de los productos y la incorporación de criterios de *ECODISEÑO*.

El concepto de prefabricado de hormigón se puede considerar como una variante industrializada de construcción que, de inicio, asegura una mejor adaptación a las exigencias de partida ya que, entre otros aspectos destacables figuran los siguientes:

- La actividad industrializada genera una menor cantidad de residuos, y los que se generan son más sencillos y económicos de gestionar y aprovechar, al localizarse en la propia fábrica.
- Resultan construcciones con una probada mayor durabilidad.
- El diseño estructural está mucho más optimizado.

En la actualidad, es innegable el potencial de la construcción industrializada con elementos prefabricados de hormigón dentro de un modelo de economía circular.

Tal y como se ha representado en la Figura 1.2, una profunda reflexión acerca de las relaciones recíprocas entre todos estos conceptos, dentro del encuadre socio-económico actual, ha dado cabida a plantear la investigación llevada a cabo en la presente Tesis Doctoral:

La construcción modular y prefabricada basada en el ECODISEÑO que apuesta por el uso de nuevos materiales amigables con el medio ambiente y eco-eficientes.

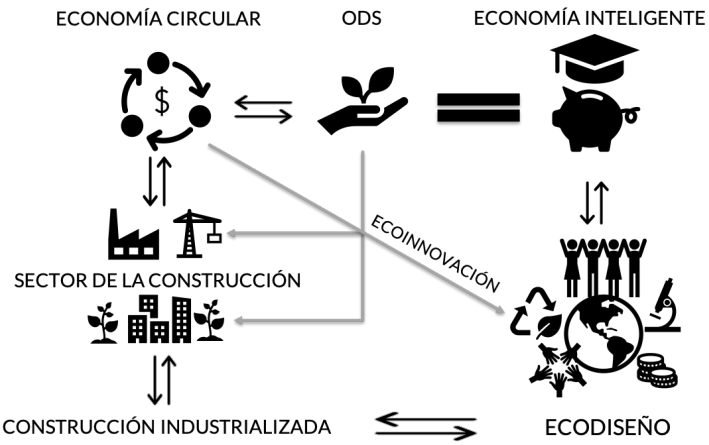

Figura 1.2: *Contexto socio-económico en el que se enmarca el desarrollo de la Tesis.*

1.2 HORMIGÓN CELULAR TRADICIONAL (TCC)

El hormigón celular tradicional (TCC) es una pasta o mortero a base de cemento Portland (Ordinary Portland Cement, OPC), y, en algunos casos, cal hidratada y/o yeso, que, en estado endurecido presenta una estructura interna repleta de microburbujas de aire estabilizadas, de tamaños consistentes, sin interconexiones y distribuidas por toda la masa. Esta estructura celular se genera mediante la incorporación de determinados agentes o aditivos, antes o durante el amasado del material.

Dependiendo del aditivo empleado y la manera en que éste reacciona, los TCC se clasifican en (Cellular Concrete Solutions, 2007; Chica and Alzate, 2019; Narayanan and Ramamurthy, 2000):

- **Hormigones celulares aireados (mediante agentes inorgánicos)**: La formación de la estructura interna del material se consigue mediante la adición, durante el proceso de amasado, de agentes generadores de gas. Estos reaccionan químicamente en el medio básico (álcalis) propio del cemento o cal, desprendiendo hidrógeno gaseoso. Por tanto, se puede decir que se trata de un proceso químico de inclusión de burbujas. Su aplicación suele llevarse a cabo en piezas prefabricadas. Dentro de estos hormigones celulares, existen dos subgrupos en función de los agentes (Melo, 2013):
    - Dos productos químicos que reaccionan entre sí, como por ejemplo la mezcla del hipoclorito cálcico y agua oxigenada que al reaccionar produce oxígeno; o ácido clorhídrico y bicarbonato sódico, que produce dióxido de carbono; o carburo de calcio y agua que al reaccionar desprende acetileno.
    - Un producto químico que reacciona en el medio al que se adiciona, como son los polvos metálicos (aluminio, zinc, magnesio, calcio, bario o litio) que generan gas hidrógeno, o sales (carbonatos y bicarbonatos) que liberan CO_2.
- **Hormigones celulares espumados (mediante agentes orgánicos)**: En este caso, las microburbujas de aire se forman mediante un proceso mecánico. Se adicionan espumas a base de proteínas o surfactantes (tensoactivos, como el lauril sulfato de sodio) o bien productos que sufren un proceso de fermentación (levaduras orgánicas y fermentaciones lácticas). En este caso, la adición de espumantes puede realizarse de manera previa al amasado (pre-espumados) o durante el mismo. Este tipo de hormigones celulares se puede emplear in-situ o en piezas prefabricadas.

- **Hormigones celulares mixtos**: los que combinan los procedimientos químicos y mecánicos nombrados anteriormente (generación de gas con espumas).

Una característica intrínseca de este material es el procedimiento del curado. En el caso de aplicaciones in-situ (esto es, únicamente en el caso de los hormigones celulares espumados), el curado se lleva a cabo a temperatura ambiente, bajo las mismas condiciones que un hormigón convencional. Sin embargo, para la mayor parte de aplicaciones, se requiere de tratamientos en autoclave, con la finalidad de que el carácter cementante de los silicatos cálcicos hidratados formados resulte más fuerte y con una estructura final más robusta que cuando el curado se lleva a cabo a temperatura ambiente. Como resultado se obtiene un material con mejores prestaciones mecánicas. El procedimiento de curado en autoclave se lleva a cabo en el caso de la fabricación industrial de piezas prefabricadas donde (Grupo Xella, 2019; Pytlik and Saxena, 1992):

- Tras el amasado, el material se vierte en moldes de grandes dimensiones donde se deja finalizar por completo las reacciones que dan lugar a la expansión del material.
- Una vez la mezcla está consolidada se procede al dimensionado de las piezas requeridas y a su corte mediante el uso de una cortadora de hilo de acero.
- Finalmente, las piezas se introducen en autoclave (cámara estanca con vapor) y se someten a un tratamiento bajo presiones de entre 8 y 11 kg/cm^2 (entre 7.7 y 10.6 atmósferas), temperaturas de entre 175 a 190 °C, durante tiempos que oscilan entre 8 y 48 horas, en función de las condiciones finales del material que se quieren obtener.

Como consecuencia de su configuración interna, el TCC adquiere una serie de propiedades que lo convierten en un material de especial interés para su aplicación en determinadas situaciones constructivas, tanto como complemento de los materiales tradicionales como por él mismo, cuando sus cualidades resultan ventajosas respecto a las del hormigón convencional.

A grandes rasgos, es un material caracterizado por su baja densidad (valores entre los 300 y 1400 kg/m^3) con resistencias mecánicas del orden de 1 a 15MPa (Ramamurthy et al., 2009) y por presentar conductividades térmicas entre un 5 % y un 30 % menores que el hormigón convencional (Jones and McCarthy, 2006)(Wongkeo et al., 2012). Además, presenta una alta resistencia al ataque de bacterias y al fuego (Dolton and Hannah, 2006; Melo, 2013; Zulkarnain and Ramli, 2011).

Debido a las características técnicas del producto, citadas anteriormente, a lo largo de los últimos años, diversos autores han coincidido en que el TCC es un material idóneo para la nueva concepción de economía circular en el sector industrial de la **construcción mediante piezas prefabricadas** (Chica and Alzate, 2019; Chindaprasirt and Rattanasak, 2011; Dolton and Hannah, 2006; Falliano et al., 2018) facilitando la nueva concepción de *ECODISEÑO* por las siguientes razones:

- En primer lugar, su ligereza permite optimizar las cantidades de material a emplear en lugares de relleno, así como en todas aquellas situaciones constructivas con requerimientos estructurales moderados. Cuando los requerimientos estructurales son superiores se puede proyectar su uso como complemento del hormigón tradicional y, de igual manera, se consigue optimizar el uso de recursos.
- También relacionado con su baja densidad, permite reducir las cargas muertas estructurales en las construcciones. En lo referente a la actividad de construcción en sí, se proyecta con una disminución del coste de transporte, así como con una mejora en los tiempos y procedimientos de construcción. Las piezas de TCC son ligeras y fáciles de manejar e instalar en obra (Raj et al., 2019).
- Por otra parte, su capacidad aislante, tanto térmica como acústica, contribuye a una notable mejora en la eficiencia energética de las edificaciones. Sus características higrotérmicas contribuyen a un mayor bienestar y confort climático, garantizando la salubridad. En este sentido, el TCC resulta un material con elevado potencial para su aplicación en edificaciones de consumo energético casi nulo, de acuerdo con lo establecido en la Directiva de Eficiencia Energética en Edificios (EPBD en sus siglas en inglés – Energy Performance of Buildings Directive) del Parlamento Europeo y del Consejo (Hogeling and Derjanecz, 2018). Mediante modelos y tipologías de edificios en consecuencia, con paramentos verticales a base de hormigón celular, se consume entre un 85 y un 90 % menos de energía que en un edificio a base de materiales tradicionales (Grupo Xella - Noticias, 2016).
- Por último, el TCC es un material incombustible con bajo coeficiente de conductividad térmica y además presentan baja absorción de agua, presenta alta tolerancia a los cambios bruscos de temperatura y presenta una excelente resistencia química, por lo que se puede considerar un material de elevada durabilidad (Jerman et al., 2013; Narayanan and Ramamurthy, 2000).

Actualmente, en Europa, existen diversas empresas de producción de hormigón celular con varias características técnicas y múltiples prestaciones, ya sea en forma de bloques simples, bloques armados, paneles de muros o losas. Ytong, Siporex, Hebel y Celcon son las que presentan mayor actividad en el sector (Celcon, 2019; Hebel, 2019; Siporex, 2019; Ytong, 2019). Se fabrican tanto elementos estructurales (bloques y dinteles para la construcción de muros de carga y de cerramientos) como elementos no estructurales (tabiques, dinteles, placas para trasdosado o incluso piezas de consolidación de minas).

1.3 PROBLEMÁTICA ASOCIADA Y SOLUCIONES INDIVIDUALES: HORMIGONES CELULARES ALTERNATIVOS

Como se ha visto hasta ahora, el TCC se presenta como un material alternativo al empleo del hormigón convencional con un elevado potencial en determinadas situaciones constructivas. Sin embargo, desde el punto de vista ecológico, este material presenta una serie de impactos medioambientales asociados tanto a los materiales que lo constituyen como a su proceso de fabricación.

A continuación, y de manera esquemática, se presenta una relación de los problemas y las posibles soluciones individuales, propuestas por la comunidad científica. Cada uno de los antecedentes (problema – solución) que aquí se plantean se expone con mayor detalle en el Capítulo 4 de la presente Tesis Doctoral como introducción de las publicaciones, en función de los objetivos parciales de cada una de ellas:

- **Materiales constituyentes (i)**

Problema i.a) CEMENTO PORTLAND (OPC)

Como se ha introducido en el punto 1.2 del presente capítulo, los TCCs se fabrican a base de OPC y, en los tiempos actuales, ya es bien conocida la problemática asociada a este conglomerante en torno a tres focos bien diferenciados: el consumo desmesurado de materias primas no renovables, la elevada demanda energética y las emisiones de CO_2 a la atmosfera derivadas fundamentalmente a la decarbonatación de las calizas (constituyente mayoritario del Clinker) durante su fabricación, así como la quema de combustibles fósiles (Luukkonen et al., 2018; Mo et al., 2016).

Solución i.a) MATERIALES DE ACTIVACIÓN ALCALINA O GEOPOLIMEROS

Ante esta problemática, hay investigaciones centradas en el estudio de la sustitución parcial del OPC por materias primas alternativas. La ceniza volante y/o el humo de sílice han sido alternativas muy estudiadas. Mediante la sustitución del OPC en porcentajes de hasta el 20 %, además del beneficio medioambiental, se consigue mejorar las características físicas de los sistemas celulares endurecidos, debido a la actividad puzolánica y su influencia en el calor de hidratación cuando se combina con el cemento (Gökçe et al., 2019; She et al., 2018; Zulkarnain and Ramli, 2011). Otros trabajos presentan los beneficios de incorporar metakaolin (Sepulcre Aguilar et al., 2013) o escoria de alto horno (Pan et al., 2014) en porcentajes superiores al 30 % del peso del OPC, y se ha descrito que estos materiales mejoran los procesos de expansión al incorporar los agentes aireantes.

En la actualidad, los investigadores se centran en la obtención de hormigones alternativos con la sustitución total del OPC mediante la aplicación de conglomerantes de activación alcalina (AAM, del inglés Alkali Activated Cement) y los geopolímeros (Collins et al., 2017; Davidovits, 2002; Duxson et al., 2007; Palomo and López de la Fuente, 2003; Provis, 2016).

Los nuevos cementos de activación alcalina (AAM) se obtienen a partir de precursores con estructura amorfa (normalmente residuos o sub-productos), compuestos principalmente de sílice (SiO_2), alúmina (Al_2O_3) y calcio (CaO) como es el caso de la escoria de alto horno (BFS, del inglés Blast Furnace Slag)(Fernández-Jiménez et al., 1999; Frost, 2016; Provis, 2016; Puertas et al., 2018). Por su parte, el término geopolímero (GP) se emplea para los materiales alternativos obtenidos a partir de la activación de precursores minerales, también con estructura amorfa y procedentes de una actividad secundaria, pero en este caso de naturaleza silico-aluminosa (SiO_2-Al_2O_3), como el metakaolin (MK)(Istuque et al., 2016; Pelisser et al., 2013; Tchakouté et al., 2017; Tippayasam et al., 2016), el catalizador gastado de craqueo catalítico (FCC)(Rodríguez et al., 2013; Tashima et al., 2013, 2012) o diversas arcillas calcinadas(Buchwald et al., 2009; Elimbi et al., 2011; Ogundiran and Kumar, 2016; Reig et al., 2013). En ambos casos, los precursores se hacen reaccionar con una solución acuosa de elevada alcalinidad mediante sustancias solubles que aportan cationes: hidróxidos alcalinos, silicatos, óxidos, carbonatos, sulfatos o aluminatos. Como resultado de los procesos de hidratación tenemos que (Lecomte et al., 2006; Provis, 2016; Torres-Carrasco and Puertas, 2017):

- En el caso de los AAM se forma principalmente un gel de silicoaluminato de calcio (C-A-S-H) similar al gel de hidratación del OPC, pero con menor relación CaO/SiO_2. Como productos secundarios, dependiendo de la composición del precursor y de los activadores empleados, se generan fases ricas en magnesio y aluminio, como la hidrotalcita ($Mg_6Al_2CO_3(OH)_{16}{\cdot}4H_2O$) o fases de hidratos de aluminato tetracálcico $(C,M)_4AH_{13}$.
- En el caso de los GP, la disolución parcial del precursor sólido da lugar a la poli-condensación de las especies disueltas que finalmente se consolida en un gel de aluminosilicato sódico (N) o potásico (K) amorfo, tipo N-A-S-H o K-A-S-H, dependiendo de la naturaleza del activador. Estos geles se constituyen por cadenas poliméricas que forman una estructura tridimensional donde se distribuyen aleatoriamente tetraedros de silicio SiO_4 y aluminio AlO_4 interconectados por átomos de oxígeno compartidos. Como productos secundarios se forman zeolitas tales como hidrosodalita, zeolita tipo P o tipo Y, chabacita-sódica y faujasita.

Tanto los materiales de activación alcalina, como los geopolímeros presentan una alcalinidad y un calor de hidratación elevados. Además, como resultado se obtiene matrices estables, con buenas prestaciones mecánicas (incluso superiores a las de los de OPC) y buena durabilidad. En este sentido, la aplicación de esta tecnología en la fabricación de hormigones celulares resulta una alternativa interesante, por lo que recientes investigaciones se han

centrado en estos nuevos conglomerantes, introduciendo por tanto una nueva línea de investigación centrada en los **hormigones celulares geopoliméricos (GCC) y los hormigones celulares de activación alcalina (AACC).**

Problema i.b) DISOLUCIONES ALCALINAS CONVENCIONALES

Los nuevos AACC o GCC permiten obviar el empleo de OPC, sin embargo, llevan asociado un inconveniente medioambiental y económico relacionado con los reactivos químicos de las disoluciones alcalinas. Normalmente se emplea una mezcla de silicatos (sódicos o potásicos) con hidróxidos (sódicos o potásicos) caracterizadas por la molaridad de sodio o potasio activador y las relaciones molares SiO_2/Na_2O o SiO_2/K_2O.

Investigaciones recientes han mostrado que se evitan los problemas medioambientales del OPC, pero el uso de los silicatos alcalinos de la solución activadora representa un escalón a superar; tras él, se presenta otro aspecto a resolver: los hidróxidos. Los componentes del activador alcalino presentan elevadas emisiones de CO_2 a la atmósfera producidas en su manufactura. Además, debe considerarse el relativamente elevado coste económico de ambos reactivos (Cristelo et al., 2015; Mellado et al., 2014).

Solución i.b) DISOLUCIONES ALCALINAS ALTERNATIVAS

Ante esta situación, en la actualidad se están contemplando diversas líneas para la obtención de activadores alternativos en base a dos vertientes: por una parte, los silicatos o fuentes de sílice alternativos, y, por otra parte, las fuentes de sodio o potasio alternativas.

En el primer caso, las disoluciones activadoras alternativas estarían compuestas por NaOH o KOH mezclados con una fuente de sílice amorfa procedente de residuos agrarios o industriales. La ceniza de cascara de arroz (RHA, Rice Husk Ash), la tierra de diatomeas naturales (DE, diatomaceus earth), residuos de vidrio, ceniza de hojas de caña de azúcar (SCSA, sugar cane straw ash) o humo de sílice (SF, silica fume) son los más utilizados (Bernal et al., 2015; Bouzón et al., 2014; Font et al., 2018; Mejía et al., 2016; Tchakouté et al., 2016). En estos casos, el agente alcalino acaba solubilizando parte de la sílice, creándose unas mezclas ricas en silicato alcalino.

Finalmente, la producción de materiales alternativos a base de 100 % residuos que se fundamentan en la sustitución del álcali de las disoluciones se centran en: i) los residuos de procesos industriales, generalmente ricos en sodio, como el residuo de lodo rojo resultante en el proceso Bayer de obtención de la alúmina, o el residuo de la solución cáustica empleada en el proceso de limpieza industrial del aluminio (Hu et al., 2018; Nie et al., 2019; Shirley and Black, 2011); y b) los residuos agroindustriales ricos en potasio, como la ceniza de biomasa de maderas o la ceniza de la mazorca de maíz, entre otros (Cheah et al., 2015; Peys et al., 2016).

La aplicación de estas alternativas en la fabricación de los sistemas GCC O AACC da lugar a la obtención de una alternativa medioambientalmente limpia y ecoeficiente y contribuye un paso más hacia la adopción de la economía circular.

Si el hormigón celular se fabrica a partir de un AAM o de un GP basado en el uso de precursores procedentes de residuos y en la aplicación de activadores alcalinos generados a partir de residuos, estaríamos en la línea de la obtención de hormigones eco-celulares (ECC, Eco-cellular Concrete). En la actualidad existen investigaciones de ECC en los que se emplean fuentes de sílice alternativas como el residuo de vidrio (Xuan et al., 2019), sin embargo, hasta donde ha alcanzado la búsqueda bibliográfica realizada a lo largo de la presente investigación, no existen investigaciones centradas en la sustitución de los hidróxidos alcalinos y, por tanto, en la elaboración de disoluciones alcalinas 100 % residuales.

Es evidente que, siguiendo la línea medioambientalmente amigable del material, en el desarrollo de los nuevos ECCs debería considerarse adicionalmente el uso de agentes aireantes también procedentes de residuos.

Problema i.c) REACTIVOS DE AIREACIÓN

De entre todos los agentes que se pueden utilizar como aireantes (ver punto 1.2 del presente capítulo), responsables de generar una estructura repleta de micro-porosidades en las matrices de los TCCs, el aluminio en polvo es el material empleado por excelencia (Kazaryan and Belyaev, 2019).

Este reactivo, a pesar de su baja dosificación (0.05 % a 0.5 % del peso del OPC) resulta tener un elevado impacto económico y ambiental. Para obtener una tonelada de aluminio puro de bauxita se requieren 15000 kWh de calor generado por energía eléctrica y se producen cinco toneladas de residuos (Ayres, 1995; U.S. Department of Energy, 2007). Además, existe una importante contribución adicional del tratamiento posterior a la fabricación del polvo de aluminio mediante el fresado de sellos, el fresado de bolas en condiciones secas, el fresado en húmedo, el fresado por atrición y el fresado por vibración (Ding et al., 2012).

Según el informe medioambiental del sector, en términos de consumo total, el impacto ambiental, Potencial de Calentamiento Global (en inglés Global Warming Potential (GWP)[1]), de la fabricación del aluminio primario utilizado en Europa en el año 2018 fue (European Aluminium Association, 2018):

[1] Potencial de Calentamiento Global (Global Warming Potential (GWP)): Define el efecto del calentamiento integrado a lo largo del tiempo que produce una liberación instantánea de 1kg de un gas de efecto invernadero, en comparación con el causado por el CO_2. Se suele calcular para periodos de 20, 100 o 500 años, siendo 100 el más frecuente.

- LCA (modalidad cradle to gate[1]) para la producción de aluminio primario: 8.6 kg CO_2eq por kg de aluminio[2].
- LCA (molalidad gate to gate[3]) para el proceso de extrusión: 0.7 kg CO_2eq por kg de aluminio.
- LCA (modalidad gate to gate) para la producción de papel de aluminio: 1.3 kg CO_2eq por kg de aluminio.

Solución i.c) MÉTODOS DE AIREACIÓN ALTERNATIVOS

En este sentido, desde hace varios años varios autores han presentado trabajos de investigación en los que se ha propuesto medios alternativos de aireación de distintas procedencias: aluminio procedente de chatarra (Araújo and Tenório, 2005), residuos procedentes del polvo de los filtros de gasificación en plantas de energía (Holt and Raivio, 2005) o cenizas de fondo procedentes de la incineración de residuos sólidos urbanos (Song et al., 2015; Xuan et al., 2019).

- **Procedimientos de fabricación (ii)**

Problema ii.a) CURADO EN AUTOCLAVE

Como se ha nombrado en el punto 1.2 del presente capítulo, a pesar de que el proceso de producción del TCC es relativamente sencillo y medioambientalmente limpio, para alcanzar las características físicas y mecánicas del producto es necesario un tratamiento de curado en autoclave. Este tratamiento se basa en condiciones de temperatura y presión muy elevadas, por lo que se trata de un proceso caro, que requiere de instalaciones de cierta envergadura, y que lleva asociado consumos energéticos desmesurados y emisiones de gases de efecto invernadero.

Solución ii.a) CURADO A TEMPERATURA AMBIENTE

Ante esta situación, los AAM y los GP pueden presentar buenas propiedades bajo condiciones de curado más suaves a temperatura ambiente o en las que únicamente se requiere de temperaturas moderadas (en torno a los 60-70°C)

[1] Modalidad cradle to gate de LCA (de la cuna a la puerta): es aquel que comprende todo el ciclo de vida de un producto y servicio hasta que este se encuentra listo para su empleo o instalación (extracción de materias primas, transporte y fase de producción o fabricación).
[2] kg CO_2eq: unidad de medición empleada para indicar el GWP de cada uno de los gases de efecto invernadero, en comparación con el dióxido de carbono.
[3] Modalidad gate to gate de LCA (de puerta a puerta): el análisis del ciclo de vida está limitado desde que las materias primas están preparadas para ser transformadas hasta que el producto o servicio se encuentra listo para su empleo o instalación (fase de producción o fabricación).

para configurar materiales estables con excelentes propiedades mecánicas y de durabilidad.

En lo que respecta a los sistemas celulares, siguiendo la misma línea, en la mayoría de las investigaciones actuales se evita el uso de autoclave para el curado de los materiales, tanto para la fabricación de AACCs como de GCCs, sin embargo, sí que se requiere de moderadas temperaturas (entre los 40 y los 80 °C) para obtenerse matrices estables (Esmaily and Nuranian, 2012). Hay otra parte de los trabajos publicados en los que se procede a un pre-tratamiento a altas temperaturas durante 24 o 48 horas y posteriormente los especímenes permanecen a temperatura ambiente hasta la edad de ensayo (Beghoura and Castro-Gomes, 2019; Stoleriu et al., 2019).

Recientemente, se ha documentado la obtención de AACC de escoria de alto horno, así como sistemas a base de MK o ceniza volante de GCCs, curados a temperatura ambiente sin necesidad de ningún procedimiento que requiera de consumo energético, obteniéndose matrices celulares con buenos resultados físicos y mecánicos (Alzaza et al., 2019; He et al., 2019; Stolz et al., 2018).

En resumen, para la fabricación de los nuevos ECC, se ha requerido tratamientos a temperaturas moderadas (entre los 70 y 80 °C) y hasta donde llega el análisis bibliográfico del presente trabajo, no existen trabajos en los que estos materiales se obtengan a temperatura ambiente.

Problema ii.b) PRODUCCIÓN DE LAS DISOLUCIONES ACTIVADORAS ALTERNATIVAS

El desarrollo de los nuevos ECC permite evitar el empleo de autoclave mejorando también los inconvenientes medioambientales asociados al proceso de fabricación del material. Sin embargo, se introduce otro aspecto crítico a tener en cuenta, relacionado con la producción de la disolución activadora alternativa.

En la mayoría de los casos, para la producción de las disoluciones activadoras alternativas, es necesario un tratamiento a altas temperaturas para la correcta disolución en agua de los residuos sólidos en polvo (tanto cuando se emplea una fuente de sílice alternativa, como cuando se emplea una fuente de sodio o potasio alternativa o en las que se emplean las dos) (Bouzón, 2015; Puertas and Torres-Carrasco, 2014; Tchakouté et al., 2017). En ocasiones, este tratamiento térmico no es necesario, ya que al incluir en la disolución un reactivo alcalino que induce una reacción exotérmica, se mejora el proceso de disolución de los componentes del activador. Sin embargo, en estos casos se requiere de un mecanismo de agitación continua de la mezcla activadora durante periodos que van desde las 20 a las 24 horas (Mejía et al., 2016; Villaquirán-Caicedo et al., 2017). Como consecuencia se produce un consumo energético extra contribuyendo al incremento del GWP asociado.

Solución ii.b) PRODUCCIÓN DE AAM/GP DEL TIPO "ONE-PART".

Generalmente se denominan AAMs o GPs “two-part” a aquellos que están formados por una fase sólida o precursor y una fase acuosa o disolución alcalina. En los últimos años, se está introduciendo el concepto de AAM o GP “one-part” que se basan en la mezcla en sólido de todos los constituyentes (precursores y activadores) de manera que para la fabricación del hormigón únicamente se requiere añadir agua y mezclar (Abdel-Gawwad and Abo-El-Enein, 2016; Luukkonen et al., 2018).

Esta nueva tecnología se presenta como una opción potencial a aplicar en los sistemas celulares alternativos en dos sentidos: i) agilizar y optimizar los tiempos y procesos de producción lo que lo convierte en un material interesante para la industria de los prefabricados; y ii) es una opción económicamente eficiente y más amigable con el medio ambiente ya que no requiere de ningún tratamiento térmico ni mecánico.

No se ha encontrado publicaciones científicas en las que se presente hormigones celulares alternativos (GCC o AACC) en los que se aplica la modalidad de fabricación “one-part”.

Problema ii.c) PRE-TRATAMIENTO DE MATERIAS PRIMAS

Con el objetivo de obtener un material final con emisiones asociadas muy bajas, el último aspecto a considerar es el pre-tratamiento necesario de los precursores, los residuos para las disoluciones alcalinas alternativas, así como de los agentes aireantes alternativos, para su uso en la fabricación de hormigones celulares alternativos.

En el caso de los precursores y los residuos para las disoluciones, generalmente consta de dos actividades: el secado y la molienda. En el caso de los agentes aireantes alternativos se requiere de un tratamiento de molienda con el fin de obtener la máxima reactividad posible disminuyendo el tamaño de partícula y aumentando la superficie específica.

Solución ii.c) Co-MOLIENDA DE PRECURSORES Y AGENTES AIREANTES

En base a los trabajos de documentación llevados a cabo a lo largo de la presente Tesis Doctoral, no se tiene constancia de la existencia de investigaciones científicas previas en las que se evite este tratamiento de los aireantes alternativos.

Como se va a exponer a continuación en el punto 1.4 del presente capítulo, la alumna que opta al título de doctora, introdujo el concepto de Co-molienda (Co-M) en el desarrollo de su tesina final de máster (Font, 2016). Se trata de introducir el agente aireante alternativo en el procedimiento de molienda requerido para los precursores, de modo que el tamaño de partículas

adquirido, así como la distribución de las mismas, sea homogéneo entre ambos materiales, favoreciendo la reacción de aireación en las matrices.

La Co-molienda puede permitir adaptar la modalidad de fabricación "one-part" expuesta anteriormente (solución ii.b) a la tecnología de los nuevos ECC, de modo en que se obtengan materiales eco-eficientes compuestos por un 100 % de residuos y cuyo procedimiento de fabricación tenga asociado un GWP casi nulo.

1.4 ANTECEDENTES EXPERIMENTALES Y APROXIMACIÓN A LA INVESTIGACIÓN

El trabajo de investigación asociado al desarrollo de la presente Tesis Doctoral, tiene sus orígenes en septiembre del año 2014, cuando la alumna inicia los estudios del Máster Universitario en Ingeniería del Hormigón (MUIH), y se incorpora como colaboradora en Grupo de Investigación en Química de los Materiales (GIQUIMA) del Instituto de Ciencia y Tecnología del Hormigón (ICITECH), de la Universitat Politècnica de València (UPV).

El grupo GIQUIMA, formado por los doctores Jordi Payá Bernabeu, María Victoria Borrachero Rosado, José María Monzó Balbuena, Ana Mellado Romero y Lourdes Soriano Martínez, tiene un amplio recorrido científico en el estudio microestructural de materiales de construcción y en la investigación y desarrollo de nuevos conglomerantes de activación alcalina y geopolímeros. Además, participa activamente en la docencia de varias asignaturas del MUIH.

En febrero de 2015, la alumna obtuvo una Beca de Colaboración concedida en la primera convocatoria de proyectos I+D+i de la Cátedra de Empresa C.S.A con un proyecto titulado "*HORMIGONES CELULARES GEOPOLIMÉRICOS, NUEVOS DESARROLLOS*", bajo la dirección del Dr. Jordi Payá Bernabeu. El plan de trabajo se desarrolló durante 16 meses y sirvió de precedente para el desarrollo de la Tesina Final de Master (TFM) que la alumna defendió en abril de 2016 titulada: *"HORMIGÓN CELULAR GEOPOLIMÉRICO (HCG) AIREADO CON ALUMINIO RECICLADO: DESARROLLO Y CARACTERIZACIÓN DE UN MATERIAL DE BAJO COSTE ECONÓMICO Y MEDIOAMBIENTAL"* (Font, 2016).

En dicha TFM, se llevaron a cabo los trabajos preliminares previos necesarios para conocer el comportamiento de las matrices geopoliméricas y de activación alcalina con la introducción de agentes de aireación procedentes de fuentes de aluminio residuales. El trabajo fue presentado en noviembre de 2016 a los "*PREMIOS A TESIS FIN DE MÁSTER DEL AULA-EMPRESA CEMEX SOSTENIBILIDAD*" obteniendo la primera posición en el apartado de tesinas de máster.

Tras la defensa del TFM y la obtención del título de máster, la alumna continuó con los trabajos experimentales de investigación, desarrollando un nuevo plan de trabajo que se culmina con lo expuesto en el presente documento para la obtención del título de Doctora.

1.5 REFERENCIAS BIBLIOGRÁFICAS

Abdel-Gawwad, H.A., Abo-El-Enein, S.A., 2016. A novel method to produce dry geopolymer cement powder. HBRC J. https://doi.org/10.1016/j.hbrcj.2014.06.008

AENOR, 2012. UNE-EN 15978: Sostenibilidad en la construcción. Evaluación del comportamiento ambiental de los edificios. Métodos de cálculo, 2012.

AENOR, 2011. UNE-EN ISO 14006: Sistemas de gestión ambiental. Directrices para la incorporación del ecodiseño.

Alfonso, C., Avellaner, J., Lozano, B., Estévez, R., Marinas, I., Morino, A., Prieto, A., Santamarta, J., 2018. I Anuario De Economía Circular En España 2018. Resum. Ejec.

Alzaza, A., Mastali, M., Kinnunen, P., Korat, L., Abdollahnejad, Z., Ducman, V., Illikainen, M., 2019. Production of Lightweight Alkali Activated Mortars Using Mineral Wools. Materials (Basel). 12, 1695. https://doi.org/10.3390/ma12101695

Araújo, E.G. de, Tenório, J.A.S., 2005. Cellular Concrete with Addition of Aluminum Recycled Foil Powders. Mater. Sci. Forum 498–499, 198–204. https://doi.org/10.4028/www.scientific.net/MSF.498-499.198

Ayres, R.U., 1995. Life cycle analysis: A critique. Resour. Conserv. Recycl. 14, 199–223. https://doi.org/10.1016/0921-3449(95)00017-D

Beghoura, I., Castro-Gomes, J., 2019. Design of alkali-activated aluminium powder foamed materials for precursors with different particle sizes. Constr. Build. Mater. 224, 682–690. https://doi.org/10.1016/j.conbuildmat.2019.07.018

Bernal, S.A., Rodríguez, E.D., Mejía de Gutiérrez, R., Provis, J.L., 2015. Performance at high temperature of alkali-activated slag pastes produced with silica fume and rice husk ash based activators. Mater. Construcción 65, e049. https://doi.org/10.3989/mc.2015.03114

BOE-RD 105, 2008. Real Decreto 105/2008, de 1 de febrero, por el que se regula la producción y gestión de los residuos de construcción y demolición, Boletin Oficial del Estado.

Bouzón, N., 2015. ACTIVADORES ALCALINOS ALTERNATIVOS A PARTIR DE LA CENIZA DE CÁSCARA DE ARROZ PARA LA FABRICACIÓN DE GEOPOLÍMEROS. Universitat Politècnica de València.

Bouzón, N., Payá, J., Borrachero, M. V., Soriano, L., Tashima, M.M., Monzó, J.,

2014. Refluxed rice husk ash/NaOH suspension for preparing alkali activated binders. Mater. Lett. 115, 72–74. https://doi.org/10.1016/j.matlet.2013.10.001

Buchwald, A., Hohmann, M., Posern, K., Brendler, E., 2009. The suitability of thermally activated illite/smectite clay as raw material for geopolymer binders. Appl. Clay Sci. 46, 300–304. https://doi.org/10.1016/j.clay.2009.08.026

Celcon, 2019. CELCON, Hormigón Celular [WWW Document]. URL https://www.celcon.cl (accessed 11.17.19).

Cellular Concrete Solutions, 2007. What is Cellular Concrete... and if It is So Great, Why Doesn't Everyone Use it? Smart Foam Liq. Conc. Solut. Ser.

Cheah, C.B., Part, W.K., Ramli, M., 2015. The hybridizations of coal fly ash and wood ash for the fabrication of low alkalinity geopolymer load bearing block cured at ambient temperature. Constr. Build. Mater. 88, 41–55. https://doi.org/10.1016/j.conbuildmat.2015.04.020

Chica, L., Alzate, A., 2019. Cellular concrete review: New trends for application in construction. Constr. Build. Mater. 200, 637–647. https://doi.org/10.1016/j.conbuildmat.2018.12.136

Chindaprasirt, P., Rattanasak, U., 2011. Shrinkage behavior of structural foam lightweight concrete containing glycol compounds and fly ash. Mater. Des. 32, 723–727. https://doi.org/10.1016/j.matdes.2010.07.036

Collins, F.G., Turner, L.K., Collins, F.G., 2017. Carbon dioxide equivalent (CO 2 -e) emissions : A comparison between geopolymer and OPC cement concrete and OPC cement concrete. Constr. Build. Mater. 43, 125–130. https://doi.org/10.1016/j.conbuildmat.2013.01.023

Comisión Europea, 2014. Hacia una economía circular: un programa de cero residuos para Europa (COM(2014) 398 final/2).

Comisión Europea - Medio Ambiente, 2019. Creado el Comité de Normalización de UNE sobre Economía Circular (CNT 323) [WWW Document]. URL http://www.cepco.es/noticia.asp?id_rep=11134 (accessed 10.23.19).

Comisión Europea - Medio Ambiente, 2015. La ECOINNOVACIÓN en el corazón de las políticas europeas [WWW Document]. URL https://ec.europa.eu/environment/ecoap/frontpage_es (accessed 10.23.19).

Comité Técnico ISO/TC 207, Gestión ambiental, Subcomité SC 5, A. del ciclo de vida., 2017. ISO 14040:2006(a) Gestión ambiental — Análisis del

ciclo de vida — Principios y marco de referencia.

Consejo Económico y Social (CES), 2016. El papel del sector de la construcción en el crecimiento económico, Coleccion informes.

Cristelo, N., Miranda, T., Oliveira, D. V., Rosa, I., Soares, E., Coelho, P., Fernandes, L., 2015. Assessing the production of jet mix columns using alkali activated waste based on mechanical and financial performance and CO<inf>2</inf> (eq) emissions. J. Clean. Prod. 102, 447–460. https://doi.org/10.1016/j.jclepro.2015.04.102

CTN 22 Minería y explosivos, 2019. UNE 22480: Sistema de gestión minero-mineralúrgica-metalúrgica sostenible. Requisitos.

Davidovits, P.J., 2002. 30 Years of Successes and Failures in Geopolymer Applications . Market Trends and Potential Breakthroughs . Geopolymer 2002 Conf. 1–16. https://doi.org/10.1017/CBO9781107415324.004

Ding, N., Gao, F., Wang, Z., Gong, X., Nie, Z., 2012. Environment impact analysis of primary aluminum and recycled aluminum. Procedia Eng. 27, 465–474. https://doi.org/10.1016/j.proeng.2011.12.475

Dolton, B., Hannah, C., 2006. Cellular Concrete : Engineering and Technological Advancement for Construction in Cold Climates 1–11.

Duxson, P., Provis, J.L., Lukey, G.C., van Deventer, J.S.J., 2007. The role of inorganic polymer technology in the development of "green concrete." Cem. Concr. Res. 37, 1590–1597. https://doi.org/10.1016/j.cemconres.2007.08.018

Elimbi, A., Tchakoute, H.K., Njopwouo, D., 2011. Effects of calcination temperature of kaolinite clays on the properties of geopolymer cements. Constr. Build. Mater. 25, 2805–2812. https://doi.org/10.1016/j.conbuildmat.2010.12.055

Esmaily, H., Nuranian, H., 2012. Non-autoclaved high strength cellular concrete from alkali activated slag. Constr. Build. Mater. 26, 200–206. https://doi.org/10.1016/j.conbuildmat.2011.06.010

European Aluminium Association, 2018. Environmental Profile Report for the European Aluminium Industry.

Falliano, D., De Domenico, D., Ricciardi, G., Gugliandolo, E., 2018. Experimental investigation on the compressive strength of foamed concrete: Effect of curing conditions, cement type, foaming agent and dry density. Constr. Build. Mater. 165, 735–749. https://doi.org/10.1016/j.conbuildmat.2017.12.241

Fernández-Jiménez, A., Palomo, J.G., Puertas, F., 1999. Alkali-activated slag mortars: Mechanical strength behaviour. Cem. Concr. Res. https://doi.org/10.1016/S0008-8846(99)00154-4

Font, A., 2016. Hormigón Celular Geopolimérico (Hcg) Aireado Con De Un Material De Bajo Coste Económico Y Medioambiental. Universitat Politècnica de València.

Font, A., Soriano, L., Reig, L., Tashima, M.M., Borrachero, M. V., Monzó, J., Payá, J., 2018. Use of residual diatomaceous earth as a silica source in geopolymer production. Mater. Lett. 223, 10–13. https://doi.org/10.1016/j.matlet.2018.04.010

Frost, A., 2016. Alkali-activated cementitious materials. Concrete. https://doi.org/10.1016/j.cemconres.2017.02.009

Funfación Conama - Grupo de trabajo GT-6, 2018. Economía circular en el sector de la construcción. Congr. Nac. del Medio Ambient. 2018.

Gökçe, H.S., Hatungimana, D., Ramyar, K., 2019. Effect of fly ash and silica fume on hardened properties of foam concrete. Constr. Build. Mater. 194, 1–11. https://doi.org/10.1016/j.conbuildmat.2018.11.036

Green building council españa (GBCe), 2017. Informe de posicionamiento de GBCe sobre Economía Circular 8.

Grupo Xella, 2019. Proceso de fabricación bloques Ytong [WWW Document]. URL https://www.ytong.es/proceso_productivo.php (accessed 10.28.19).

Grupo Xella - Noticias, 2016. Una vivienda inteligente proyectada con Ytong, elegida como modelo en un congreso de edificios de bajo consumo en Madrid [WWW Document]. URL https://www.ytong.es/noticias_1939.php (accessed 10.25.19).

He, Juan, Gao, Q., Song, X., Bu, X., He, Junhong, 2019. Effect of foaming agent on physical and mechanical properties of alkali-activated slag foamed concrete. Constr. Build. Mater. 226, 280–287. https://doi.org/10.1016/j.conbuildmat.2019.07.302

Hebel, 2019. La Solución Inteligente Para La Construcción: Concreto Celular Autoclavado [WWW Document]. URL https://www.hebel.mx/#_sub1399 (accessed 11.17.19).

Hogeling, J., Derjanecz, A., 2018. The 2nd recast of the Energy Performance of Buildings Directive (EPBD). Sustain. Dev. 1–30.

Holt, E., Raivio, P., 2005. Use of gasification residues in aerated autoclaved

concrete. Cem. Concr. Res. 35, 796–802. https://doi.org/10.1016/j.cemconres.2004.05.005

Hu, W., Nie, Q., Huang, B., Shu, X., He, Q., 2018. Mechanical and microstructural characterization of geopolymers derived from red mud and fly ashes. J. Clean. Prod. 186, 799–806. https://doi.org/10.1016/j.jclepro.2018.03.086

Istuque, D.B., Reig, L., Moraes, J.C.B., Akasaki, J.L., Borrachero, M. V., Soriano, L., Payá, J., Malmonge, J.A., Tashima, M.M., 2016. Behaviour of metakaolin-based geopolymers incorporating sewage sludge ash (SSA). Mater. Lett. 180, 192–195. https://doi.org/10.1016/j.matlet.2016.05.137

Jerman, M., Keppert, M., Výborný, J., Černý, R., 2013. Hygric, thermal and durability properties of autoclaved aerated concrete. Constr. Build. Mater. 41, 352–359. https://doi.org/10.1016/j.conbuildmat.2012.12.036

Jones, M.R., McCarthy, A., 2006. Heat of hydration in foamed concrete: Effect of mix constituents and plastic density. Cem. Concr. Res. 36, 1032–1041. https://doi.org/10.1016/j.cemconres.2006.01.011

Kazaryan, R., Belyaev, K., 2019. The sustainable energy approach in the manufacture of cellular concrete. E3S Web Conf. 91. https://doi.org/10.1051/e3sconf/20199102024

Lecomte, I., Henrist, C., Liégeois, M., Maseri, F., Rulmont, A., Cloots, R., 2006. (Micro)-structural comparison between geopolymers, alkali-activated slag cement and Portland cement. J. Eur. Ceram. Soc. 26, 3789–3797. https://doi.org/10.1016/j.jeurceramsoc.2005.12.021

Luukkonen, T., Abdollahnejad, Z., Yliniemi, J., Kinnunen, P., Illikainen, M., 2018. One-part alkali-activated materials: A review. Cem. Concr. Res. https://doi.org/10.1016/j.cemconres.2017.10.001

Mejía, J.M., Mejía De Gutiérrez, R., Montes, C., 2016. Rice husk ash and spent diatomaceous earth as a source of silica to fabricate a geopolymeric binary binder. J. Clean. Prod. 118, 133–139. https://doi.org/10.1016/j.jclepro.2016.01.057

Mellado, A., Catalán, C., Bouzón, N., Borrachero, M. V., Monzó, J.M., Payá, J., 2014. Carbon footprint of geopolymeric mortar: study of the contribution of the alkaline activating solution and assessment of an alternative route. RSC Adv. 4, 23846–23852. https://doi.org/10.1039/C4RA03375B

Melo, J.P., 2013. Desarrollo y caracterización de un material celular de alta

porosidad con base cementicia activada mediante agentes inorgánicos.

Ministerio de Agricultura y Alimentación Pesca y Medio Ambiente (MAPAMA), Ministerio de Economía Industria y Competitividad (MINECO), 2018. España Circular 2030 - Estrategia Española de Economía Circular.

Ministerio de Fomento - Gobierno de España, 2018. CTE-HE. Código Técnico de la Edificación. Basic document HE (Energy saving). June 68.

Mo, K.H., Alengaram, U.J., Jumaat, M.Z., Yap, S.P., Lee, S.C., 2016. Green concrete partially comprised of farming waste residues: A review. J. Clean. Prod. 117, 122–138. https://doi.org/10.1016/j.jclepro.2016.01.022

Naciones Unidas, 2018. Asamblea de las Naciones Unidas sobre el Medio Ambiente del Programa de las Naciones Unidas para el Medio Ambiente - Plan de ejecución "Hacia un planeta sin contaminación" [WWW Document]. UNEP/EA.4/3. URL https://papersmart.unon.org/resolution/uploads/k1804193-1.pdf

Naciones Unidas, 2015a. Convención Marco sobre el Cambio Climático - Aprobación del Acuerdo de París [WWW Document]. FCCC/CP/2015/L.9. URL https://unfccc.int/resource/docs/2015/cop21/spa/l09s.pdf (accessed 10.22.19).

Naciones Unidas, 2015b. Proyecto de documento final de la cumbre de las Naciones Unidas para la aprobación de la agenda para el desarrollo después de 2015 - Agenda 2030 para el Desarrollo Sostenible [WWW Document]. A/69/L.85. URL https://www.cooperacionespanola.es/sites/default/files/agenda_2030_desarrollo_sostenible_cooperacion_espanola_12_ago_2015_es.pdf (accessed 10.22.19).

Narayanan, N., Ramamurthy, K., 2000. Prediction models based on gel-pore parameters for compressive strength of aerated concrete 2, 206–212.

Nie, Q., Hu, W., Huang, B., Shu, X., He, Q., 2019. Synergistic utilization of red mud for flue-gas desulfurization and fly ash-based geopolymer preparation. J. Hazard. Mater. 369, 503–511. https://doi.org/10.1016/j.jhazmat.2019.02.059

Noticias-Parlamento Europeo, 2015. Economía circular: definición, importancia y beneficios [WWW Document]. 20151201STO05603. URL https://www.europarl.europa.eu/news/es/headlines/economy/20151201STO05603/economia-circular-definicion-importancia-y-beneficios

(accessed 10.23.19).

Ogundiran, M.B., Kumar, S., 2016. Synthesis of fly ash-calcined clay geopolymers: Reactivity, mechanical strength, structural and microstructural characteristics. Constr. Build. Mater. 125, 450–457. https://doi.org/10.1016/j.conbuildmat.2016.08.076

Palomo, A., López de la Fuente, J.I., 2003. Alkali-activated cementitous materials: Alternative matrices for the immobilisation of hazardous wastes - Part I. Stabilisation of boron. Cem. Concr. Res. 33, 281–288. https://doi.org/10.1016/S0008-8846(02)00963-8

Pan, Z., Li, H., Liu, W., 2014. Preparation and characterization of super low density foamed concrete from Portland cement and admixtures. Constr. Build. Mater. 72, 256–261. https://doi.org/10.1016/j.conbuildmat.2014.08.078

Pelisser, F., Guerrino, E.L., Menger, M., Michel, M.D., Labrincha, J.A., 2013. Micromechanical characterization of metakaolin-based geopolymers. Constr. Build. Mater. 49, 547–553. https://doi.org/10.1016/j.conbuildmat.2013.08.081

Peys, A., Rahier, H., Pontikes, Y., 2016. Potassium-rich biomass ashes as activators in metakaolin-based inorganic polymers. Appl. Clay Sci. 119, 401–409. https://doi.org/10.1016/j.clay.2015.11.003

Provis, J.L., 2016. Alkali-activated materials. Cem. Concr. Res. https://doi.org/10.1016/j.cemconres.2017.02.009

Puertas, F., González-Fonteboa, B., González-Taboada, I., Alonso, M.M., Torres-Carrasco, M., Rojo, G., Martínez-Abella, F., 2018. Alkali-activated slag concrete: Fresh and hardened behaviour. Cem. Concr. Compos. https://doi.org/10.1016/j.cemconcomp.2017.10.003

Puertas, F., Torres-Carrasco, M., 2014. Use of glass waste as an activator in the preparation of alkali-activated slag. Mechanical strength and paste characterisation. Cem. Concr. Res. 57, 95–104. https://doi.org/10.1016/j.cemconres.2013.12.005

Pytlik, E.C., Saxena, J., 1992. Autoclaved Cellular Concrete: the Building Material for the 21St Century. Proc. 3rd RILEM Int. Symp. Autoclaved Aerated Concr. 18.

Raj, A., Sathyan, D., Mini, K.M., 2019. Physical and functional characteristics of foam concrete: A review. Constr. Build. Mater. 221, 787–799. https://doi.org/10.1016/j.conbuildmat.2019.06.052

Ramamurthy, K., Kunhanandan Nambiar, E.K., Indu Siva Ranjani, G., 2009. A

classification of studies on properties of foam concrete. Cem. Concr. Compos. 31, 388–396. https://doi.org/10.1016/j.cemconcomp.2009.04.006

Reig, L., Tashima, M.M., Borrachero, M. V, Monzó, J., Cheeseman, C.R., Payá, J., 2013. Properties and microstructure of alkali-activated red clay brick waste. Constr. Build. Mater. 43, 98–106. https://doi.org/https://doi.org/10.1016/j.conbuildmat.2013.01.031

Rodríguez, E.D., Bernal, S.A., Provis, J.L., Gehman, J.D., Monzó, J.M., Payá, J., Borrachero, M.V., 2013. Geopolymers based on spent catalyst residue from a fluid catalytic cracking (FCC) process. Fuel 109, 493–502. https://doi.org/10.1016/j.fuel.2013.02.053

Schroeder, P., Anggraeni, K., Weber, U., 2018. The Relevance of Circular Economy Practices to the Sustainable Development Goals: Circular Economy and SDGs. J. Ind. Ecol. https://doi.org/10.1111/jiec.12732

Sepulcre Aguilar, A., Pinilla Melo, J., Hernández Olivares, F., 2013. Microstructural analysis of aerated cement pastes with fly ash, Metakaolin and Sepiolite additions. Constr. Build. Mater. 47, 282–292. https://doi.org/10.1016/j.conbuildmat.2013.05.082

Servicio de Estudios del Parlamento Europeo (EPRS), 2015. Pleno 2/7/2015 del Parlamento Europeo - Avanzar hacia una economía circular.

She, W., Du, Y., Zhao, G., Feng, P., Zhang, Y., Cao, X., 2018. Influence of coarse fly ash on the performance of foam concrete and its application in high-speed railway roadbeds. Constr. Build. Mater. 170, 153–166. https://doi.org/10.1016/j.conbuildmat.2018.02.207

Shirley, R., Black, L., 2011. Alkali activated solidification/stabilisation of air pollution control residues and co-fired pulverised fuel ash. J. Hazard. Mater. 194, 232–242. https://doi.org/10.1016/j.jhazmat.2011.07.100

Siporex, 2019. SIPOREX, créations en béton cellulaire [WWW Document]. URL https://www.siporex.fr (accessed 11.17.19).

Song, Y., Li, B., Yang, E.H., Liu, Y., Ding, T., 2015. Feasibility study on utilization of municipal solid waste incineration bottom ash as aerating agent for the production of autoclaved aerated concrete. Cem. Concr. Compos. 56, 51–58. https://doi.org/10.1016/j.cemconcomp.2014.11.006

Stoleriu, S., Vlasceanu, I.N., Dima, C., Badanoiu, A.I., Voicu, G., 2019. Alkali activated materials based on glass waste and slag for thermal and acoustic insulation. Mater. Construcción 69, 194. https://doi.org/10.3989/mc.2019.08518

Stolz, J., Boluk, Y., Bindiganavile, V., 2018. Mechanical, thermal and acoustic properties of cellular alkali activated fly ash concrete. Cem. Concr. Compos. 94, 24–32. https://doi.org/10.1016/j.cemconcomp.2018.08.004

Tashima, M.M., Akasaki, J.L., Castaldelli, V.N., Soriano, L., Monzó, J., Payá, J., Borrachero, M. V., 2012. New geopolymeric binder based on fluid catalytic cracking catalyst residue (FCC). Mater. Lett. 80, 50–52. https://doi.org/10.1016/j.matlet.2012.04.051

Tashima, M.M., Akasaki, J.L., Melges, J.L.P., Soriano, L., Monzó, J., Payá, J., Borrachero, M. V., 2013. Alkali activated materials based on fluid catalytic cracking catalyst residue (FCC): Influence of SiO_2/Na_2O and H_2O/FCC ratio on mechanical strength and microstructure. Fuel 108, 833–839. https://doi.org/10.1016/j.fuel.2013.02.052

Tchakouté, H.K., Rüscher, C.H., Kong, S., Kamseu, E., Leonelli, C., 2017. Thermal Behavior of Metakaolin-Based Geopolymer Cements Using Sodium Waterglass from Rice Husk Ash and Waste Glass as Alternative Activators. Waste and Biomass Valorization 8, 573–584. https://doi.org/10.1007/s12649-016-9653-7

Tchakouté, H.K., Rüscher, C.H., Kong, S., Kamseu, E., Leonelli, C., 2016. Geopolymer binders from metakaolin using sodium waterglass from waste glass and rice husk ash as alternative activators: A comparative study. Constr. Build. Mater. 114, 276–289. https://doi.org/10.1016/j.conbuildmat.2016.03.184

Telos digital - Fundación Telefónica, 2018. Telos digital - Fundación Telefónica [WWW Document]. URL https://telos.fundaciontelefonica.com/la-multi-revolucion-mato-la-economia-circular/grafico-economia-lineal-vs-economia-circular/ (accessed 10.23.19).

Tippayasam, C., Balyore, P., Thavorniti, P., Kamseu, E., Leonelli, C., Chindaprasirt, P., Chaysuwan, D., 2016. Potassium alkali concentration and heat treatment affected metakaolin-based geopolymer. Constr. Build. Mater. https://doi.org/10.1016/j.conbuildmat.2015.11.027

Torres-Carrasco, M., Puertas, F., 2017. Alkaline activation of different aluminosilicates as an alternative to Portland cement: Alkali activated cements or geopolymers | La activación alcalina de diferentes aluminosilicatos como una alternativa al Cemento Portland: cementos activados alcaliname. Rev. Ing. Constr. 32, 5–12. https://doi.org/10.4067/S0718-50732017000200001

U.S. Department of Energy, 2007. U.S. Energy Requirements for Aluminum Production: Historical Perspective, Theoretical Limits and Current Practices. Ind. Technol. Progr. Energy Effic. Renew. Energy 150.

Villaquirán-Caicedo, M.. A., Mejía de Gutiérrez, R., Gallego, N.C.C., 2017. A Novel MK-based Geopolymer Composite Activated with Rice Husk Ash and KOH : Performance at High Temperature. Mater. Construcción 67, 1–13. https://doi.org/10.3989/mc.2017.02316

Wongkeo, W., Thongsanitgarn, P., Pimraksa, K., Chaipanich, A., 2012. Compressive strength, flexural strength and thermal conductivity of autoclaved concrete block made using bottom ash as cement replacement materials. Mater. Des. 35, 434–439. https://doi.org/10.1016/j.matdes.2011.08.046

Xuan, D., Tang, P., Poon, C.S., 2019. MSWIBA-based cellular alkali-activated concrete incorporating waste glass powder. Cem. Concr. Compos. 95, 128–136. https://doi.org/10.1016/j.cemconcomp.2018.10.018

Ytong, 2019. YTONG, el material de construcción natural [WWW Document]. URL https://www.ytong.es (accessed 11.17.19).

Zulkarnain, F., Ramli, M., 2011. Durability of Performance Foamed Concrete Mix Design with Silica Fume for Housing Development. J. M 5, 518–527.

CAPÍTULO II: ENFOQUE DE LA TESIS DOCTORAL

CONTENIDO

2 ENFOQUE DE LA TESIS DOCTORAL

2.1 OBJETIVO GENERAL DE LA TESIS DOCTORAL

El objetivo de la presente Tesis Doctoral es el desarrollo de hormigones eco-celulares basados 100% en residuos y aplicando la tecnología "one-part": los nuevos **ECC-OP**. Estos materiales cumplirán con las especificaciones funcionales de los hormigones celulares tradicionales (TCC) y mejorarán el ciclo de vida del material reduciendo las emisiones de gases de efecto invernadero y contribuyendo a la implantación de la economía circular en el sector.

2.2 OBJETIVOS ESPECÍFICOS DE LA TESIS DOCTORAL

Para llegar al objetivo general claramente marcado, es necesaria una planificación progresiva de objetivos específicos que se detallan a continuación:

i. Aplicación de la tecnología de los materiales geopoliméricos en la fabricación de hormigones celulares. Empleo del catalizador gastado de craqueo catalítico (FCC) para el desarrollo de hormigones celulares geopoliméricos (GCC).

ii. Aplicación de la tecnología de los materiales de activación alcalina en la fabricación de los hormigones celulares. Empleo de la escoria de alto horno (BFS) para el desarrollo de hormigones celulares de activación alcalina (AACC).

iii. Búsqueda y estudio de alternativas al empleo del polvo de aluminio (A) comercial que sean más amigables con el medio ambiente: a) papel de aluminio doméstico reciclado (A_R); b) peróxido de hidrogeno (H_2O_2); y c) Sub-productos de las escorias salinas (Paval granulado, PG). Aplicación en matrices de GCC y AACC, caracterización completa de los materiales, estudio de sus propiedades y establecimiento de relaciones entre las mismas.

iv. Influencia del tipo de aireación en los GCC y AACC: a) estudio de la aireación mecánica mediante la adición de lauril sulfato de sodio (SLS); y ii) estudio de la combinación de métodos (activaciones mecánica y química) mediante la adición de SLS y A.

v. Estudio y mejora medioambiental de las matrices GCC y AACC mediante la sustitución de del silicato de sodio comercial (WG) que se emplea en la preparación de la disolución activadora, por una fuente de sílice procedente de un residuo agrícola: la ceniza de cáscara de arroz (RHA). Aproximación al desarrollo de los nuevos hormigones eco-celulares ECC.

vi. Búsqueda de un comportamiento predecible de los GCC, AACC y ECC en función de sus constituyentes, dosificaciones y propiedades esperadas.

vii. Estudio medioambiental comparativo entre los TCC, GCC, AACC y los ECC: Cálculo de la huella de carbono.

viii. Desarrollo de matrices con base 100 % residuos. Estudio preliminar de la ceniza de biomasa de hueso de oliva (OBA) como posible fuente de potasio en la preparación de disoluciones alcalinas. Caracterización microestructural y física de la ceniza y primeras aplicaciones en la activación de BFS.

ix. Estudio del comportamiento de los sistemas binarios compuestos por BFS y OBA (sistemas BAAM). Estudio comparativo respecto a matrices activadas con los reactivos químicos comerciales (KOH y NaOH) con distintas concentraciones. Investigación de la posible combinación de influencia química y física de la ceniza en el material resultante: comparación con matrices a las que se adiciona un inerte para conocer el posible efecto filler de la OBA.

x. Combinación de la RHA, como fuente de sílice, y la OBA, como fuente de potasio, en la preparación de disoluciones alcalinas para la activación de BFS. Desarrollo de nuevos materiales ternarios de activación alcalina (TAAM). Estudio comparativo de las propiedades de los materiales en función de la dosificación y las condiciones de curado.

xi. Aplicación de los sistemas TAAM (BFS/RHA/OBA) a la tecnología del hormigón celular. Optimización medioambiental del material: compuesto a base de 100 % de residuos, que cumpla las especificaciones funcionales (densidad, resistencia mecánica y aislamiento) para su empleo en la industria de los prefabricados y cuyo proceso de fabricación se vea reducido a la mezcla de un material sólido con agua (tecnología “one-part”).

xii. Análisis comparativo del ciclo de vida (LCA) de los materiales resultantes en cada uno de los pasos de mejora planteados: TCC, AACC, ECC y ECC-OP.

2.3 ESQUEMA CONCEPTUAL DEL DESARROLLO EXPERIMENTAL Y PUBLICACIONES CIENTÍFICAS QUE ENMARCAN LA PRESENTE TESIS DOCTORAL

2.3.1 Problemática abordada y objetivos de mejora planteados

Llegados a este punto, ya se han dispuesto todas las bases necesarias para poder seguir el transcurso de la investigación objeto de la presente Tesis Doctoral.

El plan de trabajo se planteó como un desarrollo de mejoras "paso a paso" partiendo del material tradicional (el TCC) y culminando en el objetivo general de la investigación: el nuevo ECC-OP. Cada uno de los objetivos parciales marcan un "paso individual" de mejora y a su vez estos se han clasificado atendiendo a la fase del LCA a la que favorece su introducción: obtención de materias primas o proceso de fabricación del material. La Figura 2.1 y la Tabla 2.1 se presentan como herramientas de encuadre del recorrido experimental llevado a cabo en el desarrollo de la Tesis.

A continuación, se muestra un esquema en el que se pueden diferenciar las problemáticas abordadas y los objetivos de mejora planteados para cada una de ellas (Figura 2.1).

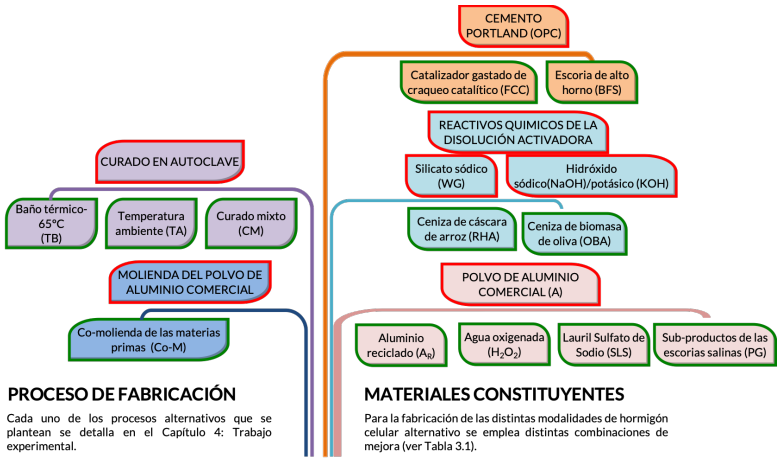

Figura 2.1: *Esquema conceptual de clasificación de problemáticas abordadas y objetivos de mejora planteados en el estudio "paso a paso"*

Una vez enmarcados cada uno de los aspectos de mejora individuales, en la Tabla 2.1, se presentan los materiales que se han ido obteniendo en función de las materias primas empleadas para su fabricación.

Tabla 2.1: *Modalidad de hormigón celular estudiado en función de los materiales constituyentes.*

	FASE SÓLIDA	FÁSE LÍQUIDA	PRODUCTO DE AIREACIÓN
Hormigón celular tradicional (TCC)	OPC	H_2O	A SLS H_2O_2
Hormigón celular geopolimérico (GCC)	FCC	WG + NaOH + H_2O	A A_R H_2O_2 SLS PG
Hormigón celular activado alcalinamente (AACC)	BFS	WG + NaOH + H_2O	A A_R H_2O_2 SLS PG
Hormigón eco-celular (ECC)	FCC BFS	RHA + NaOH + H_2O	A_R
Morteros binarios de activación alcalina (BAAM)	BFS	OBA + H_2O	-
Morteros ternarios de activación alcalina (TAAM)	BFS BFS + OBA	RHA + OBA + H_2O	-
Hormigón eco-celular "one-part" (ECC-OP)	BFS + OBA + RHA	H_2O	A_R

2.3.2 Publicaciones que enmarcan la presente Tesis Doctoral

La investigación llevada a cabo por la alumna Alba Font Pérez para la obtención del título del Doctora se ha distribuido a la comunidad científica mediante las siguientes publicaciones:

i. Alba Font, María Victoria Borrachero, Lourdes Soriano, José Monzó y Jordi Payá, ***"Geopolymer eco-cellular concrete (GECC) based on fluid catalytic cracking catalyst residue (FCC) with addition of recycled aluminium foil powder",*** Journal of Cleaner Production 168 (2017) 1120 – 1131.

ii. Alba Font, José Monzó, Lourdes Soriano, María Victoria Borrachero y Jordi Payá, ***"Nuevos Hormigones Celulares Geopoliméricos aireados con agua oxigenada: síntesis y propiedades",*** HAC2018, V Congreso Iberoamericano de hormigón autocompactable y hormigones especiales (5-6 marzo, 2018).

iii. Alba Font, José Monzó, Lourdes Soriano, María Victoria Borrachero y Jordi Payá, ***"New cellular geopolymer concretes (CGC) base on blast furnace slag and spent FCC catalyst",*** NOCMAT17, Non-Conventional Materials and Technologies. Materials Research Proceedings, 7 (2018) 685 – 694.

iv. Alba Font, Lourdes Soriano, José Monzó, Joao Claudio Bassan Moraes, María Victoria Borrachero y Jordi Payá, ***"Salt slag recycled by-products in high insulation alternative environmentally friendly cellular concrete manufacture",*** Construction and Building Materials 231 (2020) 117114.

v. Alba Font, María Victoria Borrachero, Lourdes Soriano, José Monzó, Ana Mellado y Jordi Payá, ***"New eco-cellular concretes: sustainable and energy-efficient materials",*** Green Chemistry 20 (2018) 4684 – 4694.

vi. Alba Font, María Victoria Borrachero, Lourdes Soriano, José Monzó y Jordi Payá, **"Air-void system characterisation of new eco-cellular concretes".** Sent to International Journal of Applied Ceramic Technology, status: peer-review (04/02/2019).

vii. Alba Font, Lourdes Soriano, Joao Claudio Bassan Moraes, Mauro M. Tashima, José Monzó, María Victoria Borrachero y Jordi Payá, ***"A 100% waste-based alkali-activated material by using olive-stone biomass ash (OBA) and blast furnace slag (BFS)"*** Materials Letters 203 (2017) 46 – 49.

viii. Sayonara María de Moraes Pinheiro, Alba Font, Lourdes Soriano, Mauro M. Tashima, José Monzó, María Victoria Borrachero, Jordi Payá, ***"Olive-stone biomass ash (OBA): An alternative alkaline source for***

the blast furnace slag activation", Construction and Building Materials 178 (2018) 327 – 338.

ix. Alba Font, Lourdes Soriano, Sayonara María de Moraes Pinheiro, Mauro M. Tashima, José Monzó, María Victoria Borrachero, Jordi Payá, ***"Design and properties of 100% waste-based ternary alkali-activated mortars: blast furnace slag, olive-stone biomass ash and rice husk ash",*** Journal of Cleaner Production 243 (2020) 118568.

x. Alba Font, Lourdes Soriano, Mauro M. Tashima, José Monzó, María Victoria Borrachero, Jordi Payá, ***"Step-by-step development of one-part eco-cellular concretes (ECC-OP) for precast industry: functional features and life cycle assessment (LCA)"*** Sent to Journal of Cleaner Production, status: peer-review (04/02/2020).

CAPÍTULO III: TRABAJO EXPERIMENTAL

CONTENIDO

3 TRABAJO EXPERIMENTAL

Se presenta un breve recorrido, de las materias primas empleadas y los diversos trabajos experimentales que se han llevado a cabo, a lo largo del presente trabajo de investigación.

3.1 MATERIAS PRIMAS

Una relación de las materias primas, **clasificadas por su tipología y su procedencia**, se lista en la Tabla 3.1. Por tipología nos referimos al empleo que se va a hacer de ellas como constituyentes de los diversos materiales objeto de estudio. Además, en la Tabla 3.1, se referencia las publicaciones en las que se ha hecho uso de ellas y que se citaron en el apartado 2.3.2.

Tabla 3.1:
Materias primas, procedencia y publicaciones en las que se emplean.

Precursores:		
	Procedencia	**Publicaciones**
OPC	Lafarge S.A (Puerto de Sagunto)	**i, ii, iii, v, vi, x**
FCC	BP Oil (Grao de Castellón)	**i - vi**
BFS	Cementval S.A (Puerto de Sagunto)	**ii-x**
Activadores alcalinos:		
Reactivos químicos	**Procedencia**	**Publicaciones**
NaOH	Meck S.L (Valencia)	**i, ii, iv, x**
	Panreac Química S.L.U (Castellar del Vallès)	**iii, v, vi, viii,**
KOH	Panreac Química S.L.U (Castellar del Vallès)	**vii, viii**
WG	Merck S.L (Valencia)	**i - vi, x**
Biomasa – alternativos		
RHA	DACSA S.A (Tabernes Blanques)	**v, vi, ix, x**
OBA	Almazara Candela (Elche)	**vii - x**
Agentes generadores de gas:		
	Procedencia	**Publicaciones**
A	Schlenk Metallic Pigments GmbH (Barcelona)	**i, iii - vi, x**
A_R	Departamento de Ecosistemas Agroforestales (UPV)	**i, v, vi, x**
H_2O_2	JT Baker (Madrid)	**ii**
SLS	Panreac Química S.L.U (Castellar del Vallès)	**iii**
PG	Befesa Aluminio S.L (Valladolid)	**iv**

Kephalite

El kephalite se ha empleado como adición inerte a los morteros de BFS (sistemas BAAM) con la finalidad de estudiar el posible efecto filler de la OBA en la **publicación xiii.**

Arena

La arena para la fabricación de los BAAM (**publicaciones xii y xiii)**, así como para los TAAM (**publicación ix)** son una mezcla de arena silícea (10 % arena fina, 12 % arena media y 78 % arena gruesa) que cumple con las especificaciones de UNE-EN 196-1.
Han sido suministrados por Sílices Carrión Martínez S.L (Llíria).

La caracterización física y microestructural de las materias primas se detalla más adelante en el Capítulo 4 para cada una de las fases experimentales en las que se emplean.

3.2 PRODUCCIÓN DE ESPECÍMENES

3.2.1 Pre-tratamiento de materias primas

Las **materias primas alternativas** empleadas en la investigación, sin hacer distinción de su tipología, han sido: BFS, FCC, RHA, OBA, A_R y PG. Todas ellas, requieren de un tratamiento, previo a su aplicación en la fabricación de los distintos materiales de activación alcalina o geopoliméricos. Las actividades de pre-tratamiento son el **secado** y la **molienda**.

En el caso del **secado** se ha aplicado a la BFS y la OBA con la finalidad de quitar completamente la humedad de los materiales para que, posteriormente, el proceso de molienda se pueda realizar de manera efectiva. El proceso consiste en mantener las materias primas en estufa a una temperatura de 100 ºC durante 24 horas.

La BFS, el FCC y la RHA han sido previamente estudiadas y tienen unas condiciones determinadas en cuanto a tamaño de partícula que mejoran su efectividad como precursores (BFS, FCC) (Payá et al., 1999; Wang et al., 2005, 1995) o como fuente de sílice alternativa en la preparación de disoluciones alcalinas (RHA) (Bouzón et al., 2014). Para la OBA, el A_R y el PG, los condicionantes asociados a su **molienda** han sido estudiados en la presente Tesis Doctoral con la finalidad de conseguir un óptimo comportamiento de los mismos como constituyentes de los distintos materiales alternativos planteados. Finalmente, como avance tecnológico y mejora medioambiental en el proceso de fabricación de hormigones celulares alternativos se introduce el concepto de **co-molienda (Co-M)**. En el caso de los GCCs, los AACCs y los ECCs se trata de introducir los agentes aireantes alternativos (A_R o PG) en el proceso de molienda de los precursores (BFS, FCC) y en el caso de los nuevos ECC-OP se trata de la molienda conjunta de todas las materias primas sólidas que constituyen el material (BFS/OBA/RHA/A_R):

- El uso individual de la RHA se ha llevado a cabo en dos condiciones: en su estado original (sin moler) en los primeros trabajos experimentales (**publicaciones v y vi**) y molida en un molino industrial durante 4 horas (Bouzón, 2015) en los últimos trabajos experimentales (**publicación ix y x**). Para su aplicación en la Co-M se ha empleado la RHA original (**publicación x**).

- En cuanto a la **molienda**, se va a distinguir entre **molienda individual y Co-M**. La molienda individual de la BFS, el FCC y la OBA, así como para la Co-M, se ha llevado a cabo mediante un molino de bolas modelo Gabrielli Mill-2. Se trata de un recipiente de cerámica de un litro de capacidad donde se introducen bolas de alúmina (diámetro = 2 cm) junto con el material que se quiere moler. Los condicionantes

de los que depende la granulometría obtenida son: el tiempo de molienda, el número de bolas y la cantidad de material introducido (ver Tabla 3.2*)*.

- En el caso del papel de aluminio reciclado (A_R), para el procedimiento de molienda individual se lleva a cabo tres etapas: i) se corta manualmente en trozos de entre 2 – 4 mm; ii) se muele con una picadora de alimentos Moulinex A320R1 (0.6 L de capacidad – 700 W de potencia) durante 5 minutos, haciendo paradas de 5 segundos cada minuto; iii) finalmente, el material se tamiza y se selecciona la fracción < 125 μm.

Tabla 3.2:
Características de los procesos de molienda individual y Co-M con la nomenclatura empleada en cada caso

Molienda individual				
Materia prima	Nomenclatura	*Cantidad de material (g)*	*Nº bolas*	*Tiempo (min)*
FCC	**FCC**	300	98	20
BFS	**BFS**	450		30
OBA	**OBA**	250	80	20
PG	**PG10**			10
	PG15			15
	PG20	250	98	20
	PG25			25
	PG30			30

Co-M				
Materias primas	Nomenclatura	*Cantidad de material (g)*	*Nº bolas*	*Tiempo (min)*
FCC + A_R	**FCCRm**	FCC = 300 A_R = 0.6	98	20
BFS + A_R	**BFSRm**	BFS = 450 A_R = 0.9		30
FCC + PG	**FCCPGm**	FCC = 300 PG = 6		20
BFS + PG	**BFSPGm**	BFS =450 PG = 9		30
BFS/A_R/RHA/OBA	**BRm-RO**	BFS = 360 A_R = 0.9 RHA = 40 OBA = 180		30

3.2.2 Procedimiento de fabricación: amasado y curado de los especímenes

Para la fabricación de los especímenes se han empleado dos equipos distintos en función del volumen de material que se requería amasar:

- Amasadora convencional para morteros de cemento (**NM**): de acuerdo con la norma UNE-EN 196 – 1 (AENOR, 2005), con capacidad de 5 litros, fijada a un bastidor que contiene la pala de la amasadora.

- Mezcladora de pintura (**PD**): para amasadas de más de 5 litros se procedió mediante una mezcladora de pintura conectada a un taladro eléctrico modelo AEG SBE705RE.

En la Tabla 3.3, se ha expuesto la cronología llevada a cabo en la fabricación de los distintos materiales según su tipología y el volumen de material requerido (equipo empleado) y además se facilita la publicación en que aparece cada una de ellas.

Tabla 3.3:
Resumen de la fabricación de los distintos materiales en función de la tipología o el equipo de amasado empleado.

Hormigón	Equipo		Publicaciones
TCC	NM	**OPC + (A o SLS)** 1. Mezcla en seco del OPC y el agente aireante 2. Adición a la amasadora del agua junto con los sólidos y amasado durante 90 segundos.	i, iii,
	PD	**OPC + A** 1. Mezcla en seco del OPC y el agente aireante 2. Adición al recipiente del agua junto con los sólidos y amasado durante 180 segundos.	v, vi, x
		OPC + H_2O_2 1. Mezcla del OPC con el H_2O durante 150 segundos 2. Adición del H_2O_2 y amasado durante 90 segundos.	ii
GCC AACC	NM	**FCC/BFS + (A, A_R, PG o SLS)** 1. Preparación de la disolución activadora 2/3 horas previas al amasado 2. Mezcla en seco del PRECURSOR y el agente aireante 3. Mezcla en la amasadora de la disolución 30 segundos 4. Adición el sólido durante los siguientes 60 segundos 5. Amasado durante 90 segundos	i, iii, iv
		FCC + H_2O_2 1. Preparación de la disolución activadora 2/3 horas previas al amasado 2. Mezcla en la amasadora de la disolución 30 segundos 3. Adición el FCC durante los siguientes 60 segundos 4. Amasado durante 60 segundos 5. Adición del H_2O_2 y amasado durante 90 segundos	ii
		FCCRm o FCCPGm / BFSRm o BFSPGm 1. Preparación de la disolución activadora 2/3 horas previas al amasado 3. Mezcla en la amasadora de la disolución 30 segundos 4. Adición el sólido durante los siguientes 60 segundos 5. Amasado durante 90 segundos	i, iv
GCC AACC	PD	**FCC/BFS + A** 1. Preparación de la disolución activadora 2/3 horas previas al amasado 2. Mezcla en seco del PRECURSOR y el A 3. Mezcla con el PD de la disolución 30 segundos 4. Adición del sólido durante los siguientes 60 segundos 5. Amasado durante 180 segundos	iv, x
		FCC/BFS + H_2O_2 1. Preparación de la disolución activadora 2/3 horas previas al amasado 2. Mezcla con el PD de la disolución 30 segundos 3. Adición del PRECURSOR durante los siguientes 60 segundos 4. Amasado durante 140 segundos 5. Adición del H_2O_2 y amasado durante 90 segundos	ii
		FCCRm o FCCPGm / BFSRm o BFSPGm 1. Preparación de la disolución activadora 2/3 horas previas al amasado 2. Mezcla con el PD de la disolución 30 segundos 3. Adición del sólido durante los siguientes 60 segundos 4. Amasado durante 180 segundos	iv, v, vi, x
ECC	PD	**FCCRm / BFSRm** 1. Preparación de la disolución activadora 24 horas previas al amasado 2. Mezcla con el PD de la disolución 30 segundos 3. Adición del sólido durante los siguientes 60 segundos 4. Amasado durante 180 segundos	v, vi, x
BAAM TAAM	NM	1. Preparación de la disolución activadora 24/2-3 horas previas al amasado (dependiendo de si se emplea RHA). 2. Mezcla en la amasadora de la disolución 30 segundos 3. Adición del precursor durante los siguientes 60 segundos 4. Mezclado durante 30 segundos 5. Adición de la arena y amasado hasta 4 minutos y 30 segundos	xii - ix

Los materiales se vierten en el molde pertinente y se procede a:

- En el caso de los BAAM y los TAAM su vibrado, enrasado y almacenamiento bajo las condiciones de curado seleccionadas hasta la edad de ensayo.
- En el caso de los hormigones celulares se almacenan directamente bajo las condiciones de curado requeridas, tras 24 horas se procede a su enrasado con una sierra dentada (Font, 2016) y finalmente se almacenan de nuevo hasta la edad de ensayo.

Respecto al curado de las probetas, se trata de uno de los objetivos de mejora planteados en cuanto a la ecoeficiencia de los hormigones celulares alternativos en su proceso de fabricación. A lo largo del plan de trabajo se han llevado a cabo las siguientes tipologías en busca de evitar el curado en autoclave tradicional y comparar las características funcionales de los materiales obtenidos:

- Baño térmico a 65 °C y 100 % HR (**TB**).
- Temperatura ambiente a 20 – 23 °C y 100 % HR (**TA**).
- Método combinado (**CM**): 24h en TB y TA hasta la edad de ensayo.

En el Capítulo 4 se especifica qué metodología de amasado y curado se ha llevado a cabo en cada una de las etapas experimentales que comprenden la presente Tesis Doctoral.

3.3 ENSAYOS DE CARÁCTERIZACIÓN

Los ensayos de caracterización realizados a lo largo de la investigación se han dividido en dos grupos principales: los ensayos de caracterización de las materias primas y los ensayos de caracterización de los especímenes. A su vez, dentro de la caracterización de los especímenes, se ha procedido (dependiendo del caso de análisis) a la verificación de las características funcionales del material, el estudio de la matriz porosa y finalmente a la evaluación ambiental del material. En la Tabla 3.4 se especifican los ensayos correspondientes a cada uno de estos propósitos.

Tabla 3.4:
Clasificación de los ensayos de caracterización de las materias primas y de los especímenes

ENSAYOS DE CARÁCTERIZACIÓN DE MATERIAS PRIMAS	• Fluorescencia de rayos-X (XRF) • Cálculo de pH • Análisis de partículas por difracción de rayos láser (PSD) • Microscopía electrónica de barrido de emisión de campo (FESEM) y microanálisis por energía dispersiva de rayos-X (EDS) • Difracción de rayos-X (XRD) • Cálculo de cantidad de aluminio por emisiones de hidrógeno	
ENSAYOS DE CARÁCTERIZACIÓN DE LOS ESPECIMÉNES	• Análisis termogravimétrico de pastas (TGA) • Difracción de rayos-X de pastas (XRD) • Microscopía electrónica de barrido de emisión de campo (FESEM) y microanálisis por energía dispersiva de rayos-X (EDS)	
	Características funcionales	• Resistencia mecánica a la compresión (Rc) • Densidad natural (D_N) • Conductividad térmica (λ)
	Evaluación de la matriz porosa	• Porosimetria de intrusión de mercurio (MIP) • Ensayos hídricos • Microscopía electrónica de barrido de emisión de campo (FESEM) • Microscopía óptica (OM) • ImageJ
	Evaluación ambiental del material	• Cálculo de la huella de carbono (CO_2/m^3 de material) • Análisis del ciclo de vida (LCA)

3.3.1 Fluorescencia de Rayos-X (XRF)

Para la obtención de la composición química elemental cuantitativa de las materias primas empleadas (BFS, FCC, OBA y RHA) se ha utilizado un espectrómetro secuencial de rayos-X modelo Philips Magix PRO (PW2400).

El análisis se basa en la irradiación con fotones de rayos-X sobre los átomos de una muestra, que provoca la creación de huecos electrónicos. El llenado de estos huecos con electrones de orbitales externos da lugar a transiciones que liberan energía en forma de fotones de rayos-X secundarios. La longitud de onda es inversamente proporcional a la energía, y son características para cada elemento (determinación cualitativa). La intensidad (número de fotones), es proporcional a la concentración del elemento responsable (determinación cuantitativa) (Servicios Técnicos de Investigación. Universitat d'Alacant, 2019).

Una vez llevado a cabo el ensayo, es necesario introducir el valor de la LOI (pérdida al fuego) para el ajuste de los análisis. Para determinar la LOI se

calcina por duplicado (en crisoles de alúmina previamente calcinados y tarados) 1 gramo de material durante 1 hora a 950 °C.

3.3.2 Cálculo de pH

El pH en suspensión acuosa de la OBA se ha medido con un pHmetro Crison microp H2001 (ver **publicación vii**).

3.3.3 Análisis de Partículas por Difracción de Rayos Láser (PSD)

La curva granulométrica y los parámetros granulométricos básicos ($d_{(0.1)}$, $d_{(0.5)}$, $d_{(0.9)}$ y D_{med}) de las materias primas tras el proceso de molienda (ver punto 3.2.1 del presente capítulo) se han obtenido mediante la técnica de análisis de partículas por difracción de rayos láser (PSD).

La técnica consiste en hacer incidir un frente de luz monocromática sobre las partículas de la materia analizada, de modo en que se produce una dispersión que captan los detectores ópticos. La información captada es procesada y mediante una serie de modelos ópticos que consideran las partículas como esferas se obtiene la distribución del tamaño de partículas (Malvern Panalytical, 2019).

El equipo que se ha utilizado es un Mastersizer 2000 de Malvern Instruments que permite medir partículas en el rango de 0.02 a 2000 micras y tiene como principio de medición la dispersión de Fraunhofer y Mie. Las medidas se llevaron a cabo por vía húmeda empleando como dispersante agua desionizada. El equipo cuenta con una fuente de ultrasonidos que se emplea para ayudar en la dispersión de muestras muy apelmazadas.

3.3.4 Difracción de Rayos-X (XRD)

La difracción de rayos-X (XRD) es una técnica de análisis no destructiva que permite identificar elementos y compuestos químicos cristalinos que constituyen el material analizado.

Se ha utilizado un difractómetro de rayos-X, modelo Bruker AXS D8 Advance. Se ha utilizado la radiación Kα de Cu y monocromador secundario (filtro de Níquel) que elimina la radiación K_β de Cu. La intensidad y voltaje del tubo generador de rayos X se ha ajustado en todas las medidas a 20 mA y 40 KV respectivamente. Se registraron los difractogramas para el intervalo de 2θ entre 5° y 70°, con un ángulo de paso de 0.02° y un tiempo de acumulación de 2 segundos.

El fundamento del ensayo es la medida de la desviación que sufre un haz primario o monocromático de rayos-X cuando incide sobre la muestra. Los ángulos de desviación están íntimamente relacionados con la distancia entre los planos de la red cristalina del material, siguiendo la ley de Bragg (Eq. 3.1):

$$n \cdot \lambda = 2d \cdot sen\theta \quad (3.1)$$

Donde:
n: = orden de reflexión
λ = longitud de onda
d = distancia interplanar entre dos planos atómicos paralelos sucesivos en el cristal
θ = ángulo formado con el plano atómico entre el haz incidente y el reflejado

Cada sustancia cristalina genera un patrón característico que se compara con el resultante en el análisis. Posteriormente utilizando el software DRXWin podemos comparar patrones almacenados en bases de datos con los picos que aparecen en la muestra objeto de estudio.

La XRD se ha llevado a cabo sobre muestras en polvo para la caracterización de materias primas, así como de pastas.

En el caso de las **materias primas** se han analizado todas tras el proceso de molienda (ver punto 3.2.1 del presente capítulo). Las muestras se tamizan seleccionando las fracciones menores a 125 μm que se someten a un proceso de secado en estufa durante 30 minutos a 65ºC.

En el caso de la aplicación para **caracterización de pastas** ha sido necesario un proceso previo de acondicionamiento:

- Molienda en un mortero de ágata. Se realiza añadiendo acetona con la finalidad de detener el proceso de hidratación.
- Filtrado de la muestra mediante bomba de vacío
- Secado en estufa durante 30 minutos a 65°C
- Tamizado de la muestra por el tamiz de 125 μm. La fracción que pasa es la que se emplea para el análisis.

Las muestras en polvo se colocan en un portamuestras descubierto, de manera que la superficie superior quede lo más lisa posible.

3.3.5 Cálculo de cantidad de aluminio por emisiones de hidrogeno (H_2)

Este procedimiento se ha aplicado para estimar el rendimiento de los agentes aireantes alternativos (A_R y PG) dentro de las matrices en que se adicionan. Dentro de las aplicaciones del ensayo se puede distinguir:

Publicación i:

- Evaluar la reactividad del papel de aluminio reciclado (A_R) y compararla con el polvo de aluminio comercial A.
- Evaluar la reactividad del A_R cuando es introducido en el procedimiento de molienda de los precursores ($FCCA_R$ y $BFSA_R$).

Publicación iv:

- Estimar la cantidad de aluminio reactivo presente en el PG.
- Comparar la reactividad de PG con distintos tiempos de molienda (10-30 minutos, ver Tabla x del punto 4.2.1 del presente capítulo).
- Evaluar la reactividad del PG cuando es introducido en el procedimiento de molienda de los precursores (FCCPGm y BFSPGm).

Las medidas se basan en el hidrógeno (H_2) generado por la reacción resultante del aluminio metálico puro en medio alcalino (Eq. 3.2):

$$Al\ (s) + 3H_2O + OH^-{}_{(ac)} \rightarrow Al(OH)^-{}_4\ (ac) + \frac{3}{2} H_{2\ (G)} \qquad (3.2)$$

El ensayo se fundamenta en el calcímetro de Bernard (empleado para determinar la cantidad de carbonatos en suelos (AENOR, 2014). En este caso, el gas que se mide es el hidrógeno (en vez de CO_2 generado en el caso de los carbonatos), que desplaza a una columna de agua; el reactivo que activa la descomposición (realmente se trata de una reacción de oxidación-reducción) es una disolución concentrada (7.5 M) de NaOH (en lugar de disolución de HCl empleada en el caso de los carbonatos). El esquema del montaje que se ha realizado para los ensayos se puede consultar en la **publicación i** (Capítulo 4).

Para la realización de las medidas, se pesa una cantidad determinada de muestra, se hace reaccionar en medio básico y se determina el volumen de H_2 liberado a través de la medida del desplazamiento de una columna de agua en una bureta (tubo regulado) conectada al matraz de reacción.

Para una temperatura (T) y presión (P) constantes, es posible calcular la cantidad de aluminio consumida (m_{Al}) aplicando la ecuación de los gases ideales (Eq. 3.3) y la Ecuación 3.4:

$$P \cdot V = n_{H_2} \cdot R \cdot T \qquad (3.3)$$

Donde:
R = Constante de los gases ideales (0.082 L atm K^{-1} mol^{-1})
nH_2 = moles de H_2 medidos

$$m_{Al} = \frac{n_{H_2}}{3/2} \cdot M_{(Al)} \qquad (3.4)$$

Donde:
$M_{(Al)}$ = masa molar del aluminio (26.98 g mol^{-1})

3.3.6 Análisis Termogravimétrico (TGA)

El análisis termogravimétrico (TGA) es una técnica basada en registrar de manera continua la pérdida o ganancia de la masa de una muestra, colocada en una atmosfera controlada, a medida que se aumenta la temperatura de la muestra (normalmente de manera lineal con el tiempo).

El ensayo nos da como resultado la curva de descomposición térmica o termograma (curva TG), donde se pueden observar pérdidas o ganancias de masa correspondientes a los procesos químicos experimentados por la muestra (descomposición, hidratación, oxidación…)

Cuando las variaciones de masa son muy pequeñas o se producen en intervalos de temperatura muy próxima se recurre a la curva derivada termogravimétrica (DTG) que permite identificar con mayor facilidad los cambios en la muestra. La DTG representa la velocidad de pérdida o ganancia de masa en función del tiempo o la temperatura.

El equipo que se ha utilizado ha sido un módulo TGA 850 Mettler-Toledo que cuenta con una micro-electrobalanza horizontal (0.1 μg de precisión), un horno y sensores de temperatura que se comunican con un ordenador donde se registran los datos para poder ser procesados.

En este trabajo de investigación los ensayos de termogravimetría se han realizado para la caracterización de pastas con el fin de observar los compuestos resultantes de las reacciones de hidratación, geopolimerización y activación en los distintos materiales empleados. Los ensayos han sido llevados a cabo para un rango de temperaturas de entre 35 y 600 °C, velocidad de calentamiento de 10 °C min^{-1} en atmosfera de nitrógeno (N_2).

Una vez procesados los datos, la pérdida de masa total ha servido para realizar los cálculos teóricos de dosificación de los hormigones celulares objeto de la presente Tesis Doctoral con la finalidad de proceder a la evaluación ambiental del material (ver punto 3.3.12 del presente capítulo).

El acondicionamiento previo de las muestras necesario para el análisis es el mismo que el realizado para llevar a cabo el ensayo de XRD (descrito en el punto 4.3.4 del presente capítulo). El material en polvo se introduce en un crisol de aluminio (capacidad de 100μl) con una tapa que tiene un micro-orificio (para favorecer la salida de gases y permitir la generación de una atmosfera controlada) que se sella en un instrumento diseñado para tal fin.

3.3.7 Microscopía Electrónica de Barrido de Emisión de Campo (FESEM) y Microanálisis por Energía Dispersiva de Rayos-X (EDS)

La microscopía electrónica de barrido de emisión de campo (FESEM) y el microanálisis por energía dispersiva de rayos-X (EDS) permite conocer cualitativa y cuantitativamente la morfología y topografía de **materias primas**

en polvo (originales, molidas o en Co-M), así como caracterizar los compuestos resultantes en las reacciones de hidratación de los materiales analizados (**porciones de pasta**).

Además, las micrografías tomadas mediante FESEM han servido para estudiar cualitativamente la topografía interna de los distintos hormigones celulares y complementar el análisis de la red porosa de los mismos (ver punto 3.3.3-ii del presente capítulo).

El fundamento del ensayo se basa en barrer la superficie de una muestra sólida de material con un haz de electrones muy fino. El barrido sigue un modelo raster similar al usado en un tubo de rayos catódicos: recorrido de ida y vuelta en línea recta y desplazamiento hacia abajo a una distancia establecida. Por tanto, los condicionantes de este ensayo son la intensidad de barrido y la distancia de trabajo. El proceso se repite hasta que el área de trabajo ha sido barrida por completo. Cuando el haz de electrones se proyecta con una intensidad de barrido elevada se producen, entre otras, señales de electrones retro-dispersados y secundarios, que sirven de base en el microanálisis (EDS) (Servicio de Microscopía Electrónica. Universitat Politècnica de València, 2019).

El equipo utilizado es un microscopio FESEM modelo ULTRA 55 de la marca ZEISS, en el que se han configurado los datos en función del tipo de información requerida:

- Micrografías: intensidad de barrido de 3 a 5 kV y distancia de trabajo 7 mm.
- EDS: intensidad de barrido de 15 a 20 kV y distancia de trabajo entre 6 -8 mm.

Las muestras destinadas a este ensayo han de cumplir dos condiciones: deben estar secas y ser conductoras. El procedimiento seguido es el siguiente:

- El proceso de **secado** ha de llevarse a cabo preservando al máximo la estructura original de la muestra:
  - En el caso de las **materias primas en polvo** estas se pueden analizar antes o después del proceso de molienda. En cualquiera de los casos estos se secan en estufa a 60 °C durante 30 minutos.
  - En el caso de **porciones de pastas**: Estas se deben extraer de la zona interior de la matriz y han de ser lo más finas posibles (de modo que no se den diferencias significativas de altura entre zonas del área analizada). Las muestras se mantienen sumergidas en acetona durante 1 hora para detener el proceso de hidratación a la edad determinada de ensayo y posteriormente se secan en estufa a 60 °C durante 30 minutos.

- Colocación en el portamuestras:
  - **Muestras en polvo**: se colocan sobre cinta adhesiva de carbono y se soplan para retirar el excedente y las partículas sueltas.
  - **Porciones de pastas**: se colocan sobre cinta adhesiva de carbono y se metalizan mediante un puente de grafito coloidal (esto hace que la muestra sea conductora).

- Finalmente, antes de introducir los portamuestras en el equipo se realiza un recubrimiento con carbono mediante un recubridor de alto vacío, modelo EM MED020 de la marca LEICA, durante un tiempo de exposición que depende de la porosidad de las muestras (30 segundos para los BAAM y TAAM, y de 60 a 120 segundos para los hormigones celulares).

3.3.8 Evaluación de la matriz porosa

Teniendo en cuenta la clasificación de la Unión Internacional de Química Pura y Aplicada (IUPAC) (Rouquerol J et al., 1994) los materiales estudiados en el presente trabajo de investigación se pueden clasificar según el diámetro medio de poros (D_{med}) en:

- BAAMs y TAAMs son **meso-porosos** con 2nm < D_{med} < 50nm
- Los hormigones celulares (TCC, GCC, AACC, ECC y ECC-OP) son **macro-porosos** con D_{med} > 50 nm

Además, según la IUPAC los poros se pueden diferenciar según su diámetro (ϕ) entre: microporos: ϕ < 2nm; poros capilares o mesoporos: 2nm < ϕ < 50nm; macroporos: 50nm < ϕ < 50μm y poros artificiales de aire: ϕ > 50 μm (Rouquerol J et al., 1994).

Para los materiales del tipo **BAAM y TAAM**, el estudio de la red porosa ha de centrarse en los **micro-poros y** los **poros capilares**, característicos de las matrices en materiales cementicios (Abdelkader et al., 2008; Molina Bas et al., 2009), por lo que se ha seleccionado como técnica para su análisis la porosimetría por intrusión de mercurio (MIP).

Por su parte, para la evaluación de la matriz porosa de los **hormigones celulares**, el interés se centra en los **macroporos** y sobre todo en los **poros artificiales de aire** ya que son los que caracterizan al material y van a influir directamente en sus propiedades. Para su análisis, se ha combinado una serie de técnicas tradicionalmente empleadas (Esmaily and Nuranian, 2012; Lawrence and Jiang, 2017; Novais et al., 2019, 2016): la microscopía electrónica de barrido (FESEM), la microscopía óptica (OM), el procesamiento de imágenes mediante ImageJ y finalmente la realización de ensayos hídricos.

i. Porosimetría por Intrusión de Mercurio (MIP)

La porosimetría por intrusión de mercurio (MIP) se fundamenta en los fenómenos de capilaridad generados por los líquidos que no mojan los sólidos

con los que están en contacto. En estos casos, un líquido no humectante, como es el mercurio (Hg), precisa de una presión (p) para su introducción en los conductos capilares que es inversamente proporcional al radio de los mismos (Eq. 3.5):

$$r = 2\,\sigma \cdot cos\alpha / p \tag{3.5}$$

Donde:
σ = tensión superficial del mercurio
α = ángulo de contacto sólido-líquido

El ensayo consiste en la aplicación de presión para forzar la entrada de Hg en el entramado poroso del sólido y registrar el volumen de mercurio absorbido. Se distinguen tres intervalos de presión: un primer intervalo de baja presión (entre 0 y 345 kPa), un segundo intervalo de alta presión (entre presión atmosférica y 228 MPa) y finalmente una fase de extrusión. Para cada intervalo de presión considerado, el volumen de mercurio absorbido nos indica el volumen de poros de la muestra que presentan un determinado intervalo de acceso. Con este análisis se determina el área y el volumen de poros; y se calcula la distribución de la porosidad del material.

El equipo de medida es un Micrometrics modelo Auto-Pore IV 9500 de Instrument Corporation que mide poros desde 91.25 μm hasta 5.5nm. El ensayo se realiza por duplicado a porciones de muestra representativos del material, con un tamaño de entre unos 1 y 2 cm^3.

ii. FESEM, microscopía óptica (OM) y software ImageJ

La combinación de estas tres técnicas permite caracterizar cualitativa y cuantitativamente los poros de los hormigones celulares, dentro de un área determinada de estudio.

Para el caso particular del presente trabajo de investigación se han estudiado los poros artificiales de aire (ϕ > 50 μm) y se ha considerado la siguiente diferenciación:

- **Microporos** artificiales de aire: 0.05 mm < ϕ < 0.1 mm
- **Macroporos** artificiales de aire: ϕ > 0.1 mm

Mediante la técnica de **FESEM** se han procesado y analizado las micrografías de porciones de muestra de entre unos 7 y 10 mm, tomadas entre 50 y 200 aumentos (ver punto 3.3.2 del presente capítulo donde se ha detallado la técnica y el procedimiento de preparación de las muestras). El software informático adaptado al FESEM permite realizar un conteo y medición (ϕ) de las superficies marcadas manualmente como porosidades.

Para la **microscopía óptica (OM)** se emplea un Estereomicroscopio Apocromático de la marca Leica, modelo S8 APO, que ofrece detalles exactos de estructuras finas y de bajo contraste. Técnicamente, el estereomicroscopio tiene aumentos de 8-80x, distancia de trabajo 75mm y ángulos de observación de 38º. Tiene oculares adaptados para gafas, antiestáticos y ofrece salida de vídeo/foto. La iluminación de las muestras es perfectamente regulable mediante 4 lámparas de anillo LED en la parte superior y 3 LED de iluminación oblicua. En total dispone de 5 ajustes de iluminación programados de modo que se consigue reducir la fatiga visual y evitar los reflejos.

El estereomicroscopio empleado se complementa con la incorporación de una cámara digital a color con resolución de 5 megapíxeles para análisis, documentación y presentación de imágenes Leica DFC 420. La cámara captura imágenes brillantes y nítidas procedentes del microscopio, transformándolas al lenguaje digital y transfiriéndolas a ordenador para su posterior edición mediante el software informático de procesamiento y edición que incorpora la propia cámara.

El ensayo se lleva a cabo sobre probetas cúbicas de 4 x 4 x 4 cm^3 que son previamente cortadas en dos partes de 2 cm de ancho, con lo que se nos quedan dos especímenes de 2 x 4 x 4 cm^3. Para cortar las probetas se emplea una sierra de sobremesa de la marca Struers, con sistema de refrigeración por agua y discos de diamante de 250 mm de diámetro. Las superficies analizadas mediante OM son las dos caras lisas y libres de cada una de las porciones, de 16 cm^2.

Finalmente, las muestras analizadas mediante OM se sumergen en una solución de tinte universal color bermellón 790 y disolvente 302 NC universal, ambos de la marca Tkarom, de concentración del 0.4 % en volumen. El conjunto se introduce en un desecador y mediante una bomba de vacío se favorece la impregnación completa de los poros accesibles de la superficie. Las probetas se extraen del disolvente y se dejan en la campana de extracción durante 24 horas para su completo secado.

Para la toma de imágenes la superficie de las muestras se lija de modo que únicamente queda tinte en las porosidades. Se colocan sobre un fondo blanco y se realizan fotografías de la superficie completa que son analizadas con el software informático **ImageJ**, mediante la siguiente secuencia:

- Alisado de la imagen mediante la función automática “smooth” y a continuación se configura el contraste de la fotografía.
- Calibración del programa mediante el escalado de la imagen (distancia en pixeles en base a una distancia conocida).
- Selección y medición del área de la fotografía que se va a analizar (superficie de la probeta).
- Duplicado de la imagen para poder trabajar sobre ésta y tener la original como referencia.

- Ejecución del comando "Threshold" (umbralización de la imagen) que convierte la imagen de 8 bits en una imagen pseudo-binaria. En este punto se aconseja intensificar la escala de rojos para que los poros queden bien definidos. El "thresholding" permite elegir los píxeles que representan los poros según la intensidad. De este modo podemos ajustar (over/under) los objetos (que aparecerán en gris) que se van a contabilizar y se descartará los pixeles que quedan por encima (verde) o debajo (en azul) de los seleccionados.
- Ejecución del comando "Binary" que asigna a los poros el valor 1 (blanco) y al resto de la superficie el 0 (negro).
- Selección de los valores que se desea obtener y ejecución del comando "Analyse".

iii. Ensayos hídricos

Los ensayos hídricos se han llevado a cabo para obtener la densidad aparente ($\mathbf{D_{AP}}$) y absoluta ($\mathbf{D_{ABS}}$) secas de los hormigones celulares estudiados, con la finalidad de conocer los valores de porosidad total (**ΦT**), abierta (**Φa**) y cerrada (**Φc**) de los mismos. Se han seguido las especificaciones de la norma UNE-EN 772-13:2001, "*Métodos de ensayo para piezas de fábrica de albañilería. Parte 13: Determinación de la densidad absoluta seca y de la densidad aparente seca de piezas para fábrica de albañilería (excepto piedra natural)*" (AENOR, 2001), así como trabajos de investigación precedentes en el campo (Font, 2016; Melo, 2013; Sepulcre Aguilar et al., 2013).

Los ensayos se han llevado a cabo sobre pobretas cúbicas de dimensiones 4 x 4 x 4 cm^3. A la edad determinada (7 o 28 días) los especímenes se extraen de las condiciones de curado, se dejan al aire durante 2 horas y se pesan, obteniéndose su peso natural ($\mathbf{P_N}$). A continuación, se realiza la siguiente secuencia de actividades:

- Determinación del peso seco ($\mathbf{P_S}$): Secado a 105ºC ± 5ºC y peso de las mismas cada 24 horas hasta masa constante (variación < 0.2 %).
- Determinación del peso saturado ($\mathbf{P_{SAT}}$): Saturación de las muestras en agua introduciéndolas en un vaso de vidrio cubiertas de agua durante 24 horas y peso de las mismas.
- Determinación del peso sumergido ($\mathbf{P_{SUM}}$): En estado de saturación, peso con balanza hidrostática.
- Determinación del volumen real ($\mathbf{V_R}$): Desecado de la muestra (105ºC ± 5ºC) y pulverización de la misma mediante mortero de ágata y obtención del volumen real mediante volumenómetro de Le Chatelier.

Con estos datos y considerando los precedentes indicados en las Ecuaciones 3.7 y 3.8, se procede a realizar los siguientes cálculos para obtener las densidades y porosidades de la muestra (Eqs. 3.6 y 3.9 - 3.15).

$$V_{AP} = \frac{P_{SAT} - P_{SUM}}{\gamma_{LIQ}} \quad (3.6)$$

Donde:
V_{AP} *= Volumen aparente*
γ_{LIQ} *= Densidad del líquido empleado para las medidas.*

Y considerando:

$$P_{SAT} = P_S + V_{AB} \cdot \gamma_{LIQ} \quad (3.7)$$

(peso saturado es el peso de las muestras más el peso del agua en los poros accesibles).

$$P_{SUM} = P_S - (V_{AP} - V_{AB}) \cdot \gamma_{LIQ} \quad (3.8)$$

(peso sumergido es el peso de la muestra seca menos el empuje hidrostático (principio de Arquímedes).

Se tiene, por tanto:

Densidad aparente (**D_{AP}**):

$$D_{AP} = \frac{D_S}{V_{AP}} \quad (3.9)$$

Densidad real/absoluta (**D_{ABS}**):

$$D_{ABS} = \frac{D_S}{V_R} \quad (3.10)$$

Densidad relativa (**D_{REL}**):

$$D_{REL} = \frac{D_{AP}}{D_{ABS}} \quad (3.11)$$

Porosidad total (**ΦT (%)**):

$$\Phi\mathrm{T} = \left[1 - \frac{D_{AP}}{D_{ABS}}\right] \cdot 100 \quad (3.12)$$

Porosidad abierta (**Φa (%)**):

$$\Phi\mathrm{a} = \left[\frac{P_{SAT} - P_S}{P_{SAT} - P_{SUM}}\right] \cdot 100 \quad (3.13)$$

Porosidad cerrada (**Φc (%)**):

$$\Phi\mathrm{c} = \Phi\mathrm{T} - \Phi\mathrm{a} \quad (3.14)$$

Compacidad (**C (%)**):

$$C = 100 - \Phi T \quad (3.15)$$

3.3.9 Características funcionales

Los morteros de activación alcalina (BAAM y TAAM) se han caracterizado mecánicamente siguiendo las especificaciones de la norma UNE-EN 196-1:2005, "*Métodos de ensayo de cementos. Parte 1: Determinación de resistencias mecánicas*" (AENOR, 2005).

En el caso de los hormigones celulares, en la presente Tesis Doctoral se analizan los requerimientos funcionales que debe de cumplir el material bajo lo establecido en la norma europea UNE-EN 771-4:2011+A1, "*Especificaciones de piezas para fábrica de albañilería. Parte 4: Bloques de hormigón celular curado en autoclave*" (AENOR, 2016a) y además se comparan con lo establecido en la guía-comité 523.2-R96 del Instituto Americano del Hormigón (ACI), "*Guide for Precast Cellular Concrete*" (Babbitt et al., 2014).

En estas normativas se establecen unos valores de referencia de resistencia a compresión (Rc), densidad natural (D_N) y conductividad térmica (λ).

iv. Resistencia mecánica de los morteros binarios y ternarios de activación alcalina

Las características mecánicas analizadas para los BAAM y TAAM han sido la resistencia a compresión (Rc) y la resistencia a flexión (Rf) de probetas prismáticas de 4 x 4 x 16 cm^3. Se ensayaron para cada edad de rotura 3 probetas obteniéndose 3 valores de Rf y 6 valores de Rc. Se calculó el valor promedio de los resultados (media aritmética de los valores) afectados por una desviación estándar menor al 10 %.

v. Densidad natural (**D_N**) y resistencia a compresión (**Rc**) de los hormigones celulares

La densidad natural (**D_N**) de los hormigones celulares objeto del presente trabajo de investigación se ha determinado tomando su peso antes de proceder al ensayo de resistencia a compresión y dividiéndolo por el volumen bruto de las probetas. Las probetas se extraen de sus condiciones de curado y se mantienen al aire 2 horas antes de las mediciones.

La resistencia a compresión (**Rc**) se determina siguiendo las especificaciones de la norma UNE EN 772-1 "*Métodos de ensayo de piezas para fábrica de albañilería. Parte 1: Determinación de la resistencia a compresión*" (AENOR, 2016b) con una máquina universal INSTRON 3282. Esta máquina dispone de un bastidor con capacidad máxima de carga de 100 kN y células de carga de 5 kN y 100 kN. La velocidad de carga requerida (0.05 MPa por segundo) se ajusta con una velocidad de desplazamiento de 1 mm por minuto.

Se ensayan 6 probetas cúbicas, de cada modalidad de hormigón celular, con dimensiones de 4 x 4 x 4 cm^3 o de 10 x 10 x 10 cm^3 en función del caso de estudio. Las medidas resultantes del ensayo se procesan mediante el software informático Bluehill que tiene conexión directa con la prensa. Este programa proporciona un análisis de datos estadístico de cada una de las series introducidas.

vi. Conductividad térmica (λ)

Para determinar, la conductividad térmica de los hormigones celulares se han empleado dos métodos, en ambos casos siguiendo las especificaciones establecidas en la norma europea UNE EN 1745 "*Fábrica de albañilería y componentes para fábrica. Métodos para determinar las propiedades térmicas*" (AENOR, 2013).

Al inicio del periodo experimental de la presente Tesis Doctoral se utilizó un analizador **TCI™** de conductividad térmica y efusividad de la marca C-Therm Technologies. Se trata de un ensayo no destructivo que no requiere calibración ni preparación previa de la muestra. El sistema trabaja con rangos de conductividad entre 0 a 500 W/mK y temperaturas de -50ºC a 200ºC y realiza las mediciones en tiempos de entre 0.8 a 3 segundos.

El funcionamiento del equipo TCI se basa en la **técnica de fuente plana transitoria modificada (MTPS)** que utiliza un sensor de reflectancia de calor interfacial (por un solo lado). Mediante el sensor se aplica una fuente de calor conocida constante y momentánea a la muestra. Se produce un incremento de temperatura en la interfase entre el sensor y la muestra (normalmente menor a 2 °C), que induce un cambio en la caída del voltaje del elemento sensor. Las propiedades termo-físicas de la muestra de material son inversamente proporcionales al grado de incremento en el voltaje del sensor. Cuanto más aislante térmicamente es el material mayor resulta la caída del voltaje (Technologies Ltd., 2019).

A la edad determinada de ensayo se midieron las propiedades térmicas de 6 probetas cúbicas de 4 x 4 x 4 cm^3.

Más adelante, el grupo de investigación adquirió un equipo **KD2-Pro** desarrollado por la empresa Decagon Devices (NE Hopkins Court Pullman, EEUU) y comercializado en España por LabFerrer (Madrid, España). A este equipo se ha incorporado un **sensor RK-1** para rocas y hormigones, que mide las propiedades térmicas en base al "**Método de la Aguja Térmica**" recogido en las normas ASTM D5334-08 (ASTM International, 2008) y IEEE Standard 442-1981 (IEEE STANDARDS ASSOCIATION, 1981).

Este método es conocido como "método de calentamiento transitorio de aguja" y como su nombre indica se trata de un método transitorio para medir la conductividad térmica (λ) de materiales con una sonda metálica en forma de aguja que se calienta por medio de la aplicación de una corriente eléctrica

durante un periodo de tiempo y por medio de expresiones matemáticas se obtiene la (λ) en pocos minutos (Mosquera Arancibia, 2013).

El KD2-Pro se enlaza con un software específico que utiliza un algoritmo patentado por la marca que ajusta los datos de tiempos y temperaturas con funciones integrales exponenciales usando un método no lineal de mínimos cuadrados (Decagon Devices, 2016). Las mediciones se obtienen en tiempos de entre 1 y 10 minutos, introduciendo la aguja metálica dentro del material y los valores de conductividad térmica se obtienen con una incertidumbre del ±10 %.

El sensor RK-1 es una aguja con dimensiones 6 mm de longitud y 3.9 mm de diámetro que se utiliza para medir conductividad (y resistividad) térmica en materiales de dureza elevada (rocas y hormigones). Tiene un rango de medidas entre 0.1 y 6.0 W/mK con una incertidumbre de ± 10 % en medidas de 0.2 a 6.0 W/mK y de 0.02 W/mK en medidas de 0.1 a 0.2 W/mK (Decagon Devices, 2016).

Para cada modalidad de hormigón celular, se ensayaron 4 probetas cúbicas de 10 x 10 x 10 cm^3 a la edad determinada de ensayo. Para poder introducir el sensor en las probetas es necesario hacer un agujero que ajuste con las dimensiones del mismo utilizando un taladro. Se realizan 10 perforaciones en cada una de las probetas distribuidas entre sus 6 caras (Figura 3.1), de modo en que se distribuyan las medidas en toda la envolvente térmica del material.

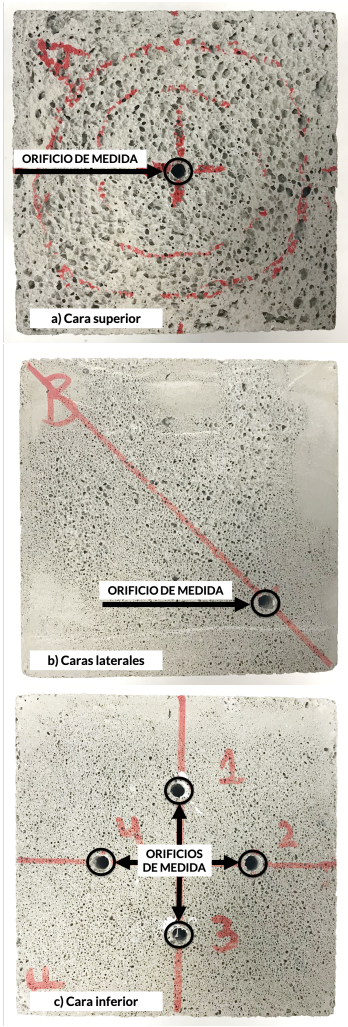

Figura 3.1: *Distribución de orificios entre las distintas caras de las probetas para introducir el sensor RK-1 y realizar las medidas de conductividad térmica del material: a) Cara superior de las probetas (cara que queda al aire cuando están en el molde); b) Cara lateral de la probeta (en total son 4 medidas de las cuatro caras laterales); y c) Cara inferior de las probetas (la que queda dentro del molde).*

3.3.10 Evaluación ambiental del material

i. Cálculo de la huella de carbono (**kgCO_2/m^3 material**) - materias primas y fabricación

En la primera etapa experimental del presente trabajo de investigación se llevó a cabo un cálculo básico de la huella de carbono de los hormigones celulares alternativos y una comparación con las emisiones asociadas al material tradicional.

Estos cálculos se basaron en la obtención de las emisiones de dióxido de carbono (CO_2) asociadas a la fabricación de los materiales bajo las mismas condiciones. Se siguió las directrices establecidas en 2006 por el Panel Intergubernamental para el Cambio Climático (IPCC) para la realización de inventarios nacionales de gases de efecto invernadero (IPCC, 2006). La metodología consiste en estimar las emisiones asociadas a un determinado proceso de acuerdo con la Ecuación 3.16.

$$E_i = A_i \cdot EF_i \tag{3.16}$$

Donde:
E_i = *emisión de CO_2 (Kg) por cada material de partida y operación realizada "i".*
A_i = *cantidad de actividad o material fabricado "i".*
EF_i = *factor de emisión asociado a cada unidad de actividad o material fabricado.*

Dentro de estos cálculos se consideraba las emisiones parciales asociadas a la fabricación de los hormigones celulares teniendo en cuenta dos procesos: i) la obtención de materias primas; y ii) las actividades de amasado y curado del material (proceso de fabricación). Los cálculos se hacen para la obtención de 1m^3 de hormigón celular (ver Figura 3.2).

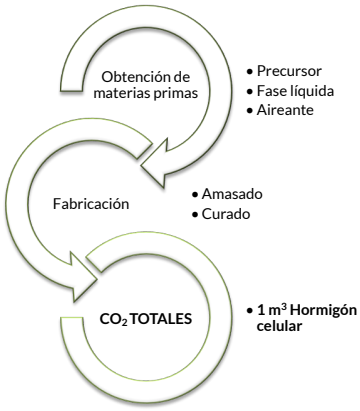

Figura 3.2: *Esquema conceptual del cálculo de la huella de carbono (CO_2/m^3) en la primera etapa experimental.*

ii. Análisis del ciclo de vida del material (LCA)

Más adelante, se abordó un estudio más profundo del impacto medioambiental y se realizó un Análisis del Ciclo de Vida (ACV) siguiendo las normas ISO 14040-2006a "*Gestión ambiental. Análisis del ciclo de vida. Principios y marco de referencia*" (Comité Técnico ISO/TC 207, Gestión ambiental, Subcomité SC 5, 2017a) e ISO 14044-2006b "*Gestión ambiental. Análisis del ciclo de vida. Requisitos y directrices*" (Comité Técnico ISO/TC 207, Gestión ambiental, Subcomité SC 5, 2017b). Con este análisis se cuantifica y compara el potencial de calentamiento global (GWP - Global Warming Potential) de los hormigones celulares estudiados en el presente trabajo de investigación.

El GWP es una medida relativa de cuánto calor puede ser atrapado por un determinado gas de efecto invernadero, en comparación con un gas de referencia, que por lo general es el CO_2. Este factor se calcula para un periodo de tiempo determinado que puede ser 20, 100 o 500 años; y se expresa como un factor de CO_2 (cuyo GWP está estandarizado en 1).

El alcance del análisis se ha limitado mediante la modalidad parcial "candle to gate". Se trata de una evaluación del ciclo de vida del producto analizado que tiene en cuenta desde la extracción de los recursos (cuna) hasta la puerta de la fábrica (es decir, antes de ser transportado al consumidor) (Chai, 2014; Tillman, 2000).

En la presente Tesis Doctoral, para llevar a cabo el ACV, se ha empleado el software de uso libre OpenLCA 1.7.2, desarrollado por GreenDelta en 2012. Para la generación del inventario se ha importado la base de datos de libre acceso Ecoinvent 3.3 de Open LCA Nexus. El método de cálculo empleado ha sido el que marcan las directrices del Panel Intergubernamental para el Cambio Climático 2006 (IPCC) (IPCC, 2006) obteniéndose el índice GWP para un periodo de 100 años (**GWP-100**) que proporciona un equivalente al calor que puede ser atrapado por un gas de efecto invernadero en comparación al dióxido de carbono (**$kgCO_2eq$**).

Con todo, se ha obtenido el GWP-100 para la fabricación de 1 m^3 de hormigón celular, desde la extracción de las materias primas hasta la fabricación del producto, antes de ser transportado al consumidor, mediante el modelo de flujos de entradas y salidas expuesto en la Figura 3.3.

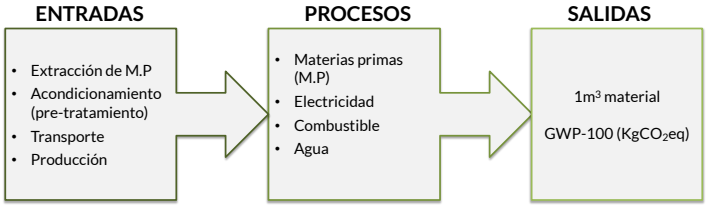

Figura 3.3: *Matriz de flujos desarrollada en el "Candle to Gate" del LCA. (Entradas-procesos abordados-salidas).*

3.4 REFERENCIAS BIBLIOGRÁFICAS

Abdelkader, S., Moragues, A., Reyes, E., 2008. Influencia de la estructura porosa de hormigones utilizados en ambientes marinos frente al transporte generado por gradiente de presión. Xxv Encuentro Del Grup. Español Fract. 25, 641–646.

AENOR, 2016a. UNE-EN 771-4:2011+A1: Especificaciones de piezas para fábrica de albañilería. Parte 4 Bloques de hormigón celular curado en autoclave.

AENOR, 2016b. UNE-EN 772-1:2011+A1: Métodos de ensayo de piezas para fábrica de albañilería. Parte 1: Determinación de la resistencia a compresión.

AENOR, 2014. UNE-EN ISO 10693:2014: Calidad del suelo. Determinación del contenido en carbonato. Método volumétrico.

AENOR, 2013. UNE-EN 1745: Fábrica de albañilería y componentes para fábrica. Métodos para determinar las propiedades térmicas.

AENOR, 2005. UNE-EN 196-1, Methods of Testing Cement – Part 1: Determination of Strength.

AENOR, 2001. UNE-EN 772-13: Métodos de ensayo de piezas para fábrica de albañilería. Parte 13: Determinación de la densidad absoluta seca y de la densidad aparente seca de piezas para fábrica de albañilería (excepto piedra natural) 9.

ASTM International, 2008. ASTM D5334 - 14 Standard Test Method for Determination of Thermal Conductivity of Soil and Soft Rock by Thermal Needle Probe Procedure [WWW Document].

Babbitt, F., Barnett, R.E., Cornelius, M.L., Dye, B.T., Liotti, D.L., Schmidt, S.B., Tanner, J.E., Valentini, S.C., 2014. ACI 523.3R-14 Guide for Cellular Concretes above 50 lb/ft3 (800 kg/m3).

Bouzón, N., 2015. ACTIVADORES ALCALINOS ALTERNATIVOS A PARTIR DE LA CENIZA DE CÁSCARA DE ARROZ PARA LA FABRICACIÓN DE GEOPOLÍMEROS. Universitat Politècnica de València.

Bouzón, N., Payá, J., Borrachero, M. V., Soriano, L., Tashima, M.M., Monzó, J., 2014. Refluxed rice husk ash/NaOH suspension for preparing alkali activated binders. Mater. Lett. 115, 72–74. https://doi.org/10.1016/j.matlet.2013.10.001

Chai, C., 2014. Life Cycle Assessment: an Introduction to Concepts and Applications. Azo Cleantech 1–4.

Comité Técnico ISO/TC 207, Gestión ambiental, Subcomité SC 5, A. del ciclo de vida., 2017a. ISO 14040:2006(a) Gestión ambiental — Análisis del ciclo de vida — Principios y marco de referencia.

Comité Técnico ISO/TC 207, Gestión ambiental, Subcomité SC 5, A. del ciclo de vida., 2017b. ISO 14044:2006(b) Gestión ambiental — Análisis del ciclo de vida — Requisitos y directrices.

Decagon Devices, I., 2016. KD2 Pro Thermal Properties Analyzer - Operator's Manual.

Esmaily, H., Nuranian, H., 2012. Non-autoclaved high strength cellular concrete from alkali activated slag. Constr. Build. Mater. 26, 200–206. https://doi.org/10.1016/j.conbuildmat.2011.06.010

Font, A., 2016. Hormigón Celular Geopolimérico (Hcg) Aireado Con De Un Material De Bajo Coste Económico Y Medioambiental. Universitat Politècnica de València.

IEEE STANDARDS ASSOCIATION, 1981. IEEE 442-1981 - IEEE Guide for Soil Thermal Resistivity Measurements [WWW Document].

IPCC, 2006. Introducción a las Directrices de 2006 1–13.

Lawrence, M., Jiang, Y., 2017. Bio-aggregates Based Building Materials. https://doi.org/10.1007/978-94-024-1031-0

Malvern Panalytical, 2019. Mastersizer 2000. User manual [WWW Document]. URL https://www.malvernpanalytical.com/es/support/product-support/mastersizer-range/mastersizer-2000 (accessed 10.21.19).

Melo, J.P., 2013. Desarrollo y caracterización de un material celular de alta porosidad con base cementicia activada mediante agentes inorgánicos.

Molina Bas, O.I., Moragues Terrades, A., Gálvez Ruiz, J.C., 2009. Procesos de hidratacion del cemento portland, porosidad. Rev. Int. Desastr. Nat. Accid. e Infraestruct. Civ. p46-55.

Mosquera Arancibia, P., 2013. Medida de la conductividad térmica con el método de la aguja térmica, basado en la fuente lineal de calor transitorio, para su aplicación en los cerramientos de adobes y bloques de tierra comprimida. Volumen I. UNIVERSIDAD POLITÉCNICA DE MADRID.

Novais, R.M., Buruberri, L.H., Ascensão, G., Seabra, M.P., Labrincha, J.A., 2016. Porous biomass fly ash-based geopolymers with tailored thermal conductivity. J. Clean. Prod. 119, 99–107. https://doi.org/10.1016/j.jclepro.2016.01.083

Novais, R.M., Senff, L., Carvalheiras, J., Seabra, M.P., Pullar, R.C., Labrincha, J.A., 2019. Sustainable and efficient cork - inorganic polymer composites_ An innovative and eco-friendly approach to produce ultra-lightweight and low thermal conductivity materials. Cem. Concr. Compos. 97, 107–117. https://doi.org/10.1016/j.cemconcomp.2018.12.024

Payá, J., Monzó, J., Borrachero, M. V., 1999. Fluid catalytic cracking catalyst residue (FC3R): An excellent mineral by-product for improving early-strength development of cement mixtures. Cem. Concr. Res. 29, 1773–1779. https://doi.org/10.1016/S0008-8846(99)00164-7

Rouquerol J, D, A., W, F.C., H, E.D., M, H.J., N, P., F, R.J.D., W, S.K.S., K, U.K., 1994. Recommendations for the characterization of porous solids

(Technical Report). Pure Appl. Chem. https://doi.org/10.1351/pac199466081739

Sepulcre Aguilar, A., Pinilla Melo, J., Hernández Olivares, F., 2013. Microstructural analysis of aerated cement pastes with fly ash, Metakaolin and Sepiolite additions. Constr. Build. Mater. 47, 282–292. https://doi.org/10.1016/j.conbuildmat.2013.05.082

Servicio de Microscopía Electrónica. Universitat Politècnica de València., 2019. Microscopía electrónica de barrido de emisión de campo [WWW Document]. URL http://www.upv.es/entidades/SME/info/859071normalc.html (accessed 10.21.19).

Servicios Técnicos de Investigación. Universitat d'Alacant, 2019. Espectroscopía de fluorescencia de rayos X. [WWW Document]. URL https://sstti.ua.es/es/instrumentacion-cientifica/unidad-de-rayos-x/espectroscopia-de-fluorescencia-de-rayos-x.html (accessed 10.21.19).

Technologies Ltd., C.-T., 2019. C-Therm TCi-Thermal Conductivity Analyzer. Principios de Operación [WWW Document]. URL https://ctherm.com/products/tci_thermal_conductivity/how_the_tci_works/mtps/lang/es/ (accessed 10.21.19).

Tillman, A.M., 2000. Significance of decision-making for LCA methodology. Environ. Impact Assess. Rev. 20, 113–123. https://doi.org/10.1016/S0195-9255(99)00035-9

Wang, P.Z., Trettin, R., Rudert, V., 2005. Effect of fineness and particle size distribution of granulated blast-furnace slag on the hydraulic reactivity in cement systems. Adv. Cem. Res. 17, 161–167. https://doi.org/10.1680/adcr.2005.17.4.161

Wang, S.-D., Pu, X.-C., Scrivener, K.L., Pratt, P.L., 1995. Alkali-activated slag cement and concrete: a review of properties and problems. Adv. Cem. Res. 7, 93–102. https://doi.org/10.1680/adcr.1995.7.27.93

CAPÍTULO IV: DESARROLLO DE LOS NUEVOS ECC-OP

CONTENIDO

4 DESARROLLO DE LOS NUEVOS HORMIGONES ECO-CELULARES "ONE-PART" (ECC-OP)

4.1 INTRODUCCIÓN

A continuación, se presentan los trabajos de investigación correspondientes al recorrido experimental llevado a cabo durante el desarrollo del la presente Tesis Doctoral.

Antes de abordar este punto es importante señalar algunos aspectos clave a tener en cuenta para seguir correctamente el hilo de la investigación:

- La investigación se ha organizado en **dos fases** fundamentales. La primera fase se corresponde con el estudio "paso a paso" en que los objetivos parciales se fueron investigando e implantando (punto 5.2 del presente capítulo). La segunda fase se corresponde con el punto 5.3 del presente capítulo y engloba los trabajos que culminan la Tesis Doctoral, con los que se aborda el objetivo general.
- Cada una de las fases se divide en **dos etapas** y estas etapas son **progresivas,** de modo que hay un **total de cuatro etapas.** Cada una de ellas será introducida a medida que se avanza en la lectura del documento. En la Figura 4.1 se presenta de manera esquemática la organización de la investigación y los materiales en cuyo desarrollo se centra cada una de ellas.

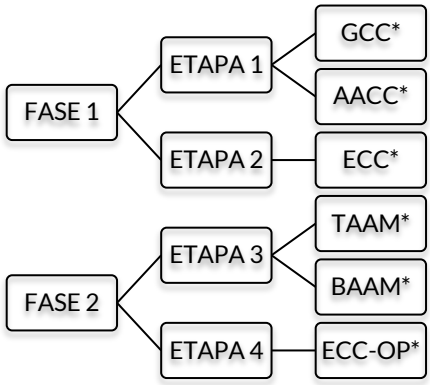

*Nota: Consultar la nomenclatura de los materiales en la Tabla 2.1 del Capítulo 2 – sección 2.3

***Figura 4.1** Organización de la investigación: Fases, etapas y materiales en cuyo desarrollo se centran.*

- El orden en que a continuación se presentan las publicaciones no coincide con cronología temporal de las mismas debido a que: i) algunas de las etapas se desarrollaron experimentalmente de manera paralela; ii) motivos editoriales de las revistas a las que se indexa cada publicación científica.
- Cabe recordar que, con el fin de dar continuidad y coherencia al estudio evolutivo de los distintos materiales, a efectos del presente documento, se han renombrado los materiales correspondientes a las distintas etapas. En algunos casos, la nomenclatura de los hormigones celulares alternativos empleada no se corresponde con la de la publicación.
- Para facilitar la aplicación de todos estos precedentes, cada una de las publicaciones se introduce con una "ficha" en la que se da una visión general del trabajo. En ella aparecen los objetivos de mejora abordados (consultar la Figura 2.1 y la Tabla 2.1 del Capítulo 2 – sección 3.3), el procedimiento experimental (consultar la Tabla 3.4 del Capítulo 3 – sección 3.3) y finalmente los resultados y conclusiones más relevantes con los que se establece el punto de avance hacia la siguiente etapa experimental.

4.2 ESTUDIO "PASO A PASO" DE LA CONSECUCIÓN DE LOS OBJETIVOS PARCIALES DE LA TESIS

En la **primera etapa** se han introducido los **GCC** con el empleo de FCC como precursor, así como los **AACC** con el empleo de BFS como precursor. En ambos casos se ha estudiado distintas dosificaciones, metodologías de fabricación (curado y amasado) y se ha comparado su caracterización con materiales control (**TCC**). Además, se ha introducido diversas alternativas de aireación para cada uno de estos sistemas alternativos.

En la **segunda etapa**, y para cerrar esta primera fase, se presentan los nuevos **ECC** y una aproximación a los beneficios medioambientales del material.

4.2.1 Hormigones Celulares Geopoliméricos (GCC) y Hormigones Celulares de Activación alcalina (AACC)

Forman parte de esta **primera etapa** experimental las siguientes publicaciones:

i. Geopolymer eco-cellular concrete (GECC) based on fluid catalytic cracking catalyst residue (FCC) with addition of recycled aluminium foil powder

ii. Nuevos Hormigones Celulares Geopoliméricos aireados con agua oxigenada: síntesis y propiedades

iii. New cellular geopolymer concretes (CGC) based on blast furnace slag and spent FCC catalyst

iv. Salt slag recycled by-products in high insulation alternative environmentally friendly cellular concrete manufacture

i. Geopolymer eco-cellular concrete (GECC) based on fluid catalytic cracking catalyst residue (FCC) with addition of recycled aluminium foil powder

AUTORES: Alba Font, María Victoria Borrachero, Lourdes Soriano, José Monzó y Jordi Payá

REFERENCIA DE LA PUBLICACIÓN: Journal of Cleaner Production 168 (2017) 1120-1131
DOI: http://dx.doi.org/10.1016/j.jclepro.2017.09.110

Factor de impacto/Cuartil (2017): 5.651/Q1	**Citas (excluyendo auto citas): 6**

OBJETIVOS PARCIALES ABORDADOS

MATERIALES	FABRICACIÓN
• **TCC:** OPC + H_2O + A • **GCC:** FCC + [WG+NaOH+H_2O] + A • **GCC:** FCC + [WG+NaOH+H_2O] + A_R	• **CO-M:** FCC + A_R = $FCCR_m$ • **CURADO:** TB, TA y CM • **Amasado con:** NM

PROCEDIMIENTO EXPERIMENTAL

CARÁCTERIZACIÓN DE MATERIAS PRIMAS	CARÁCTERIZACIÓN DE ESPECÍMENES
• PSD • FESEM • XRD • Emisiones de hidrógeno	• Densidad natural (D_N) • Resistencia mecánica (Rc) • Conductividad térmica (C-Therm TCi) (λ) • Ensayos hídricos (D_{AP} y ΦT) • Evaluación de la matriz porosa (FESEM, OM, ImageJ)

RESULTADOS Y CONCLUSIONES MÁS RELEVANTES DE LA INVESTIGACIÓN

- La reactividad del polvo de aluminio comercial (A) resultó más rápida y efectiva en las matrices geopoliméricas (GCC) que en el sistema tradicional (TCC) a temperatura ambiente. La elevada temperatura de la reacción de geopolimerización favorece la reacción y se genera mayor cantidad de hidrógeno. Este hidrógeno sale de la matriz durante el periodo previo de endurecimiento en un momento en que la consistencia de la pasta permite que se queden burbujas estables de aire atrapado. Para conseguir este efecto en las matrices de TCC fue necesario el curado a altas temperaturas.
- El empleo de papel de aluminio doméstico A_R como reactivo generador de gas resultó con muy buenos resultados. Los ensayos del potencial del material por emisiones de hidrógeno mostraron una reactividad muy similar a la obtenida con A.
- Cuando se procede a la Co-M, el $FCCR_m$ resulta con un tamaño de partícula menor que A_R (el molido en laboratorio para incorporarlo de manera individual a la mezcla) y esto mejora la efectividad de la aireación.
- Tras 7 días de curado a temperatura ambiente se obtuvieron los siguientes valores:

Material	D_N (kg/m³)	Rc (MPa)	D_{AP} (kg/m³)	ΦT (%)	D_{med} (μm)	λ (W/mK)
GCC aireados con A	590	1.8	680	75	595	0.622
GCC aireados con A_R	983	3.5	790	60	890	0.700
GCC con FCCRm	690	3.5	630	70	373	0.581

Abstract: This study presents a new cellular concrete design focused on the energy eco-efficiency and the sustainability concept: geopolymer eco-cellular concrete (GECC). Geopolymer systems made from alkali-activated fluid cracking catalyst residue (FCC) aerated by recycled aluminium foil powders (R) were designed. Commercial aluminium powder (A) was also used as an aerating agent in GECC matrix and its effect was compared with traditional cellular concrete (TCC) made with ordinary Portland cement (OPC). The more alkaline medium of the GECC system improved the hydrogen reaction rate and consequently a higher efficiency in the pore matrix development can be found. Aluminium powder addition of 0.2% by mass of the precursor (FCC) was enough to yield cellular concrete with a natural density significantly lower than that found for TCC. The replacement of A by R made it possible to produce an alternative GECC in which the recycling of the waste aluminium has an important eco-efficiency role because its low cost and its energy saving function. Ground R has less aeration effectiveness than A. However, when co-milling of FCC. R was carried out, advantageous performance GECC was attained. Very interesting properties were obtained for this material: good pore size and its proper distribution in the matrix, low natural density (600-700 kg/m^3), relatively high compressive strength (2.5-3.5 MPa), low open/closed porosity ratio (1.15) and the lowest thermal conductivity (0.581 W/mK). This opens an interesting way of reusing both FCC as precursor and aluminium foil waste as an aerating agent in the preparation of new geopolymer eco-cellular concrete (GECC).

Keywords: Cellular concrete, Geopolymers, Ecoefficiency, Waste valorization

Abbreviations:
TCC: Traditional cellular concrete
GECC: Geopolymer cellular concrete
GFC: Geopolymer foam concrete
OPC: Ordinary Portland cement
FCC: Fluid catalytic cracking residue
A: Commercial aluminium powder
R: Recycled aluminium foil
FCCRM: FCC and R co-milled

HIGHLIGHTS:

- Spent fluid catalytic cracking residue (FCC) was activated and foamed with aluminium.
- Simple method was designed and tested for quantifying aluminium in powered samples.
- The more alkaline medium of the fresh geopolymer improved the hydrogen reaction rate.
- Co-milling of FCC and aluminium foil waste presented advantageous performance.
- Low thermal conductivity and natural density for eco-cellular systems were obtained.

1. Introduction

Traditional cellular concrete (TCC) is formed by ordinary Portland cement (OPC) paste (in some cases hydrated lime is added), with the addition of an inorganic (metallic powders) or an organic surfactant reagent (foaming agent). Commercial aluminium powder (A) is the most used reagent in TCC production, and is oxidized immediately when it comes in contact with mixing water and the alkaline medium from OPC hydration, releasing hydrogen gas (Sepulcre Aguilar et al., 2013). The result is a material characterized by its internal air-void structure (gas bubbles trapped in fresh state), which has been stabilized with an autoclaving-accelerated hardening treatment (N. Narayanan and Ramamurthy, 2000). Owing to the air-void structure, this material has low density (values of 300-1400 kg/m3) (Ramamurthy et al., 2009), low thermal conductivity (5e30% of those measured on normal weight concrete) (Jones and McCarthy, 2006; Wongkeo et al., 2012), great acoustic insulation, freeze-thaw resistance (to a defined saturation level) (Namsone et al., 2017; Tikalsky et al., 2004) and high fire resistance (above 600 ^{o}C keeping their properties unchanged) (Tanaçan et al., 2009). Due to these properties, TCC is a more durable material than traditional concrete (Dolton and Hannah, 2006; Melo, 2013; Zulkarnain and Ramli, 2011). Conversely, TCC is limited by its low mechanical strength and its high inelastic deformation (Ramamurthy et al., 2009). The volume expansion of the fresh paste depends on the amount of aluminium powder that is added: hydrogen bubbles are homogeneously distributed in the paste, yielding a low-density composite. Different materials can be designed in terms of density and strength: usually, higher density materials develop higher mechanical properties (Hamad, 2014; N Narayanan and Ramamurthy, 2000).

There are several construction advantages in the use of TCC: a) its low density allows the reduction of the dead load in elements with low structural requirements, a faster building rate and lower haulage cost (Wongkeo et al., 2012); and b) its performance promotes its application as an insulation material for non- and semi-structural elements in building structures (Ramamurthy et al., 2009).

In general, TCC represents an interesting alternative material to improve the energy efficiency, climate comfort and sustainability in construction situations for either developed or undeveloped contexts. Nevertheless, TCC has some environmental and economic problems related with its raw materials and its fabrication process.

Driven by an ecological motivation, the production of this type of concrete requires a large amount of Portland cement (70% by weight), the production of which is characterized by high energy demand, the consumption of non-renewable raw materials (Mo et al., 2016) and the emission of greenhouse gases (its manufacture contributes around 5-7% of global CO_2 emissions) (Puertas and Torres-Carrasco, 2014). Alternative ways to produce cellular concrete by using new alkali-activated cement, commonly referred to as “geopolymer foam concrete (GFC)”, are currently in the relatively early stages

of study (Bai et al., 2016; Sanjayan et al., 2015). A complete review of GFC can be found in Zhang et al. (2014) (Zhang et al., 2014). Specifically, there are several authors focused on GFC production with A addition as the aerating agent: Jay G. Sanjayan et al. (2015) as well as Hlavacek et al. (2014) have studied GFC based on alkali- activated fly ashes (Hlavacek, 2014; Sanjayan et al., 2015), Arellano Aguilar et al. (2010) have combined metakaolin and fly ash binder in the geopolymeric mix (Arellano Aguilar et al., 2010). Also, the use of metakaolin-based binders was studied by Keawpapasson et al. (2014), and Esmaily and Nuranian (2012) have designed a non-autoclaved high strength cellular concrete from alkali-activated slag (Esmaily and Nuranian, 2012; Keawpapasson et al., 2014). The literature, however, does not show any work focused on GFC made from alkali-activated FCC. It is well known that this petroleum waste has a high pozzolanic reactivity and now Tashima et al. (2013) have shown its great behaviour as an alkali-activated precursor (Payá et al., 2009, 1999; Tashima et al., 2013).

A further negative aspect related to the energy saving is the curing treatment by autoclaving to obtain stable matrix with the medium compressive strength and low shrinkage needed in TCC design. The autoclaved method involves high temperature and high-pressure conditions and consequently means both a great energy consumption and major economic impact. The new geopolymer cellular binders achieve stable matrix with curing treatments using a wet chamber and temperatures in the range 70-90 ^{o}C. Arellano Aguilar et al. (2010) compared 20$\pm$2^{o}C and 75$\pm$5^{o}C curing temperatures and concluded that with the highest temperature the development of the compressive and flexural strengths was accelerated during the first day although in the long term the results for both curing treatments yielded the same performance (Arellano Aguilar et al., 2010). Sanjayan et al. (2015) kept the specimens for 24 h at room temperature until demolding and then they were oven cured at 60^{o} C for 24 h (Sanjayan et al., 2015). Hlavacek (2014) maintained the specimens under laboratory conditions at 22^{o}C for 2 h and subsequently put them in the oven for 12 h (Hlavacek, 2014). And Esmaily and Nuranian (2012) (Esmaily and Nuranian, 2012) replicated the curing regime of 2+ 3+6+3, consisting of: pre-curing at 25$\pm$1^{o}C for 2 h to complete the gas production, ramping to the maximum temperature for 3 h, soaking at the maximum temperature for 6 h and cooling down to room temperature for 3 h. The maximum temperatures tested were 70, 78 and 87 ^{o}C.

Finally, powdered aluminium also has a high environmental and economic impact as a component in TCC manufacture. To obtain a tonne of pure aluminium from bauxite requires 15000 kWh of heat and electrical energy, and 5 tons of residues are produced (European Aluminium Foil Association, n.d.). Then, there are several methods for aluminium powder manufacture such as stamp milling, ball milling under dry conditions, wet ball milling, attrition milling and vibration milling (Hong et al., 2000): all of these involve high environ- mental and economic costs. Thus, there arises the need to identify better alternatives in terms of environmental issues. The treatment and use of residual metallic aluminium could be an interesting alternative.

Some authors have attempted to resolve this issue by reusing reactive waste. The following applications in TCC have been reported: Araújo and Tenório (2005) (Araújo and Tenório, 2005) have investigated the possibility of incorporating aluminium recycled powders from recycled scrap in cellular concrete manufacture as an aerating agent. Holt and Raivio (2005) (Holt and Raivio, 2005) have tried to add residues from an energy pilot plant (gasification) that contains a substantial proportion of metallic aluminium. And more recently, Song et al. (2015) have worked with the use of residual ashes from municipal solid waste (Song et al., 2015).

The goal of this contribution is to present a new environmentally friendly cellular concrete made from fluid catalytic cracking catalyst residue (FCC) as raw material and using recycled aluminium foil powders (R) as the aerating agent, hereinafter called "geopolymer eco-cellular concrete (GECC)". First, a proper milling pre-treatment of FCC and R is described, followed by volumetric tests to ensure the aerating effect of R. Then, the GECC specimens will be characterized: physical and mechanical characteristics pore system structure, bulk density, porosity parameters and thermal conductivity.

2. Materials and methods

2.1. Materials

Ordinary Portland cement (OPC) was supplied by Lafarge (Puerto de Sagunto, Spain). FCC is a waste from the petroleum industry, and was supplied by the BP Oil Company from its plant in Grao Castellón (Spain). The chemical compositions of both OPC and FCC are summarized in **Table 4.i.1**. Sodium hydroxide pellets (98% purity) and sodium silicate (8% Na_2O, 28% SiO_2 and 64% H_2O) were used for the preparation of the alkali activator and were supplied by Merck-Spain.

Two kinds of aluminium were tested: i) commercial aluminium powder (A) supplied by Schlenk Metallic Pigments GmbH which had a 30 mm mean particle diameter; ii) recycled aluminium foil (R) which was supplied by Agricultural-Forest Ecosystem Department from Universitat Politècnica de València. R was recycled after using it to cover crop glass containers in autoclaving treatments.

Table 4.i.1
Chemical compositions of OPC and FCC (wt%).

	SiO_2	Al_2O_3	Fe_2O_3	CaO	MgO	SO_3	K_2O	Na_2O	P_2O_5	TiO_2	LOI*
OPC	20.80	4.60	4.80	65.60	1.20	1.70	1.00	0.07	-	-	0.23
FCC	47.76	49.26	0.60	0.11	0.17	0.02	0.02	0.31	0.01	1.22	0.52

*Loss on ignition

2.2. *Experimental methodology*

The present investigation was carried out by an experimental procedure structured in four consecutive phases (**Fig.4.i.1**). The first concerns the pre-treatment of raw materials: a milling procedure, in order to attain a suitable particle size and homogenize the particles for their appropriate use in cellular concrete fabrication. In the second phase, the reactivity of A and R was compared by a new and simple volumetric method to assess their aerating effect in the cement matrix. In the third phase some cellular concretes of GECC and TCC were designed and prepared. These were cured by different treatments and the physical characteristics of the resulting materials were studied and compared. In the last phase, some selected GECC systems aerated by each of the proposed methods were prepared and compared: the air-void structure was obtained by a combination of electronic and analytical techniques and the porosity parameters were obtained by hydric tests. Finally, the thermal conductivity of the samples was determined to ensure the proposed GECC insulation properties. The overview of the experimental procedure of the current work is shown in **Fig.4.i.1**.

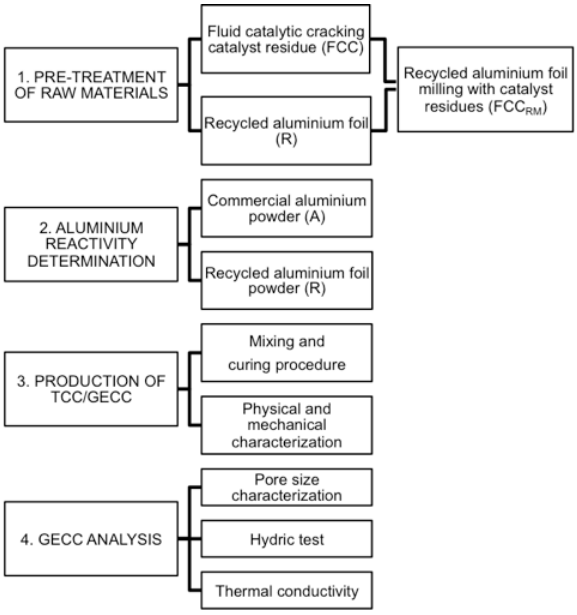

Fig.4.i.1 *Overview of experimental procedure of the current work.*

2.3. Pre-treatment of raw materials

The original FCC was milled for 20 min in a ball mill Gabrielli Mill-2 to attain a lower diameter and homogenize the particles. This is necessary to improve its reactivity in alkali medium and to encourage geopolymeric synthesis (Payá et al., 1999). The particle sizes of both the original and milled FCC were measured by means of a Malvern Instruments Mastersizer 2000. Regarding R, since the production of TCC requires aluminium powders with fractions finer than 100 or 50 mm in order to obtain the required mechanical properties (Hamad, 2014) and appropriate air-void distribution, both cutting up and milling pre-treatments were necessary. By obtaining a finer particle diameter, the aluminium reaction in alkaline matrixes is improved. In this respect, firstly the R had to be reduced into small sheets with diameters less than 4 cm by manual cutting. Then, these particles were processed by means of a food grinder Moulinex A320R1 of 0.6 L capacity and 700-Watt power. The material was ground for 5 min, stopping for 5 s in every minute. The resulting particles had to be sieved and the particles passing of 125μm sieve were collected. The morphology of these particles was characterized by field emission scanning electron microscopy (FESEM) in an ULTRA 55-ZEISS microscope. Finally, with the aim of being able to obtain a lower size of R particles, the milling procedure was improved by means of blending the R into the FCC milling process. To this end, firstly, the R had to be reduced into sheets of 35 mm length and 4 mm width by means of paper confetti cut shredder Rexel Pro-style of 1.2 L capacity. These sheets of R (0.2% by weight) were included in the abovementioned FCC milling procedure, obtaining a new raw material for cellular concrete manufacture: FCC_{RM}. The particle size of the FCC_{RM} was measured by means of the Malvern Instruments Mastersizer 2000. X-ray diffraction (XRD) patterns for ground FCC and FCC_{RM} were obtained by using a Bruker AXS D8 Advance in the Bragg's Angle (2θ) range of 5-70^{o}.

2.4. Aluminium reactivity determination

The aerating effect in the matrix of the cellular concrete was provided by the aluminium powder, which is oxidized when it comes into contact with mixing water or alkali solution and produces H_2 gas. In this investigation the reactivity of R is determined by H_2 generation measurements. Comparisons between the hydrogen generated by A and R were carried out. To develop this analysis, a new and simple gas volumetric method was designed, the set-up diagram of which is shown in **Fig.4.i.2**. It is based on the Bernard Calcimeter method, commonly used to determine carbonates in soils. The test measures the displacement of a water column by H_2 gas when aluminium powder (either A or R) comes into contact with a concentrated solution of NaOH (7.5 M), according to the following reaction (**Equation (4.i.1)**):

$$Al\,(s) + 3H_2O + OH^-\,(ac) \Longrightarrow Al(OH)_4^-\,(ac) + 3/2\,H_2\,(g) \qquad (4.i.1)$$

For given temperature (T) and pressure (P) values, the displaced H_2 volume makes it possible to calculate the amount of aluminium consumed by applying the ideal gas **Equation (4.i.2).**

$$P \cdot V = n_{H2} \cdot R \cdot T \qquad (4.i.2)$$

where *R* is the ideal gas constant (0.082 L atm K^{-1} mol^{-1}) and n_{H_2} is the number of moles of H_2. Thus, the mass of reactive aluminium (m_{Al}) in the sample can be calculated as follows (**Equation (4.i.3)**):

$$m_{Al} = n_{H_2}/(^3/_2) \cdot M_{Al} \qquad (4.i.3)$$

where $M_{(Al)}$ is the molar mass of aluminium (26.98 g mol^{-1}).

Three different aliquots, 10 mg, 15 mg and 20 mg, of each aluminium powder sample were tested and the ratio between the measured weight and the calculated weight by the amount of H_2 liberated in the reaction was obtained.

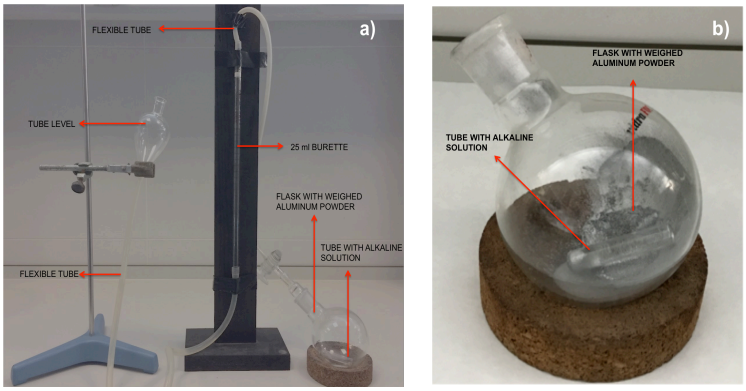

Fig.4.i.2 *Set-up diagram to perform hydrogen generation tests: a) general view; b) flask with weighed aluminium powder and tube with alkaline solution (7.5M NaOH) detail.*

2.5. Mixing and curing procedure

Some trials were performed previously in order to make a first assessment of the material expansion and rheological behaviour to help the mix design. In general, for the production of both the GECC and TCC samples, raw materials (precursor) were dry-mixed with the corresponding aluminium powder and the mixture was then added into water (for TCC) or alkaline solution (for GECC).

In particular, the following dosages were studied:

- The reference system (TCC) was composed of OPC (binder, b), water in a w/b ratio equal to 0.45 and 0.2% (by weight with respect to OPC) of A. The dry blend of OPC with A was added to the water and mixed for 4 min. For each mix, six cube specimens of dimensions 4 x 4 x 4 cm^3 were moulded and cured by different methods until testing.

- Regarding the GECC, three different dosages were designed using FCC as the mineral precursor (binder) and differing in the kind of added aluminium powder: i) A; ii) R; or iii) in the form of FCC_{RM}. In all of these, the w/b ratio was 0.5 and the amount of aluminium was 0.2% (by weight with respect to the precursor). The alkaline activator had a Na^+ molality of 7.5 and the SiO_2/Na_2O molar ratio was 1.7. For each mix, six cube specimens of dimensions 4 x 4 x 4 cm^3 were moulded and cured by different methods until testing.

Due to the expansion process in the matrix of the pastes, no compacting treatment was carried out, in order to avoid the gas escaping from the cementing matrix.

The curing treatments were carried out: i) in a wet chamber (23ºC and 100% RH); ii) in a thermal bath (65 ºC) with 100% RH; and iii) with a combined method: 4 h in the thermal bath until demoulding and then the wet chamber until testing. The free surface of the cubes had to be cut out with a saw blade just at the moment before demoulding.

The samples used in this study are named as *XYct*, where: *X* is the type of cellular concrete (T in TCC case or G in GECC case); *Y* refers to the aerating agent added in the mixtures (A for commercial aluminium powder, R for ground recycled aluminium foil and FCC_{RM} for recycled aluminium foil milled with the precursor); *c* is the curing treatment (*wc* for wet chamber, *tb* for thermal bath and *cm* for combined method) and *t* refers to the curing time until testing (1, 3 or 7 days, or 4 h). More details relating to the specimens, mixing proportions and curing treatments are summarized in **Table 4.i.2.**

Table 4.i.2
Summary of the specimen names, mixing proportions and curing treatments.

	SAMPLES (XYct) [a]	ALUMINIUM POWDER		LIQUID PHASE		CURING METHOD	TEST AGES
		Type	%wt	w/b	Alkali solution [b]		
TCC (OPC)	**TAwc1d**	Commercial aluminium **A**	0.2%	0.45	-	Wet chamber 23ºC 100% RH	24 hours
	TAwc3d						24 hours till demoulding plus 2 days = 3 DAYS
	TAwc7d						24 hours till demoulding plus 6 days = 7 DAYS
	TAtb4h					Thermal bath 65ºC	4 hours
	TAtb1d						4 hours till demoulding plus 20 hours = 24 HOURS
	TAtb7d						4 hours till demoulding plus 6 days and 20 hours = 7 DAYS
	TAcm7d					Combined method	4 hours thermal bath plus 6 days wet chamber = 7 DAYS
GECC (FCC)	**GAwc1d**	Commercial aluminium **A**	0.2%	0.5	7.5/1.7	Wet chamber 23ºC 100% RH	24 hours
	GAwc3d						24 hours till demoulding plus 2 days = 3 DAYS
	GAwc7d						24 hours till demoulding plus 6 days and 20 hours = 7 DAYS
	GAtb4h					Thermal bath 65ºC	4 hours
	GAtb1d						4 hours till demoulding plus 20 hours = 24 HOURS
	GAtb7d						4 hours till demoulding plus 6 days and 20 hours = 7 DAYS
	GAcm7d					Combined method	4 hours till demoulding plus 6 days WC = 7 DAYS
	GRwc1d	Recycled aluminium foil **R**	0.2%	0.5	7.5/1.7	Wet chamber 23ºC 100% RH	24 hours
	GRwc3d						24 hours till demoulding plus 2 days = 3 DAYS
	GRwc7d						24 hours till demoulding plus 6 days and 20 hours = 7 DAYS
	GRtb4h					Thermal bath 65ºC	4 hours
	GRtb1d						4 hours till demoulding plus 20 hours = 24 HOURS
	GRtb7d						4 hours till demoulding plus 6 days and 20 hours = 7 DAYS
	GRcm7d					Combined method	4 hours till demoulding plus 6 days WC = 7 DAYS
	GFCC$_{RM}$wc1d	Recycled aluminium foil milled with the precursor **FCC$_{RM}$**	0.2%	0.5	7.5/1.7	Wet chamber 23ºC 100% RH	24 hours
	GFCC$_{RM}$wc3d						24 hours till demoulding plus 2 days = 3 DAYS
	GFCC$_{RM}$wc7d						24 hours till demoulding plus 6 days and 20 hours = 7 DAYS
	GFCC$_{RM}$tb4h					Thermal bath 65ºC	4 hours
	GFCC$_{RM}$tb1d						4 hours till demoulding plus 20 hours = 24 HOURS
	GFCC$_{RM}$tb7d						4 hours till demoulding plus 6 days and 20 hours = 7 DAYS
	GFCC$_{RM}$cm7d					Combined method	4 hours till demoulding plus 6 days and 20 hours = 7 DAYS

[a] X: type of cellular concrete (T for TCC; G for GECC); Y: aerating agent added in mixtures (A: commercial aluminium powder; R: ground recycled aluminium foil; FCC$_{RM}$: recycled aluminium foil milled with the precursor); c is the curing treatment (wc for wet chamber, tb for thermal bath and cm for combined method) and t refers to the curing time until testing (1, 3 or 7 days, or 4 h).
[b] Composition of the solution is described as Na^+ molality/SiO_2/Na_2O molar ratio

2.6. Physical and mechanical characterization

Considering the natural density as the volumetric mass density (mass per unit volume), it was determined by means of the weight of the cubic samples before compressive strength testing. The compression test was carried out by means of an INSTRON 3282 universal testing machine.

The natural density assessment and compression test were performed for six specimens of each paste dosage, and averages and standard deviation values were calculated.

2.7. Pore system characterization

The pore system characterization of the GECC was investigated with an organized test plan based on the combination of electronic and analytical techniques. To analyse the micropore structure by FESEM, a cube of each GECC mixture was crushed in a porcelain mortar. A small piece (7-10 mm) from the inner part of the cube was selected and immersed in acetone for 30 min and dried at 65ºC for 40 min. FESEM micrographs of these samples covered with carbon were taken by an ULTRA 55-ZEISS electron microscope at 200x magnification, and the micropore diameters were measured. To determine the macropore structure, six 4 x 4 x 4 cm^3 cubes of each GECC mixture were cut into slices 2 cm thick, perpendicular to the cast face, using a diamond rotary saw. The samples were observed by a Leica S8 APO optical microscope. Pictures were taken by a Leica DFC 420 digital camera and the images were processed using Leica LAS image analysis software. A magnification of 10× was selected with a pixel representing 12 mm. A total of 24 images (16 cm^2 per image) were captured for each mix (two images per each two internal surfaces). Finally, all of the cut-off surfaces (from the previous optical microscopy analysis) were submerged in a concentrated solution (0.4% by volume) of universal dye (colour vermilion 780) and universal solvent (302 NC), both from TKROM. Submerged samples were introduced into a desiccator connected to a vacuum pump to be suitable for the impregnation of empty pores. Finally, the surface was sanded with sandpaper. The pore diameter distribution histograms were obtained by measuring all the pore diameters in the original magnification using ImageJ software. Each image was digitalized, processed with a few morphological operations (dilation, erosion, opening, closing and hole fill) to refine the shape of the objects, and finally converted into binary form.

2.8. Hydric tests

Hydric tests were carried out to determine the bulk density and porosity of the GECC and they were compared with the corresponding ones of TCC. To calculate the bulk density, the Archimedes method was used. Five 4 × 4 × 4 cm^3 cubes of each studied material were dried for 24 h in a furnace at 105°C and were then weighed to obtain their dry weight values. Then the samples were fully saturated by water immersion for 24 h and weighed (saturated weight).

In the saturation state the samples were weighed using a hydrostatic balance (submerged weight). Finally, to calculate the true density, a Le Chatelier flask was used after crushing 50 g of each sample.

2.9. Thermal conductivity measurements

A C-Therm TCi Thermal Conductivity Analyzer was employed to determine the thermal conductivity and effusivity of the samples. It employs a one-sided, interfacial heat reflectance sensor that applies a momentary constant heat source to the sample. The thermal conductivity and effusivity were measured directly, with no user-calibration or sample preparation and providing a detailed overview of the thermal characteristics of the sample. The test was carried out on four free surfaces of each cube with 16 cm^2 area. Then the weighted average of those measures was calculated.

3. Results and discussion

3.1. Materials characterization

After the milling pre-treatment of R, the resulting particles less than 125 µm were selected to use in TCC and GECC pastes as alternative aerating agents. To compare the size and morphology of A and R, FESEM micrographs with the same magnification of each one (100x) were taken and are shown in **Fig.4.i.3a** presents the A particles characterized by a homogeneous distribution and a flake-like shape. Most of these particles had a diameter less than 50 µm and showed a flat surface. On the other hand, **Fig.4.i.3b** shows ground R particles of less than 125 µm after the milling process. They are shown as irregular chips with a varied morphology. Many particles showed an apparent size greater than 125 µm, which is due to the aspect ratio.

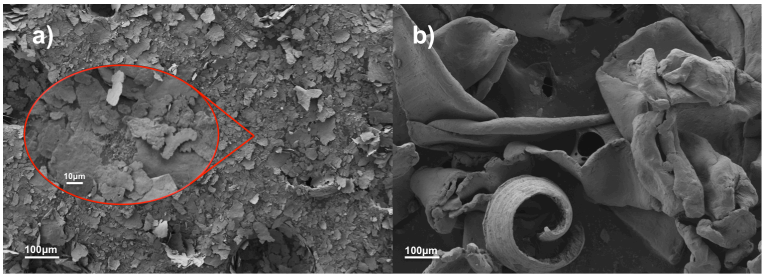

Fig.4.i.3 *FESEM micrographs of aerating agents: a) commercial aluminium powder (A), the red line delimits an enlarged area; b) recycled aluminium foil powder (R).*

It is well known that a low average size of aluminium powder particles allows a more effective aerating reaction in the cement matrix. Thus, recycled aluminium R will be less effective in the preparation of cellular concrete.

The original FCC is not sufficiently fine for being activated by means of the alkali-activation process. FCC had a milling pre- treatment and the particle size diameter was drastically reduced (18.91 µm for the ground sample vs 81.34 µm for the original one). Additional granulometric parameters for both materials are listed in **Table 4.i.3.**

Table 4.i.3
Main granulometric parameters for catalyst residue (FCC) in its original and ground states, and recycled aluminium foil milling with catalyst residue (FCC_{RM}).

Material	d_{mean} (µm)	Percentile Parameters		
		$d_{[0.1]}$ (µm)	$d_{[0.5]}$ (µm)	$d_{[0.9]}$ (µm)
Original FCC	81.34	47.63	79.36	131.65
Milling FCC	18.91	0.21	11.72	49.05
FCC_{RM}	18.43	0.21	11.35	47.92

An FCC precursor containing recycled aluminium was obtained by milling a blend of FCC and small sheets of aluminium foil. The resulting FCC_{RM} presented similar granulometric parameters to those obtained for the milling of original FCC (see **Table 4.i.3**). Certainly, the mean diameter of the aluminium particles would be much less than that obtained in the grinding/sieving treatment in which particles larger than 100 µm were found. That means a probable improvement of the reaction of R in alkaline medium, being more homogeneous and effective in the binder matrix.

Finally, **Fig.4.i.4** shows the XRD pattern of ground FCC and FCC_{RM}. As might be expected, the X-ray diffractogram of ground FCC showed peaks corresponding to zeolite type faujasite ($Na_2Al_{2-}Si_4O_{12}{\cdot}8(H_2O)$), as well as the minority presence of mullite ($Al_6Si_2O_{13}$). For the FCC_{RM} diffractogram, there is a clear difference from the mineralogical composition, and the presence of metallic aluminium in the mineral precursor is evidenced by the peaks above $2\theta = 35^{o}$ corresponding to aluminium pattern: 38.45º, 44.71º and 65.09º (corresponding to [111], [200] and [220] Miller planes), as highlighted with red in **Fig.4.i.4**.

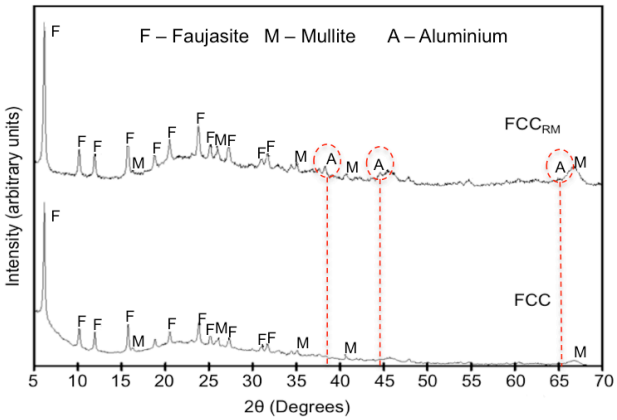

Fig.4.i.4 *XRD patterns for ground FCC and FCC_{RM}.*

3.2. Aluminium reactivity determination

The commercial aluminium powder (A) used in this study had a minimum purity of 92%. However, in taking this reagent as reference material in our study, initially 100% purity will be considered. Measurements of emitted hydrogen gas in the volumetric tests were carried out and the moles of H_2 (**Equation (4.i.2))** and mass of aluminium (**Equation (4.i.3))** were calculated. Aliquots of 10, 15 and 20 mg of A were tested and the theoretical (assuming 100% purity) and experimental aluminium contents were assessed. As can be seen in **Fig.4.i.5**, a good correlation between the calculated and experimental amounts of aluminium was achieved. The results obtained from 10 mg samples deviated from the x = y line, suggesting that for the lowest mass selected the accuracy of the measurements has a significant influence (lower hydrogen volume, lower accuracy in the weighing of sample). The results demonstrated that the purity of A was much greater than the minimum purity declared by the company.

In general, the values of aluminium calculated in this designed gas volumetric method are lower compared to the aluminium mass used. The correspondence between the aluminium used for the test and the aluminium calculated is highest with the greatest amount of tested aluminium. With the weighed values of 10 mg, the results of the aluminium calculated are clearly displaced below the x = y line. As the amount of aluminium used in the measurements increases to 15 mg the deviation is lower.

Finally, when the 20 mg weighed value is used the deviation is almost negligible. This may be for two reasons: the first is that H_2 is a very diffusive gas and consequently a slight amount of the gas is lost through the assembly joints; secondly the purity of the aluminium is probably slightly lower than 100%. The latter is related to the oxidation of the external surface of the aluminium particles (the formation of a thin passivation layer of aluminium oxide or hydroxyl oxide). The purity of the recycled aluminium foil was unknown. However, when the volumetric measurements are compared to those obtained for commercial aluminium powder, very similar values were obtained. This means that the purity of recycled aluminium is also very high, close to 100%.

In general terms, the results reveal the applicability of the designed test in order to determine the purity of aluminium samples. Additionally, this method makes it possible to calculate the maximum volume of hydrogen generated in the cellular concrete.

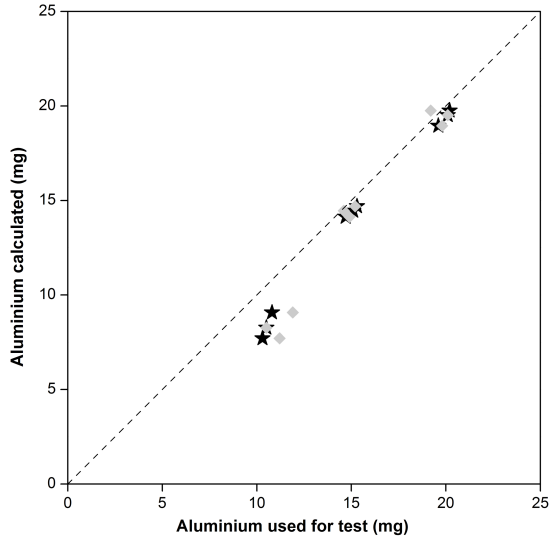

Fig.4.i.5 *Results of aluminium powder reaction test: aluminium used for each test with respect to aluminium calculated (Key: ★: commercial aluminium powder; ◆: recycled foil; ---: x=y line).*

3.3. Physical and mechanical characterization

The natural density and compressive strength of both TCC and GECC concrete aerated by the addition of A and cured by the three proposed methods are shown in **Table 4.i.4**.

For the TCC, the lowest natural density was obtained in samples cured by the combined method (642 kg/m^3) and it yielded the lowest strength after 7 days of curing (1.94 MPa). TCC cured in a thermal bath had a similar natural density, slightly higher (666 kg/m^3) than that from the combined method. However, the material cured in the wet chamber conditions developed a higher density, which is related to the expansion rate in fresh conditions. At 20ºC, the hydrogen evolution into the OPC matrix is slow and setting of the system is produced before complete oxidation of the aluminium. In these conditions, the evolved gas after setting escaped without producing expansion.

In the case of GECC, the lowest natural density value was also obtained by means of the combined method (510 kg/m^3), but in this case it yielded the highest strength (2.19 MPa at 7 days). However, the difference in density with respect to the wet chamber curing method is significantly less among GECC specimens in comparison to TCC specimens. This means that in this medium, the transformation rate of aluminium is faster than that produced in the OPC

medium. Thus, a larger part of the hydrogen evolved before setting, trapping the gas bubbles in the matrix. Serendipitously, the strength developed after 7 days of curing was the highest, suggesting that the cementitious products and gas bubbles were better spatially distributed. Generally, the geopolymeric systems allow lower natural density values to be obtained compared to traditional systems. Due to the higher alkaline medium in GECC, the aluminium powder reaction is faster and more aggressive. In addition, as can be observed, the highest compressive strengths were obtained for GECC cured in the thermal bath (2.12 MPa) and the combined method, which confirms that the great polymerization of the geopolymer systems at mildly elevated temperature conditions is not affected by the aeration process.

On the whole, regardless of the curing method, for all mixtures the compressive strength rises with increasing curing time.

Considering the same aluminium powder dosage, when the curing method was the wet chamber, the average natural densities for 1 day of curing were 912 kg/m^3 for TCC and 592 kg/m^3 for GECC, respectively. For these samples, after 7 days of curing, the gain of compressive strength compared to the values after 1 and 3 days of curing was 21.9% and 13.8% for TCC and 38.3% and 55.7% for GECC respectively.

On the other hand, when the samples were cured in the thermal bath at 65 ºC, the average natural density at 4 h of curing were 669 kg/m^3 for TCC and 532 kg/m^3 for GCC, respectively. For these samples, after 7 days of curing the gain of compressive strength compared to the values after 4 h and 3 days of curing were 33.8% and 28.6% for TCC and 67.2% and 3.8% for GCC respectively.

There is a significant difference in the natural density values for TCC samples if wet chamber or thermal bath curing conditions are used. In contrast, the effect of the curing method for GECC samples had less influence on the natural density. The percentage decrease of the average natural density from the wet chamber to the thermal bath treatment was 26.7% for TCC and 10.3% for GECC respectively. This reveals the high temperature requirement in traditional TCC systems to allow a suitable generation and entrapment of hydrogen bubbles. Even so, in the case of the compressive strength development, there were percentage differences after 7 days of curing between the wet chamber and thermal bath treatments: 21.9% reduction for TCC and 34.9% gain for GCC respectively. Advantageously, for GECC systems, the evolution of gas generation and entrapping was successful for both curing treatments.

The results for the combined method of curing in both GECC and TCC systems reveal that is not necessary to keep the thermal bath conditions for more than 4 h to improve the physical and mechanical features.

In general, since the structural requirements of cellular concrete are not very high, and considering the TCC results, the manufacturing of GECC aerated by

commercial aluminium powder was successful in terms of natural density and compressive strength when the samples were cured at room temperature.

By using ground R as the agent to aerate the geopolymeric matrix (GR mixtures), natural density values of about 1000 kg/m^3 for all of the proposed curing methods were obtained and there were no significant differences among them. After 7 days of curing, the natural density was in the range 950e983 kg/m^3, a range significantly higher than that found for GA (510e590 kg/m^3). Since the R particle size was not fine enough, the relatively high-density values may have been due to three different situations: i) a complete aluminium reaction was not possible and the aeration results were insufficient; ii) the reaction took place too fast and the hydrogen diffused before the paste matrix had enough consistency to entrap it; iii) a combination of the above two situations.

A better behaviour was observed when R was previously blended into the FCC milling treatment (mixtures GFCC$_{RM}$) and the average natural densities for the wet chamber, thermal bath and combined method were 690, 635 and 633 kg/m^3 respectively, values very close to those found for the GA mixtures.

Table 4.i.4
Natural density and compressive strength of TCC (TA samples) and GECC (GA samples) aerated concretes with commercial aluminium powder (A).

	TA samples (prepared with OPC)							GA samples (prepared with FCC)						
	wc [a]			tb [b]			cm [c]	wc [a]			tb [b]			cm [c]
	1d	3d	7d	4h	1d	7d	7d	1d	3d	7d	4h	1d	7d	7d
Natural density (kg/m^3)	912	909	908	669	667	666	642	592	590	590	532	531	528	510
Standard deviation	7.37	5.76	3.85	5.35	5.08	4.88	7.54	6.51	6.36	6.36	5.73	6.94	4.57	8.75
Compressive strength (MPa)	1.75	2.24	2.60	0.96	1.45	2.03	1.94	0.50	0.81	1.83	0.67	2.04	2.12	2.19
Standard deviation	0.4	0.12	0.13	0.12	0.35	0.34	0.04	0.04	0.03	0.11	0.13	0.29	0.38	0.17

[a] wc: wet chamber at 23°C and 100% RH;
[b] tb: thermal bath at 65°C
[c] cm: combined method

Table 4.i.5
Natural density and compressive strength of GECC aerated concretes with recycled aluminium foil (R) and for GFCC$_{RM}$.

	GR samples							GFCC$_{RM}$ samples						
	wc [a]			tb [b]			cm [c]	wc [a]			tb [b]			cm [c]
	1d	3d	7d	4h	1d	7d	7d	1d	3d	7d	4h	1d	7d	7d
Natural density (kg/m^3)	987	985	983	954	950	950	950	695	693	690	637	637	635	633
Standard deviation	4.92	4.60	4.58	3.65	4.91	5.85	9.13	8.92	9.92	9.24	5.17	5.40	5.30	5.47
Compressive strength (MPa)	0.74	1.66	3.56	1.03	1.86	3.54	3.89	0.35	1.67	3.50	0.51	1.36	2.87	2.51
Standard deviation	0.10	0.27	0.23	0.34	0.14	0.47	0.55	0.04	0.34	0.23	0.07	0.10	0.22	0.30

[a] wc: wet chamber at 23°C and 100% RH;
[b] tb: thermal bath at 65°C
[c] cm: combined method

Fig.4.i.6 shows both relative coefficients related to natural density and compressive strength. In terms of natural density, the ratio (φ_d) was obtained according to **Equation (4.i.4),** where a φ_d value lower than 1 means that the

aeration was more effective than for commercial aluminium A. In terms of strength, the ratio (θ_s) was obtained according to **Equation (4.i.5)**, where a θ_s value higher than 1 means a more resistant structure for recycled aluminium.

$$\varphi_d = \rho_A / \rho_R \quad (4.i.4)$$

Where ρ_A is the natural density for GECC aerated with A, and ρ_R is the density when aerated with R or with FCC_{RM}.

$$\theta_s = r_A / rR \quad (4.i.5)$$

Where r_A is the compressive strength for GECC aerated with A, and r_R is the compressive strength when aerated with R or with FCC_{RM}.

As can be seen, the natural density coefficients (φ_d) were close to unity for $GFCC_{RM}$ mixtures, whereas for GR the values were close to 0.5. This indicates the excellent effectiveness of the FCC_{RM} system aeration. The values of φ_d decrease slightly with the curing temperature, for both GR and $GFCC_{RM}$ samples.

The compressive strength coefficients were greater than those in all the recycled aluminium containing mixtures. Obviously, this behaviour indicates that the compressive strength of GECC by the addition of R (as GR or as $GFCC_{RM}$) was greater than GECC aerated by A.

It is noticeable that in the case of the wet chamber cured samples for the $GFCC_{RM}$ system; the natural density was in the same range as that obtained in the GA system (φ_d = 0.99), whereas a significantly higher compressive strength (θ_s = 1.91) was achieved. This means that the new proposal for preparing the binder by grinding FCC and R together represents an excellent alternative in terms of physical/mechanical properties. Additionally, this preparation procedure makes it possible to have a very good homogenization of the recycled aluminium, taking advantage of the FCC milling. This proposal does not increment the complexity of the process.

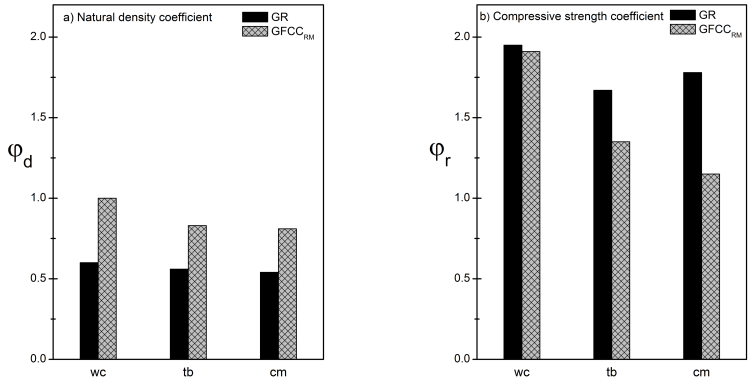

Fig.4.i.6 *Comparisons between commercial aluminium aerated systems and recycled aluminium foil (R) aerated systems: a) natural density coefficient (φ_d); b) compressive strength coefficient (θ_s).*

3.4. Pore system characterization

There have been several investigations dealing with the pore system of TCC and three different classifications have been proposed: i) artificial air pores, intercluster and interparticle pores; ii) macropores formed due to the expansion of the mass caused by aeration and micropores which appear in the walls between the macropores; and iii) microcapillaries (<50 nm), macrocapillaries (>50 nm to 50 µm) and artificial air pores (>50 µm) (Esmaily and Nuranian, 2012).

Ramamurthy et al. (2009) reported the TCC air voids characterization on the basis of volume, size distribution, shape and spacing, concluding that they had a strong influence on the strength and density (Ramamurthy et al., 2009).

In this paper, the internal air-void structure of GECC aerated by A and R (ground and included in the FCC milling treatment), after 7 days of curing in the wet chamber (wc) was compared. The following criteria to distinguish the range of pores were considered: micropores or pores less than or equal to 0.1 mm and macropores or pores greater than 0.1 mm. The area analysed for each image was 16 cm^2, and the number of different size pores was counted.

The GAwc7d sample (aerated with A) presented a predominance of 20-60 µm micropores located in the solid phases between the macropores with a homogeneous distribution and with no interconnection among them (**Fig.4.i.7.a**). Regarding the macro scale, the predominant pore size is 0.3-2 mm with the presence of few macropores over 5 mm (**Fig.4.i.7.b**). In general, this GECC presents an average of 677 pores in the 16 cm^2 area, with an average diameter equal to 595 µm and a predominant number of pores between 300 and 600 µm (**Fig.4.i.7.c**).

Due to the fast reaction of commercial aluminium in the geopolymer matrix, there is a large amount of macropores and the surrounding solid material among them contained small non- interconnected micropores. This configuration may prove the low natural density obtained in GAwc7d mixtures as well as this low compressive strength.

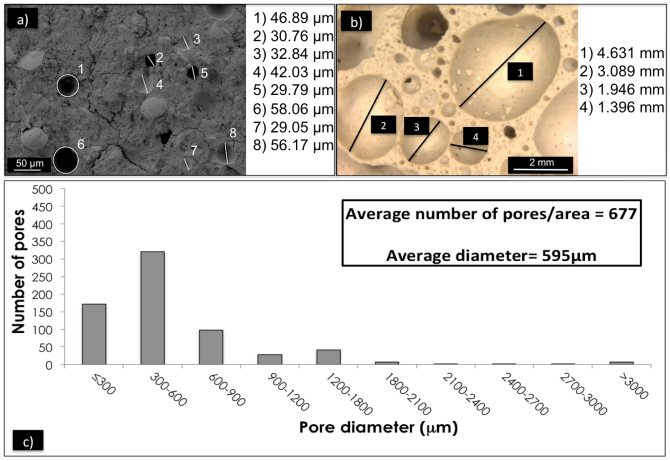

Fig.4.i.7 *Pore system characterization of* ***GAwc7d****: a) FESEM micropores sizing; b) OM macropores sizing; c) pore diameter distribution in 16 cm² area.*

The GRwc7d sample presents predominance of 30-90 µm micropores that have irregular distribution and with some interconnection among them (**Fig.4.i.8.a**). Regarding the macro scale, the predominant pore size is 1-5 mm with the presence of some 0.3e0.8 mm micropores inside the internal walls (**Fig.4.i.8.b**). In general, this GECC presents an average of 455 pores in the 16 cm² area, with an average diameter equal to 890 µm and a predominant number of pores of 600-900 µm (**Fig.4.i.8.c**). These values observed in **Fig.4.i.8c** are very different from those obtained in the GAwc7d sample.

This configuration reveals the lower aeration effectiveness in the matrix with the addition of R compared to the results obtained from the GAwc7d analysis. The interconnection between pores and their irregular shapes show that the big particles of R caused an aggressive and more localized reaction, and the entrapping of H_2 released into the fresh matrix cannot be guaranteed.

Finally, with the use of FCC_{RM} as the precursor, a similar pore structure to that obtained in the GA sample has been achieved. The $GFCC_{RM}$wc7d sample presents a homogeneous micropore distribution with sizes of 20-100 µm (**Fig.4.i.9.a**). Regarding the macro scale, the predominant pore sizes of 1-1.5 mm show some macropores interconnection (**Fig.4.i.9.b**). This GECC presents an average number of 981 pores in the 16 cm² area, with an average diameter equal to 373 µm and a predominant number of pores smaller than 300 µm (**Fig.4.i.9.c**).

In general, the inclusion of R in FCC milling achieved a better uniform size and distribution of pores in GECC, correlating highly with the density and strength values. The high number of micro and macropores is the cause of the low density of the material. However, given the existing interconnections among several of the macropores, its natural density was slightly greater than that obtained for the GAwc7d mixture. The predominance of micropores in the spaces between macropores leads to better mechanical properties.

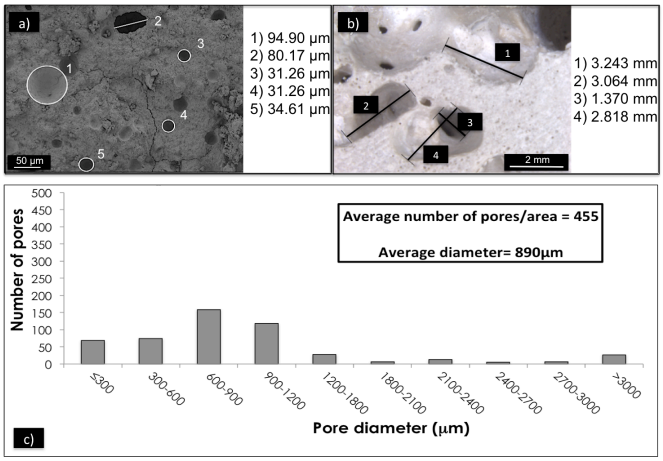

Fig.4.i.8 *Pore system characterization of sample* ***GRwc7d****: a) FESEM micropores sizing; b) OM macropores sizing; c) pore diameter distribution in 16 cm² area.*

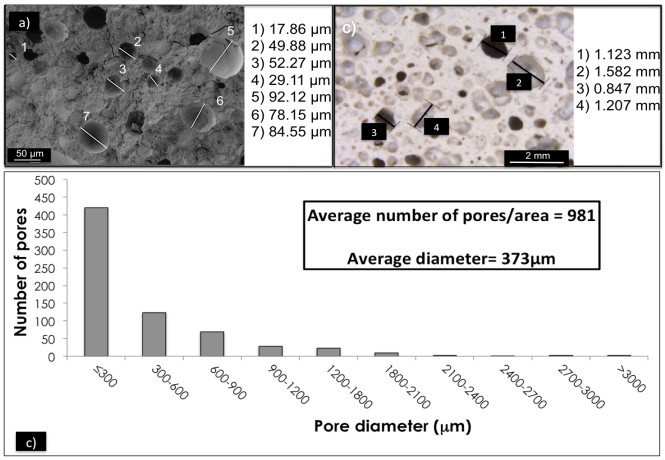

Fig.4.i.9 *Pore system characterization of sample* ***GFCC$_{RM}$wc7d****: a) FESEM micropores pore sizing; b) OM macropores pore sizing; c) pore diameter distribution in 16 cm² area*

3.5. Hydric tests

The thermal conductivity in cellular concrete is the consequence of its lightweight due to the hydrogen bubbles trapped in the matrix paste. The bulk density is the main parameter that determines the amount of these pores in the final material (Melo, 2013).

On the other hand, regarding porosity, the proportion of closed porosity (ΦCL) has a direct influence on the thermal insulation behaviour due to the hindrance of air circulation through the pores network. Contrarily, a higher proportion of open porosity (ΦOP) can favours liquid or gas access into the matrix and its circulation. Finally, the total porosity (ΦT) allows better acoustic insulation conditions.

The samples compared in this test were: TCC aerated by commercial aluminium powder and cured in the wet chamber for 7 days (TAwc7d) and GECC aerated by: commercial aluminium powder, recycled aluminium powder and recycled aluminium powder milled with FCC, cured in the wet chamber for 7 days (GAwc7d, GRwc7d and $GFCC_{RM}$wc7d, respectively). **Table 4.i.6** shows the results of the hydric test for each one.

The greatest compactness values were for the lowest total porosity values, indicating the acoustic insulation properties of each GCC compared to TCC. As expected, due to the high purity of A and the elevated alkaline medium, GAwc7d presents the highest total porosity and the lowest compactness.

Regarding open porosity and water absorption, the GRwc7d mixture had the greatest open porosity proportion, but its water absorption was the lowest. These results agree with this pore system configuration regarding the interconnection and irregular macropores and, obviously with the lowest total porosity. In this context, for the remaining GECC, GAwc7d and $GFCC_{RM}$wc7d, the durability conditions obtained were better than TCC, resulting in $GFCC_{RM}$wc7d mixtures with the greatest relations.

In general, lower values of bulk density correspond with a lower ratio between open and closed porosity. This ratio shows the amount of air entrapped due to the aeration reaction. Both GAwc7d and $GFCC_{RM}$wc7d were found to have a high closed porosity pro- portion and therefore had lower bulk densities values than that found for TAwc7d. This behaviour reveals the better thermal insulating properties of GECC with respect to TCC. Accordingly, it should be noted that the results of $GFCC_{RM}$wc7d confirm the ecoefficiency advantages of this new environmentally friendly material.

Table 4.i.6
Results of hydric tests.

Sample	Bulk density (kg/m³)	Porosity (%)				Compactness (%)	Water absorption (%)
		ΦT	ΦOP	ΦCL	ΦOP/ ΦCL	C	e
TAwc7d	710	65.62	47.20	18.42	2.56	34.38	67.32
GAwc7d	680	74.68	51.55	23.13	2.22	25.33	47.10
GRwc7d	790	59.67	52.22	7.46	7	40.33	41.05
GFCC$_{RM}$wc7d	630	69.14	46.03	23.11	1.15	30.85	59.30

3.6. Thermal conductivity

The thermal conductivity (k) measurements for selected GECC systems are shown in **Table 4.i.7**. Four samples of each type were measured. As can be seen, the thermal conductivity of GRwc7d (0.700 W/mK), for which aluminium foil is dry added to the precursor, was higher than that found for GECC aerated by commercial aluminium powder, GAwc7d (0.622 W/mK), a behaviour attributed to the large difference in terms of natural density (983 kg/m^3 versus 590 kg/m^3). Interestingly, when aluminium foil is added into the FCC milling process (GFCC$_{RM}$wc7d), the thermal conductivity results were the lowest (mean value 0.581 W/mK), although its natural density (690 kg/m^3) was slightly higher than that obtained for the GAwc7d system. Obviously, this behaviour may be related to the number of pores, their size and their distribution (the finer the pores, the better the insulation) (N Narayanan and Ramamurthy, 2000). These results agree with data collected from the hydric tests.

In general, the use of FCC as raw material and the introduction of recycled aluminium foil have been able to produce cellular concretes with great insulation properties. Notice that the co-milling process of FCC R allows the insulation properties of the material to be improved when compared to the use of commercial aluminium powder. The GFCC$_{RM}$7d mixtures resulted in the lowest thermal conductivities and consequently the greatest thermal insulation. This fact is directly related with energy saving terms.

Table 4.i.7
Individual and mean thermal conductivity values (k) for GECC samples.

		GAwc7d	GRwc7d	GFCC$_{RM}$wc7d
k (W/mK)	i	0.617	0.698	0.580
	ii	0.623	0.699	0.584
	iii	0.624	0.701	0.582
	iv	0.624	0.700	0.581
AVERAGE		**0.622**	**0.700**	**0.581**
STD. DEVIATION		**0.0018**	**0.0012**	**0.0034**

4. Conclusions

Cellular concrete based on alkali-activated FCC has been designed and tested, concluding that stable aerated concrete can be obtained in soft conditions: i) at 23ºC with 100% RH and ii) at 65ºC in a thermal bath. In general, good performance of this new type of cellular concrete was observed. This waste becomes an interesting raw material for cellular concrete purposes, thus opening a new method of waste valorisation.

Comparisons with OPC-based cellular concrete (traditional system, TA) showed that the reaction of commercial aluminium powder in the characteristic alkaline medium of alkali-activated mixtures (geopolymer system, GA) is faster and thus more effective. This behaviour is attributed to the fact that most of the hydrogen in the GA system was produced before setting due to the high temperatures of the geopolymerization reaction, and consequently more bubbles developed and were entrapped in the fresh material. To achieve a similar gas development in the traditional system, thermal treatment of the fresh mixture must be carried out. From the additional ecoefficiency and sustainability points of view, the replacement of commercial aluminium powder A, which needs high technological development in its production and has a high energy cost, by recycled aluminium foil (R) was successfully carried out.

The main reactivity characteristic of R is the generation of hydrogen when it is introduced into an alkaline medium. A very simple method to measure the potential hydrogen evolution based on the Bernard Calcimeter technique has been described and applied to this aluminium foil waste. It was also compared with the reactivity of A. Similar reactivity of both aluminium types was found.

Appropriate physical and mechanical characteristics for these new geopolymer eco-cellular concretes (GECC) containing FCC and R were obtained. The replacement of 0.2% of A by the same amount of R made it possible to produce cellular concrete with a natural density in the range of 500-1000 kg/m^3 and with compressive strength in the range of 2-4 MPa.

Specifically, the effectiveness of R was enhanced when this aluminium waste was co-milled with FCC: in these conditions, the particle size of the aluminium was significantly lower and the size and distribution of pores in the hardened cellular concrete were valuably improved. GECC prepared with co-milled FCC/R led to the production of the material with the best performance from the insulation point of view: an average pore diameter of 373 µm, a predominance of pores smaller than 300 µm, the lowest open/ closed porosity ratio (1.15) and the lowest thermal conductivity (0.581 W/mK).

In summary, an interesting way has been opened for reusing both FCC as precursor and aluminium foil waste as a foaming agent in the preparation of new geopolymer eco-cellular concretes (GECC).

Acknowledgements

This work was developed within the scope of the project Geocelplus (internal project, Universitat Politècnica de València). The authors give special grateful to Dra. Mrs. Josefa L. Roselló Caselles for kindly support and recycled aluminium foil supply. The authors also thank the Electron Microscopy Service of the Universitat Politècnica de València (Spain).

References

Araújo, E.G. de, Tenório, J.A.S., 2005. Cellular Concrete with Addition of Aluminum Recycled Foil Powders. Mater. Sci. Forum 498–499, 198–204. https://doi.org/10.4028/www.scientific.net/MSF.498-499.198

Arellano Aguilar, R., Burciaga Díaz, O., Escalante García, J.I., 2010. Lightweight concretes of activated metakaolin-fly ash binders, with blast furnace slag aggregates. Constr. Build. Mater. 24, 1166–1175. https://doi.org/10.1016/j.conbuildmat.2009.12.024

Bai, C., Franchin, G., Elsayed, H., Conte, A., Colombo, P., 2016. High strength metakaolin-based geopolymer foams with variable macroporous structure. J. Eur. Ceram. Soc. 36, 4243–4249. https://doi.org/https://doi.org/10.1016/j.jeurceramsoc.2016.06.045

Dolton, B., Hannah, C., 2006. Cellular Concrete : Engineering and Technological Advancement for Construction in Cold Climates 1–11.

Esmaily, H., Nuranian, H., 2012. Non-autoclaved high strength cellular concrete from alkali activated slag. Constr. Build. Mater. 26, 200–206. https://doi.org/10.1016/j.conbuildmat.2011.06.010

European Aluminium Foil Association, n.d. Did you know? - EAFA - The home of aluminium foil [WWW Document].

Hamad, A.J., 2014. Materials, Production, Properties and Application of Aerated Lightweight Concrete: Review. Int. J. Mater. Sci. Eng. 2, 152–157. https://doi.org/10.12720/ijmse.2.2.152-157

Hlavacek, P., 2014. Engineering properties of alkali activated composites 1–88.

Holt, E., Raivio, P., 2005. Use of gasification residues in aerated autoclaved concrete. Cem. Concr. Res. 35, 796–802. https://doi.org/10.1016/j.cemconres.2004.05.005

Hong, S.H., Lee, D.W., Kim, B.K., 2000. Manufacturing of aluminum flake powder from foil scrap by dry ball milling process. J. Mater. Process. Technol. 100, 105–109. https://doi.org/10.1016/S0924-

0136(99)00469-0

Jones, M.R., McCarthy, A., 2006. Heat of hydration in foamed concrete: Effect of mix constituents and plastic density. Cem. Concr. Res. 36, 1032–1041. https://doi.org/10.1016/j.cemconres.2006.01.011

Keawpapasson, P., Tippayasam, C., Ruangjan, S., Thavorniti, P., Panyathanmaporn, T., Fontaine, A., Leonelli, C., Chayasuwan, D., 2014. Metakaolin-Based Porous Geopolymer with Aluminium Powder. Key Eng. Mater. 608, 132–138. https://doi.org/10.4028/www.scientific.net/KEM.608.132

Melo, J.P., 2013. Desarrollo y caracterización de un material celular de alta porosidad con base cementicia activada mediante agentes inorgánicos.

Mo, K.H., Alengaram, U.J., Jumaat, M.Z., Yap, S.P., Lee, S.C., 2016. Green concrete partially comprised of farming waste residues: A review. J. Clean. Prod. 117, 122–138. https://doi.org/10.1016/j.jclepro.2016.01.022

Namsone, E., Šahmenko, G., Korjakins, A., 2017. Durability Properties of High Performance Foamed Concrete. Procedia Eng. 172, 760–767. https://doi.org/10.1016/j.proeng.2017.02.120

Narayanan, N., Ramamurthy, K., 2000. Structure and properties of aerated concrete: A review. Cem. Concr. Compos. 22, 321–329. https://doi.org/10.1016/S0958-9465(00)00016-0

Narayanan, N, Ramamurthy, K., 2000. Prediction models based on gel-pore parameters for compressive strength of aerated concrete 2, 206–212.

Payá, J., Borrachero, M. V., Monzó, J., Soriano, L., 2009. Estudio del comportamiento de diversos residuos de catalizadores de craqueo catalítico (FCC) en cemento Portland. Mater. Construcción 59, 37–52. https://doi.org/10.3989/mc.2009.48108

Payá, J., Monzó, J., Borrachero, M. V., 1999. Fluid catalytic cracking catalyst residue (FC3R): An excellent mineral by-product for improving early-strength development of cement mixtures. Cem. Concr. Res. 29, 1773–1779. https://doi.org/10.1016/S0008-8846(99)00164-7

Puertas, F., Torres-Carrasco, M., 2014. Use of glass waste as an activator in the preparation of alkali-activated slag. Mechanical strength and paste characterisation. Cem. Concr. Res. 57, 95–104. https://doi.org/10.1016/j.cemconres.2013.12.005

Ramamurthy, K., Kunhanandan Nambiar, E.K., Indu Siva Ranjani, G., 2009. A classification of studies on properties of foam concrete. Cem. Concr.

Compos. 31, 388–396. https://doi.org/10.1016/j.cemconcomp.2009.04.006

Sanjayan, J.G., Nazari, A., Chen, L., Nguyen, G.H., 2015. Physical and mechanical properties of lightweight aerated geopolymer. Constr. Build. Mater. 79, 236–244. https://doi.org/10.1016/j.conbuildmat.2015.01.043

Sepulcre Aguilar, A., Pinilla Melo, J., Hernández Olivares, F., 2013. Microstructural analysis of aerated cement pastes with fly ash, Metakaolin and Sepiolite additions. Constr. Build. Mater. 47, 282–292. https://doi.org/10.1016/j.conbuildmat.2013.05.082

Song, Y., Li, B., Yang, E.H., Liu, Y., Ding, T., 2015. Feasibility study on utilization of municipal solid waste incineration bottom ash as aerating agent for the production of autoclaved aerated concrete. Cem. Concr. Compos. 56, 51–58. https://doi.org/10.1016/j.cemconcomp.2014.11.006

Tanaçan, L., Ersoy, H.Y., Arpacioğlu, Ü., 2009. Effect of high temperature and cooling conditions on aerated concrete properties. Constr. Build. Mater. 23, 1240–1248. https://doi.org/10.1016/j.conbuildmat.2008.08.007

Tashima, M.M., Akasaki, J.L., Melges, J.L.P., Soriano, L., Monzó, J., Payá, J., Borrachero, M. V, 2013. Alkali activated materials based on fluid catalytic cracking catalyst residue (FCC): Influence of SiO 2 / Na 2 O and H 2 O / FCC ratio on mechanical strength and microstructure 108, 833–839.

Tikalsky, P.J., Pospisil, J., MacDonald, W., 2004. A method for assessment of the freeze-thaw resistance of preformed foam cellular concrete. Cem. Concr. Res. 34, 889–893. https://doi.org/10.1016/j.cemconres.2003.11.005

Wongkeo, W., Thongsanitgarn, P., Pimraksa, K., Chaipanich, A., 2012. Compressive strength, flexural strength and thermal conductivity of autoclaved concrete block made using bottom ash as cement replacement materials. Mater. Des. 35, 434–439. https://doi.org/10.1016/j.matdes.2011.08.046

Zhang, Z., Provis, J.L., Reid, A., Wang, H., 2014. Geopolymer foam concrete: An emerging material for sustainable construction. Constr. Build. Mater. 56, 113–127. https://doi.org/10.1016/j.conbuildmat.2014.01.081

Zulkarnain, F., Ramli, M., 2011. Durability of Performance Foamed Concrete Mix Design with Silica Fume for Housing Development. J. M 5, 518–527.

ii. Nuevos Hormigones Celulares Geopoliméricos aireados con agua oxigenada: síntesis y propiedades

AUTORES: Alba Font, José Monzó, Lourdes Soriano, María Victoria Borrachero y Jordi Payá

REFERENCIA DE LA PUBLICACIÓN: Articulo de conferencia. HAC2018, V Congreso Iberoamericano de hormigón autocompactable y hormigones especiales (5-6 marzo, 2018)
DOI: http://dx.doi.org/10.4995/HAC2018.2018.6453

OBJETIVOS PARCIALES ABORDADOS

MATERIALES	FABRICACIÓN
• **TCC:** OPC + H2O + H2O2 • **GCC:** FCC + [WG+NaOH+H_2O] + H_2O_2 • **AACC:** BFS + [WG+NaOH+H2O] + H_2O_2	• **CURADO:** TA • **Amasado con:** NM y PD

PROCEDIMIENTO EXPERIMENTAL

CARACTERIZACIÓN DE MATERIAS PRIMAS	CARACTERIZACIÓN DE ESPECÍMENES
-	• TGA y XRD de las pastas • Densidad natural (D_N) • Resistencia mecánica (Rc) • Conductividad térmica (KD2-Pro) (λ) • Evaluación de la matriz porosa (FESEM y OM)

RESULTADOS Y CONCLUSIONES MÁS RELEVANTES DE LA INVESTIGACIÓN

- La capacidad de generación de oxígeno resultante de la descomposición del H_2O_2 y, por tanto, la formación de burbujas de aire en las matrices cementantes, resulta más estable en los sistemas alternativos (con FCC y BFS) que en los TCC, debido a la elevada alcalinidad del medio.
- La dosificación óptima de H_2O_2 en las mezclas resultó ser de un 2% respecto al peso del precursor. Una dosificación menor dio como resultado una aireación insuficiente de las matrices. Con un mayor porcentaje resulta una reacción más agresiva con poros que pierden la forma esférica y se interconectan.
- Tras 7 días de curado a temperatura ambiente se obtuvieron los siguientes resultados:

Material	D_N (kg/m^3)	Rc (MPa)	Tamaño de poros [dmin-dmáx] µm	λ (W/mK)
GCC aireados con H_2O_2	812	3.0	53.9-1014	0.236
AACC aireados con H_2O_2	711	3.8	-	0.194

Resumen: El peso propio de las estructuras resulta habitualmente del mismo orden o superior al de las cargas que tienen que soportar, lo que las hace en la mayoría de los casos poco eficientes. La solución radica en la sustitución total o parcial de hormigón tradicional por un material más ligero. El hormigón celular se considera una solución interesante y además sus propiedades aislantes termo-acústicas los hacen mas eficientes desde el punto de vista energético. En este trabajo se presenta una variante del hormigón celular tradicional a favor del medioambiente. Se diseñan hormigones celulares geopoliméricos a partir de la activación alcalina del residuo catalizador gastado de craqueo catalítico (FCC) y la adición de agua oxigenada (H_2O_2). Los materiales resultantes se caracterizan a nivel microestructural y a nivel mecánico. Finalmente se evalúan sus propiedades térmicas y se comparan con las de otros hormigones celulares tradicionales y geopoliméricos. Destaca la obtención de hormigones celulares geopoliméricos de 812 kg/cm^3 y 3.01MPa a partir de dicho precursor FCC aireado con H_2O_2. Además, se presenta como un material aislante cuya conductividad térmica se reduce hasta un 50% respecto al material tradicional fabricado a base de cemento Portland (OPC).

Palabras clave: Hormigón Celular, geopolímeros, agua oxigenada.

1. Introducción

Un Hormigón Ligero (HL) es aquel que mediante diversos métodos aplicados en el proceso de su elaboración resulta más ligero que el hormigón tradicional (R- et al., 1999). Esta disminución en la densidad permite obtener un material que reduce las cargas muertas estructurales, una mayor rapidez de construcción y supone un menor coste de transporte. Además, este tipo de hormigones se caracterizan por tener una importante capacidad aislante, por ello, es un material óptimo desde el punto de vista de la eficiencia energética (Kim et al., 2012).

La propiedad intrínseca de los HL es su baja densidad, que se consigue por la inclusión de aire en la matriz de hormigón (R- et al., 1999). Una de las tipologías de este tipo de hormigones es el hormigón celular tradicional (HCT): se trata de una pasta o mortero de cemento Portland (OPC), y en algunos casos con adición de cal hidratada, con un sistema cerrado de microburbujas de aire que ocupa hasta el 85% del material. Este sistema de burbujas se puede generar mediante la adición de: i) agentes tensoactivos; o ii) agentes generadores de gas. Entre estos últimos se encuentra el polvo de aluminio metálico (por generación de hidrógeno molecular) y el peróxido de hidrogeno (H_2O_2) (por generación de oxígeno molecular).

Algunos estudios sobre las propiedades de los HCTs revelan que en general se caracterizan por alcanzar valores de densidad en el intervalo de 300 a 1400 kg/m^3, con resistencias mecánicas del orden de 1-15 MPa (Ramamurthy et al., 2009). Además, reducen la conductividad térmica en un 5% - 30% respecto a la del hormigón tradicional (Jones and McCarthy, 2006; Wongkeo et al., 2012) y resultan interesantes desde el punto de vista de la durabilidad ya que son

resistentes al ataque de bacterias y al fuego (Dolton and Hannah, 2006; Melo, 2013).

Sin embargo, desde el punto de vista ecológico, el HCT presenta un alto impacto medioambiental debido al elevado consumo de OPC necesario para su producción (70% en masa). Es bien conocido que la producción del OPC lleva asociada una importante demanda energética, el consumo de materias primas no renovables (Mo et al., 2016) y contribuye en un 5-7% de las emisiones globales de CO_2 a la atmosfera (Puertas and Torres-Carrasco, 2014).

Una forma de obtener este tipo de hormigones celulares con menor impacto medioambiental es por medio del uso de matrices geopoliméricas, de modo que el OPC es sustituido por un precursor mineral y una disolución activadora alcalina: son los conocidos como hormigones celulares geopoliméricos (HCG) (Arellano Aguilar et al., 2010; Esmaily and Nuranian, 2012).

El objetivo de la presente investigación es analizar el efecto aireante que produce el agua oxigenada (H_2O_2) en matrices geopoliméricas de residuo de catalizador de craqueo catalítico (FCC). Para ello se ha fabricado una serie de HCGs (con una dosificación constante a base de este precursor) a los que se ha adicionado distintos porcentajes de H_2O_2. El fundamento de uso de este generador de gas es la formación de oxígeno molecular a partir de la descomposición en medio alcalino. El H_2O_2 es termodinámicamente inestable y se descompone fácilmente en agua y gas oxígeno (**Ecuación 4.ii.1**):

$$2H_2O_2 \rightarrow 2H_2O + O_2 \qquad (4.ii.1)$$

Los materiales han sido caracterizados a nivel microestructural, y se han estudiado los productos cementantes, mediante las técnicas de termogravimetría y difracción de rayos X (DRX). A continuación, se ha procedido a su caracterización mecánica y física, determinando su densidad natural (ρ) y resistencia mecánica a compresión (Rc) a la edad de 7 días, así como la caracterización de su red porosa mediante las técnicas de microscopía óptica (OM) y microscopía electrónica de barrido con emisión de campo (FESEM). Estos ensayos han permitido determinar el porcentaje óptimo de adición de H_2O_2 con el que se consigue fabricar HCGs de FCC con matrices estables y con buenas propiedades. Finalmente se ha procedido al estudio de las propiedades térmicas de los HCGs seleccionados. Las características físicas, mecánicas y térmicas de estos últimos se han comparado con los obtenidos para sistemas de HCT a base de OPC, así como, para otros sistemas de HCGs con escoria de alto horno (BFS) como precursor mineral.

2. Materiales y métodos

2.1. Materiales y propiedades

Para la síntesis de HCGs se ha empleado dos precursores minerales: i) FCC es un residuo de la industria petroquímica, compuesto principalmente por SiO_2

(47.76%) y Al_2O_3 (49.26%) y ha sido suministrado por la planta de la empresa BP Oil (Grao de Castellón, España); y ii) BFS está compuesta por CaO (40.15%), SiO_2 (30.53%) y Al_2O_3 (10.55%) y ha sido suministrada por la empresa Cementval S.A (Puerto de Sagunto, España). El OPC para la fabricación de HCT, ha sido suministrado por Lafarge (Puerto de Sagunto, España). Para la elaboración de la disolución activadora en HCGs se ha empleado hidróxido de sodio en pellets (pureza del 98%) y silicato de sodio (8% Na_2O, 28% SiO_2 y 64% H_2O), ambos suministrados por la empresa Merck (España). Como reactivo generador de gas se ha empleado una solución 30% w/w de peróxido de hidrógeno H_2O_2, suministrada por J.T Baker (España).

2.2. Procedimiento experimental

El procedimiento experimental seguido para el desarrollo del presente estudio se ha dividido en dos fases: la fase (i) en la que se compara el efecto del porcentaje de H_2O_2 sobre el HCG (en base FCC) y la fase (ii) en la que se comparan las características del mejor HCG de la fase (i) con las de HCT (con cemento Portland, OPC) y otro tipo de HCG (con escoria, E).

En la primera fase (i) experimental se ha fabricado 6 probetas cúbicas de 64 cm^3 con adiciones de H_2O_2 del 2%, 2.5% y 3% respecto al peso del precursor y con una relación agua/precursor de 0.50. Para la segunda fase (ii) se ha fabricado 8 probetas cúbicas de 1000cm^3 con un 2% de H_2O_2 y con una relación agua/precursor para los HCGs de 0.5 con el empleo de FCC y de 0.25 con BFS. Los HCT tienen una relación agua/OPC de 0.40. La disolución activadora en todos los casos ha sido X/Y = 7.5/1.7, donde X representa la concentración molar de sodio en el activador (Na^+) e Y es la relación molar SiO_2/Na_2O.

Respecto a la fabricación de los hormigones celulares, el H_2O_2 se ha incorporado a las mezclas tras el amasado previo del precursor y de la disolución activadora (el agua en el caso del HCT), y se ha agitado durante 90 segundos. El curado se ha llevado a cabo en cámara húmeda a 23ºC y 100% H.R. Las muestras han sido enrasadas con una sierra dentada de manera manual a las 24 horas de la mezcla en el molde y, posteriormente, se ha procedido al desmoldeado de las mismas. En la **Fig.4.ii.1** se pueden observar los moldes empleados para la confección de probetas cúbicas, el procedimiento de enrasado/corte y las probetas cúbicas resultantes para cada una de las fases experimentales.

La nomenclatura empleada para la identificación de los materiales viene dada por: (A)-(B)POX, donde: (A) se corresponde con la materia prima empleada como precursor (FCC, BFS o OPC); y (B) representa el porcentaje de H_2O_2 adicionado.

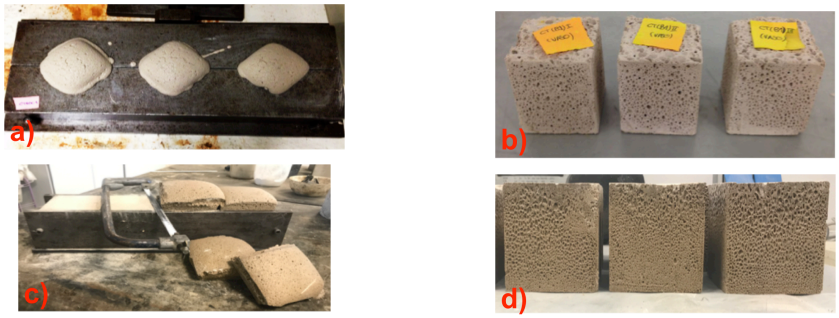

Fig.4.ii.1 *Moldes y probetas preparadas: a) molde para 3 probetas cúbicas de 64 cm^3, con el material expandido por generación de gas en el interior; b) probetas de 64cm^3 para la primera fase (i) experimental; c) molde para 4 probetas cúbicas de 1000 cm^3 en el momento previo al desmoldeado tras su enrase; d) probetas de 1000 cm^3 para la segunda fase (ii) experimental.*

Para realizar la caracterización microestructural en cada una de las amasadas, se ha tomado una muestra de material fresco en un recipiente cilíndrico de plástico con cierre hermético. Los ensayos termogravimétricos se han realizado utilizando un módulo TGA 850 Mettler-Toledo. La técnica de DRX se ha se ha llevado a cabo con un difractómetro modelo Bruker AXS D8 Advance. La densidad natural (ρ) se ha determinado mediante el peso de las probetas cúbicas antes del ensayo de resistencia a compresión. El ensayo mecánico de resistencia a compresión (Rc) se ha realizado con una máquina de ensayo universal INSTRON 3282. Con los resultados obtenidos se han calculado los promedios y los valores de desviación estándar. Se ha medido los diámetros de poro mediante el procesado de: i) micrografías tomadas con un microscopio electrónico de barrido de emisión de campo (FESEM) modelo ULTRA 55 de la marca ZEISS; y ii) fotografías de las superficies internas de las probetas (16 cm^2), tomadas con un microscopio óptico modelo S8 APO de la marca Leica en comunicación con una cámara digital modelo DFC 420 de la marca Leica. Los ensayos de conductividad térmica se han llevado a cabo con un equipo KD2-Pro desarrollado por la empresa Decagon Devices (NE Hopkins Court Pullman, EEUU) y comercializado en España por Lab Ferrer (Madrid, España). Se ha incorporado un sensor RK-1 para rocas y hormigones, que mide las propiedades térmicas en base al "Método de la Aguja Térmica" recogido en las normas ASTM D5334-08 y IEEE Standard 442-1981 (ASTM International, n.d.; "IEEE 442-1981 - IEEE Guide for Soil Thermal Resistivity Measurements," n.d.).

3. Resultados y discusión

3.1. Primera fase (i) experimental

En los ensayos termogravimétricos se ha observado para todos los materiales una evolución muy similar de los productos de hidratación. Las curvas DTG presentan un pico característico en el intervalo de temperaturas de 100ºC a 200ºC que se corresponde con la formación de geles tipo NASH durante la

reacción de geopolimerización. A los 7 días de curado aparece como un doble pico y con el tiempo se observa un ensanchamiento, que deja un pico de mayor intensidad con un hombro a baja temperatura. Con el paso del tiempo de curado, se observa un ensanchamiento del pico hacia temperaturas altas, lo que sugiere que se incrementa la cantidad de agua combinada químicamente y que los enlaces son más robustos. (**Fig.4.ii.2a y 4.ii.2b**). Además, con el tiempo de curado se produce un aumento de la pérdida de masa total (en el intervalo 35-600ºC) (**Fig.4.ii.2a y 4.ii.2b**): lo que nos indica que se está produciendo una formación progresiva de producto gel. Este comportamiento concuerda con las conclusiones de trabajos previos sobre conglomerantes activados alcalinamente de FCC (Tashima et al., 2013).

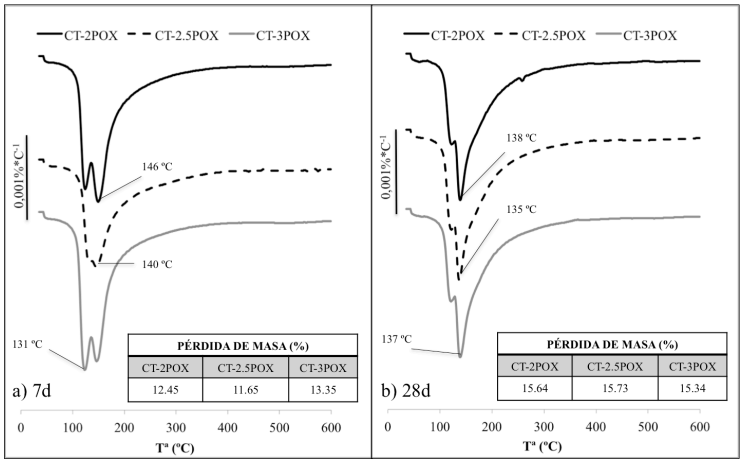

Fig.4.ii.2 *Resultados de termogravimetría de las pastas: a) curvas DTG y % relativo de pérdida de masa a los 7 días de edad; b) curvas DTG y % relativo de pérdida de masa a los 28 días de edad.*

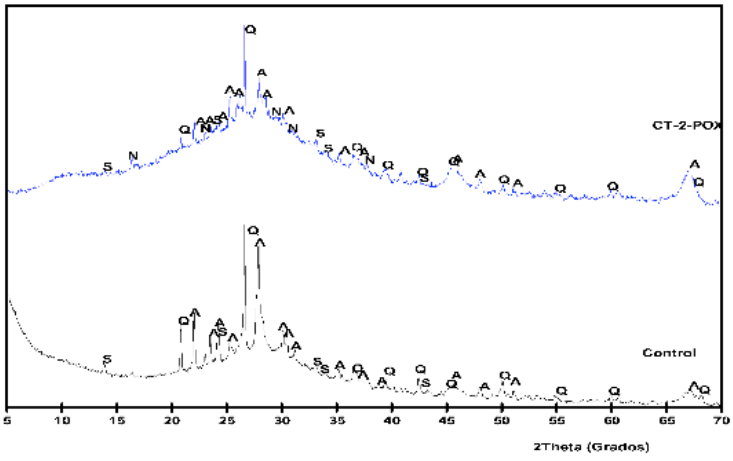

Fig.4.ii.3 *Difractogramas correspondientes a las pastas HCG*

En la **Fig.4.ii.3** se muestran los difractogramas de una pasta de FCC y de la pasta CT-2POX, ambas a 7 días de curado. En ambas muestras se observa los picos cristalinos del cuarzo (Q) (PDF Card 331161) y albita (PDF Card 191184), así como trazas de la formación de una zeolita, la hidrosodalita (PDF Card 311271). En la pasta tratada con agua oxigenada, además se ha detectado natrón (PDF Card 150800), posiblemente debido a una pequeña carbonatación de la pasta. También se detecta una fuerte desviación de la línea base, en el intervalo 20-35º 2θ debido a la formación de geles amorfos tipo NASH. Esta zona está mucho más desarrollada en la pasta tratada con agua oxigenada que en la pasta control de FCC.

Por otra parte, los resultados obtenidos de densidad natural (ρ) y resistencia mecánica a compresión (Rc) a los 7 días de curado en cámara húmeda, se reflejan en la **Tabla 4.ii.1**. Todos los valores de densidad natural obtenidos están por debajo de 1000 kg/m^3 y las prestaciones mecánicas han resultado superiores a 1MPa.

Tabla 4.ii.1
Primera fase experimental: resultados de densidad (ρ), resistencia mecánica a compresión (Rc) e intervalo de tamaño de poros (7 días de curado).

			Tamaño de poro (mm)	
Material	*ρ (kg/m^3)*	*Rc (MPa)*	*Máx.*	*Mín.*
CT-2POX	965±4	2.67 ± 0.17	0.539	1.014
CT-2.5POX	938±5	1.87 ± 0.03	0.110	2.009
CT-3POX	902±5	1.05 ± 0.35	0.052	4.002

Los valores dejan de manifiesto que la ρ decrece de manera ligera a medida que el porcentaje de H_2O_2 aumenta. La Rc también decrece, aunque en este caso el cambio que experimenta esta propiedad a medida que aumenta la cantidad de H_2O_2 resulta de mayor magnitud. Así, cuando comparamos un 2% con un 2.5% de adición, la ρ decrece en un 3% y la Rc disminuye 0.80 MPa. En el caso de comparar el 2.5% con el 3% de adición, la disminución en la ρ resulta de un 4% y la Rc desciende en 0.82 MPa. Finalmente, si comparamos los valores extremos entre un 2% y un 3%, observamos que la ρ ha disminuido únicamente un 7% mientras que la Rc se ha reducido en 1.62 MPa (60% de pérdida). Según estos resultados se puede afirmar que la reacción de aireación no esta siendo lo suficientemente efectiva al aumentar el porcentaje de H_2O_2 ya que las densidades no experimentan una disminución tal que avale la pérdida de resistencia mecánica (ver datos en **Tabla 4.ii.1**).

El análisis de la red porosa de los HCGs de FCC permite diferenciar la influencia que ejerce la dosificación del H_2O_2 sobre el desarrollo de la matriz interna del material. Mediante esta técnica microscópica/óptica se consigue comparar el tamaño de poros (tanto en escala micro como macro), la distribución de los mismos y, además, es posible comprobar la compacidad resultante de la matriz del material y su posible influencia tanto en la ρ como en la Rc.

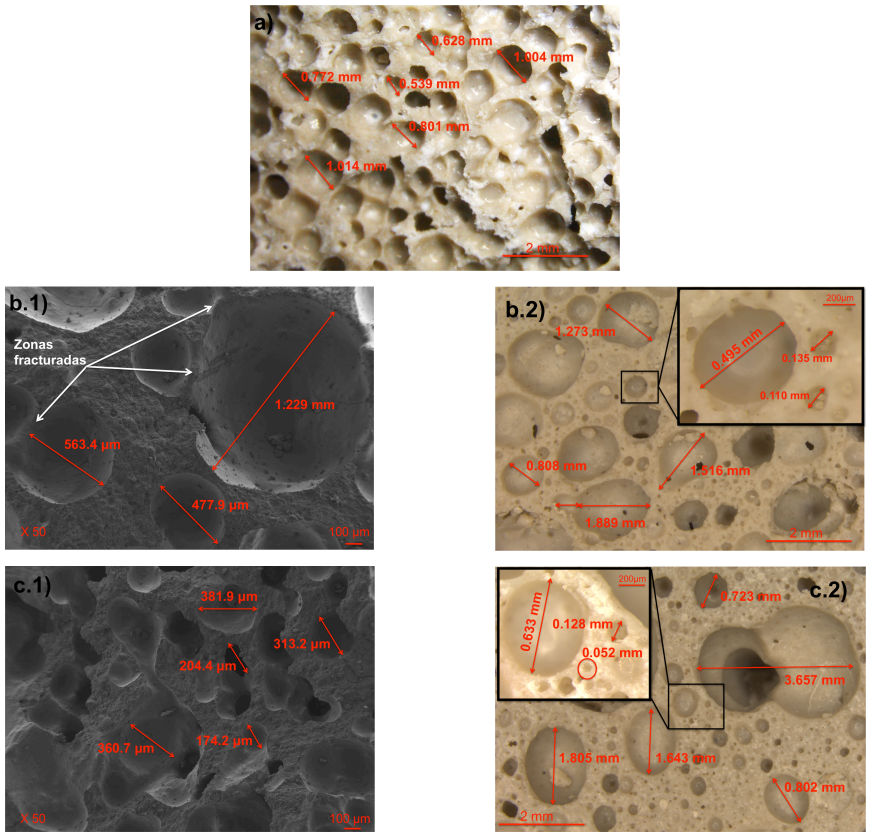

Fig.4.ii.4 *Análisis de la red porosa: a) muestra CT_2POX: Fotografía lupa de una superficie (16cm^2); b) muestra CT_2.5POX: 1. Micrografía FESEM de una porción, 2. Fotografía lupa de una superficie (16cm^2); c) muestra CT_3POX: 1. Micrografía FESEM de una porción, 2. Fotografía lupa de una superficie (16cm^2).*

El sistema CT-2POX se caracteriza por tener una matriz densa con huecos que tienen un diámetro esférico constante y que en la mayoría de casos se encuentran aislados sin interconexión entre los mismos. El material presenta huecos de tamaños en el intervalo de 0.539 a 1.014 mm (**Fig.4.ii.4a**). En el caso de aumentar el porcentaje de H_2O_2 a 2.5%, se observa que la distribución de poros, en cuanto a su tamaño, deja de ser homogénea y la matriz contiene poros que van desde 0.110 a 2.009 mm (**Fig.4.ii.4b1 y 4.ii.4b2**). Además, la forma de los poros empieza a tener una geometría ovalada en algunos casos, debido a la interconexión entre los de mayor tamaño con los de menor tamaño. Este cambio geométrico se ve mucho más acentuado en las micrografías y fotografías correspondientes a CT-3POX, donde los poros observados tienen un intervalo de tamaños desde 0.052 a 4.002 mm, mucho mayor que en los casos anteriores (**Fig.4.ii. 4c1 y 4.ii.4c2**).

Este cambio en la configuración de la red porosa de los materiales, a medida que aumenta el porcentaje de adición de H_2O_2, podría explicar la caída de resistencia observada entre CT-2POX y CT3POX. En el caso de adicionar un 2% de H_2O_2 la cinética de descomposición hace que se generen cantidades importantes de oxígeno, pero que no son lo suficientemente grandes como para producir la conexión entre burbujas. De este modo, se produce una mejor distribución de la matriz cementante alrededor de las burbujas de gas generadas. Cuando se aumenta el porcentaje de H_2O_2, la reacción resulta más agresiva y la cantidad de oxígeno liberada es mayor. La matriz cementante fresca deja de tener la resistencia suficiente para vencer el empuje que ejerce el gas sobre la interfase aire/pasta, provocando así su rotura. Es por tanto evidente, que la reología de la pasta juega un papel fundamental sobre el desarrollo de la estructura celular del HCG producido con H_2O_2.

3.2. Segunda fase (ii) experimental

La conductividad térmica resultante para los HCG tanto de FCC como de BFS, así como para el HCT se recoge en la **Tabla 4.ii.2**, junto con los valores de densidad y la resistencia mecánica a compresión a los 7 días de curado.

Tabla 4.ii.2
Segunda fase experimental: resultados de densidad (ρ), resistencia mecánica a compresión (Rc) y conductividad térmica (K) (7 días de curado).

Material	*ρ (kg/cm³)*	*Rc (MPa)*	*K (w/mk)*
CT-2POX	812±10	3.01 ± 0.13	0.236 ± 0.01
E-2POX	711±4	3.83 ± 0.06	0.194 ± 0.02
OPC-2POX	1042±19	6.50 ± 0.12	0.473 ± 0.01

A partir de los datos de densidad, se debe hacer notar que la densidad obtenida para los HCGs (CT-2POX y E-2POX) es significativamente menor que la obtenida para HCT (OPC-2POX): se produce una diferencia de unos 200-300 kg/m^3. Esta diferencia, a pesar de haber usado la misma cantidad de H_2O_2, puede ser debida a que la reacción de descomposición es más rápida para los sistemas geopoliméricos. Estos sistemas tienen una mayor alcalinidad, y por ello hacen que la estabilidad de H_2O_2 se vea influenciada de forma notable, de modo que la velocidad de generación del oxígeno se produce mayoritariamente mientras la mezcla se encuentra en estado fresco (fase previa al fraguado).

Por otra parte, la resistencia mecánica, se ha reducido a la mitad para los HCGs (CT-2POX y E-2POX), respecto al HCT. Esto se puede atribuir a los valores de densidad obtenidos para cada uno de los materiales (ver **Tabla 4.ii.2**).

Finalmente, con respecto a los valores de conductividad térmica, se ha observado una clara correlación entre esta propiedad y la densidad de los materiales. Se ha obtenido una mayor capacidad aislante con ambos sistemas de HCGs respecto a los sistemas a base de OPC. Con el empleo de FCC (CT-2POX) se consigue reducir los valores de conductividad térmica a los 7 días de

edad, respecto al HCT, un 50% y con el empleo de BFS (E-2POX) un 60%, (ver **Tabla 4.ii.2**).

4. Conclusiones

Los ensayos microestructurales de caracterización química evidencian que el desarrollo del proceso de geopolimerización y la evolución de los productos cementantes propios de los materiales de FCC activado alcalinamente, no se ven alterados al incorporar H_2O_2 en las mezclas, independientemente del porcentaje adicionado.

Se ha obtenido un material ligero, con buenas prestaciones mecánicas y con una red porosa estable, continua y homogénea mediante la adición de un 2% de H_2O_2. Como resultado, se ha desarrollado un HCG a base de FCC con 812.1 kg/cm^3 y 3.01 MPa, cuya conductividad térmica resulta un 50% menor que la correspondiente a un HCT

Con un aumento en el porcentaje de H_2O_2 resulta una reacción de generación de gas más agresiva, con poros que pierden la forma esférica y se interconectan. Como consecuencia, la densidad del material disminuye, y se produce una pérdida significativa de resistencia mecánica.

Se ha demostrado que la capacidad de generación de oxígeno resultante de la descomposición del H_2O_2 y la formación de burbujas de gas en los matrices cementantes resulta mucho más estable en los sistemas geopoliméricos debido a su elevada alcalinidad.

El presente estudio pone de manifiesto la posibilidad de fabricar nuevos hormigones celulares geopoliméricos aireados con agua oxigenada, utilizando como precursor un residuo de la industria petroquímica como es el FCC.

Agradecimientos

Los autores del presente documento quieren mostrar su especial agradecimiento a GEOCELPLUS (proyecto interno de la Universitat Politècnica de València). Se agradece también al Servicio de Microscopía Electrónica de la UPV.

Referencias

Arellano Aguilar, R., Burciaga Díaz, O., Escalante García, J.I., 2010. Lightweight concretes of activated metakaolin-fly ash binders, with blast furnace slag aggregates. Constr. Build. Mater. 24, 1166–1175. https://doi.org/10.1016/j.conbuildmat.2009.12.024

ASTM International, n.d. ASTM D5334 - 14 Standard Test Method for Determination of Thermal Conductivity of Soil and Soft Rock by Thermal Needle Probe Procedure [WWW Document].

Dolton, B., Hannah, C., 2006. Cellular Concrete : Engineering and Technological Advancement for Construction in Cold Climates 1–11.

Esmaily, H., Nuranian, H., 2012. Non-autoclaved high strength cellular concrete from alkali activated slag. Constr. Build. Mater. 26, 200–206. https://doi.org/10.1016/j.conbuildmat.2011.06.010

IEEE 442-1981 - IEEE Guide for Soil Thermal Resistivity Measurements [WWW Document], n.d.

Jones, M.R., McCarthy, A., 2006. Heat of hydration in foamed concrete: Effect of mix constituents and plastic density. Cem. Concr. Res. 36, 1032–1041. https://doi.org/10.1016/j.cemconres.2006.01.011

Kim, H.K., Jeon, J.H., Lee, H.K., 2012. Workability, and mechanical, acoustic and thermal properties of lightweight aggregate concrete with a high volume of entrained air. Constr. Build. Mater. 29, 193–200. https://doi.org/https://doi.org/10.1016/j.conbuildmat.2011.08.067

Melo, J.P., 2013. Desarrollo y caracterización de un material celular de alta porosidad con base cementicia activada mediante agentes inorgánicos.

Mo, K.H., Alengaram, U.J., Jumaat, M.Z., Yap, S.P., Lee, S.C., 2016. Green concrete partially comprised of farming waste residues: A review. J. Clean. Prod. 117, 122–138. https://doi.org/10.1016/j.jclepro.2016.01.022

Puertas, F., Torres-Carrasco, M., 2014. Use of glass waste as an activator in the preparation of alkali-activated slag. Mechanical strength and paste characterisation. Cem. Concr. Res. 57, 95–104. https://doi.org/10.1016/j.cemconres.2013.12.005

R-, a C.I., Committee, a C.I., Mechanics, F., Cedolin, L., Darwin, D., Hawkins, N.M., Isenberg, J., Li, V.C., Lin, F., Mccabe, S.L., Mau, S., Mazars, J., Naaman, A.E., Norman, C.D., Pfeiffer, P. a, Vellore, S.J., Pijaudier-cabot, G., Saouma, V., Sierakowski, R.L., Sward, S.E., Tsubaki, T., Gettu, R., Hillerbor, A., 1999. Fracture Mechanics of Concrete : Concepts , Models and Determination of Material Properties Secretary 91, 1–2.

Ramamurthy, K., Kunhanandan Nambiar, E.K., Indu Siva Ranjani, G., 2009. A classification of studies on properties of foam concrete. Cem. Concr. Compos. 31, 388–396. https://doi.org/10.1016/j.cemconcomp.2009.04.006

Tashima, M.M., Akasaki, J.L., Melges, J.L.P., Soriano, L., Monzó, J., Payá, J., Borrachero, M. V., 2013. Alkali activated materials based on fluid catalytic cracking catalyst residue (FCC): Influence of SiO_2/Na_2O and H_2O/FCC ratio on mechanical strength and microstructure. Fuel 108, 833–839. https://doi.org/10.1016/j.fuel.2013.02.052

Wongkeo, W., Thongsanitgarn, P., Pimraksa, K., Chaipanich, A., 2012. Compressive strength, flexural strength and thermal conductivity of autoclaved concrete block made using bottom ash as cement replacement materials. Mater. Des. 35, 434–439. https://doi.org/10.1016/j.matdes.2011.08.046

iii. New cellular geopolymer concretes (CGC) based on blast furnace slag and spent FCC catalyst

AUTORES: Alba Font, José Monzó, Lourdes Soriano, María Victoria Borrachero y Jordi Payá

REFERENCIA DE LA PUBLICACIÓN: Articulo de conferencia. NOCMAT17, Non-Conventional Materials and Technologies. Materials Research Proceedings, 7 (2018) 685-694
DOI: http://dx.doi.org/10.21741/9781945291838-66

OBJETIVOS PARCIALES ABORDADOS

MATERIALES	FABRICACIÓN
• **TCC:** OPC + H_2O + SLS • **TCC:** OPC + H_2O + SLS/A • **GCC:** FCC + [WG+NaOH+H_2O] + SLS • **GCC:** FCC + [WG+NaOH+H_2O] + SLS/A • **AACC:** BFS + [WG+NaOH+H_2O] + SLS • **AACC:** BFS + [WG+NaOH+H_2O] + SLS/A	• **CURADO:** TA • **Amasado con:** NM

PROCEDIMIENTO EXPERIMENTAL

CARACTERIZACIÓN DE MATERIAS PRIMAS	CARACTERIZACIÓN DE ESPECÍMENES
-	• Densidad natural (D_N) • Resistencia mecánica (Rc) • Evaluación de la matriz porosa (FESEM y OM)

RESULTADOS Y CONCLUSIONES MÁS RELEVANTES DE LA INVESTIGACIÓN

- El proceso mecánico de formación de poros mediante la adición de agentes espumantes (SLS) suele resultar más controlable que el proceso químico mediante la adición de aireantes (A). La investigación reveló que la combinación de ambos métodos resulta en mayor efectividad en la configuración de la matriz porosa para los GCC y para los AACC.
- La adición de un 0.2 % de SLS combinado con un 0.05 % de A (dosificaciones en peso respecto del precursor) resultó óptima. Los resultados obtenidos fueron mejores que cuando únicamente se adicionó a las mezclas un 2 % de SLS.
- Tras 7 días de curado a temperatura ambiente se obtuvieron los siguientes resultados:

Material	D_N (kg/m^3)	Rc (MPa)	Tamaño de poros [dmin-dmáx] (µm)
GCC aireados con SLS	1276	5.7	20.1-695
GCC aireados con SLS/A	1143	6.9	22.1-3594
AACC aireados con SLS	1345	6.8	15.6-470
AACC aireados con SLS/A	1046	8.6	24.6-2611

Abstract: In current society, the study and development of new construction materials with the aim of improve its sustainability and clean production represents an important goal to be achieved by scientific communities worldwide. This work presents the preliminary studies of new cellular geopolymer concretes (CGC), which combines energy and economic savings achievable through the use of cellular concrete, with the reduction of greenhouse gas emissions well-known linked with the substitution of traditional Portland cement binder by new geopolymer binder. Blast furnace slag (BFS) and spent FCC catalyst (FCC) were used as mineral precursors in CGC preparation, and two methods of pore formation were evaluated in each matrix: (i) mechanical, by addition of commercial grade synthetic surfactant (sodium lauryl sulphate); and (ii) a combined procedure, by mixing of this surfactant and aluminium powder. Pore distribution analyses were also performed. The results confirm the viability of producing cellular geopolymer concretes based on FCC as well as BFS by combined both foaming and aerating techniques. The obtained CGCs were mechanically characterized (5-8 MPa), yielding densities 30% lower respect to OPC systems, showing a compacted matrix and a homogeneous pore structure.

Keywords: Cellular concrete, geopolymer, aluminium powder, sodium lauryl sulphate

1. Introduction

Traditional cellular concrete (TCC) is a lightweight material consisting either Portland cement (OPC) paste or mortar with a homogeneous pore structure, created by the addition of suitable reagents. Depending on the method of air entrapped into the matrix, cellular concrete is conventionally classified in three groups (Narayanan and Ramamurthy, 2000): (i) by chemical reaction of metallic powders in high alkaline medium, generating a gas (aerated concrete or gas concrete); (ii) by mechanical procedures with adding bubble stabilizer or surfactant (foamed concrete); and (iii) by combination of chemical and mechanical procedures. The air-bubbles are entrapped into the fresh cement matrix and they are stabilized before setting. As a result, a low-density composite with moderate strength and good performance in acoustic and thermal insulations is achieved. It combines great properties of constructive and insulation materials (Hamad, 2014; Namsone et al., 2017; Othuman and Wang, 2011; Wongkeo et al., 2012).

The production of TCC requires a large amount of Portland cement; about 70% by weight is confirmed by this material (Mo et al., 2016). Since, it is well known that the production of Portland cement requires a high-energy demand, the consumption of non-renewable raw materials (Wongkeo et al., 2012) and the emission of greenhouse gases (around 5-7% of global CO_2 emissions) (Huntzinger and Eatmon, 2009), it is evident that alternative ways to produce cellular concretes are needed. Thus, the use of new alkali-activated cement, commonly referred to as “Geopolymer foam concrete (GFC)”, are currently on study (Arellano Aguilar et al., 2010; Esmaily and Nuranian, 2012;

Sanjayan et al., 2015; Zhang et al., 2014), in order to contribute to the current phenomenon of global warming and the corresponding environmental impact.

Geopolymers (or alkali activated materials) are inorganic polymeric materials which manufacture involves a chemical reaction between amorphous alumino-silicate raw materials and alkali silicate-hydroxide solutions (in high concentration) yielding stable three-dimensional polymeric structures. As a result, the production of "green concrete" with a lower both energy requirement and carbon footprint can be achieved (Duxson et al., 2007). Several types of by-products and/or wastes are generally reported as suitable precursors for preparing geopolymeric binders such as fly ash, blast furnace slag or calcined clay. Besides the viability of using spent FCC catalyst, a waste from the petroleum industry, as a precursor in geopolymers by means alkali activation was demonstrated by some authors (Tashima et al., 2012).

In cellular concrete, the chosen method of pore formation, (by gas release, by foaming or by combined method) influences the microstructure, the resultant pore structure, and thus its properties. For foamed concretes, in order to develop an optimal and stable void system into the matrix, the controlled range of paste consistency is vital therefore a controlled water/binder is required (Tashima et al., 2012; Zhang et al., 2014). In case of aerated concrete, in order to improve the reaction of aerating agent and the development of a material with great air-void system, the alkalinity of the medium, a controlled consistency and fast setting time are the primordial factors (Narayanan and Ramamurthy, 2000). The improvement of structural and functional properties is directly affected by a stable structure and spherical cell structure. Besides, to obtain composites with uniform density the pores have to be uniformly distributed. The materials with a void system where macropores are dominant are reported to reduce the density significantly and it involves an important strength drop. The compressive strength of cellular concretes decreases exponentially with a reduction in density (Ramamurthy et al., 2009; Sanjayan et al., 2015; Zhang et al., 2014).

In this research the use of geopolymeric binder is proposed for the preparation of alternative cellular concrete: cellular geopolymer concrete (CGC). To this end, two precursors were tested: blast furnace slag (BFS) and spent FCC catalyst (FCC), also to compare and value the potential of the geopolymeric binders to cellular systems production, two methods of air entrapping were carried out: (i) foaming by means the addition of commercial grade synthetic surfactant (sodium lauryl sulphate (SLS)); and (ii) by combining mechanical (foaming) and chemical procedures, with the mixing of this surfactant (SLS) and metallic aluminium powder (A). The materials obtained were compared to that obtained by using Portland cement (OPC) (obtained by the same void-forming methods), meaning a traditional cellular concrete (TCC) system. Density, compressive strength development and air-void distributions for TCC and CGC were analysed.

2. Materials and methods

2.1. Materials

Two precursors were used to prepare the CGC mixes object of the present study. On the one hand, FCC, that was supplied by BP Oil Company (Grao de Castellón, Spain). FCC is a waste from the petrochemical industries rich in SiO_2 (47.76%) and Al_2O_3 (49.26%), and is characterized by its mixed structure which is amorphous and contains some crystalline phases of zeolites type faujasite ($Na_2Al_2Si_4O_{12}{\cdot}8(H_2O)$), as well as mullite ($Al_6Si_2O_{13}$). And, on the other hand, BFS that was supplied by Cementval S.A (Puerto de Sagunto, Spain). This precursor is an amorphous industrial by-product rich in CaO (40.15%), SiO_2 (30.53%) and Al_2O_3 (10.55%), which contains some crystalline phases such as calcite ($CaCO_3$) and merwinite $Ca_3Mg(SiO_4)_2$. A previous milling treatment of the FCC as well as BFS was necessary in order to improve their behaviour as a geopolymer precursors, obtaining: d_{50}= 17.1µm for the FCC; and d_{50}= 26.6µm for the BFS. A ball mill (Gabrielli Mill-2) was used for grinding the raw materials and the particle sizes were measured by means Malvern Instruments Mastersizer 2000. Ordinary Portland cement (OPC), used in TCC mixes, was supplied by Lafarge (Puerto de Sagunto, Spain).

Alkali activating solution used for the synthesis of geopolymers was made from a mix of sodium hydroxide pellets (Panreac, 98% purity) and a waterglass solution (Merck, 8% Na_2O, 28% SiO_2 and 64% H_2O) The alkaline activator stoichiometry is defined by X/Y factor, where X is the Na^+ molality and Y represents the SiO_2/Na_2O molar ratio.

Sodium lauryl sulphate (SLS) is a synthetic foaming agent (bubble stabilizer agent), an alkyl sulphate from (Panreac); and commercial aluminium powder (A) for the gas production in the paste (by its reaction in alkali medium, **Equation. 4.iii.1**.) which was supplied by Schlenk Metallic Pigments GmbH (98% of purity with mean diameter size of 30 µm).

$$Al\,(s) + 3H_2O + OH^-_{(ac)} \Rightarrow Al(OH)_4^-{}_{(ac)} + 3/2\,H_{2\,(g)} \qquad (4.iii.1)$$

2.2. Experimental procedure

The first step to prepare the CGCs samples (as by the use of FCC as BFS) was to ready the alkali solution and wait for 2 or 3 hours until it reached room temperature. Then this solution is putting in the mechanical mixer and shaken

for 30 seconds. The solid precursor was dry pre-mixed with SLS or A/SLS (in each case) and it was added during the follow 60 seconds into the mixer. The CGC was plus mixed for 90 seconds. For the TCC reference material the OPC dry pre-mixed with SLS or A/SLS (in each case) and it was mechanically mixed with water for 90 seconds. Due to the expansion process of the pastes, no compacting treatment was carried out, in order to avoid the gas escaping from the cementing matrix during the setting process. For each resulting paste, six cube specimens of dimensions 4x4x4 cm^3 were moulded and cured in a wet chamber (23ºC and 100% R.H) for 24 hours. After this, the free surface of the cubes had to be cut out with a saw blade and the specimens were de-moulded. Finally, the samples were kept in wet chamber until testing at 7 days. An overview of samples and its composition can be found in **Table 4.iii.1**. C-S, F-S and B-S samples were prepared with SLS, and C-AS, F-AS and B-AS were prepared with a mixture of aluminium powder and SLS. The water/binder ratio (w/b, binder was the amount of precursor) was varied for each mixture, in order to have an appropriate viscosity for good air-void development in the matrix.

Table 4.iii.1
Overview of samples and its composition

	Precursor	A (% by wt)	SLS (% by wt)	Liquid phase	
				w/b	Alkali solution (X/Y)
C-S	OPC	-	2	0.45	-
C-AS		0.05	0.2		
F-S	FCC	-	2	0.5	7.5/1.7
F-AS		0.05	0.2		
B-S	BFS	-	2	0.35	
B-AS		0.05	0.2		

Considering the natural density as the volumetric mass density (mass per unit volume), it was determined by means of the weight of the cubic samples before compressive strength testing. The compression test was carried out by means of an INSTRON 3282 universal testing machine. The natural density assessment and compression test were performed for six specimens of each cellular concrete dosage, and averages and standard deviation values were calculated.

The pore system characterization of the CGC was investigated by a combination of optical microscopy (OM) and field emission scanning electron microscopy (FESEM). A cube of each mixture was crushed in a porcelain mortar. A small piece (7–10 mm) from the inner part of the cube was selected and immersed in acetone for 30 minutes and dried at 65ºC for 40 minutes. FESEM micrographs of these samples covered with carbon were taken by an ULTRA 55-ZEISS electron microscope (at 50x, 100x and 200x magnifications), and the pore diameters were measured. On the other hand, a 4x4x4 cm^3 cube of each mixture was cut into slices 2 cm thick, perpendicular to the cast face, using a diamond rotary saw. The samples were observed by a Leica S8 APO optical microscope. Pictures were taken by a Leica DFC 420 digital camera and the images were processed using Leica LAS image analysis software.

Magnifications from 8x to 80x were selected with a pixel representing 12 microns.

3. Results and discussion

Fig.4.iii.1 shows the results of natural densities and compressive strengths comparing both: (i) the method of air entrapped into the matrix for each raw material; and (ii) the development for TCC and CGC (depending of the raw material base).

Comparing the method of bubbles generation in the matrix, in both systems (traditional and geopolymeric), the combination of agents (SLS plus A), which involves a pore generation by physical and chemical action (AS systems), yield lower natural densities than when merely S was used (pore generation by physical method), as can be seen in **Fig.4.iii.1a.** Considering a lower natural density as the optimal result, the improvement observed in each material was: 18% for samples with OPC, 10% for CGC with FCC and 22% for CGC with BFS. The chemical contribution of A in pore-system generation with the mechanical effect of SLS involves an excellent combination of gas-bubbles from H_2 release and air-burbles from foaming agent into the fresh matrix of composites (C-AS, F-AS, B-AS). The reaction of metallic aluminium has a direct influence in binder rheology: it involves a significant rise in matrix temperature, and subsequently decreases the setting time. This fact allows a higher percentage of combined gas and air bubbles get caught into the matrix. As a result, both for the TCC and CGC, a better pore-system development is achieved that was successfully stabilized before hardening, than those obtained for the foamed samples (C-S, F-S, B-S).

In general, the value of natural density obtained for CGC mixes with FCC (samples F-S and F-AS) either with BFS (samples B-S and B-AS) was below than those resulting for traditional mixes with OPC (samples C-S and C-AS). When the SLS was used as unique foaming agent, the values of natural densities reached were: 1972 kg/m^3 for C-S, 1276 kg/cm^3 for F-S (35% lower than C-S density) and 1345 kg/cm^3 for B-S (30% lower than C-S density). This means that the effectiveness of air entrapping process is better for CGC. On the other hand, when A is added in combination of SLS, the values of natural densities were: 1636kg/m^3 for C-AS, 1143 kg/cm^3 for F-AS (30% lower than C-AS density) and 1046 kg/cm^3 for B-AS(36% lower than C-AS density). These results highlight the fact that the high alkalinity medium of geopolymeric systems compared to the traditional OPC systems, allows a faster and more aggressive transformation rate of aluminium. Thus, a larger part of the hydrogen evolved before setting, trapping gas bubbles into the matrix and preventing the foam breakdown. In the case of TCC, at 20ºC curing temperature, the hydrogen evolution is slow and the setting of the system is produced before the complete oxidation of the aluminium: the evolved gas during the paste setting escaped without producing expansion and, therefore part of the air from the foaming action is either escaped.

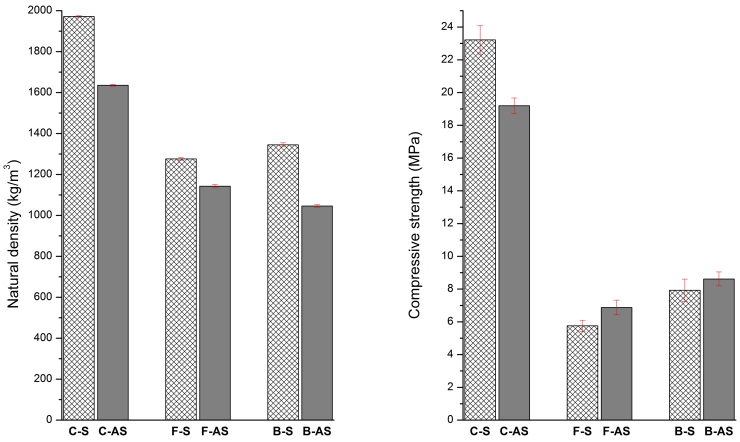

a) **b)**

Fig.4.iii.1 *Results from physical tests: a) natural densities; b) compressive strengths.*

Focused on the assess for CGC samples, for the samples with SLS, 5% of natural density improvement is reached by using FCC as the precursor, but in contrast, for the samples with SLS and A, 8% of natural density improvement is reached by using BFS as the precursor. The greatest difference is observed between CGC based on BFS (sample B-AS respect sample B-S). From these results two discussions can be presented:

(i) In order to get a stable void-system into the matrix by foaming effect from a surfactant addition, the paste must have a proper consistency. Both CGC samples have the same alkalinity rate but differ in water/binder ratio. Due to the higher mean diameter and specific surface area of FCC particles, a large water/binder ratio (w/b = 0.5) is required compared to BFS system (w/b = 0.35). Consequently, the resulting CGCs have a different rheology: samples with BFS were more fluid than samples with FCC precursor. Thus, the consistency of F-S samples results better for the inclusion of foam into the matrix before setting compared to B-S samples.

(ii) When chemical method is used by the generation of gas within the mixture and complement the SLS mechanical effect, in order to prevent the escape of the H_2 and assurance a great foam generation, the paste must have a proper consistency and fast setting time. The reactivity of BFS is faster than the reactivity of FCC, and the CGC based on BFS have a greatest polymerization at mildly low temperature conditions than CGC based on FCC. Furthermore, as stated above, the reaction of metallic aluminium involves a decrease in setting time. Thus, for B-AS sample a complete aluminium reaction was developed and, due to the increase temperature, the consistence of the paste is

enough to entrap a great volume of both air and gas resulting an optimal void-system.

Regarding de mechanical characteristics, for CGC samples the compressive strength reached was below than it for TCC in all of the experiences (**Fig.4.iii.1b**).

As it was introduced, authors argue that the compressive strength decreases exponentially with a reduction in density of cellular concrete (Ramamurthy et al., 2009). According to it, OPC samples have better mechanical behaviour when its natural density is higher (C-S sample) than when its natural density decreases (C-AS sample). Concretely, for C-S it is yielded 23.22 MPa and for C-AS 19.20 MPa, representing a 17.3 % loss. However, for CGC samples there is an increase of compressive strength when natural density is lower due to the use of combined method (foaming by SLS and gas forming by A). For F-S samples it is yield 5.76 MPa and for F-AS 6.88 MPa, representing 16.3 % gain. And for B-S samples it is yield 7.93 MPa and for B-AS 8.62 MPa, representing 8 % gain.

It should be necessary remember that, in current studies, where merely foamed agent or aerating agent is used to generate void matrix, it is discussed that despite the advantages of cellular concrete over traditional concrete, the lower mechanical properties of the former are a drawback (Arellano Aguilar et al., 2010). In this respect, these results showed an advantageous behaviour of CGC respect TCC. To sum up, when combined method of pore-formation was used, the CGC (by the use of both proposed precursors), it is yield lower natural densities with higher compressive strength.

The above studied properties of cellular concrete, such natural density and compressive strength, are directly consequence by controlling the nature, size and distribution of voids in production of the material. Furthermore, the compressive strength is also influenced by the void/paste ratio as well as spacing and interconnecting among the bubbles.

The pore-system evaluation was carried out for the CGC samples (as based on FCC as well as based on BFS) from the previous physical and mechanical characterization, which represents the optimal behaviour comparing to its reference material (TCC based on OPC) in terms of natural densities. In **Figs.4.iii.2-5**, OM images and FESEM micrographs of the CGCs are shown, in order to assess the influence of void formation method in pore-system development for the samples of each precursor (FCC and BFS).

The macropores are formed due to the expansion of paste and micropores appear in the walls between the macropores. In this investigation, the following criteria to distinguishing the range of pores was considered: Micropores are pores under or equal to 100 μm and macropores are pores greater than 100 μm.

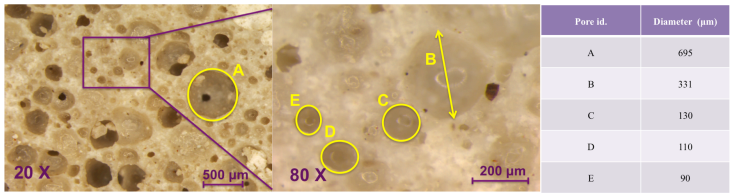

Pore id.	Diameter (µm)
A	695
B	331
C	130
D	110
E	90

a)

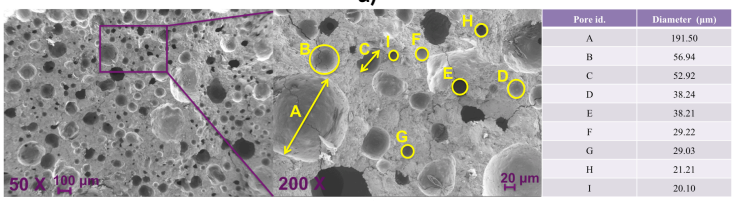

Pore id.	Diameter (µm)
A	191.50
B	56.94
C	52.92
D	38.24
E	38.21
F	29.22
G	29.03
H	21.21
I	20.10

b)

Fig.4.iii.2 *Pore system evaluation for F-S samples: a) OM images with measured voids; b) FESEM images with measured voids.*

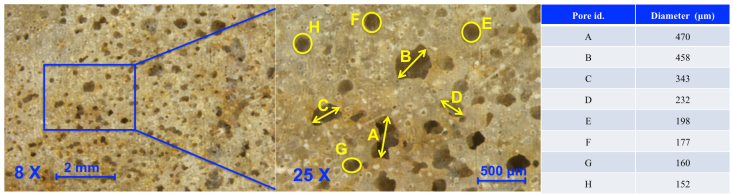

Pore id.	Diameter (µm)
A	470
B	458
C	343
D	232
E	198
F	177
G	160
H	152

a)

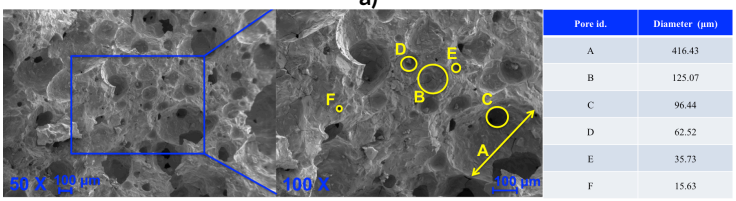

Pore id.	Diameter (µm)
A	416.43
B	125.07
C	96.44
D	62.52
E	35.73
F	15.63

b)

Fig.4.iii.3 *Pore system evaluation for B-S samples: a) OM images with measured voids; b) FESEM images with measured voids.*

When foamed method is used by the SLS addition, the resultant void-system was:

(i) By using FCC as a precursor (F-S samples) macropores from 191.5 µm to 695 µm and micropores from 20.10 µm and 90 µm could be identified (**Fig.4.iii.2**). There were many bubbles per unit area usually with spherical shape and there were not interconnected each other.

(ii) With the use of BFS as a precursor (B-S samples) there was identified a macropores distribution with sizes from 470 µm to

160 µm and micropores from 96.44 µm to 15.63 µm (**Fig.4.iii.3**). Differently from FCC case pores were irregular in shape and with interconnections among them. At micro scale (**Fig.4.iii.3b.**), it can be note that the biggest pores had the presence of smaller ones inside their internal walls.

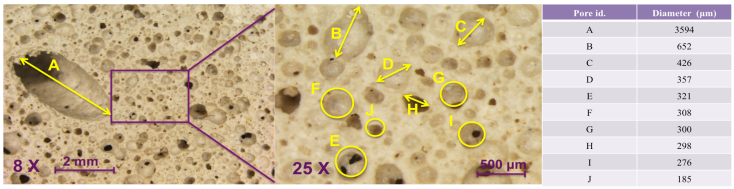

Pore id.	Diameter (µm)
A	3594
B	652
C	426
D	357
E	321
F	308
G	300
H	298
I	276
J	185

a)

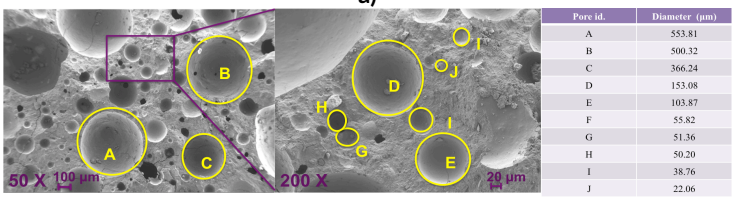

Pore id.	Diameter (µm)
A	553.81
B	500.32
C	366.24
D	153.08
E	103.87
F	55.82
G	51.36
H	50.20
I	38.76
J	22.06

b)

Fig.4.iii.4 *Pore system evaluation for F-AS samples: a) OM images with measured voids; b) FESEM images with measured voids.*

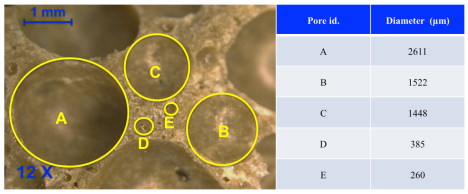

Pore id.	Diameter (µm)
A	2611
B	1522
C	1448
D	385
E	260

a)

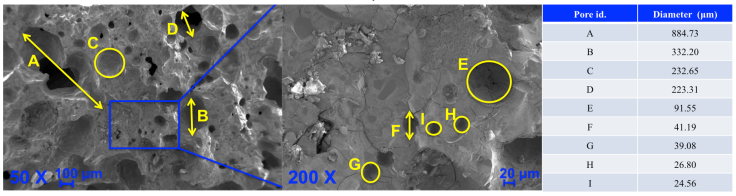

Pore id.	Diameter (µm)
A	884.73
B	332.20
C	232.65
D	223.31
E	91.55
F	41.19
G	39.08
H	26.80
I	24.56

b)

Fig.4.iii.5 *Pore system evaluation for B-AS samples: a) OM images with measured voids; b) FESEM images with measured voids.*

On the other hand, when A powder was added to complement the foaming method in the samples, the resultant void-system was:

(i) By using FCC as a precursor (F-AS samples), macropores from 3594 µm to 511 µm and micropores from 22.06 µm and 89 µm could be identified (**Fig.4.iii.4**). Besides, a higher size of

macropores was resulted the micro scale range was lower that when merely SLS was added. A similar pore structure to that the obtained in the F-S samples has been achieved. Homogeneous bubble distribution with spherical shape and no interconnection each other, have been observed.

(ii) Samples with BFS as a precursor (B-AS) presents a predominance of 2611-260 μm macropores and of 91.55-24.56 μm micropores (**Fig.4.iii.5**). The topography of the matrix is dense presenting pores with spherical shape in macro scale, but irregular forms and some interconnection among them in micro scale. Comparing with the B-S samples, a higher size of macropores was resulted and the micro scale range was lower, the same relation than the above discussed for FCC samples (F-S respect F-AS).

4. Conclusions

Despite of the most controllable pore-forming process, by foaming method using SLS, as there are no chemical reactions involved, this investigation reveals that the combination of mechanical and chemical methods involves a greatest effectiveness in both TCC and CGC production. With the addition of 0.2 % of SLS and 0.05% of A (AS mixtures) might be possible to reduce the natural density 18% in TCC, 10% in CGC with FCC and 22% in CGC with BFS than when merely SLS (2% by weight) was used. Furthermore, for the TCC systems with AS addition a direct relationship between natural density and compressive strength was found, however, for the CGCs (by the use of both proposed precursors), lower natural densities with relative higher compressive strengths were obtained.

In this research, the AS combined method, on the one hand CGCs made from FCC as a precursor with 1143 kg/cm^3 natural density and 6.88 MPa; and on the other hand, CGCs made from BFS with 1046 kg/cm^3 natural density and 8.62 MPa. These values of density constitute an improvement (reduction in natural density) of 30% and 36% respectively, respect of TCC systems.

The resultant pore system of both geopolymeric systems (FCC and BFS) by using SLS and A was higher in macro-pore scale and lower in micro-pore scale respect of the resultant with a foaming effect.

As a conclusion this paper reveals that, the geopolymeric systems based on the reuse of industrial by-products allows to obtain cellular concretes with lowest densities by using the same percentage of foaming addition, comparing to traditional systems based on OPC.

Acknowledgements

The authors acknowledge the financial support from Universitat Politècnica de València (UPV) through internal project GEOCELPLUS. The authors would like also to express special grateful to the Electronic Microscopy Service of the UPV. The first author thanks Esther Cuellar for her help with the English language.

References

Arellano Aguilar, R., Burciaga Díaz, O., Escalante García, J.I., 2010. Lightweight concretes of activated metakaolin-fly ash binders, with blast furnace slag aggregates. Constr. Build. Mater. 24, 1166–1175. https://doi.org/10.1016/j.conbuildmat.2009.12.024

Duxson, P., Provis, J.L., Lukey, G.C., van Deventer, J.S.J., 2007. The role of inorganic polymer technology in the development of "green concrete." Cem. Concr. Res. 37, 1590–1597. https://doi.org/10.1016/j.cemconres.2007.08.018

Esmaily, H., Nuranian, H., 2012. Non-autoclaved high strength cellular concrete from alkali activated slag. Constr. Build. Mater. 26, 200–206. https://doi.org/10.1016/j.conbuildmat.2011.06.010

Hamad, A.J., 2014. Materials, Production, Properties and Application of Aerated Lightweight Concrete: Review. Int. J. Mater. Sci. Eng. 2, 152–157. https://doi.org/10.12720/ijmse.2.2.152-157

Huntzinger, D.N., Eatmon, T.D., 2009. A life-cycle assessment of Portland cement manufacturing: comparing the traditional process with alternative technologies. J. Clean. Prod. 17, 668–675. https://doi.org/10.1016/j.jclepro.2008.04.007

Mo, K.H., Alengaram, U.J., Jumaat, M.Z., Yap, S.P., Lee, S.C., 2016. Green concrete partially comprised of farming waste residues: A review. J. Clean. Prod. 117, 122–138. https://doi.org/10.1016/j.jclepro.2016.01.022

Namsone, E., Šahmenko, G., Korjakins, A., 2017. Durability Properties of High Performance Foamed Concrete. Procedia Eng. 172, 760–767. https://doi.org/10.1016/j.proeng.2017.02.120

Narayanan, N., Ramamurthy, K., 2000. Structure and properties of aerated concrete: A review. Cem. Concr. Compos. 22, 321–329. https://doi.org/10.1016/S0958-9465(00)00016-0

Othuman, M.A., Wang, Y.C., 2011. Elevated-temperature thermal properties of lightweight foamed concrete. Constr. Build. Mater. 25, 705–716.

https://doi.org/10.1016/j.conbuildmat.2010.07.016

Ramamurthy, K., Kunhanandan Nambiar, E.K., Indu Siva Ranjani, G., 2009. A classification of studies on properties of foam concrete. Cem. Concr. Compos. 31, 388–396. https://doi.org/10.1016/j.cemconcomp.2009.04.006

Sanjayan, J.G., Nazari, A., Chen, L., Nguyen, G.H., 2015. Physical and mechanical properties of lightweight aerated geopolymer. Constr. Build. Mater. 79, 236–244. https://doi.org/10.1016/j.conbuildmat.2015.01.043

Tashima, M.M., Akasaki, J.L., Castaldelli, V.N., Soriano, L., Monzó, J., Payá, J., Borrachero, M. V., 2012. New geopolymeric binder based on fluid catalytic cracking catalyst residue (FCC). Mater. Lett. 80, 50–52. https://doi.org/10.1016/j.matlet.2012.04.051

Wongkeo, W., Thongsanitgarn, P., Pimraksa, K., Chaipanich, A., 2012. Compressive strength, flexural strength and thermal conductivity of autoclaved concrete block made using bottom ash as cement replacement materials. Mater. Des. 35, 434–439. https://doi.org/10.1016/j.matdes.2011.08.046

Zhang, Z., Provis, J.L., Reid, A., Wang, H., 2014. Geopolymer foam concrete: An emerging material for sustainable construction. Constr. Build. Mater. 56, 113–127. https://doi.org/10.1016/j.conbuildmat.2014.01.081

iv. Salt slag recycled by-products in high insulation alternative environmentally friendly cellular concrete manufacture

AUTORES: Alba Font, Lourdes Soriano, José Monzó, Joao Claudio Bassan Moraes, María Victoria Borrachero y Jordi Payá

REFERENCIA DE LA PUBLICACIÓN: Construction and Building Materials 231 (2020) 117114
DOI: http://dx.doi.org/10.21741/9781945291838-66

Factor de impacto/Cuartil (2018): 4.046/Q1	**Citas (excluyendo auto citas):** -

OBJETIVOS PÁRCIALES ABORDADOS

MATERIALES	FABRICACIÓN
• **GCC:** FCC + [WG+NaOH+H_2O] + A • **GCC:** FCC + [WG+NaOH+H_2O] + PG • **AACC:** BFS + [WG+NaOH+H_2O] + A • **AACC:** BFS + [WG+NaOH+H_2O] + PG	• **CO-M:** FCC + PG = FCCPGm • **CO-M:** BFS + PG = BFSPGm • **CURADO:** TA • **Amasado con:** NM and PD

PROCEDIMIENTO EXPERIMENTAL

CARÁCTERIZACIÓN DE MATERIAS PRIMAS	CARÁCTERIZACIÓN DE ESPECIMÉNES
• PDS • FESEM • DRX • Emisiones hidrógeno	• Densidad natural (D_N) • Resistencia mecánica (Rc) • Conductividad térmica (KD2-Pro) (λ) • Evaluación de la matriz porosa (FESEM, OM)

RESULTADOS Y CONCLUSIONES MÁS RELEVANTES DE LA INVESTIGACIÓN

- En la investigación se demuestra la posibilidad de utilizar sub-productos procedentes de escorias salinas (PG) como agente aireante tanto en GCC como en AACC.
- Los resultados de los ensayos correspondientes a la caracterización del PG así como del resultado de la co-molienda (FCCPGm y BFSPGm) confirmaron la presencia de aluminio metálico necesario para la reacción de aireación.
- La co-molienda resultó el método óptimo de incorporación de PG en las mezclas. La dosificación óptima fue de un 2 % respecto del peso del precursor. Con esta cantidad se obtuvieron resultados de densidad y resistencia mecánica muy cercanos a los obtenidos con el empleo de un 0.2 % de polvo de aluminio comercial (A).
- Tras 28 días de curado a temperatura ambiente se obtuvieron los siguientes resultados:

Material	D_N (kg/m^3)	Rc (MPa)	Tamaño de poros [dmin-dmáx] (μm)	λ (W/mK)
GCC aireados con A	726	6.2	-	0.260
GCC con FCCPGm	753	6.8	35.1-1872	0.310
AACC aireados con A	583	7.0	-	0.130
AACC con BFSPGm	602	7.5	12.1-2212	0.160

Abstract: This investigation presents an important contribution to the understanding of the "zero discharge in the aluminium cycle" goal. The salt slag recycled by-product was reused as alternative aerating agent in the manufacture of cellular concretes: fluid catalytic cracking catalyst (FCC) – based geopolymer (GCC) and blast furnace (BFS) – based alkali-activated (AACC). The hydrogen emission test was used to evaluate the gas releasing properties because the presence of metallic aluminium in the salt slag. Density (kg/cm^3), compressive strength (MPa) and thermal conductivity (W/mK) for GCC were 75, 6.9 and 0.31 and for AACC were 602, 7.5 and 0.16.

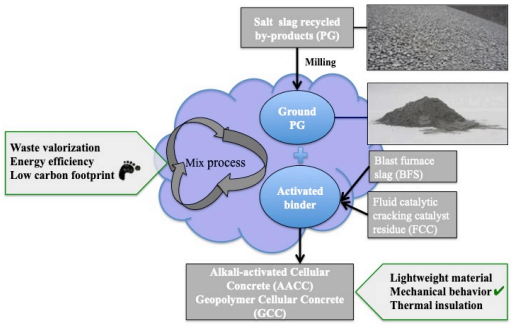

GRAPHYCAL ABSTRACT (4.iv)

Keywords: Aluminium salt slag recycled by-product, cellular concrete, geopolymer, alkali-activation, thermal insulation, waste valorisation

Abbreviations:
TCC: Traditional cellular concrete
GCC: Geopolymer cellular concrete
AACC: Alkali-activated cellular concrete
OPC: Ordinary Portland cement
FCC: Fluid catalytic cracking residue
BFS: Blast furnace slag
PG: Granulated paval
FCCPGm: FCC and PG co-milled
BFSPGm: BFS and PG co-milled

HIGHLIGHTS:

- Salt slag recycled by-products (PG) were used as aerating agent in cellular concrete.
- The PG reactivity was improved by milling.
- Co-milling of PG and the precursor was the optimal procedure for cellular concrete.
- 2% addition of PG yielded similar characteristics than 0.2% of commercial aluminium.
- PG was good aerating agent in both geopolymeric and alkali-activated systems.

1. Introduction

Traditional concrete is the most popular construction material because of its excellent structural and durability properties and consistent availability (Meyer, 2009; Petek Gursel et al., 2014). Many concrete applications require a high-density material (above 1800 kg/m^3); however, in special cases, lower-density materials yield more benefits. In this respect, the cellular concrete is a low-density material that represents an interesting cost-effective alternative material to traditional concrete because of the total material volume savings. This is because the air content is between 10% and 70% (Panesar, 2013).

Traditional cellular concrete (TCC) is a cement - based material (with sometimes lime additions) with a structured void-system matrix that results from the addition of a physical or chemical expansion agent. This material is normally manufactured with no aggregates or sand, and a partial replacement of binder can be found by pozzolanic materials to improve its properties (Dolton and Hannah, 2006). The chemical reagent most commonly used is aluminium powder, which, in contact with the alkaline medium (calcium hydroxide) from the cement, liberates hydrogen gas, as shown in **Equation 1** (Hamad, 2014). When this chemical reagent is added, a curing treatment in an autoclave (high-pressure steam curing) is usually applied. This curing method reduces the setting time and improves the early-age strength, increases the durability and reduces the drying shrinkage and moisture movement (Neville, 1982). This material is commonly known by authors as autoclaved aerated concrete (AAC) (Hamad, 2014; Holt and Raivio, 2005; Narayanan and Ramamurthy, 2000a; Neville, 1982), where:

$$2Al + 3Ca(OH)_2 + 6H_2O \Longrightarrow 3CaO \cdot Al_2O_3 \cdot 6H_2O + 3\,H_2 \quad (1)$$

Aluminium powder + hydrated lime + water $\Longrightarrow$ *tricalcium aluminate hydrate + hydrogen*

Because of the internal void system configuration that characterizes TCC, this material has low-density, moderate mechanical behaviour and good thermal and acoustic performance. It has a self -flowing behaviour in the fresh state and it is easily pumped without compaction requirement to place it (Neville, 1982). The material is commonly employed to make masonry units, such as bricks, flooring, trench filling and several insulation applications. Dolton and Hannah (Dolton and Hannah, 2006) introduced the TCC as more durable than traditional insulating materials because of its high resistance of chemical and fire exposure. Despite its great advantages, TCC manufacturing involves critical drawbacks when the environment, energy and economic issues are considered.

Traditional cellular concrete is mainly composed by ordinary Portland cement (OPC) (Mo et al., 2016) which main component is clinker. The manufacturing of clinker involves a substantial energy, the consumption of non-renewable raw materials (e.g. limestone, clay and marl,) and around 8% of the anthropogenic CO_2 emissions in the world (Luukkonen et al., 2018). In order to address the phenomenon of global warming and the corresponding environmental impact, the application of new alkali-activated cements, or geopolymers, in the cellular concrete technology is currently investigated.

The new alkali-activated cements, or geopolymers, are inorganic polymeric materials whose manufacture involves a chemical reaction between amorphous alumino-silicate raw materials with highly concentrated aqueous solution alkali compounds (i.g silicates and hydroxides). The process yields stable three-dimensional polymeric structures. The production of "green concrete" has the following advantages: (i) notice high strength, (ii) lower energy requirement and beneficial environment impact from low CO_2 emissions (Duxson et al., 2007) and (iii) beneficial impact of by-products and wastes by recycling. Diverse types of by-products and wastes are generally reported as suitable precursors for preparing cellular concretes by using geopolymeric binders (fly ash, metakaolin or spent FCC catalyst with low Ca content) as well as alkali - activated materials (blast furnace slag with high Ca content) (Ducman and Korat, 2016; Esmaily and Nuranian, 2012; Font et al., 2018, 2017).

The autoclave treatment required for TCC involves high temperature and pressure conditions, which raises important energy consumption and economic issues. The new GCC and AACC can be cured at ambient temperatures as well as at temperatures in the range 70ºC – 90ºC and achieve a stable matrix and suitable physical and mechanical behaviour. Recently, Font et al. (Font et al., 2017) reported FCC-based GCC cured at room temperature (23ºC/100% RH) with a density of 690 kg/m^3, compressive strength of 3.5 MPa and thermal conductivity of 0.581 W/mK. Arellano Aguilar et al. (Arellano Aguilar et al., 2010) presented cellular concretes with metakaolin and fly ash that yielded 600 kg/m^3, 1.7 MPa and 0.470 W/mK when the GCC was cured at 20ºC. The AACC cured at a high temperature (87ºC) was investigated by H. Esmaily et al. (Esmaily and Nuranian, 2012), who used blast furnace slag and with the product had a density of 681 kg/m^3 and 1 MPa compressive strength.

The production of 1 kg of primary aluminium from aluminium oxide (alumina, Al_2O_3) requires 15.7 kWh of electricity per the commonly used Hall-Héroult process ("RLG International cementreview," n.d.). To obtain alumina from bauxite, the Bayer process is generally employed. This process consists of grinding, digesting, dissolving, filtering, cooling, precipitating and drying sub-processes that require 13 kWh of electricity and result in 1-2 tons of residues for the production of 1 ton of alumina (World Aluminium, 2014). Furthermore, the obtained primary aluminium needs to be ground to a powder through stamp milling, ball milling under dry conditions, wet ball milling, attrition milling or vibration milling (Hong et al., 2000) The high-energy consumption and residues that are generated from the production of primary aluminium

powder have a harmfully environmental impact. Because of the high recyclability of the wasted aluminium products, the secondary aluminium production allows an energy savings of 95%. Currently, the European production of aluminium is near 87% for the secondary production process (Ashraf, 2014). In Europe, 4 million tons of recycled aluminium are annually processed from the packaging, construction and transport sectors ("Befesa :: Press :: News archive :: 2013," n.d.).

The search for an aerating reagent alternative for aluminium powder in the manufacturing of traditional cellular concretes has been carried out by several authors. The replacement of aluminium powders in the cellular concrete manufacturing process by recycled scrap (Araújo and Tenório, 2005), residues from an energy pilot plant (gasification) (Holt and Raivio, 2005), ashes from municipal solid waste (Song et al., 2015) and aluminium foil (Font et al., 2017) have been described in recent investigation reports.

Salt slags are the residues generated from the metal fusion in secondary aluminium production, where 1 ton of aluminium leaves 0.5 ton of salt slags, which may have different particle sizes as well as variable contents of aluminium, melting salts and aluminium oxide. The treatment and valorisation is carried out in specialized plants from which it is possible to recover the 5% of metallic aluminium, 45% of melting slags and 50% of the new by-product currently known as Paval (**Fig.4.iv.1**). In 2017 the 80000 – 90000 tons annual production of Paval in Befesa Aluminio S.L plant (Valladolid, Spain) has been reported. This means that all of this waste is fully converted into raw materials that can be used by the industry. The Paval by-product that is obtained in the recycling plants is ground and classified in three size fractions: i) 0 – 250 μm, referred to as Paval, Serox or BFA; ii) < 45 μm, referred to as Fine Paval (PF); and iii) 0.7 – 1.5 mm, referred to as granulated paval (PG). Since the first two size fractions are composed of 70% alumina, these provide an appealing alternative to conventional bauxite. These have been successfully used as an alternative aluminium corrector in the manufacture of OPC clinker in a number of countries, including Spain, Germany, the UK and France. However, the thicker fraction, PG, includes some fine fractions of metallic aluminium particles. Thus, their reuse is not feasible because of the reactivity of the metallic aluminium.

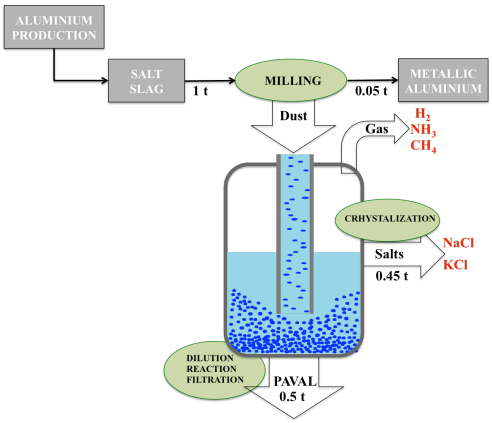

Fig.4.iv.1 *Recycling process diagram of salt slag from secondary aluminium production ("Befesa :: Press :: News archive :: 2013," n.d.).*

This research aims to study the granulated paval (PG), a by-product obtained from the processing of salt slag, as an aerating reagent in new geopolymer cellular concretes (GCC) with fluid catalytic cracking catalyst residue (FCC) and alkali-activated cellular concretes (AACC) with blast furnace slag (BFS) manufacturing. The PG was first mechanically treated and fully characterized and then it was tested as an aeration agent in the GCC matrix. The incorporation of PG in the GCC and AACC pastes was studied and compared with the use of the traditional commercial powered aluminium (A).

2. Materials and methods

2.1. Materials

Two solid precursors were selected to design the GCC and AACC aerated by the PG addition: i) FCC that was supplied by BP Oil Company (Grao de Castellon, Spain) and ii) blast furnace slag (BFS) that was supplied by Cementval S.A (Puerto de Sagunto, Spain). The chemical compositions of the FCC and BFS were analysed by X-Ray fluorescence (XRF) equipment (Magic Pro Spectrometer-Philips) and are shown in **Table 4.iv.1** (Font et al., 2017; Moraes et al., 2016). The X-ray diffractogram patterns of both precursors, FCC and BFS, are shown in **Fig.4.iv.2.** For the FCC the main peaks correspond to faujasite ($Na_2Al_2Si_4O_{12}8H_2O$, PDFcard: 391380) and minoritary peaks of mullite ($Al_6Si_2O_{13}$, PDFcard: 150776), albite ($NaSi_3O_8$, PDFcard: 711152) and quartz (SiO_2, PDFcard: 331161) can also observed. In the case of BFS an amorphous pattern can be observe with some characteristic peaks of quartz (SiO_2, PDFcard: 331161) and calcite ($CaCO_3$, PDFcard: 050586).

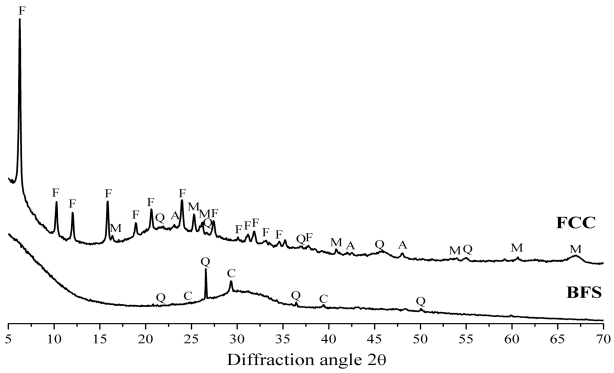

Fig.4.iv.2 *X-ray diffraction pattern of FCC and BFS (Key: F, faujasite; M, mullite; A, albite; Q, quartz; C, calcite).*

In order to obtain a finer material and improve their alkali reactivity, 450 g of these solid precursors, previously dry (24 hours at 100 °C), were milled with 98 alumina balls. The FCC was milled for 20 minutes and had a mean particle diameter (D_{mean}), d_{10}, d_{50} and d_{90} equal to 18.91 µm, 0.21 µm, 11.72 µm and 49.05 µm, respectively. The BFS was milled for 30 minutes and had a D_{mean}, d_{10}, d_{50} and d_{90} equal to 28.80 µm, 2.81 µm, 19.71 µm and 68.89 µm, respectively. The particle size of FCC and BFS was measured by means Malvern Instruments Mastersizer 2000 (in water suspension) and the distribution of both materials is shown in **Fig.4.iv.3**

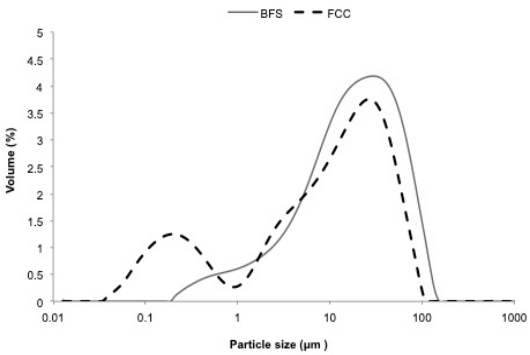

Fig.4.iv.3 *Particle size distribution curves for BFS and FCC.*

To prepare the alkaline solutions, water glass (8% Na_2O, 28% SiO_2 and 64% H_2O) and sodium hydroxide pellets (98% purity) were used. Both were acquired from Merck.

Granulated paval (PG) from Befesa Aluminio S.L (Valladolid, Spain) is the alternative reagent used for the GCC aeration in this investigation. The PG is produced by salt slag recycling, which is a waste produced by the secondary aluminium industry. Its chemical composition is also shown in **Table 4.iv.1**. The

chemical composition of PG was extracted from 2016 annual report supplied by Befesa Aluminio S.L. The PG is mostly composed of Al_2O_3 (80.57%). Commercial aluminium powder (A) was used for the control GCC sample aeration. It was supplied by Schlenk Metallic Pigments GmbH and had a 30 µm mean particle diameter.

Table 4.iv.1
Chemical compositions of FCC, BFS and PG (wt%).

	SiO_2	Al_2O_3	Fe_2O_3	CaO	MgO	SO_3	K_2O	Na_2O	P_2O_5	TiO_2	Others	LOI*
FCC	47.76	49.26	0.60	0.11	0.17	0.02	0.02	0.31	0.01	1.22	-	0.53
BFS	30.53	10.55	1.29	40.15	7.43	1.93	0.57	0.87	0.26	0.89	-	5.53
PG	10.37	80.57	1.04	2.00	0.67	0.44	0.65	1.50	0.13	0.16	1.5	0.97

*Loss on ignition

2.2. *Methods*

The experimental procedure in the present work is divided in the two sequential steps shown in **Fig.4.iv.4** where the employed methods, in each one, are indicated.

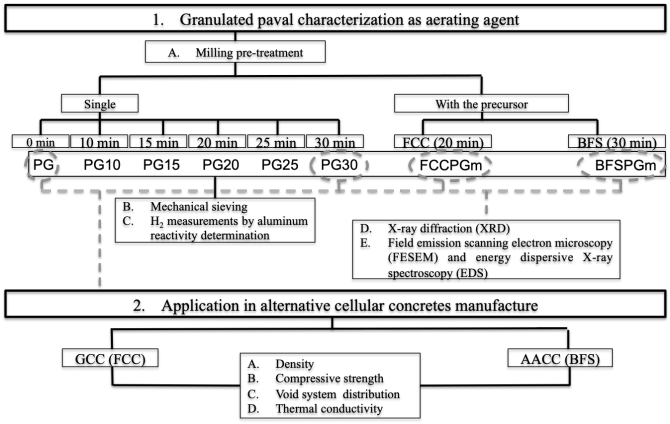

Fig.4.iv.4 *Overview of experimental procedure.*

2.2.2 Granulated paval characterization

The aerated cellular concrete structure (matrix void system distribution) and its physical properties are directly related with type and size of reagent added (Narayanan and Ramamurthy, 2000a). The original PG was milled in a Gabrielli Mill-2 ball mill by two methods. One method was done without precursor for 10, 15, 20, 25 and 30 minutes and whose resultant samples were referred to as PGX, where X represents the milling time in minutes (PG10, PG15, PG20, PG25 or PG30). The milling process was carried out with 250 g of dry material (24 hours at 100 °C) and 98 alumina balls. The other method included 2% by mass of precursor in the milling procedure. The milling parameters described above ("2.1 Materials" section: 450g of dry material with 98 alumina balls, during: i) 20 minutes when the FCC is the precursor; and ii) 30 minutes when

BFS is the precursor) were also used and the resultant samples were referred to as YPGm, where Y represents the corresponding raw material (FCCPGm or BFSPGm).

All of these resultant materials were characterized in terms of particle size distribution by mechanical sieving in dry state. Considering that the PG reaction comes from its aluminium (metal) content, H_2 measurements were carried out by aluminium reactivity determination test used by Font et al. (Font et al., 2017). This method considers the aluminium oxidation when it comes in contact with high alkali solution (NaOH, 7.5M) and measures the displacement of a water column by the released H_2 (**Equation (4.iv.2)**). Five measurements for 0.01, 0.05, 0.08, 0.1, 0.5, 1 and 1.5 g of each tested material were carried out and the equivalent arithmetic mean was calculated. The results that differed by more than 10% were rejected.

$$Al\,(s) + 3H_2O + OH^-_{(ac)} \Rightarrow Al(OH)_4^-{}_{(ac)} + 3/2\,H_{2\,(g)} \qquad (4.iv.2)$$

Aluminium powder + water + hydroxide ⇒ aluminate + hydrogen

The original PG, the PG milled for 30 minutes (PG30) and the resultant material from the precursor and PG milled together (FCCPGm and BFSPGm) were characterized by X-ray diffraction (XRD) and field emission scanning electron microscopy (FESEM) with energy dispersive X-ray spectroscopy (EDS). Both of tests were carried out to powder samples. The XRD patterns were obtained using a Bruker AXS D8 Advance in the 2θ range of 5° – 70°. The FESEM micrographs were taken by an ULTRA 55-ZEISS with a powder sample covered by carbon, and the EDS test was carried out with a 6-8mm working distance and extra high voltage of 20kV.

2.2.3 Application in alternative cellular concretes manufacture

In **Table 4.iv.2** the experimental procedure to geopolymer cellular concrete preparation and characterization is summarized.

Table 4.iv.2
Experimental data to geopolymer cellular concrete preparation and characterization.

Sample (XyZ)	Precursor (X)	Aerating agent		Water /binder		Alkali solution		Tests*	
		% (y)	Type (Z)	64 cm^3	1000 cm^3	SiO_2/Na_2O	Na^+	64 cm^3	1000 cm^3
FCC2PGm	FCC (500g)	2	PGm	0.5	0.6	1.7	7.5	D Rc VSD (7 and 28 days)	D Rc TC (28 days)
FCC1PG30		1	PG30						
FCC1.5PG30		1.5							
FCC2PG30		2							
FCC5PG		5	PG						
FCC10PG		10							
FCC0.2A		0.2	A						
BFS2PGm	BFS (500g)	2	PGm	0.3	0.35				
BFS1PG30		1	PG30						
BFS1.5PG30		1.5							
BFS2PG30		2							
BFS5PG		5	PG						
BFS10PG		10							
BFS0.2A		0.2	A						

* D: Density; Rc: Compressive strength; VSD: Void system distribution; and TC: Thermal conductivity.

GCC samples, with either FCC or BFS, as follows: i) without milling pre-treatment, in the original state (PG), in 5% and 10% proportions by mass with respect to the precursor; ii) with previous 30 minutes milling pre-treatment (PG30), in 1%, 1.5% and 2% proportions by mass with respect to the precursor; and iii) by precursor and PG co-milling (FCCPGm and BFSPGm) in 2% by mass with respect to the precursor. This difference in addition percentages between PG and PG30 was determined from the hydrogen emission tests results, as described in detail in the in Results and Discussion section below.

Depending on the test carried out, two casting moulds were used for each sample: i) nine 4x4x4 cm cubes to measure the density, compressive strength (after 7 and 28 curing days) and void system distribution; and ii) eight 10x10x10 cm cubes to measure density, compressive strength and thermal conductivity after 28 days. For the 64 cm^3 sample production, a normalize mixer machine (En et al., n.d.) with 5 litres of capacity was employed. An AEG SBE705RE power drill connected with a paint mixer was used to produce the 1000 cm^3 samples. The differences in the mixed volume and the mixing method had an influence in the material rheology and, consequently, the liquid phase stoichiometry had to be readjusted. For the alkali solution preparation, the SiO_2/Na_2O molar ratio was 1.7 with Na^+ molality of 7.5 and the water/binder (w/b) ratio varied depending on the casting mould used as follows (Font et al., 2018):

i. FCC samples: for 64 cm^3 w/b = 0.5 and for 1000cm^3 w/b = 0.6
ii. BFS samples: for 64cm^3 w/b = 0.3 and for 1000 cm^3 w/b = 0.35

The samples were cured at room temperature (23ºC and 100% R.H) for 24 hours. At this time, the free surfaces of the cubes were cut with a saw blade and the specimens were de-moulded. Finally, the samples were kept in wet chamber until testing.

The sample designation in this paper is *XyZ*, where *X* the raw material (FCC or BFS), *y* is the percentage of PG incorporated (*y*= 5, 10, 1, 1.5 or 2) and Z is the method of PG addition into the samples (original state = PG, milled during 30 minutes = PG30 or milled with the precursor = PGm). For the control samples, the designation is FCC0.2A and BFS0.2A, which had 0.2% commercial aluminium powder (A) by mass of the precursor.

The natural densities of the alternative cellular concretes were determined immediately after demolding by the specimen weight per unit of volume and the compressive strength was measured in an INSTRON 3282 universal testing machine (Babbitt et al., 2014). The void system was characterized with FESEM micrographs and optical microscopy (OM) photographs. A Leica S8 APO optical microscope was used and the pictures were taken by a Leica DFC 420 digital camera. The images were processed using the Leica LAS image analysis software. The void measurements in the FESEM micrographs and OM images considered a spherical/spheroidal shape for the voids. The thermal conductivity measurements were carried out with a KD2-Pro handheld device (Decagon Devices Inc.) with a complementary thick (6 cm long, 3.9 mm diameter) single RK-1 sensor based on the dual needle probe system (transient line source method) according to ASTM D5334-14 and IEE 442-1981 (ASTM International, n.d.; "IEEE 442-1981 - IEEE Guide for Soil Thermal Resistivity Measurements," n.d.). Before the measurements, a standard (RH-1-01116, 0.387±10% W/mK) was used to verify the good performance of the sensor.

3. Results and discussion

3.1. Granulated paval characterization

Table 4.iv.3 shows the granulometric parameters that were obtained by sieving the PG samples. The original PG (without milling) had very large particles, with more than 96% greater than 250 µm. The percentage of 250 µm particles was drastically reduced by grinding. In PG10 (10 minutes grinding), it was 38.2% and in PG30 (30 minutes grinding), it was only 18.5% by mass.

Table 4.iv.3
Particle size distribution (sieved in the dry state) for PG and ground PG samples (from 10 to 30 minutes grinding), FCC and BFS, and for PG milling jointly with catalyst residue (FCCPGm) or blast furnace slag (BFSPGm).

	Particle size distribution				
	>250 µm	250-125 µm	125-63 µm	63-45 µm	<45 µm
PG	96.7	1.0	1.5	0.7	0.0
PG10	38.2	35.2	9.6	12.8	4.1
PG15	32.8	20.5	21.4	14.1	11.1
PG20	29.6	6.8	22.0	26.2	15.4
PG25	23.7	4.6	31.4	7.1	33.2
PG30	18.5	5.4	25.8	16.8	33.5
FCC	0	0.3	1.5	29.6	68.6
FCCPGm	0	0.3	1.1	24.5	74.1
BFS	0	0.3	2.3	44.1	53.3
BFSPGm	0	0.2	2.2	49.7	47.9

The aerating reaction in the alkaline medium increased with the particle fineness. The metal powders commonly added into cellular concretes have an average grain size of 20 - 45 µm (van Boggelen, 2011). The PG30 contained over 50% of particles with a grain size less than 63 µm, which was the most similar to the commercial powder among the PG samples. The remaining shorter milling times yielded larger particle sizes. Furthermore, PG30 was significantly coarser than the precursors. Most of particles for FCC and BSF were smaller than 63 µm.

For the samples of PG and precursor that were co-milled (FCCPGm and BFSPGm), it was found (**Table 4.iv.3**) that also most of the particles had a size lower than 63 µm. This means that, by this procedure and in view of the results for the PG singly milling treatment (in all of milling experimented times), the PG particles were comminuted to a similar particle size as the precursor. One of the most influential parameters on the effectiveness of the matrix aeration in the cellular concretes is the aluminium particle oxidation. The volume of liberated hydrogen into the alkaline medium (NaOH or KOH aqueous solution) is directly related to the aluminium content, initial alkali concentration, temperature and aluminium particle surface area (Porciúncula et al., 2012). A larger surface area allows better impregnation of the aluminium particles when they come in contact with the alkali solution. The reaction of the aluminium with the alkali solution starts with the hydration of the Al atoms and the chemisorption of the hydroxide ions (Aleksandrov et al., 2003). A first-order topochemical redox reaction takes place. The inclusion of the alternative recycled aluminium foil in the milling treatment of the FCC as of the BFS was studied by Font et al. (Font et al., 2018, 2017) with great results. The foil pre-treatment reduced its particle size. The co-milling of the precursor and aluminium did not significantly modify the granulometric distribution of

the obtained powder compared to the ground precursor without aluminium foil.

The considered reference dosage of A to the cellular concretes was 0.2% (with respect the weight of precursor), and the entire A was reactive in the alkaline medium. The dependence between the resultant percentages of the equivalent reactive aluminium for each tested material (original PG and samples milled during different times) and the percentages of each material to incorporate 0.2% of aluminium in GCC manufacture are shown in **Fig.4.iv.5**.

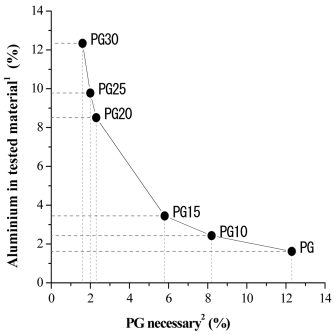

Fig.4.iv.5 *Results of H_2 emission tests.*
[1]reactive metallic aluminium content in each tested material; [2] percentage of each PG type to add in the manufacture of GCC and AACC with 0.2% of reactive metallic aluminium.

The PG (0.1g) in its original size liberated 50 mg of H_2, which indicates that the reactive metallic aluminium content was 1.8% by weight (see Y-Axis in 43). Consequently, to incorporate 0.2% (by weight) of reactive aluminium in a GCC or AACC sample, a PG addition between 12% and 13% is necessary (see X-axis in **Fig.4.iv.5**). In the other extreme modality proposed, when PG is milled for 30 minutes (PG30 sample), the liberated H_2 from 0.1g increases to 100 mg, which means there was 12.2% of reactive aluminium metallic content. Consequently, the amount of PG30 necessary to incorporate 0.2% (by weight) of reactive aluminium in GCC or AACC sample decreased to 1%-2%. It can be noted than when the milling time increases, the amount of treated PG to yield 0.2% of reactive metallic aluminium addition equivalent in the GCC or AACC samples decreases.

A controlled aerated reaction is essential to develop a good void system structure. This influences the physical behaviour of the cellular concretes. The reaction in a basic medium of the metallic aluminium contained in PG is the basis to carry out the study of its application in GCC as well as AACC mixes. The particle size difference between PG and PG30 involves a high yield of H_2 gas emissions. Consequently, a lower quantity of material must be added to incorporate the equivalence of 0.2% of metallic reactive aluminium into the mixes. The influence of the particle size in the aeration effect has been recently

verified by authors that presented commercial aluminium powder alternatives for cellular concrete aeration (Araújo and Tenório, 2005; Font et al., 2017; Song et al., 2015).

Based on these results, PG and PG30 and the innovative co-milling with the corresponding precursor (FCCPGm and BFSPGm) processes were selected for addition to the designed geopolymer cellular concretes. The percentages (with respect the precursor weight) assessed in the samples were: 10% and 5% in the case of PG addition; 1%, 1.5% and 2% for PG30 addition; and 2% for FCCPGm and BFSPGm.

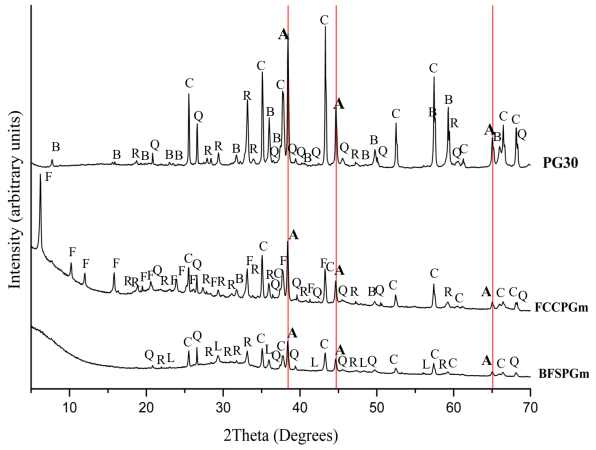

Fig.4.iv.6 *X-ray diffractograms for PG30, FCCPGm and BFSPGm. (Key: Q – quartz; C – corundum; B – beta-aluminium oxide; A – aluminium (marked with vertical red lines; R – calcium aluminates; F – faujasite; L – calcite).*

In **Fig.4.iv.6**, the XRD patterns obtained for PG30, FCCPGm and BFSPGm can be observed. The X-ray diffractogram corresponding to the ground PG sample (PG30) shows peaks from metallic aluminium (A, JCPDF card #040787) and aluminium oxide in the crystallized phases of corundum (Al_2O_3, JCPDF card #100173) as well as of beta–aluminium oxide (β-Al_2O_3, JCPDF card #100414). Traces of quartz (SiO_2, JCPDF card #331161) and calcium aluminate (Ca_3AlO_6, JCPDF card #320150) were also found.

The patterns for the materials obtained by the co-milling treatment of the precursors with PG presented the following features:

i. The FCCPGm diffractogram showed the peaks in agreement with a zeolite named faujasite ($Na_2Al_2Si_4O_{12}{\cdot}8(H_2O)$, JCPDF card #391380), which correspond with the intense peaks in the FCC diffractogram (Font et al., 2017). Furthermore, the peaks of aluminium (A, JCPDF card #040787), corundum (Al_2O_3, JCPDFcard #100173) and traces of calcium aluminate (Ca_3AlO_6, JCPDF card #320150) and quartz (SiO_2, JCPDF card #331161) indicate the

presence of PG addition. A baseline deviation in the 15°-30° range was observed, which was related to the presence of an amorphous fraction (rich in silica and alumina) in the FCC.

ii. In the XRD pattern for BFSPGm, an important baseline deviation between 25° and 35° can be observed because of the typical amorphous phases (Ca-Si-Al oxides) in the BFS mineralogical composition (Moraes et al., 2016). Overlapping of peaks attributable to the presence of crystalline products due to the presence of PG can be seen: calcite ($CaCO_3$, JCPDF card #050586), BFS and aluminium (A, JCPDF card #040787), corundum (Al_2O_3, JCPDF card #100173) and traces of calcium aluminate (Ca_3AlO_6, JCPDF card #320150) and quartz (SiO_2, JCPDF card #331161).

The peaks above 2Θ =35° corresponding to aluminium are highlighted in red (**Fig.4.iv.6**) for 2Θ values of 38.45°, 44.71° and 65.09° (corresponding to the [111], [200] and [220] Miller planes). It is evident the presence of metallic aluminium in PG30, FCCPGm and BFSPGm samples due to the co-milling treatment of the precursors with PG. These results suggested that the aeration reaction of FCCPGm and BFSPGm might be possible due to the metallic aluminium dispersed in the co-milled precursor.

The FESEM micrographs and EDX analysis of selected analysis spots from the PG, PG30, FCCPGm and BFSPGm particles are shown in **Fig.4.iv.7**.

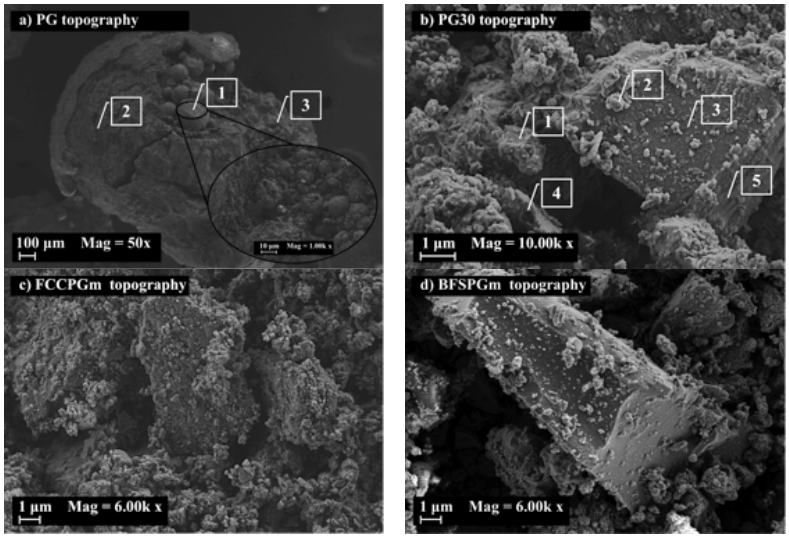

Fig.4.iv.7 *FESEM micrographs: a) PG, b) PG30, c) FCCPGm and d) BFSPGm. Some spots are marked in the micrographs where EDS analysis was done.*

The PG was found to have large spherical and spheroidal particles, which had a high porosity (**Fig.4.iv.7a**). In the case of PG30 (**Fig.4.iv.7b**), the particle

fineness increased because the original spherical and spheroidal particles were completely broken. The presence of aluminium (element) was indicated by the analysis and high aluminium contents were found in PG and PG30 powders (spot 1 in **Fig.4.iv.7a** with 82.9% and spot 1 in **Fig.4.iv.7b** with 70%). Considering the oxygen content from these EDS data, part of this aluminium element is chemically combined to Al_2O_3 formation. The resultant metallic aluminium in the EDS analysis was between 22%-64% for the PG sample (spots 1–3 in **Fig.4.iv.7a**), and 23%–70% for the PG30 sample (spots 1-5 in **Fig.4.iv.7b**).

In case of the FCCPGm and BFSPGm particles, no evidence of the PG co-milled presence was found in the FESEM micrographs or in the spectra obtained by the EDS analysis. **Figs.4.iv. 7c and 7d** show the typical texture for the ground FCC and BFS samples, respectively. The FCCPGm (**Fig.4.iv.7c**) is characterized by the presence of particles about 20 μm in diameter with particles adhering to their surfaces that are less than 2 μm in diameter. The chemical analysis showed their composition to consist of large amounts of silicon and aluminium, where Si = 21.78 %, Al =28.97 and O = 49.33 %. In the case of BFSPGm (**Fig.4.iv.7d**), the larger particles were observed to be about 30 μm in diameter with a surface covered in smaller particles (with a lower content than the FCCPGm sample). From the EDX analyses, a high content of calcium and some amount of silicon, magnesium and aluminium were detected (Ca = 31.13 %, Si = 13.7 %, Al = 7.26 %, Mg = 4.78 % and O = 43.12 %).

3.2. Application in alternative cellular concretes manufacture

The density and compressive strength obtained for the GCCs and AACCs (prepared with several PG addition modalities) are shown in **Fig.4.iv.8**. The following dosages were selected: a) for PG, an addition of 5% and 10% by weight of the precursor; b) for PG30, 1%, 1.5% and 2%; and c) for the co-milling of PG it was 2% by weight and precursor (BFS or FCC). They were compared to GCCs and AACCs with 0.2% commercial powdered aluminium (A) (see **Table 4.iv.2**).

In general, the BFS samples yield higher densities and better mechanical behaviour respect FCC samples independent of the PG addition modality. These results are in contrast with those reported by Font et al. (Font et al., 2018). In that study, when recycled aluminium foil was used as the aerating agent, the FCC-based GCCs yielded higher densities and better mechanical behaviour with respect those obtained for BFS-based AACCs. This can be attributed to the differences in the mixed sample volumes and in the w/b ratio. Yang et al. (Yang et al., 2014) established that the dry density of alkali activated slag cellular concretes depends on the unit binder content, regardless of the type of precursor used.

There were changes in the density evolution when different PG addition modality was carried out that is rather similar for the use of both precursors, FCC and BFS. When PG was used as the aerating agent, higher densities were obtained for 10% PG with respect to the 5% samples. Specifically, the

difference was 15% higher for FCC10PG vs. FCC5PG (**Fig.4.iv.8a**) and 9% higher for BFS10PG vs. BFS5PG (**Fig.4.iv.8b**). These results are in contrast with the those observed from the H_2 emission test results. In FCC10PG and BFS10PG, a vigorous chemical reaction was observed due to the large amount of H_2 released. The paste consistency was fluid and it did not have enough resistance (viscosity) to maintain the gas bubbles into the matrix before hardening. Despite the fact that there was a large amount of bubbles, the H_2 was released from the material and the aeration was not effective. For this reason, it was not possible to test a higher percentage of PG addition. When the percentage of PG was decreased by half (FCC5PG and BFS5PG), a more progressive reaction was noted and there was not a large amount of gas released from the matrix. The FCC5PG samples yielded densities that were 24% higher than the control samples (FCC0.2A). The BFS5PG density was 40% higher than the corresponding control material (BFS0.2A). This can be explained by considering the above discussion about the H_2 emission tests. The corresponding amount of PG addition modality to release the corresponding gas that is released by 0.2 % of A addition was 12%-13 % (by wt% precursor). However, the strong chemical reaction in the alkaline medium of the mixes made this percentage addition impossible. Furthermore, it can be considered that the PG particle size was too high and consequently, the gas generation was not homogeneously dispersed into the matrix. Thus, large bubbles were formed and they had a substantial pressure and escaped from the mixture.

With the use of PG30 as the aerating agent, the densities were higher than, or similar to, those obtained with the PG. Compared with FCC5PG, the density of the FCC1PG30 increased 30% and for FCC1.5PG30, it was close to FCC5PG and decreased 4% (**Fig.4.iv.8a**). In the BFS samples (**Fig.4.iv.8b**), compared with BFS5PG, the densities increased 44% and 16% for BFS1PG30 and BFS1.5PG30 samples, respectively. The chemical reaction from the 1% and 1.5% addition percentages of PG30 was apparently slow and controlled. However, not enough H_2 was released with the addition of 1% of PG30. The FCC1PG30 density was close to 1000 kg/m^3 and the BFS1PG30 density was higher than 1000 kg/m^3. When 2% of the PG30 was added, a natural density reduction was observed for the FCC samples (5% respect FCC5PG). Nevertheless, there is a slight increase in BFS2PG30 density compared to the BFS5PG (6%). As demonstrated from the H_2 emission test results, a lower quantity of milled material (PG30) with respect the original PG is required to produce the aeration level equivalent to 0.2 % of the metallic aluminium powder in the GCCs and AACCs.

The milling treatment of PG led to an evident improvement in this reaction. These results can be explained by the increase in the specific surface area of the metallic aluminium, which involves a higher contact and reactivity in alkaline medium.

The lowest densities were obtained when the addition was carried out by the co-milling treatment (FCCPGm and BFSPGm samples). It is highlighted that the PG percentage addition was 2%, the same as for the FCC2PG30 and

BFS2PG30 samples. The density values for the FCC2PGm and BFS2PGm samples were close to the control samples and yielded 4% and 7% higher densities, respectively. It is remarkable that the PG co-milling with the precursor was an excellent treatment compared to the individual grinding in terms of the obtained cellular concrete density. In the co-milling process, the effectiveness of the particle size was higher and the dispersion of the ground PG particles was better than that obtained by mixing the ground precursor and the ground PG.

From the mechanical point of view, two aspects can be discussed: i) there was an evolution with the curing time in all of the tests, which was attributed to the progress of the reaction with curing time at room temperature; and ii) the improvement of density (lower values) corresponded to a compressive strength reduction (lower values) independent of the PG addition modality. This link between the density and compressive strength is typical for cellular concretes (traditional systems as well as geopolymeric or alkali-activated systems), and it has been reported by several authors (Hamad, 2014; Narayanan and Ramamurthy, 2000a; Panesar, 2013; Sanjayan et al., 2015; Yang et al., 2014). There is an exception in this behaviour in the case of FCC2PGm, which had a low natural density (612 kg/m^3) with a high compressive strength (6.2 MPa) compared to the other PG modalities (**Fig.4.iv.8a**).

In general, the PG co-milling process with the precursors (FCC and BFS) became a practical and effective method for alternative cellular concrete production. The FCC2PGm had a compressive strength of 6.2 MPa after 28 days with a density of 612 kg/m^3. These parameters being similar to those presented for the control sample (FCC0.2A) that had a compressive strength of 5.4 MPa and density of 590 kg/m^3. In a parallel way, for BFS, the sample containing the co-milled PG (BFS2PGm) had a compressive strength of 6.4 MPa and density of 695 kg/m^3. The control (BFS0.2A) had a compressive strength of 7.8 MPa and density of 651 kg/m^3. The 2% addition of this by-product produced GCCs and AACCs with the physical and mechanical characteristics similar than those obtained when 0.2 % of the commercial aluminium powder is added. This discussion is in accordance with that affirmed by Font et al. (Font et al., 2018, 2017), where the most effective method was to incorporate the recycled aluminium foil into the mixes by co-milling with the precursor.

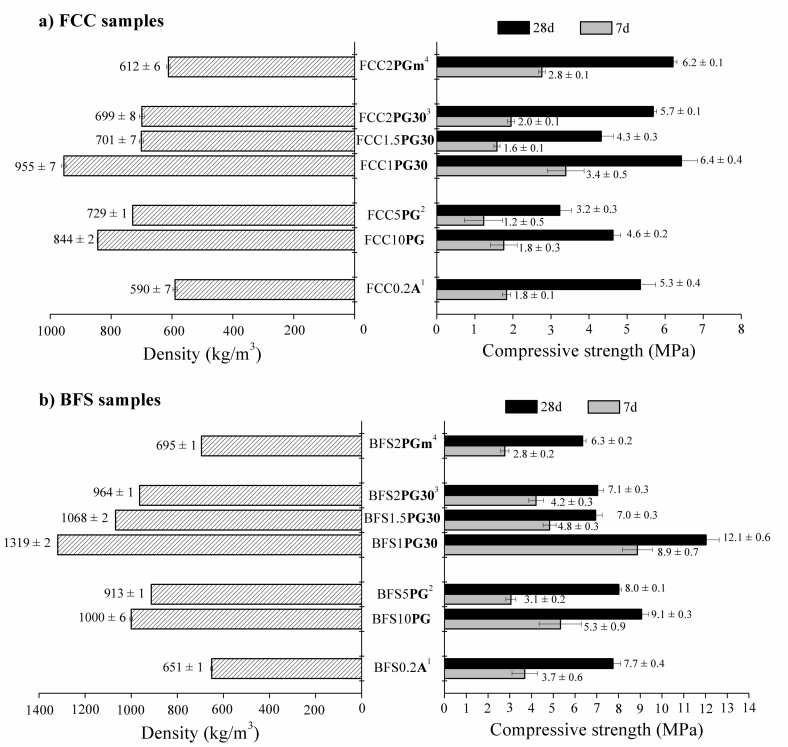

Fig.4.iv.8 *Natural densities and compressive strengths after 7 and 28 curing days for alternative cellular concretes that compares the aeration effect of PG modality: a) using FCC as precursor (GCC) and b) using BFS as precursor (AACC).*

[1] commercial aluminium; [2] PG; [3] PG 30 minutes milled; [4] PG co-milled with the precursor.

A stable void system with a homogeneous pore size and distribution is the key to providing a stable cellular concrete matrix that has good mechanical behaviour and low thermal conductivity (Nambiar and Ramamurthy, 2007; Yang et al., 2014). Narayanan and Ramamurthy (Narayanan and Ramamurthy, 2000b) reported that in cellular concretes, the zone between the cement paste and the voids represent a transition zone equivalent to the interface of cement paste with aggregates from traditional concretes. The density and the mechanical behaviour are related to the thickness and the compactness of this transition zone. The development of the regular void system (shape and size distribution) directly influences in the density and compressive strength of the cellular concrete (Alexanderson, 1979; Yang et al., 2014).

The void system configuration was analysed and compared for the PG, PG30 and PGm samples (10% wt% for PG and in 2% for PG30 and PGm). **Figs.4.iv. 9 and 10** show the FESEM micrographs, OM photographs and the void measurements tables for the FCC and the BFS studied samples, respectively.

Upon comparing the influence of the PG modality incorporation in the samples, the size of the pores is generally smaller when the PG particle size is lower. When PG10 is added to the matrix, the aeration was faster and aggressive and involved the development of large pores with irregular shapes, which are interconnected (**Figs.4.iv. 9a1, 9b1, 10a1 and 10b1).** The fresh paste is not consistent enough to entrap the generated hydrogen and the bubbles coalesce and escape. This situation is attenuated by the milling treatment of PG (when PG30 is used), as can be observed by the FESEM data (**Figs.4.iv. 9a2 and 10a2**). These samples presented a homogeneous distribution of voids with more regular shapes. The number of voids increased with the use of the finer PG powder, and was sometime located in the intermediate zone among the bigger pores. The best results were produced by FCCPGm (**Figs.4.iv. 9a3 and 9b3)** and BFSPGm (**Figs.4.iv. 10a3 and 10b3**), in which the reaction developed more slowly and the matrix retained the gas. In these samples, the void system appeared to be in a stable configuration and had a homogeneous range of sizes.

In general, two different imperfections in the void system configuration can be seen: Despite findings by Narayanan and Ramamurthy (Narayanan and Ramamurthy, 2000b) about the stronger transition zone in cellular concretes than in traditional concretes, some voids have an irregular shape due to the fracture of its transition zone.; Also, there are some unions between voids that are caused by the fracture of the wall among them. These two irregularities are a consequence of the strong gas pressure from the aerating reaction in the fresh matrix. During hardening, the paste does not have enough resistance to entrap the gas without breaking.

Alexanderson (Alexanderson, 1979) established a void system classification with differences between macropores (from the mass expansion caused by aeration) and micropores (distributed in the paste among the macropores). The small voids with a mean diameter lower than 100 μm were referred to as micropores and the bigger voids that have mean diameter equal or higher than 100 μm were referred to as macropores. The micropore and macropore size range intervals were assessed as a difference between the smallest and the biggest one. Analysing this distribution with the obtained results of density and compressive strength tests, the following observations can be made:

- For the FCC samples, the highest density and lowest compressive strength occurred for sample FCC10PG. This material yielded a micropore size range lower than for FCC2PG30 and a macropore size range larger than FCC2PG30 (**Figs.4.iv. 9a1 and 9b1** compared to **Figs.4.iv. 9a2 and 9b2**). These ranges mean that for FCC10PG, the micropores had a more regular and constant size distribution and the macropores had more irregular sizes compared to FCC2PG30. Considering the large number of large pores and their irregular shape, when PG was added without a milling treatment (FCC10PG sample), the paste was less consistent because of the interconnection between the voids. By comparing FCC2PG30 with FCC2PGm (**Figs.4.iv. 9a2 and 9b2 compared to Figs.4.iv. 9a3 and**

9b3), both the micropore range and the macropore range were lower when PG was co-milled with the precursor. The FCC2PGm samples had a good pore distribution with homogeneous mean void diameters with respect to the FCC2PG30 pore distribution. Subsequently, the void system structure was more homogeneous without pore interconnections and had a stable paste matrix (**Figs.4.iv. 9a3 and 9b3**). These observations could explain the discussion above about the lowest density and highest compressive strength for the FCC2PGm.

- In the case of the BFS mixes, BFS10PG had the highest density and mechanical strength. For this sample, the macropore range was similar and the range between micropores was lower when compared to BFS2PG30 (**Figs.4.iv. 10a1 and 10b1** compared to **Figs.4.iv. 10a2 and 10b2**). The BFS10PG sample did not present a large amount of micropores and the macropores yielded a more stable and compact paste matrix compared to the other samples. This fact explains its highest density value. For this sample, the aerating reaction was not enough to develop the required cellular structure. Sample BFS2PGm achieved the lowest values of density and compressive strength. In this case, the ranges of both the macropores and micropores were lower than those for the other systems (BFS10PG and BFS2PG30). The BFS2PGm system showed a stable and compact matrix with a homogeneous void shape and without interconnections, which enabled a cellular structure with a low density and sufficient mechanical behaviour (**Figs.4.iv. 10a3 and 10b3**).

A	B	C	D	E	F	G
66.8	74.1	55.3	52.7	38.0	40.1	30.9
H	I	J	K	L	M	
488.3	116.1	475.7	446.7	283.2	215.3	

A	B	C	D	E	F	G
106.1	89.3	65.3	57.8	39.7	26.3	105.4
H	I	J	K	L	M	N
192.5	105.1	202.0	752.1	253.3	92.7	45.6
O	P	Q	R	S	T	
47.6	89.3	719.6	241.2	25.4	832.6	

A	B	C	D	E	F	G
52.3	53.6	142.9	169.7	35.1	47.9	39.5
H	I	J	K	L	M	N
48.7	65.4	72.3	70.5	61.0	54.3	130.0
O	P	Q	R	S	T	U
669.9	305.2	253.0	265.5	168.3	384.1	339.4

A	B	C	D	E	F	G
3001	668	1900	551	432	702	
G	H	I	J	K	L	
1093	578	665	893	556	592	

A	B	C	D	E	F	G
2936	376	105	143	675	897	900
H	I	J	K	L	M	
546	1020	672	724	1520	705	

A	B	C	D	E	F	G
944	562	1065	599	765	732	345
H	I	J	K	L	M	N
396	1872	654	709	204	433	198

Fig.4.iv.9 *Void system characterization of GCC based on FCC. Void diameters (with values in µm) measured in: a) FESEM micrographs and b) OM images. For (1) FCC10PG, (2) FCC2PG30 and (3) FCC2PGm samples.*

A	B	C	D	E	F	G	H
118.3	44.7	13.4	46.3	29.8	156.3	209.1	322.0
I	J	K	L	M	N	O	P
67.3	89.0	70.0	128.8	589.5	72.1	75.6	80.1
Q	R	S					
102.3	223.0	1090					

A	B	C	D	E	F	G	H
91.5	52.3	22.2	75.92	35.6	59.5	41.2	47.1
I	J	K	L	M	N	O	P
76.5	74.9	28.0	55.4	48.1	36.7	236.7	78.9

A	B	C	D	E	F	G	H
12.3	13.4	74.1	136.2	44.3	50.9	61.6	70.2
I	J	K	L	M	N	O	P
84.8	65.4	38.5	43.7	46.5	51.0	12.1	63.8
Q	R	S	T	U	V		
218.4	187.6	94.3	192.3	370.7	464.0		

A	B	C	D	E	F	G	H
674	1982	187	334	1640	676	174	
H	I	J	K	L	M		
548	612	3102	403	2503	425		

A	B	C	D	E	F
458	987	1198	1697	2157	102
G	H	I	J	K	
98.9	549	378	422	1345	

A	B	C	D	E	F	G	H
449	345	754	2212	787	906	873	398
I	J	K	L	M	N	O	
829	392	405	769	673	231	129	

Fig.4.iv.10 *Void system characterization of AACC based on BFS: a) FESEM micrographs and b) OM images. For (1) BFS10PG, (2) BFS2PG30 and (3) BFS2PGm samples.*

The results for the density, compressive strength (after 7 and 28 curing days) and thermal conductivity for the FCC2PGm, BFS2PGm and their respective control systems that used 0.2 wt% commercial aluminium powder in are summarized in **Table 4.iv.4** for the 1000 cm^3 samples. There are noticeable differences when the properties that were measured on the 1000 cm^3 samples are compared with the same properties obtained for the 64 cm^3 samples (**Fig.4.iv.8**). When a bigger volume of material was manufactured, the density of BFS samples was lower than for the FCC samples. By comparing the 1000 cm^3 vs. 64 cm^3 samples, the densities increased 23% for FCC0.2A and FCC2PGm, and these decreased 10% for BFS0.2A and 13% for BFS2PGm. The differences among the cellular samples were attributed to the w/b ratio and to the mixing methodology.

With these results, is possible to confirm the influence of w/b ratio on the physical characteristics of the GCC and AACC. The metallic aluminium reacts with the alkali and liberates bubbles of hydrogen, which expand the matrix before setting. The paste must have a consistency that prevents the gas from escaping and allows a stable and homogeneous void system to form during the hardening process This in agreement with Esmaily et al. (Esmaily and Nuranian, 2012), who concluded than the density and compressive strength can be more intensely affected by the pore structure than for other manufacturing factors.

Table 4.iv.4
Density, compressive strength (after 7 and 28 days) and thermal conductivity (28 days) measured for 1000 cm^3 samples.

Sample	Density (kg/m^3)	Compressive strength (MPa)		Thermal conductivity (W/mK)
		7d	28d	
FCC0.2A	726 ± 3	3.9 ± 0.4	6.2 ± 0.2	0.26 ± 0.01
FCC2PGm	753 ± 2	4.1 ± 0.1	6.8 ± 0.3	0.31 ± 0.01
BFS0.2A	583 ± 4	3.8 ± 0.6	7.0 ± 0.2	0.13 ± 0.02
BFS2PGm	602 ± 7	4.2 ± 0.1	7.5 ± 0.1	0.16 ± 0.01

The results from the 1000 cm^3 samples showed a good physical performance in the FCC and BFS samples. The co-milling method of the PG by-product addition obtained densities lower than 800 kg/m^3, which were close to the control values for both utilized precursors. The FCC2PGm had a density only 3.7% higher than FCC0.2A and the BFS2PGm had a density 3.3% higher than BFS0.2A. The compressive strength values increased according to the densities. In comparison to the control samples, the strength for FCC2PGm increased 0.2 and 0.4 MPa after 7 and 28 days respectively. This represents about a 40% compressive strength gain with the curing in this period. In the case of the BFS samples, the compressive strength for BFS2PGm compared to BFS0.2A was 0.4 and 0.5 MPa higher after 7 and 28 days, respectively. This represents about a 45% compressive strength gain with the curing time at room temperature.

With respect to the thermal conductivity, the achieved values were higher with the increased density. For FCC2PGm, the thermal conductivity was 16% higher than the control samples. The same behaviour occurred for the BFS samples. Those yielded a thermal conductivity 18% higher when the PG was

used as the aerating agent with respect to the samples that used commercial aluminium powder (BFS0.2A). In any case, the thermal insulating properties for the new alternative environmentally friendly cellular concretes that contained PG were very appropriate.

4. Conclusions

In this work, the effective application of a salt slag recycled by-product (granulated paval, PG) as aerating reagent in alternative environmentally friendly cellular concretes was demonstrated. The following conclusions were drawn from the discussion of the experimental data:

- Chemical analysis indicated that the metallic aluminium content in the PG is the essential requirement for the GCC as well as AACC aeration process. The XRD patterns indicated the metallic aluminium presence in the resultant material when the precursor was milled with PG (FCCPGm and BFSPGm).
- Incorporation of PG into the milling treatment, together the precursor (FCC or BFS), is an excellent method to re-use this by-product in GCC and AACC production. This methodology might improve the productivity and reduce the costs (energy and economic). The fineness of the PG particles and their homogeneous distribution within the particles of the precursor determined the degree of aeration that yielded the most continuous and stable void system distribution in the matrix. The 2% addition of this by-product produced GCC and AACC with the physical and mechanical characteristics close to those obtained when the 0.2 wt% of commercial aluminium was added.
- There were noticeable differences in the physical and mechanical properties for the 1000 cm^3 samples with respect to those obtained for the 64 cm^3 samples. The influence of the void system configuration on the GCC and AACC properties was demonstrated. It was demonstrated that the selection of a suitable w/b ratio could be the key to obtaining a material with the consistency to prevent the gas escaping during the hardening.
- With the commercial aluminium powder replacement by PG in the new alternative environmentally friendly cellular concrete, it is possible to obtain an effective thermal insulating material.

Acknowledgements

The authors give special grateful to Befesa Aluminio S.L (Valladolid, Spain) for the granulated paval supply. The authors would also thanks to Cementval and BPOil for precursors supplying. Thanks are given to the Electron Microscopy Service of the Universitat Politècnica de València (Spain).

References

Aleksandrov, Y.A., Tsyganova, E.I., Pisarev, A.L., 2003. Reaction of Aluminum with Dilute Aqueous NaOH Solutions. Russ. J. Gen. Chem. 73, 689–694. https://doi.org/10.1023/A:1026114331597

Alexanderson, J., 1979. Relations between structure and mechanical properties of autoclaved aerated concrete. Cem. Concr. Res. 9, 507–514. https://doi.org/10.1016/0008-8846(79)90049-8

Araújo, E.G. de, Tenório, J.A.S., 2005. Cellular Concrete with Addition of Aluminum Recycled Foil Powders. Mater. Sci. Forum 498–499, 198–204. https://doi.org/10.4028/www.scientific.net/MSF.498-499.198

Arellano Aguilar, R., Burciaga Díaz, O., Escalante García, J.I., 2010. Lightweight concretes of activated metakaolin-fly ash binders, with blast furnace slag aggregates. Constr. Build. Mater. 24, 1166–1175. https://doi.org/10.1016/j.conbuildmat.2009.12.024

Ashraf, A. Al, 2014. Energy Consumption and the CO2 footprint in aluminium production.

ASTM International, n.d. ASTM D5334 - 14 Standard Test Method for Determination of Thermal Conductivity of Soil and Soft Rock by Thermal Needle Probe Procedure [WWW Document].

Babbitt, F., Barnett, R.E., Cornelius, M.L., Dye, B.T., Liotti, D.L., Schmidt, S.B., Tanner, J.E., Valentini, S.C., 2014. ACI 523.3R-14 Guide for Cellular Concretes above 50 lb/ft3 (800 kg/m3).

Befesa :: Press :: News archive :: 2013 [WWW Document], n.d. URL http://www.befesa.es/web/en/prensa/historico_de_noticias/2013/bma_20130307.html (accessed 4.15.18).

Dolton, B., Hannah, C., 2006. Cellular Concrete : Engineering and Technological Advancement for Construction in Cold Climates 1–11.

Ducman, V., Korat, L., 2016. Characterization of geopolymer fly-ash based foams obtained with the addition of Al powder or H_2O_2 as foaming agents. Mater. Charact. 113, 207–213. https://doi.org/10.1016/j.matchar.2016.01.019

Duxson, P., Provis, J.L., Lukey, G.C., van Deventer, J.S.J., 2007. The role of inorganic polymer technology in the development of "green concrete." Cem. Concr. Res. 37, 1590–1597. https://doi.org/10.1016/j.cemconres.2007.08.018

En, N.E., Une-en, N., General, B., n.d. española.

Esmaily, H., Nuranian, H., 2012. Non-autoclaved high strength cellular concrete from alkali activated slag. Constr. Build. Mater. 26, 200–206. https://doi.org/10.1016/j.conbuildmat.2011.06.010

Font, A., Borrachero, M.V., Soriano, L., Monzó, J., Mellado, A., Payá, J., 2018. New eco-cellular concretes: Sustainable and energy-efficient materials. Green Chem. https://doi.org/10.1039/c8gc02066c

Font, A., Borrachero, M.V., Soriano, L., Monzó, J., Payá, J., 2017. Geopolymer eco-cellular concrete (GECC) based on fluid catalytic cracking catalyst residue (FCC) with addition of recycled aluminium foil powder. J. Clean. Prod. 168, 1120–1131. https://doi.org/10.1016/j.jclepro.2017.09.110

Hamad, A.J., 2014. Materials, Production, Properties and Application of Aerated Lightweight Concrete: Review. Int. J. Mater. Sci. Eng. 2, 152–157. https://doi.org/10.12720/ijmse.2.2.152-157

Holt, E., Raivio, P., 2005. Use of gasification residues in aerated autoclaved concrete. Cem. Concr. Res. 35, 796–802. https://doi.org/10.1016/j.cemconres.2004.05.005

Hong, S.H., Lee, D.W., Kim, B.K., 2000. Manufacturing of aluminum flake powder from foil scrap by dry ball milling process. J. Mater. Process. Technol. 100, 105–109. https://doi.org/10.1016/S0924-0136(99)00469-0

IEEE 442-1981 - IEEE Guide for Soil Thermal Resistivity Measurements [WWW Document], n.d.

Luukkonen, T., Abdollahnejad, Z., Yliniemi, J., Kinnunen, P., Illikainen, M., 2018. One-part alkali-activated materials: A review. Cem. Concr. Res. https://doi.org/10.1016/j.cemconres.2017.10.001

Meyer, C., 2009. The greening of the concrete industry. Cem. Concr. Compos. 31, 601–605. https://doi.org/10.1016/j.cemconcomp.2008.12.010

Mo, K.H., Alengaram, U.J., Jumaat, M.Z., Yap, S.P., Lee, S.C., 2016. Green concrete partially comprised of farming waste residues: A review. J. Clean. Prod. 117, 122–138. https://doi.org/10.1016/j.jclepro.2016.01.022

Moraes, J.C.B., Tashima, M.M., Akasaki, J.L., Melges, J.L.P., Monzó, J., Borrachero, M. V., Soriano, L., Payá, J., 2016. Increasing the sustainability of alkali-activated binders: The use of sugar cane straw ash (SCSA). Constr. Build. Mater. 124, 148–154. https://doi.org/10.1016/j.conbuildmat.2016.07.090

Nambiar, E.K.K., Ramamurthy, K., 2007. Air-void characterisation of foam

concrete. Cem. Concr. Res. 37, 221–230. https://doi.org/10.1016/j.cemconres.2006.10.009

Narayanan, N., Ramamurthy, K., 2000a. Structure and properties of aerated concrete: A review. Cem. Concr. Compos. 22, 321–329. https://doi.org/10.1016/S0958-9465(00)00016-0

Narayanan, N., Ramamurthy, K., 2000b. Microstructural investigations on aerated concrete. Cem. Concr. Res. 30, 457–464. https://doi.org/10.1016/S0008-8846(00)00199-X

Neville, A.M., 1982. Properties of concrete, Fifth. ed, Journal of General Microbiology. Pearson Education Limited, England. https://doi.org/10.4135/9781412975704.n88

Panesar, D.K., 2013. Cellular concrete properties and the effect of synthetic and protein foaming agents. Constr. Build. Mater. 44, 575–584. https://doi.org/10.1016/j.conbuildmat.2013.03.024

Petek Gursel, A., Masanet, E., Horvath, A., Stadel, A., 2014. Life-cycle inventory analysis of concrete production: A critical review. Cem. Concr. Compos. 51, 38–48. https://doi.org/10.1016/j.cemconcomp.2014.03.005

Porciúncula, C.B., Marcilio, N.R., Tessaro, I.C., Gerchmann, M., 2012. Production of hydrogen in the reaction between aluminum and water in the presence of NaOH and KOH. Brazilian J. Chem. Eng. 29, 337–348. https://doi.org/10.1590/S0104-66322012000200014

RLG International cementreview, n.d.

Sanjayan, J.G., Nazari, A., Chen, L., Nguyen, G.H., 2015. Physical and mechanical properties of lightweight aerated geopolymer. Constr. Build. Mater. 79, 236–244. https://doi.org/10.1016/j.conbuildmat.2015.01.043

Song, Y., Li, B., Yang, E.H., Liu, Y., Ding, T., 2015. Feasibility study on utilization of municipal solid waste incineration bottom ash as aerating agent for the production of autoclaved aerated concrete. Cem. Concr. Compos. 56, 51–58. https://doi.org/10.1016/j.cemconcomp.2014.11.006

van Boggelen, D.R., 2011. Safe aluminium dosing in AAC plants. 5th Int. Conf. Autoclaved Aerated Concr. 45–50.

World Aluminium, 2014. Environmental Metrics Report Year 2010 Data Final 21.

Yang, K.H., Lee, K.H., Song, J.K., Gong, M.H., 2014. Properties and sustainability of alkali-activated slag foamed concrete. J. Clean. Prod.

68, 226–233. https://doi.org/10.1016/j.jclepro.2013.12.068

4.2.2 Hormigones Eco-celulares (ECC)

Forman parte de esta **segunda etapa** experimental las siguientes publicaciones:

v. New eco-cellular concretes: sustainable and energy-efficient materials

vi. Air-void system characterization of new eco-cellular concretes

v. New eco-cellular concretes: sustainable and energy-efficient materials

AUTORES: Alba Font, María Victoria Borrachero, Lourdes Soriano, José Monzó, Ana Mellado y Jordi Payá

REFERENCIA DE LA PUBLICACIÓN: Green Chemistry 20 (2018) 4684-4694
DOI: http://dx.doi.org/10.1039/C8GC02066C

Factor de impacto/Cuartil (2018): 9.405/Q1	**Citas (excluyendo auto citas): 1**

MATERIALES	FABRICACIÓN
• **TCC:** OPC + H_2O + A • **GCC:** FCC + [WG+NaOH+H_2O] + A_R • **ECC:** FCC + [RHA+NaOH+H_2O] + A_R • **AACC:** BFS + [WG+NaOH+H_2O] + A_R • **ECC:** BFS + [RHA+NaOH+H_2O] + A_R	• **CO-M:** FCC + A_R = FCCRm • **CO-M:** BFS + A_R = BFSRm • **CURADO:** TA • **Amasado con:** PD

PROCEDIMIENTO EXPERIMENTAL

CARACTERIZACIÓN DE MATERIAS PRIMAS	CARACTERIZACIÓN DE ESPECÍMENES
-	• Densidad natural (D_N) • Resistencia mecánica (Rc) • Conductividad térmica (KD2-Pro) (λ) • Cálculo de la huella de carbono (CO_2/m^3)

RESULTADOS Y CONCLUSIONES MÁS RELEVANTES DE LA INVESTIGACIÓN

- En la investigación se demuestra la posibilidad de sustituir el WG, de la disolución activadora, por RHA en la fabricación de hormigones celulares alterativos.
- Los factores que más contribuyen en la huella de carbono son el OPC en los TCC y el WG en los GCC y los AACC. En el caso de los ECC el factor más influyente es el proceso de molienda de las materias primas.
- Tras 28 días de curado a temperatura ambiente se obtuvieron los siguientes resultados:

Material	D_N (kg/m^3)	Rc (MPa)	λ (W/mK)	CO_2 / m^3
TCC	618	6.5	0.182	467.6
GCC	813	4.3	0.083	356.5
ECC-FCCRm	782	3.2	0.113	120.4
AACC	474	2.6	0.281	245.2
ECC-BFSRm	611	4.6	0.224	102.9

- Con los nuevos ECC se consigue disminuir la emisión de CO_2 a la atmósfera respecto a los TCC en un 74 % cuando se emplea FCCRm y en un 78 % cuando se emplea BFSRm.

Abstract: Chemistry is an essential science for understanding and developing construction materials. Specifically, the application of the green chemistry concept to the cement sector might allow the fabrication of new environmentally friendly materials in sustainability and energy efficiency terms. Cellular concretes are an excellent alternative to conventional concrete in thermal insulation and material saving terms. In this paper the development of waste-based cellular concrete is presented bearing out its good performance and the focus of their low environmental impact is warrantied. Three different cellular concrete systems were investigated: i) traditional cellular concrete based on ordinary Portland cement and commercial aluminium powder; ii) geopolymer cellular concrete applying the alkali activated chemical technology, by comparing the use of two precursors, fluid catalytic cracking catalyst residue (FCC) and blast furnace slag (BFS) as precursors, and recycled aluminium foil as an aerating agent; iii) eco-cellular concrete, where commercial waterglass was replaced by an agro-industrial by-product, rice husk ash (RHA), in the activating solution. The development of geopolymer cellular concrete with different precursors and activating solutions have proven that the production of this type of concrete by using different nature precursors and in several availability, context is enabled depend of the by-products and wastes availability. The density, compressive strength, and thermal properties of the three cellular concrete systems were assessed and a complete study on the carbon footprint of the developed concretes is presented. The results show alternative concretes with densities from 474 to 813 kg/m^3, with compressive strength from 2.6 to 4.6 MPa, and with thermal conductivities from 0.083 to 0.281 W/mK. In the case of the cellular concrete prepared by using RHA in the activating reagent, the heat released from dissolution of NaOH pellets in water dissolve the soluble silica present in the ash. The production implied a reduction of which carbon footprint by 78%.

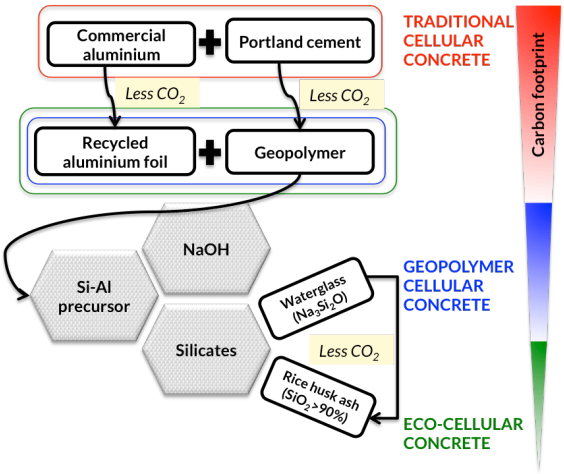

GRAPHYCAL ABSTRACT (4.v)

Abbreviations:
OPC: Ordinary Portland cement
A: Commercial aluminium powder
FCC: Fluid catalytic cracking catalyst residue
BFS: Blast furnace slag
RAF: Recycled aluminium foil
RHA: Rice husk ash
TCC: Traditional cellular concrete (OPC + commercial aluminium powder: OPCA)
GCC: Geopolymer cellular concrete: co-milling of precursor and recycled aluminium foil (RAF):

- FCCRm: Solid resulted of the co-milling of FCC and RAF
    - FR samples: Material resulted of blending FCCRm with the conventional activating solution
- BFSRm: solid resulted of the co-milling of BFS and RAF
    - SR samples: Material resulted of blending BFSRm with the conventional activating solution

ECC: Eco-cellular concrete: use the RHA as silica source in activating solution (alternative activating solution):

- FRR samples: Material resulted of blending FCCRm with alternative activating solution
- SRR samples: Material resulted of blending BFSRm with alternative activating solution

1. Introduction

Nowadays, 50% of total CO_2 emissions, 40% of used primary power and 75% of electric power generation come from the building industry(Cabeza et al., 2014; Ortiz et al., 2009). Construction materials are an important factor of these consumptions and conventional concrete is the most widely used material in this industry (Jiang et al., 2014). The use of this material structurally goes beyond requirements in most situations.

Cellular concrete can be an environmentally friendly material with great insulation and low density properties (Cavanaugh and Speck, 2002) (300–1800 kg/m^3) that yields moderate mechanical behaviour (Narayanan and Ramamurthy, 2000). It is an ordinary Portland cement (OPC) based material prepared by mixing with water, and occasionally with fine aggregates (sand or lightweight aggregates), with an internal air-void system formed by the addition of suitable reagents. There are two methods to introduce air into the matrix: a chemical reaction in the alkaline medium of metal powders (aerated concrete) or foam introduced with a surfactant addition (foamed concrete) (Zhang et al., 2014). The combination of these methods has been recently studied to improve a suitable porous structure (Esmaily and Nuranian, 2012).

The addition of metallic aluminium powder is the most widespread method employed for air-bubbles entrapping in traditional cellular concretes (TCC) (Arellano Aguilar et al., 2010). This reagent is oxidised in an OPC alkaline medium, where it comes in contact with the mixing water and the produced H_2 gas, as shown in **Equation (4.v.1**).

$$2Al + 3Ca(OH)_2 + 6H_2O \implies 3CaO \cdot Al_2O_3 \cdot 6H_2O + 3\,H_2 \qquad (4.v.1)$$

For many applications, TCC can provide cost and performance benefits compared with traditional construction materials. As this material combines insulation properties and structural capability, it is excellent for walls, floors and roofs, and its cost is sufficiently competitive with brick, wood and other materials costs (Bremner et al., 1997). Furthermore, TCC is easy to cut, shape and size, and it readily takes nails or screws. Common TCC applications are: pre-cast lightweight blocks, cast *in situ* lightweight walls, roof and floor insulation screeds, void-filling, ground stabilisation, geotechnical and mine fill applications, and roads on soft grounds (Bremner et al., 1997; Dolton and Hannah, 2006; Panesar, 2013).

Thus, TCC are an excellent alternative to conventional concrete in several structural situations. Even so its components are actually responsible for major environmental and energetic impacts.

The ordinary Portland cement represents nearly 70% (by wt) of total TCC constituents (as opposed to 11% in conventional concrete), and the impact of this binder is well-known in terms of energy demand, non-renewable materials

and the CO_2 footprint (Gartner, 2004; Scrivener and Kirkpatrick, 2008). From a chemical point of view, the application of the alkali activation aiming the OPC replacement, are commonly studied as a cleaner alternative (Davidovits, 2002; Duxson et al., 2007; Palomo and López de la Fuente, 2003). The alkali-activated cements or geopolymers consist of two essential components: a precursor, a mineral silico-aluminate raw material, rather amorphous or vitreous; and an alkali activator, a high concentrated aqueous dissolution of alkali compounds (hydroxides, silicates). The geopolymerization calls for inorganic polycondensation reaction, which results in three-dimensional zeolitic frameworks (Davidovits, 1994). For this hardening (setting) mechanism, the first step is the precursor dissolution in contact with the OH^- groups (that involves a high alkaline medium). The Al and Si ion are diffused or transported from the particle surface inward, giving rise to a gel-like phase. And finally, a rigid chains or series of intertwined tetrahedral joined by oxygen atoms are developed (species polycondensation), which must have alkaline cations enough to offset the charge from the tetra-coordinated aluminium. The result is a well-stabilised, stable and insoluble geopolymer binder.

The mineral precursor may be a synthetized product, such as metakaolin (MK), or an industrial waste, such as fluid catalytic cracking catalyst residue (FCC), fly ash or blast furnace slag (BFS). Depending on the calcium content in the precursor, they can be classified according to the nature of the reaction product: i) precursors with low calcium content (**Equation (4.v.2)**) reacts to form alumino-silicate hydrate gel (NASH); and ii) precursors with high calcium content (+ CaO > 30 %, **Equation (4.v.3)**) reacts to form calcium alumino-silicate hydrate gel (CASH).

$$Precursor + (Na,K)OH \text{ or } (Na,K)_2SiO_3 + H_2O \rightarrow (Na,K)_2O\text{-}Al_2O_3\text{-}SiO_2\text{-}H_2O \text{ (NASH gel)} \quad (4.v.2)$$

$$Precursor + (Na,K)OH \text{ or } (Na,K)_2SiO_3 + H_2O \rightarrow (\ (Na,K)_2O\text{-}CaO\text{-}Al_2O_3\text{-}SiO_2\text{-}H_2O \text{ (CASH gel)} \quad (4.v.3)$$

The applications of geopolymer systems in manufacturing cellular concretes have emerged as a novel lightweight insulation material (Zhang et al., 2014). In the geopolymer system for cellular concrete manufacture the strongly alkaline medium make effective the aluminium oxidation thus ensuring hydrogen release as shown in **Equation (4.v.4)**. Recent research has focused on studying these new materials. The use of BFS as a precursor to produce cellular concretes has been reported by Esmaily et al. (Esmaily and Nuranian, 2012) where aluminium powder aeration was combined with the sodium lauril sulphate foaming effect. Besides, Font et al. (Font et al., 2017) have recently tested FCC as a precursor in cellular concrete aerated by using recycled aluminium foil. Both of these studies obtained excellent results thanks to their easy production and good performance without any autoclave curing process requirement.

$$Al\,(s) + 3H_2O + OH^-_{(ac)} \Longrightarrow Al(OH)_4^-{}_{(ac)} + 3/2\,H_{2\,(g)} \qquad (4.v.4)$$

The alkali solution commonly used for geopolymer activation requires silicates to obtain good-performing materials, thus the SiO_4^{4-} anion favours the formation of a denser and stronger structure (Provis, 2016). By its important reactive part of silica, the commercial waterglass (WG) is the most common chemical reagent utilised, combined with NaOH/water solution. Nevertheless the WG is expensive (20 % of total cost of alkali activated cement production) and this synthesis represent a higher greenhouse gas emitter process (50 – 70 % of total emissions of alkali activated cements constituents) (Mellado et al., 2014). The sodium silicate production consists on the melting of silica (SiO_2) and sodium carbonate (Na_2CO_3) until 1400ºC (Turner and Collins, 2013), releasing a large amount of CO_2 (**Equation (4.v.5)**). For this reason, studying alternatives to replace this silica source has become the next "must have" in recent years (Dodson et al., 2013), and rice husk ash (RHA) (Bouzón et al., 2014), sugar cane straw ash (SCSA) (Moraes et al., 2018) and glass waste (Torres-Carrasco and Puertas, 2015) (GW) have been recently investigated.

$$x\,Na_2CO_3\,(s) + y\,SiO_2\,(s) \rightarrow (Na_2O)_x(SiO_2)_y\,(s) + x\,CO_2\uparrow(g) \qquad (4.v.5)$$

Near 471 million tons of rice were produced in 2014 which the hull represents 20% by weight ("EST: Publications," n.d.). The rice hull is removed and is burned to their volume reduce for disposal. This RHA contains 65 – 90 % wt % amorphous SiO_2 (Marchal et al., 2015). The appropriate management of rice husk and their ashes becomes an important environmental aspect because the contamination produced in farmland and watercourses in agricultural regions. The high silica content in rice husk ashes may allow their use in the new alternative geopolymer binders by its solubilisation in the activating solution yielding important environmental as well as economic profits. Recently, the use of RHA as a silica source in one-part slag alkali activated binders was introduced (Luukkonen et al., 2018). These binders consist on the mix of the precursor with the solid alkali activator and water is added to initiate the reaction.

Another high environmental and economic impact of TCC is caused by aluminium powder manufacturing. To obtain one tonne of pure aluminium from bauxite, 15000 kWh of heat generated by electric energy is required and five tons of residues are produced (Ayres, 1995; U.S. Department of Energy, 2007). Apart from this, there is the additional major contribution of treatment subsequent to powder manufacturing by stamp milling, ball milling under dry conditions, wet ball milling, attrition milling and vibration milling. Since aluminium never loses its performance or strength during the recycling process, the same piece of aluminium can enter the secondary production process time and time again, which multiplies cost savings and environmental benefits. Furthermore, recycling aluminium achieves up to 95% of energy savings compared to the energy required to manufacture the same amount of aluminium to avoid depletion in bauxite extraction. The result is a reduction in

power from 21 kWh in the 1950s to 14 kWh in 1997 for 1 kg of manufactured aluminium ("Arpal Asociacion para el Reciclado de Aluminio," n.d.).

The use of alternative sources of aluminium to TCC aeration have been investigated by Araujo et al. (Araújo and Tenório, 2005) by incorporating aluminium recycled scrap powders. As a result, cellular concrete blocks with densities less than 500 kg/m^3 and low compressive strength (1.5 MPa) were obtained by an autoclaved curing treatment (200ºC and 10atm). These authors concluded that milling time, oxidation level and addition of hard particles are the parameters that control the required density and strength properties.

Recycled domestic foil is another interesting alternative to use as a reagent. Annually in Europe, close to 860000 tons of aluminium foil are produced, which represents a mean use of more than 26 m^2 per habitant (European Aluminium Foil Association, n.d.). The inclusion of recycled foil in the milling procedure of FCC has been recently tested by Font et al. (Font et al., 2017) to use it as a raw material in new geopolymer cellular concrete (GCC) manufacturing. These GCC offer several advantages over traditional OPC-based cellular concretes in terms of natural densities, air-void distribution and thermal conductivity.

2. Objective

In the present paper three steps to improve the sustainability and energy-efficiency landscape of TCC are introduced, combined and discussed: i) developing a geopolymer system by using both FCC and BFS as alternative precursors to replace OPC; ii) using recycled aluminium foil (RAF) to replace commercial aluminium powder (A); iii) producing the activating solution by using rice husk ash (RHA) as an alternative silica source for replacing commercial waterglass (WG).

The study of two precursors with different nature (high calcium vs. low calcium content) is essential to test the material reproducibility depending on the manufacture context and resources availability. The fluid catalytic cracking residue (FCC) is a low calcium content precursor whose potential as geopolymer precursor was proved by Tashima et.al (Tashima et al., 2012). On the other hand, the blast furnace slag (BFS) is a high calcium precursor and CaO/SiO_2 molar ratio between 0.1 and 0.6 are considered suitable for alkaline activation (Talling and Brandstetr, 1989). The FCC was selected to continue the previous work (Font et al., 2017) where the precursor was mixed with RAF using a conventional alkali solution (NaOH + water + WG). In the case of BFS there is no previous works where cellular concrete of this activated precursor was aerated by RAF addition.

Natural density, mechanical behaviour and thermal insulation must be assessed and controlled to obtain good-performing cellular concretes. Thus, the proposed materials were tested to verify its resultant behaviour.

The aim of the present investigation is the new eco-cellular concrete development, which yields good performance and represents a potential solution front the traditional cellular concrete in terms of environmental and energy-saving impacts (measured as carbon footprint assessment).

3. Experimental

3.1. Materials

In **Table 4.v.1** an overview of the material composition of each mixture assessed in this study is shown. Three cellular concrete systems were fabricated, tested and compared:

i. Traditional cellular concrete (TCC), which consists in a traditional cellular system based on OPC aerated by commercial aluminium powder (A). These two materials were dry-mixed manually for 1 minute to homogenise, and the mix was used as raw material (OPCA) to reference material manufacture (CA).

ii. Two geopolymer cellular concretes (GCCs), designed by employing the dry solid resulting from the co-milling of the precursor with recycled aluminium foil (RAF) as the raw material: a) FCC with RAF (hereafter called FCCRm); and b) BFS with RAF (hereafter called BFSRm). The activation of each precursor (FCC or BFS) was by using an alkali solution made from sodium hydroxide and commercial waterglass (NaOH/WG).

iii. Two eco-cellular concretes (ECCs), prepared with the same raw material combinations as GCCs (FCCRm and BFSRm), where in the alkali solution the commercial waterglass was replaced with an alternative source of active silica, the rice husk ash (RHA).

Table 4.v.1
Overview of dosages.

	Mixtures	Solid phase				Liquid phase
		Precursor	Aluminium type	Pre-treatment	Raw material designation	
TCC	**CA**	OPC	A	Dry mix	**OPCA**	Water
GCC	**FR**	FCC	RAF	Co-milling	**FCCRm**	NaOH + WG
	SR	BFS			**BFSRm**	
ECC	**FRR**	FCC			**FCCRm**	NaOH + RHA
	SRR	BFS			**BFSRm**	

OPC (CEM I 52.5R) was supplied by Lafarge S.A (Puerto de Sagunto, Spain). Fluid catalytic cracking catalyst residue (FCC) was supplied by the BP Oil Company (Grao de Castellón, Spain) and blast furnace slag (BFS) was supplied as large grains by Cementval S.A (Puerto de Sagunto, Spain). The chemical compositions of OPC, FCC and BFS are summarized in **Table 4.v.2.**

Commercial aluminium powder (A) was supplied by Schlenk Metallic Pigments GmbH, whose mean particle diameter was 30 μm and the recycled aluminium foil (RAF), was supplied by the Department of Agricultural Forest Ecosystems

at the Universitat Politècnica de València (Valencia, Spain). RAF was recycled after using it to cover crop glass containers in autoclaving treatments. FCC and BFS required a previous milling treatment to obtain a fine material to be used as a solid precursor (Moraes et al., 2016; Payá et al., 1999). As previously demonstrated (Font et al., 2017) the method to incorporate RAF into the paste matrix to allow optimal reaction performance is done by blending RFA (previously reduced in small sheets: 35 mm long, 4 mm wide) in the FCC milling process. FCC and RAF sheets (0.2% wt%) were milled in a ball mill for 20 minutes to obtain a new raw material for cellular concrete manufacturing, which was designated as FCCRm (**Table 4.v.1**). Its mean particle diameter (D_{mean}) was 18.43 µm. BFS and RAF sheets (0.2% wt%) were milled in a ball mill for 30 minutes to obtain a new raw material for cellular concrete manufacturing, which was designated as BFSRm (**Table 4.v.1**). Its mean particle diameter (D_{mean}) was 26.28 µm.

To prepare the activating solutions, the following chemical reagents were used: i) sodium hydroxide (NaOH) in the form of pellets (98% purity), acquired from Panreac S.A; ii) commercial sodium silicate (or commercial waterglass - WG), supplied by Merck-Spain (8 wt% Na_2O, 28% wt% SiO_2 and 64% wt% H_2O). Finally, rice husk ash (RHA) was utilised as an alternative silica source to produce the activating solution. This ash was supplied by DACSA S.A (Tabernes Blanques, Spain). RHA is composed mainly of SiO_2 (85.6 wt%), as seen in **Table 4.v.2**, and was used without milling (D_{mean} of 62.3 µm) because the particle diameter did not influence on the mechanical properties of geopolymers, as was reported by Bouzón et al. (Bouzón et al., 2014).

Table 4.v.2
Chemical compositions of OPC, FCC, BFS and RHA (wt%).

	SiO_2	Al_2O_3	Fe_2O_3	CaO	MgO	SO_3	K_2O	Na_2O	P_2O_5	TiO_2	Cl	LOI*
OPC	20.80	4.60	4.80	65.60	1.20	1.70	1.00	0.07	-	-	-	0.23
FCC	47.76	49.26	0.60	0.11	0.17	0.02	0.02	0.31	0.01	1.22	-	0.53
BFS	30.53	10.55	1.29	40.15	7.43	1.93	0.57	0.87	0.26	0.89	-	5.53
RHA	85.58	0.25	0.21	1.83	0.5	0.26	3.39	-	0.67	-	0.32	6.99

*Loss on ignition

The experimental planning of this research was divided into two phases:

- First, the GCC and ECC mixes were prepared and tested by comparing the results with those obtained for the control samples of TCC. Density, compressive strength and thermal conductivity were studied.
- Secondly, calculation of the carbon footprint attributed to these GCCs and ECCs compared to TCC.

Samples mixing and testing

In this study, to the air bubble generation in the cellular concrete matrix (TCC, GCC and ECC), aluminium powder (A or RAF in each case) was added at 0.2% by weight of the solid precursor (OPC, FCC or BFS). This reagent percentage has been commonly tested by several authors (Muthu Kumar and Ramamurthy, 2017), which allows traditional cellular concrete with excellent physical and mechanical performances to be obtained. For the liquid phase, to gain an appropriate viscosity for good air-void development, the water/binder (w/b) ratio was selected f mixture. This ratio was: i) w/b = 0.5 for the TCC system (CA samples); ii) w/b = 0.6 for the FR mixes and w/b = 0.7 for the FRR mixes; iii) w/b = 0.35 and w/b = 0.45 for the SR and the SRR mixes, respectively. In the geopolymer systems, the alkali activator solution parameters that determine the amount of NaOH and silica (WG in GCC or RHA in ECC) remained constant as follows: the Na^+ molality was 7.5 and the SiO_2/Na_2O molar ratio was 1.7. These parameters have been previously studied by Payá et al. (Payá et al., 2009) and Bouzón et al. (Bouzón et al., 2014) and were applied to GCC based on FCC by Font et al. (Font et al., 2017). The dosages for the samples based on BFS were maintained at the same proportions to make their physical and mechanical properties comparable, and in carbon footprint calculation terms. To prepare the alkaline solution, for GCC systems, NaOH and WG were mixed with water, and rest in a plastic beaker sealed with plastic film until room temperature was reached. For ECC, NaOH and RHA were mixed with water in a thermal bottle for 1 minute. To improve the solubilisation of silica in RHA by the heat released from the NaOH dissolution in water (according to **Equation (4.v.6)**), the thermal bottle was rest during 24 hours.

$$2x\ NaOH\ (s) + y\ SiO_2\ (s) + n\ H_2O \rightarrow (Na_2O)_x(SiO_2)_y(H_2O)_{n+x}\ (solution) \qquad (4.v.6)$$

An AEG SBE705RE power drill connected to a paint mixer was used for sample preparation. For the cellular concrete manufacturing, the solid was mixed with its respective liquid phase (water for TCC or alkaline reagent for GCC and ECC) for 190 seconds in the TCC mixes and for 30 seconds for the dissolution, plus 90 seconds when the solid blend was incorporated into the GCC and ECC mixes (the total mixing time was 120 seconds). The alkali activated systems required a shorter mixing time because the high alkalinity medium provided a quick aluminium powder reaction compared to OPC systems. No compacting treatment was carried out to avoid gas escaping from the aerated concrete during the setting process. For each resulting concrete twelve 10x10x10 cm^3 cube specimens were moulded and cured at 23°C and 100% RH for 24 h when the free surface of cubes had to be cut with a saw blade. Then specimens were demoulded and kept in a wet chamber (23°C and 100% RH) until testing.

By considering natural density (ρ) to be the volumetric mass density (mass per unit volume), it was determined by means of the weight of the 10-cm cubic samples before compressive strength testing. The compressive strengths of

the cellular concretes were obtained by an INSTRON 3282 universal testing machine. The compressive test was performed after 7 and 28 curing days. Tests were carried out on four cubic specimens (10x10x10 cm^3) for each curing time, and averages and standard deviation values were calculated.

A KD2-Pro handheld device (Decagon Devices Inc.) was employed to determine thermal conductivity. Thermal measurements were taken by a thick (6 cm long, 3.9 mm diameter) single RK-1 sensor based on the dual needle probe system (transient line source method) according to ASTM D5534-08 (ASTM International, n.d.) and Standard IEEE 442-1981 ("IEEE 442-1981 - IEEE Guide for Soil Thermal Resistivity Measurements," n.d.). Before taking measurements, a standard (RH-1-01116, 0.387±10% W/mK) was used to verify the sensor's good performance. Room temperature thermal conductivity was measured on four cubic specimens (10 x 10 x 10 cm^3) of each formulation. A rotary hammer bit to drill pilot holes (6 cm long, 4 mm diameter) was necessary to accommodate the RK-1 sensor.

Carbon footprint calculation

The calculations and comparisons among the CO_2 emissions related to the TCC, GCC and ECC systems were made.

To that end, the International Panel on Climate Change (IPCC) Guidelines for National Greenhouse Gas Inventories was followed (Eggleston et al., 2006). The general methodology employed to estimate the CO_2 emissions associated with a particular process involves the product of activity level data: the amount of the material processed or the amount of energy consumed, and an associated emission factor per unit of consumption/production according to:

$$E_i = A_i EF_i \qquad (4.v.7)$$

Where E_i = the process emission (kg) of CO_2 from each component or operation 'i'; A_i = the amount of activity or processed material 'i'; and EF_i = the emission factor associated with the CO_2 per unit of activity or process material 'i'.

Two different phases were assessed: i) Phase 1: emissions associated with each single material which forms a cellular concrete (called emissions associated with the components, E_C); ii) Phase 2: emissions associated with the cellular concrete manufacture considering laboratory conditions (milling and mixing procedures) (E_M). The carbon footprint calculation result was calculated as the sum of the emissions from its two phases (**Equation (4.v.8)**).

$$E_{TOTAL,\,i} = E_{C,\,i} + E_{M,\,i} \qquad (4.v.8)$$

Where "i" is the sample (CA, FR, FRR, SR or SRR).

Calculations were made to obtain, in the same context (laboratory conditions), 1 m^3 of each material. For the volume of manufactured materials to be comparable, their same density was considered herein (600 kg/m^3). By considering this aspect, the currently commercial cellular concretes with the proposed alternatives and the same properties were compared.

The amounts of the solid precursor, combined water and solid alkali compounds present in each mix were obtained from the thermogravimetric analysis (TGA) with a Mettler–Toledo TGA 850. The obtained DTG curve provides the amount of water chemically combined in the samples in weight percentage. The weight difference corresponds to the solid phases: precursor, Na_2O and SiO_2. Whit a determined dosage (w/b ratio, Na^+ molality and SiO_2/Na_2O molar ratio) the solid phases proportion in the samples is constant, and the amount of the precursor to obtain a cellular concrete with a done density can be determined by the relationship shown in **Fig.4.v.1:**

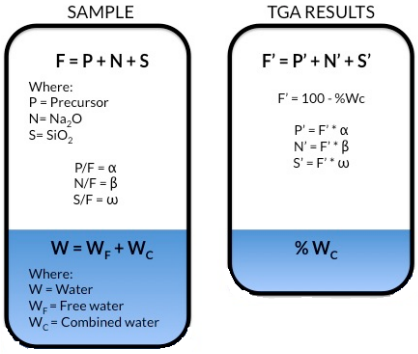

Fig.4.v.1 *Methodology for obtaining the dosages of cellular concretes from TGA analysis results.*

4. Results and discussion

4.1. Physical and mechanical characterisation

Table 4.v.3 shows a summary of the results obtained in the experimental section of the cellular concretes studied in this work.

Table 4.v.3
TCC, GCC and ECC properties obtained from tests

	Natural density (kg/m^3)	Compressive strength (MPa)		Thermal Conductivity (W/mK)
		7d	28d	
CA	618 ± 2	4.5 ± 0.4	6.5 ± 0.4	0.182 ± 0.001
FR	813 ± 2	3.5 ± 0.2	4.3 ± 0.4	0.083 ± 0.003
FRR	782 ± 4	2.6 ± 0.4	3.2 ± 0.3	0.113 ± 0.005
SR	474 ± 4	1.6 ± 0.5	2.6 ± 0.2	0.281 ± 0.007
SRR	611 ± 4	3.2 ± 0.2	4.6 ± 0.3	0.224 ± 0.007

The TCC based on OPC and commercial aluminium powder (A), CA sample, had a natural density of 618±2 kg/m^3 and its compressive strength yielded 4.5 and 6.5 MPa for 7 and 28 curing days, respectively. These values are in line with those reported in the literature, where values of 600 kg/m^3 are related with compressive strengths of 2.8 to 6.3 MPa at 28 days (Hamad, 2014; Narayanan and Ramamurthy, 2000).

For the GCC system, activated by a traditional alkali solution (NaOH, commercial waterglass and water), replacing the commercial aluminium powder (A) by recycled aluminium foil (RAF) allowed interesting cellular systems to be obtained.

With the addition of RAF, the FR resultant material yielded a natural density of 813±2 kg/m^3 (31.6% higher than the TCC system). Compressive strength varied from 3.5 after 7 days to 4.3 MPa after 28 days. In contrast with its natural density value, this mechanical behaviour represents a 34.1% reduction compared to the TCC system. These results do not agree with those reported by Font et al. (Font et al., 2017) in their previous research work where the geopolymer samples with FCC allowed the natural density to lower and yielded a compressive strength gain compared to the TCC systems. It could be attributed to the difference in the w/b ratio and to specimen dimensions. Since cellular concretes should flow to avoid compaction or vibration, for a larger volume material the required w/b ratio would have to be equal 0.6. This value involves higher fluid consistence and, consequently, extends the time spent on gaining matrix stability, which allows gas entrapping. During this time, most of the generated gas from the aluminium reaction was not entrapped, and the resultant void-system in the paste produced a poorer performing system in terms of natural density and strength. In a previous research, for foamed concrete, Nambiar and Ramamurthy (Nambiar and Ramamurthy, 2007) and Zhang et al.(Zhang et al., 2014) established that a controlled w/b range is required to develop an optimal and stable void system in the matrix.

With the use of BFS precursor, the RAF reaction into the cementitious matrix involves an effective cellular structure and the resultant average density of the SR samples was 474±4 kg/m^3 (23.3% lower than CA). The mechanical strength was 1.6 MPa after 7 curing days, and 2.6 MPa after 28 days. The strength value was 60.9% lower than the CA compressive strength. This expected behaviour in the SR samples agrees with the linear relationship between density and compressive strength in cellular concrete systems. In this case, given the low w/b ratio of 0.35, most of hydrogen gas was entrapped in the matrix, which led to lower natural density compared to TCC.

The ECC systems, where the traditional activating solution (NaOH, commercial waterglass and water) was replaced by a mixture of NaOH and RHA in water, showed interesting behaviour. Concrete prepared with FCC (FRR) had natural density of 782±4 kg/m^3, which was 26.6% higher than CA, and was similar to the FR sample. Compressive strength yielded from 2.6 MPa after 7 curing days to 3.2 MPa after 28 curing days. This mechanical behaviour was 51.3% lower than that obtained in the CA samples which, as with the FR

samples, contrasts with the strength-density linear relationship usually found in cellular concretes. This can be explained by the same discussion as that mentioned above based on the w/b ratio. In the BFS-based ECC system (SRR samples), the results showed an interesting evolution when WG was replaced by RHA and its natural density was similar to that obtained in the CA samples (611±4 kg/m^3). Compressive strength yielded 3.2 MPa after 7 days of curing and 4.6 MPa after 28 days, values significantly higher than those obtained for SR concrete.

These results highlighted that the amount of silica soluble from RHA allows obtain an appropriate alkali activator reagent, which potentially reacts with the precursors forming the cementing gels. In any case, the use of an aerating agent as well as replacing the commercial aluminium powder with recycled aluminium foil (RAF) allowed good-performance cellular concretes to be prepared.

Regarding thermal properties (**Table 4.v.3**), the traditional cellular samples (CA) yield 0.182 W/mK. With the alternative geopolymer systems, the highest value was obtained for SR sample (0.281 W/mK) followed by SRR (0.224 W/mK), FRR (0.113 W/mK) and finally FR, which yield the lowest value (0.083 W/mK). With the results obtained herein, we highlight the good insulation performance of the studied alternative cellular materials. Specifically, regards to FCC based cellular concretes, the lowest thermal conductivity was obtained despite they had the highest natural density. This behaviour suggested that the pore distribution of aerated system was very advantageous when FCC is used as precursor.

A clear visual comparative of the physical properties is shown in **Fig.4.v.2**. The following coefficients (**Equations (4.v.9) (4.v.10) and (4.v.11)**) were determined by analysing the results of the physical tests (density, compressive strength and thermal conductivity), and after considering the ratio between each alternative cellular concrete based on waste precursors and recycled aluminium foil (GCC and ECC) respect the TCC system based on OPC and commercial aluminium powder. These coefficients allowed us to compare the potential of the GCC and ECC systems in terms of the selected properties.

$$\vartheta_d = \frac{\rho_x}{\rho_R} \qquad (4.v.9)$$

Where:

ϑ_d= Density ratio coefficient

ρ_x = Density for the alternative cellular concrete (FR, FRR, SR or SRR)

ρ_R= Density for the TCC (CA)

$$\vartheta_s = \frac{r_x}{r_R} \qquad (4.v.10)$$

Where:

ϑ_S= Compressive strength ratio coefficient at 28 curing days
r_x = Compressive strength for the alternative cellular concrete at 28 days (FR, FRR, SR or SRR)
r_R= Compressive strength for the TCC (CA) at 28 curing days

$$\vartheta_t = \frac{k_x}{k_R} \qquad (4.v.11)$$

Where:

ϑ_t = Thermal conductivity ratio coefficient
k_x = Thermal conductivity for the alternative cellular concrete (FR, FRR, SR or SRR)
k_R= Thermal conductivity for the TCC (CA)

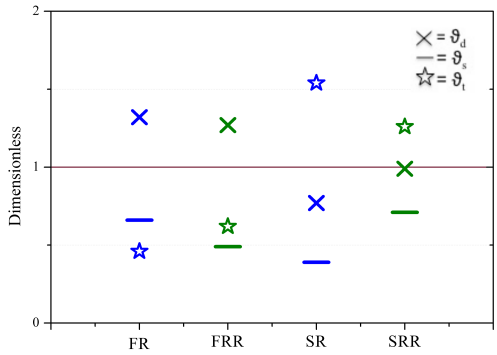

Fig.4.v.2 *Density, compressive strength and thermal conductivity ratio coefficients for the GCC and ECC systems.*

The horizontal solid line shown in **Fig.4.v.2** represents the unit value of the ratio coefficients. The values of ϑ_d, ϑ_s and ϑ_t above the line denote that the corresponding property of the material is higher than that for the CA reference, and the values below the line mean that it is lower than the CA reference one.

Since, a good performance of cellular concrete involves its low density, moderate compressive strength and low thermal conductivity, from **Fig.4.v.2** it is possible to denote that:

- FCC samples are denser than the reference material, being the FRR density ratio slightly closer to the unit. Respect to the use of BFS as

the precursor, the SR density is below the line (corresponding to the lower value), while the SRR density coefficient is the closer one of the solid line. As for FCC samples as for BFS the density coefficients are closer to the unit when RHA is used to replace the silica from WG.

- Analysing the compressive strength ratio coefficients it is clearly highlighted the directly relation with the density for FCC samples and the inverse relationship for BFS samples. The strength values for all alternative cellular concretes evaluated were lower than that obtained for CA.
- The lowest thermal conductivity values were yielded for system in which FCC is used as the precursor despite their density values.
- By considering the three physical properties coefficients, the use of RHA involves the corresponding ratio coefficients closer than the unit (solid line).

4.2. Carbon footprint calculation

The components and manufacturing process for each cellular concrete, considered with the CO_2 emissions calculations, are summarised in **Table 4.v.4**.

Table 4.v.4
Overview of each cellular concrete system component (C) and manufacturing process (M) for carbon footprint calculation.

		TCC	GCC		ECC	
		CA	FR	SR	FRR	SRR
C	Solid phase	OPCA	FCCRm	BFSRm	FCCRm	BFSRm
	Liquid phase	H_2O	NaOH/WG/H_2O		NaOH/RHA/H_2O	
M		Mix	Milling + Mix			

Two phases for three different cellular systems were assessed, which were as follows.

Phase 1: Emissions associated with components (E_C)

Table 5 shows the resultant dosage of the CA, FR, SR, FRR and SRR cellular concretes by considering that these must have a density of 600 kg/m^3 (dry conditions).

If we consider a CA sample with a density of 600 kg/m^3, it represents 600 kg of total weight, formed by OPC and combined H_2O. This water is chemically combined to form the typical CSH, ettringite, CASH, CAH and CH products, among others, from hydration reactions (C-CaO; S-SiO_2; A-Al_2O_3; H-H_2O). The total mass loss observed on the DTG curve (35–600ºC temperature range) of the CA paste (20.32%) (**Fig.4.v.3**) represents this chemically combined water. This means that 79.68% of the sample corresponds to OPCA.

The emission factor associated with clinker production was 1 kg of CO_2 per kg of cement (Duxson et al., 2007; Jiang et al., 2014; Mellado et al., 2014). If we consider that the used OPC was 95% composed of clinker, the emission factor adopted for the calculation would be 0.95 CO_2/kg. Zero emission was

considered for water supply. Regarding the emission associated with the aerating agent, the corresponding factor for gas generator production was 11.5 kg CO_2 per kg of A. In this case, the emission factor related to aluminium powder metallurgy processing (air or gas atomisation) was not considered because this value was not available from the consulted databases. Finally, by using **Equation (4.v.7**), the total CO_2 emissions associated with components per m^3 of TCC were calculated ($E_{C,CA}$), resulting 467.0 kg CO_2 /m^3 CA.

For the GCC samples, an FR sample with a density of 600 kg/m^3 represented 600 kg of the resultant weight, formed by FCC, Na_2O, SiO_2 and chemically combined water (to form NASH gel). By the total mass loss from the DTG curve (14.09%) **(Fig.4.v.3**), the chemically combined water was determined. From the alkaline solution stoichiometry (Na^+ molality=7.5 and SiO_2/Na_2O molar ratio = 1.7) and the w/b ratio (0.6), the Na_2O and SiO_2 percentages were constant compared to the solid precursor. The same ratios were considered with the SR sample, which yielded a total mass loss of 14.19% on the DTG curve and had the same stoichiometry for the activating solution, with a w/b ratio equal to 0.35.

Since FCC and BFS are industrial wastes and RAF was from recycled supply, no emission associated with them was considered. The manufacture of NaOH and commercial waterglass was taken into account (no emission associated with water supply). Both emission factors, which corresponded to NaOH and WG, were obtained from the SimaPro7.1 program databases (demo version, Pré Consultants Company of The Netherlands, LCA software specialist). The emission factors were 1.12 kg CO_2 of NaOH and 1.2 kg CO_2 per kg of the commercial waterglass solution. Finally, by using **Equation (4.v.7)**, the total CO_2 emissions associated with components per m^3 of each GCC were calculated, which were $E_{C,FR}$ = 322.5 kg CO_2/m^3 for FR and $E_{C,SR}$ = 207.7 kg CO_2/m^3 for SR.

In the ECC systems, WG was replaced with RHA. The solid components of the FRR and SRR samples were the same as for FR and SR, respectively, and the alkali solution based on H_2O, NaOH and RHA composed the liquid phase (**Table 4.v.4**). The amount of each component required in the 600 kg/m^3 FRR or SRR dosages was obtained by the same means as for FR and SR, explained above from the thermogravimetric data and stoichiometry of the activating mixture (see **Table 4.v.5** and **Fig.4.v.3**).

According to the above $E_{C,FR}$ and $E_{C,SR}$ calculations, no emissions associated with FCC, BFS and RAF were considered. Moreover, RHA is an agricultural waste, thus no emissions associated with it were considered. In this case, only the CO_2 emissions from NaOH manufacturing were contemplated. Thus, the $E_{C,FRR}$ and $E_{C,SRR}$ values were 88.3 and 65.8 kg CO_2/m^3, respectively.

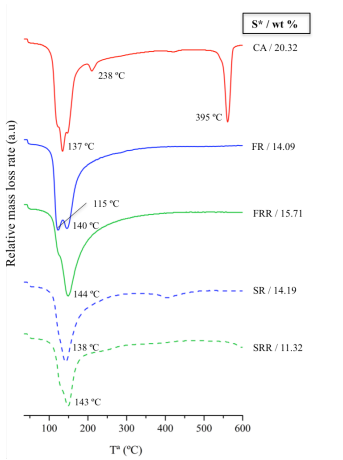

Fig.4.v.3 *The DTG curves of the CA, FR, FRR, SR and SRR samples. S*/wt % = sample/total mass loss % per weight*

Table 4.v.5
Dosages of CA, FR, SR, FRR and SRR samples to obtain a cellular concrete with a density of 600 kg/m³.

CA		FR		SR		FRR		SRR	
		FCC	397.4kg	BFS	438.8kg	FCC	375.6kg	BFS	435.2kg
OPC	480.0kg	RAF	0.8kg	RAF	0.9kg	RAF	0.8kg	RAF	0.9kg
A	0.9kg	H_2O	95.4kg	H_2O	61.4kg	H_2O	363.9kg	H_2O	195.8kg
H_2O	240.0kg	NaOH	48.5kg	NaOH	31.2kg	NaOH	78.9kg	NaOH	58.7kg
		WG	223.5kg	WG	144.0kg	RHA	76.7kg	RHA	57.1kg

Fig.4.v.4 shows the percentage of contribution to CO_2 emissions from the components and the percentage that represents each component in the final dosage material.

It is noticeable in the CA samples, that the CO2 emissions coming from the OPC (whose are 66.6% of the total dosage) represent nearly 97% of the total component emissions, and the remaining 3% is caused by the use of powdered aluminium (which represents merely 0.16% of the dosage).

The application of both proposed GCC systems yielded a marked E_C reduction compared to the TCC system emissions. $E_{C,FR}$ and $E_{C,SR}$ gave 30.9% and 55.5% less than $E_{C,CA,}$ respectively. We highlight that in these two GCC systems, the emissions from the WG manufacturing, represented nearly 83% despite this component is in 29.2% and 21.3% in the FR and SR dosages, respectively. The remaining 17% of $E_{C,}$ was related to NaOH manufacturing (**Fig.4.v.4**).

Finally regarding ECC (where the total component emissions were associated with NaOH), for the FRR samples the NaOH dosage represented 9.9% of the total weight and the resultant $E_{C,FRR}$ was 88.3 kg CO_2/m^3 FRR. This $E_{C,FRR}$ was 72.6% lower than $E_{C,FR}$ and 81.1% lower than $E_{C,CA}$. For the SRR samples, the NaOH dosage represented 7.8% of the total weight and the resultant $E_{C,SRR}$

was 65.8 kg CO_2 /m^3 SRR. This $E_{C,SRR}$ was 68.3% lower than $E_{C,SR}$ and 85.9% lower than $E_{C,CA}$.

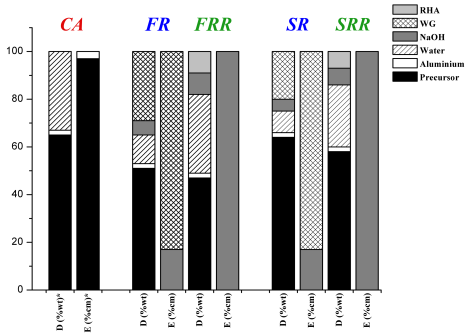

Fig.4.v.4 *Comparison of the contribution percentage to the CO_2 emissions from components (* E (%cm):) and the percentage that represents each component in the final dosage material (D (% wt): weight percentage) for the CA, FR, FRR, SR and SRR cellular concretes.*

It can be focus this noticeable reduction in CO_2 emissions in relation to the cellular concrete components mainly on the replacement of chemically synthetic reagent WG. The synthesis of commercial waterglass consists in the reaction of quartz and sodium carbonate, which is carried out at high temperature (above 1300ºC) and involves CO_2 emissions from sodium carbonate decomposition (**Equation (4.v.5)**) and the energy required to heat the quartz/Na_2CO_3 mixture in a furnace. These results agree with the statements found in several works which have centred on searching for an alternative silica source in alkali-activated materials (Mellado et al., 2014; Torres-Carrasco et al., 2015; Turner and Collins, 2013).

It is worth considering that the aluminium contributions in emissions were much lower: 3% for TCC production, and were completely null for the alternative GCC and ECC systems. However, we must take into account that no aluminium powder metallurgy processing was considered for TCC production. In any case, the way proposed to include RAF in the FCC/BFS milling process became a new ecological material to remove the emissions associated with this commercial gas-generating reagent.

Phase 2: Emissions associated with the manufacture process (E_M)

The manufacturing of TCC, GCC and ECC involves assessing three different activities: i) the pre-treatment of raw materials; ii) the mixing procedure; iii) the curing procedure. The evaluated cellular concrete samples were cured at room temperature and, for this reason, only the first two activities were considered herein. Additionally, with ECC systems, no emissions associated with dissolution preparations in a thermal bottle were produced. Since no industrial process exists for GCC and ECC production, calculations were made

by considering the same manufacture conditions as those used to produce concrete in a laboratory.

The raw materials used to prepare TCC (OPC and A) have an industrial manufacture system and their pre-treatment was not necessary. For the GCC and ECC systems, as in Section 2.2 "Materials" was explained, FCCRm and BFSRm solid mixes were achieved by the grinding treatment. To obtain FCCRm, FCC and RAF were co-milled in a ball mill at 0.3 kW electric powers, and capacity was 300 g and grinding time was 20 minutes. The same ball mill was used to obtain BFSRm but, in this case, capacity was 450 g for 30 minutes.

The mixing procedure was the same for the TCC, GCC and ECC systems, and only mixing time differed. As explained in Section 2.2 "Experimental procedure", an AEG SBE705RE power drill connected to a paint mixer was used for samples preparation. This power drill works at 0.705 kW and the capacity for each mix cycle was 0.012 m^3. For the CA samples the mixing time lasted 150 seconds (2.5 minutes), but it was 120 seconds (2 minutes) for the GCC and ECC systems.

For these calculations, and as with the mill and mix procedures, we took the national average value provided by IDAE as the emission factor of energy use, which is 0.25 kg CO_2 per kWh (Ministerio de Industria, Energía y Turismo, Secretaría de Estado de Energía, Madrid, n.d.).

With these considerations, the calculations of the emissions associated with the manufacture that corresponded to each sample were made by **Equation (4.v.7)** and the results were: $E_{M,CA}$ = 0.6 kg CO_2/m^3 CA, $E_{M,FR}$ = 34 kg CO_2/m^3 FR, $E_{M,SR}$ = 37.5 kg CO_2/m^3 SR, $E_{M,FRR}$ = 32.1 kg CO_2/m^3 FRR and $E_{M,SRR}$ = 37.1 kg CO_2/m^3 SRR.

Fig.4.v.5 shows a comparison of the CO_2 emissions from the different materials and operations for each concrete. Calculated kg of CO_2 per m^3 of material, the relative values are plotted and absolute values are provided.

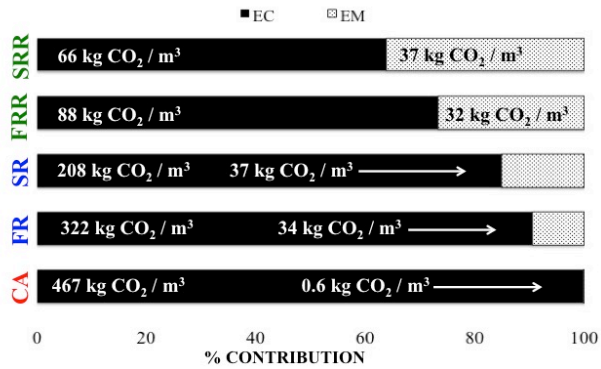

Fig.4.v.5 *Comparison of the relative CO_2 emissions contributions from the components (E_C) and manufacture processes (E_M) for the CA, FR, SR, FRR and SRR cellular concretes. The absolute CO_2 emissions values are given in each bar.*

As we can see, no influence of the TCC manufacture process was perceived, and total emission was related mainly to its components. However, as in both the GCC and ECC systems, manufacturing influenced the total CO_2 emissions. Indeed, the effect of the milling procedure was more important than the mixing procedure for all the samples. An analysis of the results revealed that: $E_{M,\,FR}$ represents 9.5%, with 97.5% from milling and 2.5% from mixing; $E_{M,\,SR}$ represents 15.3%, with 97.7% from milling and 2.3% form mixing; $E_{M,\,FRR}$ represents 26.7%, with 97.3% from milling and 2.7% form mixing; $E_{M,\,SRR}$ represents 31.1%, with 97.7% from milling and 2.3 % form mixing. The absolute CO_2 emissions produced from manufacturing were higher when the required solid material increased (**Table 4.v.5**) due to the high-energy requirement of pre-treatment.

These results can be explained because, nowadays for TCC, an industrial process of OPC and A manufacturing exists, and no pre-treatment in laboratory is required. If the same conditions for GCC and ECC systems could be considered, the emissions of this materials would be lower.

Finally, the resultant carbon footprint of each material was calculated by **Equation (4.v.8)**. **Fig.4.v.6** shows a comparison of the total CO_2 emissions from the CA, FR, SR, FRR and SRR cellular concretes analysed in the present study.

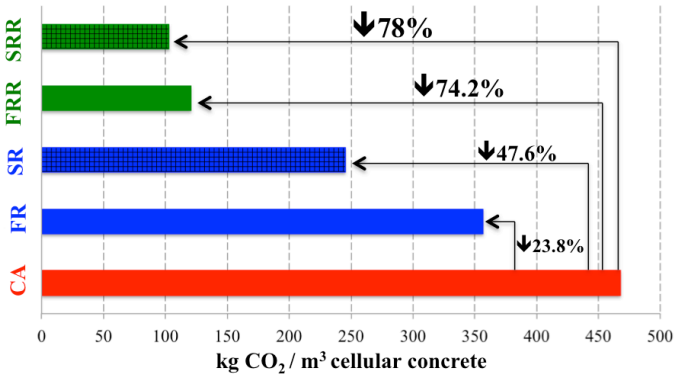

Fig.4.v.6 *The total CO_2 emissions associated with cellular concretes CA, FR, SR, FRR and SRR and reductions in CO_2 emissions compared to the CA sample (the TCC system).*

For TCC, total emissions were 467.6 kg CO_2/m^3 CA. For GCC, where OPC and A were replaced with alternative raw materials (FCCRm and BFSRm, respectively), the total CO_2 emissions significantly reduced: i) the total emissions for the FR sample were 356.5 kg CO_2/m^3 FR, which is 23.8% lower than those for the CA sample; ii) for the SR sample, they were 245.2 kg CO_2/m^3 SR, 47.6% lower than those for CA. The last development step, where commercial waterglass was replaced by RHA (ECC systems), gave a relevant reduction in the total carbon footprint: 66.2% *vs.* FR and 74.2% *vs.* CA for the FRR system (120.4 kg CO_2/m^3 FRR), and 58% vs. SR and 78% vs. CA for the SRR systems (102.9 kg CO_2/m^3 SRR).

5. Conclusions

In this research, the density of the proposed alternative cellular concrete (FR, FRR, SR and SRR) was lower than 1000 kg/m^3, which represents suitable lightweight insulation behaviour. Besides, mechanical behaviour came close to TCC in all the evaluated alternative cellular concretes.

The obtained results for the new proposed ECC demonstrated the high effectiveness of soluble silica from RHA to replace the silica from WG. Replacing the traditional alkaline solution by a mixture of RHA and NaOH allowed new cellular concrete to be prepared with similar properties to those found for the equivalent systems with WG. This implies an interesting chance to reduce the use of synthetic chemical reagents for preparing this cellular concrete type.

The results of the carbon footprint calculations revealed that with the new ECC it is possible to minimise CO_2 emissions by more than 70% *versus* TCC emissions. The factors that most contributed to the carbon footprint were: i) the OPC in TCC; ii) WG as well as milling in the GCC systems; iii) only milling in the ECC systems. Calculations were made by considering laboratory conditions: if the industrial milling of the alternative raw materials required

for the GCC and ECC systems manufacturing could be considered, the emissions from milling would be much lower. For the GCC systems, the contribution of commercial waterglass (WG) was more than 80%. Indeed, the new alternative ECC allowed the possibility of reducing greenhouse gas emissions and contributing to sustainable development by integrating green chemistry principles into construction materials by reusing wastes, including those related to aluminium-based gas generators.

Acknowledgements

The authors acknowledge the financial support from the Universitat Politècnica de València (UPV) through internal project GEOCELPLUS. The authors like also to express special grateful to Dra. Mrs. Josefa L. Roselló Caselles for recycled aluminium foil, and to the Electronic Microscopy Service of the UPV. Thanks are given to DACSA for supplying the RHA sample.

References

Araújo, E.G. de, Tenório, J.A.S., 2005. Cellular Concrete with Addition of Aluminum Recycled Foil Powders. Mater. Sci. Forum 498–499, 198–204. https://doi.org/10.4028/www.scientific.net/MSF.498-499.198

Arellano Aguilar, R., Burciaga Díaz, O., Escalante García, J.I., 2010. Lightweight concretes of activated metakaolin-fly ash binders, with blast furnace slag aggregates. Constr. Build. Mater. 24, 1166–1175. https://doi.org/10.1016/j.conbuildmat.2009.12.024

Arpal Asociacion para el Reciclado de Aluminio [WWW Document], n.d.

ASTM International, n.d. ASTM D5334 - 14 Standard Test Method for Determination of Thermal Conductivity of Soil and Soft Rock by Thermal Needle Probe Procedure [WWW Document].

Ayres, R.U., 1995. Life cycle analysis: A critique. Resour. Conserv. Recycl. 14, 199–223. https://doi.org/10.1016/0921-3449(95)00017-D

Bouzón, N., Payá, J., Borrachero, M. V., Soriano, L., Tashima, M.M., Monzó, J., 2014. Refluxed rice husk ash/NaOH suspension for preparing alkali activated binders. Mater. Lett. 115, 72–74. https://doi.org/10.1016/j.matlet.2013.10.001

Bremner, T.W., Carkner, P.M., Healy, M., Litvin, A., 1997. Guide for Precast Cellular Concrete Floor, Roof, and Wall Units. Man. Concr. Pract. 2–6.

Cabeza, L.F., Rincón, L., Vilariño, V., Pérez, G., Castell, A., 2014. Life cycle assessment (LCA) and life cycle energy analysis (LCEA) of buildings and the building sector: A review. Renew. Sustain. Energy Rev. 29, 394–416. https://doi.org/10.1016/j.rser.2013.08.037

Cavanaugh, K., Speck, J.F., 2002. Guide to Thermal Properties of Concrete and Masonry Systems Reported by ACI Committee 122. Concrete 1–21.

Davidovits, J., 1994. Properties of Geopolymer Cements. First Int. Conf. Alkaline Cem. Concr. 131–149.

Davidovits, P.J., 2002. 30 Years of Successes and Failures in Geopolymer Applications . Market Trends and Potential Breakthroughs . Geopolymer 2002 Conf. 1–16. https://doi.org/10.1017/CBO9781107415324.004

Dodson, J.R., Cooper, E.C., Hunt, A.J., Matharu, A., Cole, J., Minihan, A., Clark, J.H., Macquarrie, D.J., 2013. Alkali silicates and structured mesoporous silicas from biomass power station wastes: the emergence of bio-MCMs. Green Chem. 15, 1203. https://doi.org/10.1039/c3gc40324f

Dolton, B., Hannah, C., 2006. Cellular Concrete : Engineering and Technological Advancement for Construction in Cold Climates 1–11.

Duxson, P., Provis, J.L., Lukey, G.C., van Deventer, J.S.J., 2007. The role of inorganic polymer technology in the development of "green concrete." Cem. Concr. Res. 37, 1590–1597. https://doi.org/10.1016/j.cemconres.2007.08.018

Eggleston, S., Buendia, L., Miwa, K., Ngara, T., Tanabe, K., 2006. Foreword Preface 2006 IPCC Guidelines for National Greenhouse Gas Inventories. 2006 IPCC Guidel. Natl. Greenh. Gas Invent. 6.

Esmaily, H., Nuranian, H., 2012. Non-autoclaved high strength cellular concrete from alkali activated slag. Constr. Build. Mater. 26, 200–206. https://doi.org/10.1016/j.conbuildmat.2011.06.010

EST: Publications [WWW Document], n.d. URL http://www.fao.org/economic/est/publications/publicaciones-sobre-el-#.WrfjcGYrw_U (accessed 3.25.18).

European Aluminium Foil Association, n.d. Did you know? - EAFA - The home of aluminium foil [WWW Document].

Font, A., Borrachero, M.V., Soriano, L., Monzó, J., Payá, J., 2017. Geopolymer eco-cellular concrete (GECC) based on fluid catalytic cracking catalyst residue (FCC) with addition of recycled aluminium foil powder. J. Clean. Prod. 168, 1120–1131. https://doi.org/10.1016/j.jclepro.2017.09.110

Gartner, E., 2004. Industrially interesting approaches to "low-CO2" cements. Cem. Concr. Res. 34, 1489–1498. https://doi.org/10.1016/j.cemconres.2004.01.021

Hamad, A.J., 2014. Materials, Production, Properties and Application of Aerated Lightweight Concrete: Review. Int. J. Mater. Sci. Eng. 2, 152–157. https://doi.org/10.12720/ijmse.2.2.152-157

IEEE 442-1981 - IEEE Guide for Soil Thermal Resistivity Measurements [WWW Document], n.d.

Jiang, M., Chen, X., Rajabipour, F., Hendrickson, C.T.C.T., 2014. Comparative Life Cycle Assessment of Conventional, Glass Powder, and Alkali-Activated Slag Concrete and Mortar. J. Infrastruct. Syst. 20, 04014020. https://doi.org/10.1061/(ASCE)IS.1943-555X.0000211

Luukkonen, T., Abdollahnejad, Z., Yliniemi, J., Kinnunen, P., Illikainen, M., 2018. Comparison of alkali and silica sources in one-part alkali-activated blast furnace slag mortar. J. Clean. Prod. 187, 171–179. https://doi.org/10.1016/j.jclepro.2018.03.202

Marchal, J.C., Krug III, D.J., McDonnell, P., Sun, K., Laine, R.M., 2015. A low cost, low energy route to solar grade silicon from rice hull ash (RHA), a sustainable source. Green Chem. 17, 3931–3940. https://doi.org/10.1039/C5GC00622H

Mellado, A., Catalán, C., Bouzón, N., Borrachero, M. V., Monzó, J.M., Payá, J., 2014. Carbon footprint of geopolymeric mortar: study of the contribution of the alkaline activating solution and assessment of an alternative route. RSC Adv. 4, 23846–23852.

https://doi.org/10.1039/C4RA03375B
Ministerio de Industria, Energía y Turismo, Secretaría de Estado de Energía, Madrid, S., n.d. IDAE 2011 [WWW Document]. URL http://www.idae.es/ (accessed 3.12.18).
Moraes, J.C.B., Font, A., Soriano, L., Akasaki, J.L., Tashima, M.M., Monzó, J., Borrachero, M.V., Payá, J., 2018. New use of sugar cane straw ash in alkali-activated materials: A silica source for the preparation of the alkaline activator. Constr. Build. Mater. 171. https://doi.org/10.1016/j.conbuildmat.2018.03.230
Moraes, J.C.B., Tashima, M.M., Akasaki, J.L., Melges, J.L.P., Monzó, J., Borrachero, M. V., Soriano, L., Payá, J., 2016. Increasing the sustainability of alkali-activated binders: The use of sugar cane straw ash (SCSA). Constr. Build. Mater. 124, 148–154. https://doi.org/10.1016/j.conbuildmat.2016.07.090
Muthu Kumar, E., Ramamurthy, K., 2017. Influence of production on the strength, density and water absorption of aerated geopolymer paste and mortar using Class F fly ash. Constr. Build. Mater. 156, 1137–1149. https://doi.org/10.1016/j.conbuildmat.2017.08.153
Nambiar, E.K.K., Ramamurthy, K., 2007. Air-void characterisation of foam concrete. Cem. Concr. Res. 37, 221–230. https://doi.org/10.1016/j.cemconres.2006.10.009
Narayanan, N., Ramamurthy, K., 2000. Microstructural investigations on aerated concrete. Cem. Concr. Res. 30, 457–464. https://doi.org/10.1016/S0008-8846(00)00199-X
Ortiz, O., Castells, F., Sonnemann, G., 2009. Sustainability in the construction industry: A review of recent developments based on LCA. Constr. Build. Mater. 23, 28–39. https://doi.org/10.1016/j.conbuildmat.2007.11.012
Palomo, A., López de la Fuente, J.I., 2003. Alkali-activated cementitous materials: Alternative matrices for the immobilisation of hazardous wastes - Part I. Stabilisation of boron. Cem. Concr. Res. 33, 281–288. https://doi.org/10.1016/S0008-8846(02)00963-8
Panesar, D.K., 2013. Cellular concrete properties and the effect of synthetic and protein foaming agents. Constr. Build. Mater. 44, 575–584. https://doi.org/10.1016/j.conbuildmat.2013.03.024
Payá, J., Borrachero, M. V., Monzó, J., Soriano, L., 2009. Estudio del comportamiento de diversos residuos de catalizadores de craqueo catalítico (FCC) en cemento Portland. Mater. Construcción 59, 37–52. https://doi.org/10.3989/mc.2009.48108
Payá, J., Monzó, J., Borrachero, M. V., 1999. Fluid catalytic cracking catalyst residue (FC3R): An excellent mineral by-product for improving early-strength development of cement mixtures. Cem. Concr. Res. 29, 1773–1779. https://doi.org/10.1016/S0008-8846(99)00164-7
Provis, J.L., 2016. Alkali-activated materials. Cem. Concr. Res. https://doi.org/10.1016/j.cemconres.2017.02.009
Scrivener, K.L., Kirkpatrick, R.J., 2008. Innovation in use and research on cementitious material. Cem. Concr. Res. 38, 128–136. https://doi.org/10.1016/j.cemconres.2007.09.025
Talling, B., Brandstetr, J., 1989. Trondheim Conference, in: Present State and Future of Alkali-Activated Slag Concretes. American Concrete Institute,

pp. 1519–1546.
Tashima, M.M., Akasaki, J.L., Castaldelli, V.N., Soriano, L., Monzó, J., Payá, J., Borrachero, M. V., 2012. New geopolymeric binder based on fluid catalytic cracking catalyst residue (FCC). Mater. Lett. 80, 50–52. https://doi.org/10.1016/j.matlet.2012.04.051
Torres-Carrasco, M., Puertas, F., 2015. Waste glass in the geopolymer preparation. Mechanical and microstructural characterisation. J. Clean. Prod. 90, 397–408. https://doi.org/10.1016/j.jclepro.2014.11.074
Torres-Carrasco, M., Rodríguez-Puertas, C., Del Mar Alonso, M., Puertas, F., Alonso, M. del M., Puertas, F., 2015. Alkali activated slag cements using waste glass as alternative activators. Rheological behaviour 54, 45–57.
Turner, L.K., Collins, F.G., 2013. Carbon dioxide equivalent (CO2-e) emissions: A comparison between geopolymer and OPC cement concrete. Constr. Build. Mater. 43, 125–130. https://doi.org/10.1016/j.conbuildmat.2013.01.023
U.S. Department of Energy, 2007. U.S. Energy Requirements for Aluminum Production: Historical Perspective, Theoretical Limits and Current Practices. Ind. Technol. Progr. Energy Effic. Renew. Energy 150.
Zhang, Z., Provis, J.L., Reid, A., Wang, H., 2014. Geopolymer foam concrete: An emerging material for sustainable construction. Constr. Build. Mater. 56, 113–127. https://doi.org/10.1016/j.conbuildmat.2014.01.081

vi. Air-void system characterization of new eco-cellular concretes

AUTORES: Alba Font, María Victoria Borrachero, Lourdes Soriano, José Monzó y Jordi Payá

REFERENCIA DE LA PUBLICACIÓN: Enviado a International Journal of Applied Ceramic Technology (En revisión)

Factor de impacto/Cuartil (2018): 1.074/Q2	**Citas (excluyendo auto citas): -**

OBJETIVOS PARCIALES ABORDADOS

MATERIALES	FABRICACIÓN
• **TCC:** OPC + H_2O + A • **GCC:** FCC + [WG+NaOH+H_2O] + A_R • **ECC:** FCC + [RHA+NaOH+H_2O] + A_R • **AACC:** BFS + [WG+NaOH+H_2O] + A_R • **ECC:** BFS + [RHA+NaOH+H_2O] + A_R	• **CO-M:** FCC + A_R = FCCRm • **CO-M:** BFS + A_R = BFSRm • **CURADO:** TA • **Amasado con:** PD

PROCEDIMIENTO EXPERIMENTAL

CARACTERIZACIÓN DE MATERIAS PRIMAS	CARACTERIZACIÓN DE ESPECÍMENES
-	• Ensayos hídricos (D_{AP}, ΦT, Φa y Φc) • Evaluación de la matriz porosa (FESEM, MO, ImageJ)

RESULTADOS Y CONCLUSIONES MÁS RELEVANTES DE LA INVESTIGACIÓN

- Tras 7 días de curado a temperatura ambiente se obtuvieron los siguientes resultados:

Material	D_{AP} (kg/m^3)	POROSIDAD			D_{med} (µm)	N° medio poros/area
		ΦT (%)	Φa (%)	Φc (%)		
TCC	614	80	39	41	612	509
GCC	797	69	21	48	513	619
ECC-FCCRm	740	70	27	44	649	492
AACC	584	70	46	24	819	378
ECC-BFSRm	616	66	40	26	408	408

- Se establece una clara relación entre la densidad natural y la conductividad térmica con los parámetros del sistema poroso analizados: el número medio de poros por área del material y el diámetro medio del poro.
- La densidad natural presenta una dependencia lineal positiva con la porosidad cerrada y negativa con la porosidad abierta.
- La predominancia de poros cerrados se relaciona con la predominancia de poros de menor tamaño sin interconexiones. Las matrices son mas estables debido a que la reacción de aireación ha sido menos agresiva.
- Respecto a la conductividad térmica, presenta una relación lineal negativa respecto a la porosidad cerrada y positiva respecto a la porosidad cerrada.
- A mayor porosidad cerrada, mayor densidad de las muestras y menor aislamiento.
- Una distribución homogénea de poros, con ausencia de interconexión entre ellos y formas regulares de tamaños dentro de un mismo rango de valores, favorece la obtención de hormigones celulares alternativos con bajas densidades y matrices estables (resistencia a la compresión competente).

Abstract: Cellular concrete is an alternative to conventional concrete as a low-density and high-insulating building material. The new eco-cellular concretes (ECC) based on the geopolymer technology have been recently introduced by the scientific community. A form of ECC was herein studied, in which the fluid catalytic cracking residue and the blast furnace slag were employed as precursors, the rice husk ash was utilised as an alternative silica source in the activator and the aerating reagent was replaced with recycled aluminium foil. Field emission scanning electron microscopy, optical microscopy and the ImageJ software were employed to characterize the void distribution. Bulk density and porosity were determined by hydric tests. The results revealed that lowest densities without strength loss were obtained when the cementing matrix had a homogeneous void-system: similar spacing between pores, narrow size ranges and non-interconnected pores. A relation between open/close porosity with both density and thermal conductivity was established.

Abbreviations:
TCC: Traditional cellular concrete
GCC: Geopolymer cellular concrete
ECC: Eco-cellular concrete
FCC: Fluid catalytic cracking residue
BFS: Blast furnace slag
RHA: Rice husk ash
RAF: Recycled aluminium foil
A: Commercial aluminium powder

HIGHLIGHTS:

- The air-void system for cellular concretes was assessed by different techniques.
- Eco-cellular concrete (ECC) and geopolymer cellular concrete (GCC) were characterized.
- ECC showed a similar air-void system than traditional cellular concrete (TCC).
- ECC developed materials are greener cellular concrete alternatives.
- Bulk density and open/closed porosity related to the functional properties.

1. Introduction

Traditional cellular concrete (TCC) is a Portland cement-based paste or mortar (with sand or fly ash) to which a controlled aerating agent (commonly aluminium powder), which results in a lightweight high-insulation material with medium-low mechanical behaviour(Ramamurthy et al., 2009). Compared to other construction materials, a cost-effective solution, better performance and faster construction are achieved when cellular concrete is used. This material is commonly employed in masonry units for floors, roofs and walls(Bremner et al., 1997). Dolton and Hannah(Dolton and Hannah, 2006) presented cases studies of cellular concrete applications in cold climates, and highlighted the easy application in an insulation solution as shallow utilities, pipeline and tank, frost-protected shallow foundations or below-ground grouting voids, among others.

Hence density, compressive strength and thermal insulation must be assessed and controlled to obtain good-performing cellular concretes. These properties are directly related with their void system configuration (volume, mean diameter and distribution of formed internal air pores)(Ramamurthy et al., 2009). Porosity and strength are related to the empirical models proposed by Narayanan and Ramamurthy(N Narayanan and Ramamurthy, 2000) and by Kearsley and Wainwright(Kearsley and Wainwright, 2001). A concise study was done by Nambiar and Ramamurthy(Nambiar and Ramamurthy, 2007), which established a direct relationship between pore parameters (volume, size and spacing) and the bulk density and strength of traditional cellular concretes. These authors reported that pore shape did not influence final cellular concrete properties. Moreover, a linear relation between thermal conductivity and dry bulk density was reported by Zhang et al.(Zhang et al., 2015), and closed porosity with thermal conductivity correlations were also demonstrated by Topçu et al.(Topçu and Uygunoğlu, 2007). Wee et al.(Wee et al., 2006) revealed that optimal air content was enclosed in the traditional cellular concretes matrix to obtain a homogeneous air-void distribution and, consequently, low densities without strength loss. These authors showed that more air entrapped caused mechanical behaviour to worsen because of an interconnection of bigger sized pores. Othuman and Wang(Othuman and Wang, 2011) reported the strong influence of pore size distribution in the thermal conductivity and physical properties of prediction models for cellular concrete manufacturing. Recently, the same conclusion was reached by Almalkawi et al.(Almalkawi et al., 2018), who confirmed that a well-organised air-bubbles system in a matrix with a more spherical shape avoided internal water circulation, which gave good compressive strength and thermal conductivity.

Void system research works have been mainly done by scanning electron microscopy (SEM), mercury intrusion porosimetry (MIP), gas permeability, X-ray computer tomography or optical microscopy(Akthar and Evans, 2010; Almalkawi et al., 2018; Nambiar and Ramamurthy, 2007; N. Narayanan and Ramamurthy, 2000a; Yang et al., 2014). In recent research, the measurement of void parameters (shape, size, volume and distribution) has been carried out

by 2D image analysis processing and using computer software, such as Avizo(Ducman and Korat, 2016), Photoshop(Panesar, 2013) or ImageJ(Esmaily and Nuranian, 2012). The bulk density and porosity of cellular concretes have been traditionally tested by hydric tests(Colangelo et al., 2018; Pinilla Melo et al., 2014).

It is well-known that the scientific community currently focuses on developing new materials that offer a healthy and environmental-friendly alternative to conventional ones. TCC is 60% to 70% based on Portland cement (OPC). The environmental impact of OPC and its non-renewable raw materials consumption have led the scientific community to investigate new alternatives.

The application of alkali activation or geopolymers technology to cellular concrete manufacturing has rapidly gained importance in the last few years. Many authors have published works in which greener geopolymer cellular concretes (GCCs) were developed and analysed(Bai et al., 2016).

Fly ash and blast furnace slag (BFS) have been the most widely used precursors to new GCCs development. The combination of Class F fly ash and blast furnace slag has been employed as precursors by Zang et al.(Zhang et al., 2015) to develop GCC activated by an NaOH and sodium silicate dissolution. The best results were obtained with 30% of BFS, which specimens yielding 3 MPa, 720 kg/m^3 and 0.15 W/mK after a curing treatment consisting in: 24 h at 40ºC, plus 27 days under ambient conditions. More recently, Stolz et al(Stolz et al., 2018) also studied the physical characteristics of GCC systems based on fly ash activated by NaOH and sodium silicate dissolution, and by incorporating glass fibres into mixes to improve mechanical behaviour. Specimens were cured at room temperature, and densities between 1000 and 1400 kg/m^3 and compressive strengths from 3 to 9 MPa were obtained. Esmaily and Nuranian(Esmaily and Nuranian, 2012) presented non-autoclaved GCCs by employing BFS activated with NaOH and sodium silicate. Specimens were compared depending on curing temperature (70ºC, 78ºC and 87ºC) and the best results were obtained for the GCCs cured at 87ºC, which yielded 946 kg/m^3 and 3.7 MPa. The experimental work includes a void system characterisation, and the mean diameter for these samples was 608 µm. The authors concluded that the pore structure more strongly influenced compressive strength than curing treatment.

Xuan et al.(Xuan et al., 2019) introduced the use of municipal solid waste incineration bottom ash (MSWIBA) combined with waste-glass powder (WGP) as a precursor. With a 20% of WGP, GCCs were obtained that fell within the ranges of 494-1295 kg/m^3, 0.9-10.4 MPa and 0.14-0.38 W/mK. That research work showed alternative materials with a wider internal voids size distribution than TCCs (within the 0.02-3.0 mm range), but no correlation with the obtained physical characteristics was made.

In a recent research work, Font et al.(Font et al., 2018) presented a novel alternative cellular concrete development, where the functional properties

and carbon footprint were assessed. Three cellular systems were studied: i) traditional cellular concrete (TCC) based on OPC and commercial aluminium (A); ii) Geopolymer cellular concretes (GCC) by using fluid catalytic cracking residue (FCC) or blast furnace slag (BFS) as a precursor, activated by a traditional activating solution (sodium hydroxide (NaOH), plus commercial waterglass (WG)), and aerated by means recycled aluminium foil (RAF); iii) Eco-cellular concretes, with a similar composition to GCC, where commercial waterglass was replaced with rice husk ash (RHA). The physical properties of the developed cellular concretes are summarised in **Table 4.vi.1**.

The authors carried out a comparative carbon footprint calculation with the three cellular systems (TCC, GCC and ECC) by considering the associated emissions of the components and the manufacturing process. By taking the total TCC carbon footprint as a reference, the following conclusions were reached: i) the use of geopolymer technology and the aluminium source replacement (GCC systems) allows to reduce the total CO_2 emissions by 24% in the FCC system and by 48% in the BFS system; ii) when WG was replaced with RHA, these emission was cut by 74% and 78% when using FCC and BFS, respectively.

Table 4.vi.1
Composition and selected properties of the different cellular concretes(Font et al., 2018).

	Precursor	Aerating agent	Liquid Phase	Mixtures	Density (kg/m³)	Compressive strength (MPa)	Thermal conductivity (W/mK)
TCC	OPC	A	Water	**CA**	618 ± 2	6.5 ± 0.4	0.182 ± 0.001
GCC	FCC	RAF	NaOH + WG	**FR**	813 ± 2	4.3 ± 0.4	0.083 ± 0.003
	BFS			**SR**	474 ± 4	2.6 ± 0.2	0.281 ± 0.007
ECC	FCC		NaOH + RHA	**FRR**	782 ± 4	3.2 ± 0.3	0.113 ± 0.005
	BFS			**SRR**	611 ± 4	4.6 ± 0.3	0.224 ± 0.007

These results were the first evidence for a new eco-friendly alternative with acceptable functional properties in its applicability. At this point, a number of research steps are necessary to improve its properties and to manage dose variability effects.

In the present work, the air-void system of the aforementioned new developed materials was investigated. Characterisation was done by combining several techniques: i) field emission scanning electron microscopy (FESEM), optical microscopy (OM), and the image software analysis were employed to obtain the void size distribution; ii) bulk density and porosity were determined by hydric tests.

The results allowed the comparison of the internal matrix structure formed by gas expansion from the aerating reaction in each material. Relations between the resulting final void-structure and the functional properties of each material were established.

2. Materials and methods

Table 4.vi.2 shows the materials employed in the present investigation and its origin. On the other hand, the chemical composition of the raw materials (OPC, FCC, BFS and RHA) is summarised in **Table 4.vi.3**.

Table 4.vi.2
Materials and its origin.

Ordinary Portland Cement (**OPC**)	Lafarge S.A
Fluid catalytic cracking residue (**FCC**)	BP Oil Company
Blast furnace slag (**BFS**)	Cementval S.A
Rice husk ash (**RHA**)	DACSA S.A
Commercial aluminium powder (**A**)	Schlenk Metallic Pigments GmbH
Recycled aluminium foil **RAF**	Department of Agricultural Forest Ecosystems at the Universitat Politècnica de València
NaOH (pellets - 98% purity)	Panreac S.A
WG (8 wt% Na_2O, 28% wt% SiO_2 and 64% wt% H_2O)	Merck-Spain

Table 4.vi.3
Chemical compositions of OPC, FCC, BFS and RHA (wt%).

	SiO_2	Al_2O_3	Fe_2O_3	CaO	MgO	SO_3	K_2O	Na_2O	P_2O_5	TiO_2	Cl	LOI*
OPC	20.80	4.60	4.80	65.60	1.20	1.70	1.00	0.07	-	-	-	0.23
FCC	47.76	49.26	0.60	0.11	0.17	0.02	0.02	0.31	0.01	1.22	-	0.53
BFS	30.53	10.55	1.29	40.15	7.43	1.93	0.57	0.87	0.26	0.89	-	5.53
RHA	85.58	0.25	0.21	1.83	0.5	0.26	3.39	-	0.67	-	0.32	6.99

*Loss on ignition

A summary of the materials and the dose selected to manufacture the TCC, GCCs and ECCs in the present study can be observe in the **Table 4.vi.4**.

Table 4.vi.4
Overview of the materials and doses to the specimen's manufacture.

	Solid phase			Liquid phase			
	Precursor	Aerating agent	Dose (wt%)		a/b	SiO_2/Na_2O	Na^+ molality[2]
CA	OPC[1]	A	2%	Water	0.50	-	-
FR	FCC	RAF		Water/NaOH/WG	0.60	1.70	7.50
FRR				Water/NaOH/RHA	0.70		
SR	BFS			Water/NaOH/WG	0.35		
SRR				Water/NaOH/RHA	0.45		

[1] OPC = CEM I- 52.5R.
[2] Na^+ molality = mol of sodium per kg of water.

The mix process was carried out by means a paint mixer connected to a power drill AEG SBE705RE model. The sequence to the specimen's manufacture was as follow:

To prepare TCC:

1. The OPC and A were manually mixed for 2 minutes = solid phase
2. The solid phase was mixed for 180 seconds with water

To prepare GCCs and ECCs:

1. The precursors were co-milled with the RHA in a ball mill: i) FCC + RAF during 30 minutes, obtaining the solid phase named $BFSR_m$ (D_{mean} = 18.43 µm).and ii) BFS + RAF during 20 minutes, obtaining the solid phase named $FCCR_m$ (D_{mean} = 26.28 µm).
2. The alkali dissolution (liquid phase) was shaken by the power drill for 30 seconds.
3. The solid phase was added to the liquid phase and mixed for 180 seconds.

The fresh pastes were moulded in 4x4x4 cm^3 cubes and cured at room temperature (23ºC - 100% RH). After 24 hours, the free surface of cubes had to be cut with a saw blade, the specimens were demoulded and kept in at room temperature until testing.

The number, mean diameter and distribution of the formed internal air pores were studied by FESEM, OM and the ImageJ software. A cube (4x4x4 cm^3) of each formulation was crushed in a porcelain mortar. A small piece (7-10 mm) from the inner part of the cube was selected and immersed in acetone for 30 minutes and dried at 65ºC for 40 minutes. These samples were studied by FESEM. The FESEM micrographs of the carbon-covered samples were taken by an ULTRA 55-ZEISS electron microscope (at magnifications of 100x and 200x), which allows pore section configurations and pore diameters to be measured. Another 4x4x4cm^3 cubic sample was cut into 2 cm-thick slices perpendicularly to the cast face with a diamond rotary saw. The internal 16-cm^2 surfaces were observed under a Leica S8 APO optical microscope. Pictures were taken with a Leica DFC 420 digital camera and images were processed by the Leica LAS image analysis software. 8x magnifications were selected with a pixel representing 12 microns. Then these cut-off internal 16-cm^2 surfaces were immersed in a concentrated solution (0.4% by volume) of universal dye (colour vermilion 780) and universal solvent (302 NC), both from TKROM. To complete pore impregnation, the submerged samples were placed inside a vessel connected to a vacuum pump (Fig 4.vi.1a). An image of an impregnated surface was taken (Fig 4.vi.1b) (two images of each 16-cm^2 internal surface per sample). Images were digitised and processed by the ImageJ software. Morphological operations (dilation, erosion, opening, closing and hole filling) to refine the shape of objects, and for the conversion into the binary form, were performed. Pore diameter distribution histograms were obtained by measuring all the pore diameters at the original magnification.

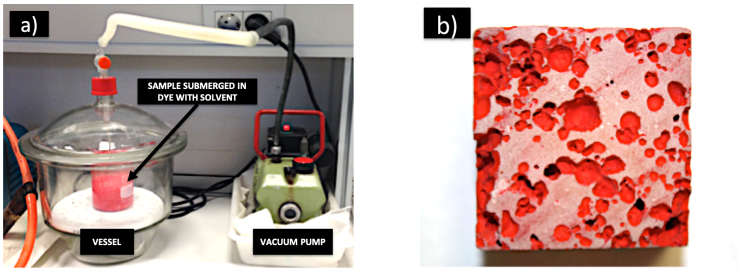

Fig 4.vi.1 *Specimen preparation for the ImageJ analyses: a) sample immersed in colour solution, connected to a vacuum pump; b) the impregnated internal surface of samples (4x4 cm² section).*

The bulk density and porosity of the cellular concretes were determined by hydric tests, which were done in six cubic samples (4x4x4 cm^3) of each cellular concrete (CA, FR, FRR, SR and SRR). Specimens were weighed and the natural density (ρ) was calculated after 7 curing days. Archimedes method was used for bulk density (ρ_{bulk}) calculations (**Equation (4.vi.1) and Equation (4.vi.2)**) by employing still water as a known density liquid (1000 kg/m^3). The cubic samples were weighed after being left to dry for 24 h in a furnace at 105°C to obtain their dry weight values (W_{dry}). Then samples were fully saturated by water immersion for 24 h and weighed (saturated weight (W_{sat})). In the saturation state, specimens were weighed by a hydrostatic balance (submerged weight (W_{sum})). To calculate the true density (ρ_{true}) (**Equation (4.vi.3)**), a Le Chatelier flask with still water was used after crushing 20 g of each material to obtain the true volume (V_{true}). The total, open and closed porosities (Φ_t, Φ_o and Φ_c) were obtained by **Equations (4.vi.4)**, **(4.vi.5)** and **(4.vi.6)**, respectively.

$$V_{bulk} = \frac{W_{sat} - W_{sum}}{\rho_{water}} \quad (4.vi.1)$$

$$\rho_{bulk} = \frac{W_{dry}}{V_{bulk}} \quad (4.vi.2)$$

$$\rho_{true} = \frac{W_{dry}}{V_{true}} \quad (4.vi.3)$$

$$\Phi_t(\%) = \left(\frac{1 - \rho_{bulk}}{\rho_{true}}\right) \times 100 \quad (4.vi.4)$$

$$\Phi_o(\%) = \left(\frac{W_{sat} - W_{dry}}{W_{sat} - W_{sum}}\right) \times 100 \quad (4.vi.5)$$

$$\Phi_c\ (\%) = \Phi_t - \Phi_o \qquad (4.vi.6)$$

Simple linear regression and correlation between density and thermal conductivity (as dependent variables) with bulk density and porosity (as explanatory variables) were carried out. The Statgraphics XVII software was employed and the linear fit tool was applied. The values of the properties for each alternative material (FR, FRR, SR and SRR) were considered a coefficient, obtained in relation to the reference traditional cellular concrete as follows:

$$\beta_x = \frac{x_m}{x_r} \qquad (4.vi.7)$$

where:

β_x: coefficient for each property (where subscript (x) can be: ρ = natural density, k = thermal conductivity, ρ_{bulk} = bulk density, φ_o = open porosity or φ_c = closed porosity) in the linear fit.

x_r: property value obtained for the reference material (CA)

x_m: property value obtained for each alternative material (FR, FRR, SR or SRR)

3. Results and discussion

The number, mean diameter and distribution of the pores obtained by FESEM, OM and the ImageJ software for samples CA, FR, FRR, SR and SRR are summarised in **Figs. 4.vi.2-6**, respectively.

The CA sample had many pores within the 300-600 μm size range, followed by the number of pores with sizes below 300 μm. A smaller proportion of pores had large diameters (from 600 to 3000 μm) and some pore dimensions exceeded 3000 μm (**Fig. 4.vi.2**). This sample presented an average pore diameter of 612 μm.

The pore distribution of samples FR and FRR (**Figs. 4.vi.3-4**) were similar to many pores whose size was under 300 μm and the number of pores lowered within each range for larger sizes. The FRR sample had a small average number of pores/area (492 μm) compared to the FR sample (619 μm), which suggests less aeration reactivity when the commercial silicate was replaced with RHA (FRR sample). As in the CA sample, the FRR specimen had several pores whose size exceeded 3000 μm. For this reason, the average pore diameter for FRR (649 μm) was larger than for FR (513 μm).

The BFS samples SR and SRR (**Figs. 4.vi.5-6**) displayed a more homogeneous pore distribution than the other cellular concretes herein studied. In these

cases, many pore diameters were above 900 µm compared to the CA, FR and FRR samples. Thus, the average pore diameters fell within the 804-819 µm range. The SRR samples had many pores bigger than 3000 µm, with a smaller average number of pores/area and a larger average diameter.

A trend in relation to the values of the number of pores/area and the average pore diameter exists. The samples with a smaller number of pores/area (SR and SRR) yielded high average diameter values. The sample with the smallest average pore diameter was FRR, which had the highest pores/area value.

The best cellular concrete in terms of physical (natural density) and mechanical (compressive strength) properties (similarly to traditional systems) was represented by the ECC alternative system based on BFS (SRR samples, 611 kg/m^3 and 4.6 MPa). By reviewing the resultant pore system distribution of SRR, the air-void shape had no influence on the cellular concrete properties, which agrees with Nambiar and Ramamurthy(Nambiar and Ramamurthy, 2007). A wide range of pore dimensions with a homogeneous distribution of pore diameters allowed us to obtain a matrix in which micropores were enclosed in the walls between macropores. Thus, a lower-density material can be obtained with no major strength loss. Conversely, the FR sample was the material with the highest density; as this GCC system had more pores/area, the diameter range of pores was narrower than it was for the other samples.

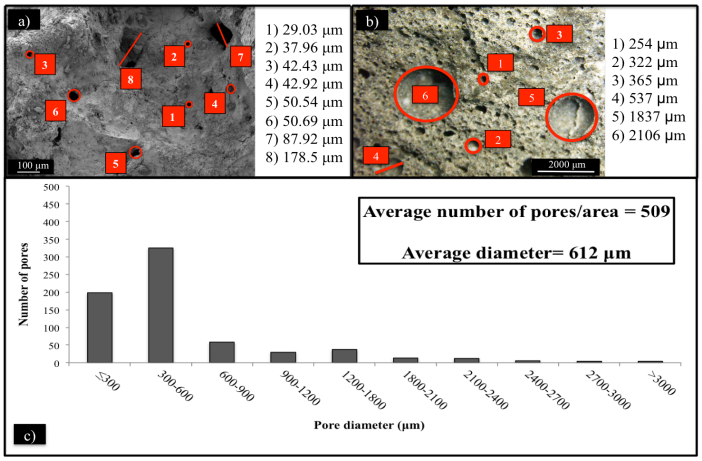

Fig 4.vi.2 *Pore system characterisation of* **CA***: a) FESEM micrograph at 100x magnifications with pore sizing; b) OM image at 8x magnifications with pore sizing; c) pore diameter distribution in the 16-cm^2 area.*

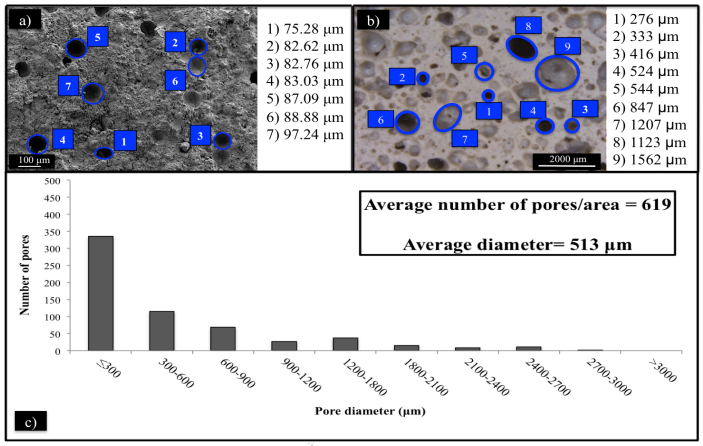

Fig 4.vi.3 *Pore system characterisation of **FR**: a) FESEM micrograph in 100x magnifications with pore sizing; b) OM image in 8x magnifications with pore sizing; c) pore diameter distribution in the 16-cm² area.*

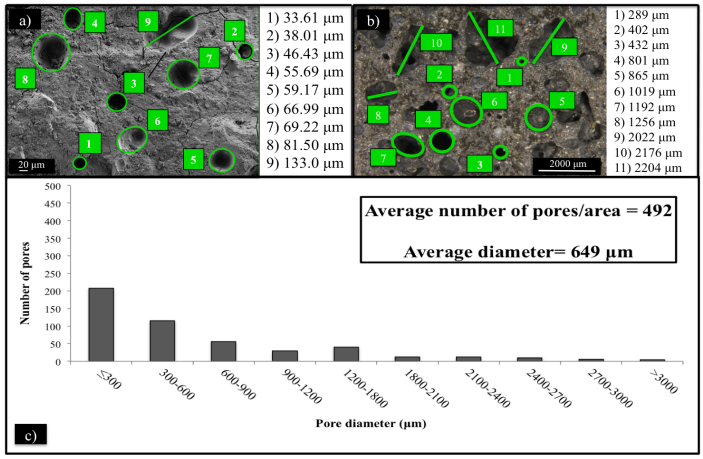

Fig 4.vi.4 *Pore system characterisation of FRR: a) FESEM micrograph in 200x magnifications with pore sizing; b) OM image in 8x magnifications with pore sizing; c) pore diameter distribution in the 16-cm² area.*

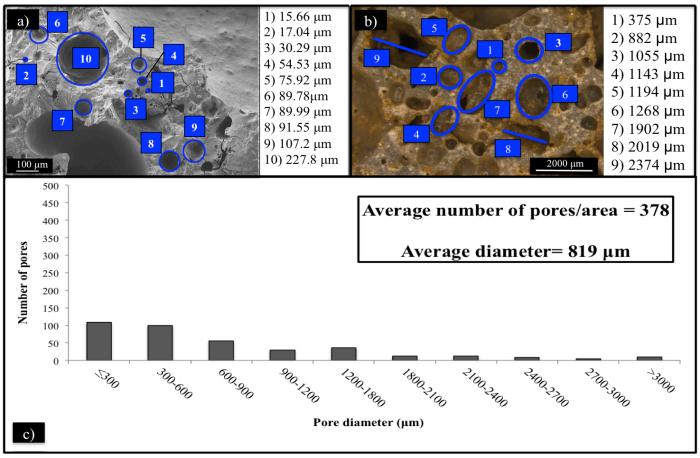

Fig 4.vi.5 *Pore system characterisation of **SR**: a) FESEM micrograph in 100x magnifications with pore sizing; b) OM image in 8x magnifications with pore sizing; c) pore diameter distribution in the 16-cm² area.*

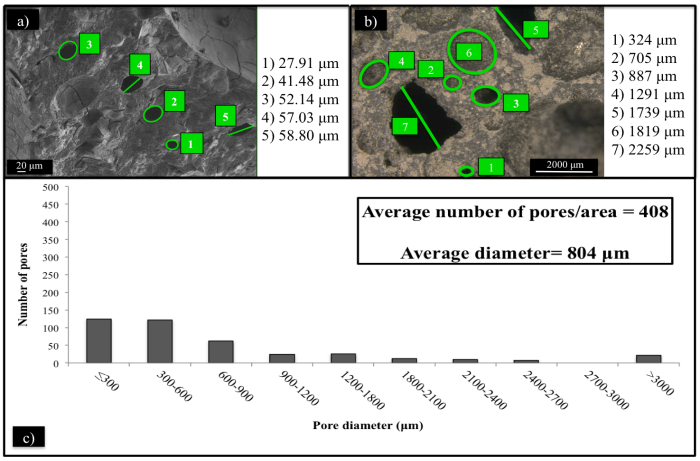

Fig 4.vi.6 *Pore system characterisation of **SRR**: a) FESEM micrograph in 200x magnifications with pore sizing; b) OM image in 8x magnifications with pore sizing; c) pore diameter distribution in the 16-cm² area.*

Table 4.vi.5 shows the bulk density and porosity (total, open and closed porosities) assessed in each studied system.

Table 4.vi.5
Values of bulk density and porosity (total, Φt; open, Φo; closed, Φc) obtained from hydric tests.

	Bulk density (kg/m^3)	Porosity (%)		
		Φt	Φo	Φc
CA	614 ± 1	80	39	41
FR	797 ± 2	69	21	48
FRR	740 ± 2	70	27	44
SR	584 ± 2	70	46	24
SRR	616 ± 3	66	40	26

When comparing bulk density with porosity in the alternative systems (FR, FRR, SR and SRR), a linear relationship was experimentally obtained. High bulk density involves a high closed porosity and, consequently, a lower open porosity was obtained. This is logical if we consider that bulk density comes from considering the bulk volume, which involves the solid volume and the volume entrapped in the closed void of the material.

After comparing the materials, it can be stated that the total porosity of the CA sample was 80% and its closed porosity/open porosity ratio (Φ_c/Φ_o) was 1.05, which indicates that closed porosity was similar to open porosity. The FR sample had 66% total porosity with a 2.28 Φ_c/Φ_o ratio, so its relative closed porosity was much higher than in the CA sample. The FRR sample obtained 70% total porosity, with its Φ_c/Φ_o between the CA and FR samples (1.62). The same total porosity of FRR was obtained for SR (70%), but its Φ_c/Φ_o ratio was 0.52 because the closed porosity was lower than the open porosity. Finally, for the SRR sample, total porosity was 66%, which came close to the total porosity of FR but, as in the SR sample, this Φ_c/Φ_o ratio was also below the unit (0.65).

The results of the linear fit obtained from the statistical analysis are plotted in **Figure 4.vi.7** for natural density and in **Figure 4.vi.9** for thermal conductivity. These graphs reveal a positive linear dependence between density and closed porosity (**Fig 4.vi.7.a**) and a negative linear dependence between natural density and open porosity (**Fig 4.vi.7.b**). In both the resultant models, the p-value was lower than 0.05, which means that a statistic significant relation between natural density and the explanatory variables (closed porosity and open porosity) existed, with a 95% confidence level. The R-squared statistic allowed to affirm that 92.17% of natural density variability was explained by the model fit assessed with closed porosity, and 96.74% by the model fit assessed with open porosity. Finally, a strong dependence of natural density with closed porosity and open porosity was found with a correlation coefficient of 0.96 and -0.98, respectively.

The reduction in natural density for the systems with higher open porosity was most probably because open porosity consists in the volume of pores connected to the outside boundary of the material, which are filled with air.

On the other extreme, the higher density of the systems when closed porosity is higher than open porosity can be explained by the increasing total volume of the solid matrix: there are many walls between closed pores. Furthermore, as observed in Figure 8, a direct relation appears between closed porosity and the number of the smallest size pore predominance (pore size < 300 μm). Thus, the volume of the solid matrix in these materials was bigger and the natural density of the material increased. A linear fit was found when considering all the studied systems (traditional system, CA sample, was included in the fitting). The initial hypothesis of a high dependence between both variables was accepted with a p-value that equalled 0.02 and the R-squared statistic equalled 92%.

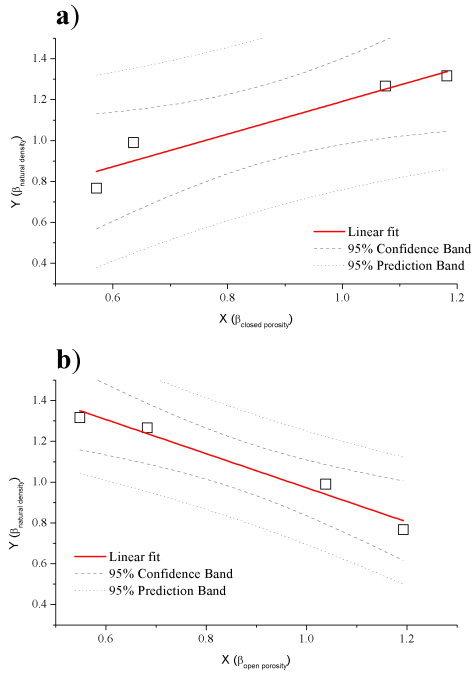

Fig 4.vi.7 *Linear fit model for: a) natural density (dependent variable) and closed porosity (explanatory variable); and b) natural density (dependent variable) and open porosity (explanatory variable).*

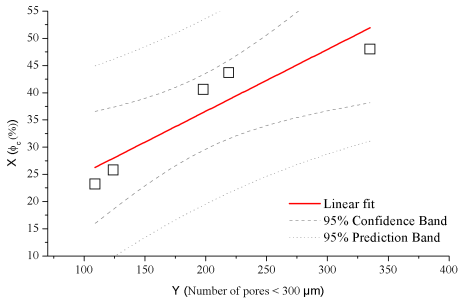

Fig 4.vi.8 *Linear fit model for closed porosity (dependent variable) and number of pores smaller than 300 μm (explanatory variable).*

Font et al.(Font et al., 2018) analysed the physical properties of each alternative material (GCC and ECC systems) by its relative values in relation to traditional cellular concrete ones (TCC) to obtain the natural density (ϑ_d) and compressive strength (ϑ_s) ratio coefficients. The authors concluded that the relation between natural density and compressive strength was direct for the FCC samples and inverse for the BFS samples.

The models that describe the relation linking thermal conductivity with bulk density (**Fig 4.vi.9.a**), closed porosity (**Fig 4.vi.9.b**) and open porosity (**Fig 4.vi.9.c**) showed an intense dependence relation, which has been commonly affirmed by other authors(N. Narayanan and Ramamurthy, 2000b; Ramamurthy et al., 2009). The model p-value was under 0.05 for the three linear fits that appeared. Thus, a statistically significant relation was found between thermal conductivity and the explanatory variables (closed porosity, open porosity, bulk density), with a 95% confidence level. The statistic R-square allowed to affirm that the model fit explained 97.24%, 99.55% and 97.58% of natural density variation in relation to closed porosity, open porosity and bulk density, respectively. Finally, the correlation coefficients were -0.98 (negative linear dependence) for closed porosity as an explanatory variable, 0.99 (positive linear dependence) for open porosity as an explanatory variable and -0.98 (negative linear dependence) for bulk density as an explanatory variable. This means a strong dependence of thermal conductivity on them.

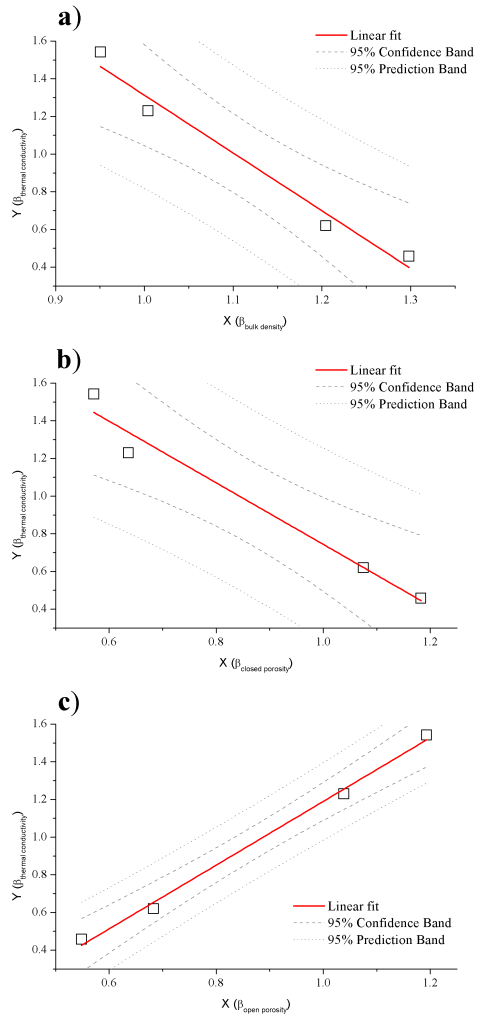

Fig 4.vi.9 *Linear fit models for: a) thermal conductivity (dependent variable) and bulk density (explanatory variable); b) thermal conductivity (dependent variable) and closed porosity (explanatory variable); c) thermal conductivity (dependent variable) and open porosity (explanatory variable).*

4. Conclusions

The void-system configuration in the new alternative alkali-activated cellular concretes (GCC) as well as eco-cellular concretes (ECC) represents a primary influence on their functional properties (density, compressive strength and thermal conductivity).

A relation clearly links natural densities and compressive strengths with the void-system analysed parameters (the average number of pores/area and the mean pore diameters). The development of a homogeneous void distribution, with non-interconnected pores, regular shapes and continuous sizes, involves an alternative cellular concrete with lower natural density and enough matrix stability to achieve relatively high compressive strength.

The amount of pores/area can be associated with aeration effectiveness, while the size of the obtained pores indicates the reaction intensity. By comparing all the materials, the cellular concretes with more pores/area (FR>CA>FRR>SRR>SR) achieved a more effective aerating reaction with a resulting matrix in which smaller pore size ranges predominated (pores smaller than 300 μm: FR>CA ≈ FRR>SRR ≈ SR). The materials with fewer pores/area had bigger sized pores (pores above 3000 μm: SRR>SR>FRR ≈ CA>FR), which indicates a more aggressive and less effective aerating reaction.

A relation between bulk density and porosity was established: with an internal void system where the Φ_c/Φ_o ratio was over the unit, and bulk density was higher than when the Φ_c/Φ_o ratio was below the unit. Furthermore, closed porosity resulted in a direct relation with voids distribution where smaller sizes predominated. Finally, bulk density and porosity were confirmed as explanatory characteristics of the thermal conductivity in the alternative cellular concretes.

In general, greener cellular concrete alternatives, the new ECC (FRR and SRR), have an internal void system with similar parameters to TCCs (CA).

Acknowledgements

The authors acknowledge the financial support from the Universitat Politècnica de València (UPV) through internal project GEOCELPLUS. The authors are especially grateful to Dr. Mrs. Josefa L. Roselló Caselles for the recycled aluminium foil, and also to the Electronic Microscopy Service of the UPV. Thanks also go to DACSA, BP Oil and Cementval for supplying the raw materials.

References

Akthar, F.K., Evans, J.R.G., 2010. High porosity (> 90%) cementitious foams. Cem. Concr. Res. 40, 352–358. https://doi.org/10.1016/j.cemconres.2009.10.012

Almalkawi, A.T., Salem, T., Hamadna, S., Darsanasiri, A.G.N.D., Soroushian, P., Balchandra, A., Al-Chaar, G., 2018. Physio-microstructural properties of aerated cement slurry for lightweight structures. Materials (Basel). 11, 1–15. https://doi.org/10.3390/ma11040597

Bai, C., Franchin, G., Elsayed, H., Conte, A., Colombo, P., 2016. High strength metakaolin-based geopolymer foams with variable macroporous structure. J. Eur. Ceram. Soc. 36, 4243–4249. https://doi.org/https://doi.org/10.1016/j.jeurceramsoc.2016.06.045

Bremner, T.W., Carkner, P.M., Healy, M., Litvin, A., 1997. Guide for Precast Cellular Concrete Floor, Roof, and Wall Units. Man. Concr. Pract. 2–6.

Colangelo, F., Roviello, G., Ricciotti, L., Ferrándiz-Mas, V., Messina, F., Ferone, C., Tarallo, O., Cioffi, R., Cheeseman, C.R., 2018. Mechanical and thermal properties of lightweight geopolymer composites. Cem. Concr. Compos. 86, 266–272. https://doi.org/10.1016/j.cemconcomp.2017.11.016

Dolton, B., Hannah, C., 2006. Cellular Concrete : Engineering and Technological Advancement for Construction in Cold Climates 1–11.

Ducman, V., Korat, L., 2016. Characterization of geopolymer fly-ash based foams obtained with the addition of Al powder or H_2O_2 as foaming agents. Mater. Charact. 113, 207–213. https://doi.org/10.1016/j.matchar.2016.01.019

Esmaily, H., Nuranian, H., 2012. Non-autoclaved high strength cellular concrete from alkali activated slag. Constr. Build. Mater. 26, 200–206. https://doi.org/10.1016/j.conbuildmat.2011.06.010

Font, A., Borrachero, M.V., Soriano, L., Monzó, J., Mellado, A., Payá, J., 2018. New eco-cellular concretes: Sustainable and energy-efficient materials. Green Chem. https://doi.org/10.1039/c8gc02066c

Kearsley, E.P., Wainwright, P.J., 2001. Porosity and permeability of foamed concrete. Cem. Concr. Res. 31, 805–812. https://doi.org/10.1016/S0008-8846(01)00490-2

Nambiar, E.K.K., Ramamurthy, K., 2007. Air-void characterisation of foam concrete. Cem. Concr. Res. 37, 221–230. https://doi.org/10.1016/j.cemconres.2006.10.009

Narayanan, N, Ramamurthy, K., 2000. Prediction models based on gel-pore parameters for compressive strength of aerated concrete 2, 206–212.

Narayanan, N., Ramamurthy, K., 2000a. Microstructural investigations on aerated concrete. Cem. Concr. Res. 30, 457–464. https://doi.org/10.1016/S0008-8846(00)00199-X

Narayanan, N., Ramamurthy, K., 2000b. Structure and properties of aerated concrete: A review. Cem. Concr. Compos. 22, 321–329. https://doi.org/10.1016/S0958-9465(00)00016-0

Othuman, M.A., Wang, Y.C., 2011. Elevated-temperature thermal properties of lightweight foamed concrete. Constr. Build. Mater. 25, 705–716. https://doi.org/10.1016/j.conbuildmat.2010.07.016

Panesar, D.K., 2013. Cellular concrete properties and the effect of synthetic and protein foaming agents. Constr. Build. Mater. 44, 575–584. https://doi.org/10.1016/j.conbuildmat.2013.03.024

Pinilla Melo, J., Sepulcre Aguilar, A., Hernández Olivares, F., 2014. Rheological properties of aerated cement pastes with fly ash, metakaolin and sepiolite additions. Constr. Build. Mater. 65, 566–573. https://doi.org/10.1016/j.conbuildmat.2014.05.034

Ramamurthy, K., Kunhanandan Nambiar, E.K., Indu Siva Ranjani, G., 2009. A classification of studies on properties of foam concrete. Cem. Concr. Compos. 31, 388–396. https://doi.org/10.1016/j.cemconcomp.2009.04.006

Stolz, J., Boluk, Y., Bindiganavile, V., 2018. Mechanical, thermal and acoustic properties of cellular alkali activated fly ash concrete. Cem. Concr. Compos. 94, 24–32. https://doi.org/10.1016/j.cemconcomp.2018.08.004

Topçu, I.B., Uygunoğlu, T., 2007. Properties of autoclaved lightweight aggregate concrete. Build. Environ. 42, 4108–4116. https://doi.org/10.1016/j.buildenv.2006.11.024

Wee, T.-H., Babu, D.S., T, T., Lim, H.-S., 2006. Air-void system of foamed concrete and its effect on Mechanical Properties. ACI Mater. J. 103, 45–52.

Xuan, D., Tang, P., Poon, C.S., 2019. MSWIBA-based cellular alkali-activated concrete incorporating waste glass powder. Cem. Concr. Compos. 95, 128–136. https://doi.org/10.1016/j.cemconcomp.2018.10.018

Yang, K.H., Lee, K.H., Song, J.K., Gong, M.H., 2014. Properties and sustainability of alkali-activated slag foamed concrete. J. Clean. Prod.

68, 226–233. https://doi.org/10.1016/j.jclepro.2013.12.068

Zhang, Z., Provis, J.L., Reid, A., Wang, H., 2015. Mechanical, thermal insulation, thermal resistance and acoustic absorption properties of geopolymer foam concrete. Cem. Concr. Compos. 62, 97–105. https://doi.org/10.1016/j.cemconcomp.2015.03.013

4.3 CULMINACIÓN DEL OBJETIVO GENERAL DE LA TESIS

4.3.1 Desarrollo de materiales de activación alcalina binarios (BAAM: BFS/OBA) y ternarios (TAAM: BFS/OBA/RHA)

En la **tercera etapa** se han englobado los trabajos correspondientes a la investigación del uso de ceniza de hueso de oliva (OBA) en la fabricación de materiales de activación alcalina (AAM). Como se viene nombrando en capítulos anteriores, la OBA se presenta como una fuente alternativa de potasio frente al empleo de reactivos químicos (NaOH/KOH) en la preparación de las disoluciones alcalinas.

Esta investigación permitió sentar las bases del empleo de una nueva materia prima, la OBA, en los materiales de activación alcalina (caracterización de la ceniza, dosificación de las mezclas, metodología de fabricación, propiedades físicas y mecánicas) para poder proceder a su aplicación en la tecnología de los hormigones celulares.

Forman parte de esta **tercera etapa** experimental las siguientes publicaciones:

vii. A 100% waste-based alkali-activated material by using olive-stone biomass ash (OBA) and blast furnace slag (BFS)

viii. Olive-stone biomass ash (OBA): An alternative alkaline source for the blast furnace slag activation

ix. Design and properties of 100% waste-based ternary alkali-activated mortars: blast furnace slag, olive-stone biomass ash and rice husk ash.

vii. A 100% waste-based alkali-activated material by using olive-stone biomass ash (OBA) and blast furnace slag (BFS)

AUTORES: Alba Font, Lourdes Soriano, Joao Claudio Bassan Moraes, Mauro M. Tashima, José Monzó, María Victoria Borrachero y Jordi Payá

REFERENCIA DE LA PUBLICACIÓN: Materials Letters 203 (2017) 46-49
DOI: https://doi.org/10.1016/j.matlet.2017.05.129

Factor de impacto/Cuartil (2017): 2.687/Q2	**Citas (excluyendo auto citas):** 6

OBJETIVOS PARCIALES ABORDADOS

MATERIALES	FABRICACIÓN
• BFS + H_2O • **BAAM:** BFS + OBA (18.8% Ad) + H_2O • **BAAM:** BFS + KOH(4M) + H_2O	• **CURADO:** TB • **Amasado con:** NM

PROCEDIMIENTO EXPERIMENTAL

CARACTERIZACIÓN DE MATERIAS PRIMAS	CARACTERIZACIÓN DE ESPECÍMENES
• XRF • Cálculo de pH • PSD • XRD • FESEM	• Resistencia a la compresión (Rc) • TGA

RESULTADOS Y CONCLUSIONES MÁS RELEVANTES DE LA INVESTIGACIÓN

- La ceniza de biomasa de hueso de oliva (OBA) presentó altas cantidades de calcio y potasio en su composición.
- En suspensión acuosa la OBA presentó elevada alcalinidad (pH = 13.5)
- Los BAAM de BFS/OBA presentaron un comportamiento mecánico mejor que la mezcla control (BFS/KOH) tras 3 y 7 días de curado:

Material	Rc (MPa)	
	3 días	**7 días**
BFS/KOH	12.7	16.9
BFS/OBA	20.6	29.9

- Se plantea una posible **combinación del efecto químico** (aporte del potasio) **con un efecto filler** (físico) de la ceniza en las mezclas.

Abstract: This study presents the use of olive-stone biomass ash (OBA) as an alkali source in alkali-activated materials (AAM) based on blast furnace slag (BFS). The OBA was physically and chemically characterized. It presented high K_2O and CaO contents, and yielded high alkalinity in water medium. The newly designed OBA + BFS mixes (a 100% waste-based AAM) reached a compressive strength of 30 MPa after 7 days of curing at 65 LC, which was higher than for BFS activated with KOH solution. Thermogravimetric studies showed the formation of C-S-H/(C,K)-A-S-H gels and hydrotalcite. The OBA presented excellent performance as a component in AAM and a good valorization was achieved.

Keywords: Biomass ash, thermal analysis, alkali-activated material, ceramics

HIGHLIGHTS:

- Olive – stone biomass ash (OBA) contains high percentages of K_2O and CaO.
- First preparation of alkali-activated material (AAM) by adding OBA.
- AMM obtained entirely from waste materials: OBA and blast furnace slag (BFS).
- Better strength in OBA/BFS system than in KOH – activated BFS.
- New better ecological and economical material containing OBA has been designed.

1. Introduction

Alkali-activated materials (AAM) are prepared by mixing a solid precursor and an alkaline solution (usually sodium or potassium hydroxides, carbonates or silicates). The precursor is an aluminosilicate-based mineral material and in many cases, this is a waste from industrial activity (e.g. fly ash, blast furnace slag, ceramic wastes). Environmental benefits are provided by the use of AAMs, compared to Portland cement, due to their low associated carbon footprint (Turner and Collins, 2013). Alternative binder solutions also have been reported by the use of mixtures of wastes, in which one of the components has a biomass waste origin: sugarcane straw ash has been successfully tested in 50/50%wt mixtures with blast furnace slag (Moraes et al., 2016) with a significant reduction in the sodium silicate content. However, the alkaline solutions are prepared by means of the use of synthetic chemical reagents, with relatively high costs in eco-nomic and environmental terms. The use of alkaline wastes could help to solve this issue. In some cases, part of chemical reagent has been successfully replaced by a waste (e.g. rice husk ash replaced silicate source in (Bouzón et al., 2014)).

In this way, some alkaline ashes can be obtained by power generation from biomass combustion. After this process, a solid by-product is generated, the biomass ash. Vassilev et al. (Vassilev et al., 2010) have classified these biomass ashes into four types, depending on the oxides compositions: S, K, C and CK types.

The challenge of finding a use for these biomass ashes needs to be addressed. Greener concrete has been developed by the use of different ashes from farming waste residues (Mo et al., 2016). Alternatively, alkali-rich ashes could be used for preparing activation solutions for AAM.

This paper presents an investigation of a waste obtained after the combustion of olive stone: olive-stone biomass ash (OBA). The residue is rich in K_2O and CaO (CK ash according to (Vassilev et al., 2010)). Olive biomass ash has already been studied in cement blends with interesting results. In these studies, the use of olive cake, pulp and stone in the combustion process produced an ash with high SiO_2 content (Cabrera et al., 2014; Cruz-Yusta et al., 2011). Peys et al. (Peys et al., 2016) studied the use of some potassium-rich bio-mass ashes as an activator in metakaolin mixtures, where they obtained a maximum compressive strength of 40 MPa after 28 days of curing.

The aim of this research is to present the potential use of olive-stone biomass ash (OBA) as an alkali source in AAMs based on blast furnace slag (BFS). The OBA was fully characterized and it was used in AAM. The OBA/BFS blend was compared to water activated BFS and KOH activated BFS to assess the effectiveness of OBA in the matrix development.

2. Experimental

2.1. Materials

Blast furnace slag (BFS) was supplied by Cementval (Valencia, Spain) (see Composition in **Table 4.vii.1**) with a mean particle diameter of 26.0 mm. Olive-stone biomass ash (OBA) was supplied by Almazara Candela (Elche, Spain). The original ash was milled for 20 min in a ball mill in order to homogenize the sample and to reduce the particle diameter. Commercial potassium hydroxide (KOH) was used (Panreac-SA, 85% purity).

Table 4.vii.1
Chemical composition (wt%) of OBA and BFS.

	SiO_2	Al_2O_3	Fe_2O_3	CaO	K_2O	MgO	P_2O_5	SO_3	Na_2O	Others	LOI*
OBA	5.33	0.70	3.45	27.77	32.16	5.13	2.68	1.67	0.78	0.95	18.90
BFS	30.53	10.55	1.29	40.15	0.57	7.43	0.26	1.93	0.87	0.89	5.53

*Loss on ignition

2.2. Methods

The OBA was characterized by X-ray fluorescence (XRF), pH in deionized water, particle size distribution (PSD), X-ray diffraction (XRD) and field emission scanning electron microscopy (FESEM). XRF was carried out using a Philips Magic Pro XRF instrument. The pH measurement was carried out by means of a Crison micro PH2001 pH meter, and the PSD was measured by means of a Malvern Instruments Mastersizer 2000. XRD was carried out by a Bruker AXS D8 Advance. FESEM micrographs were taken by an ULTRA 55-ZEISS with the sample covered by carbon.

Three different mixes were designed in this study by using BFS as precursor, where the activating solution was: a) still water with-out any alkali source (M1); b) an aqueous solution of KOH to pro-duce an alkali-activated material (M2); or c) the mixture of OBA and water in a 0.47 ratio (M3). The K^+ molarity selected in this study was 4 M for the M2. For M3, the same molarity was calculated as for the M2 based on the K_2O content in the OBA: 18.8% of OBA was added with respect to the BFS. Water:BFS and BFS:sand (for mortars) ratios were maintained as constant values of 0.40 and 1:3 by mass, respectively. Samples were cured at 65°C and 100% relative humidity. Mortars were assessed by their compressive strength (universal testing machine). Thermogravimetric analyses (TGA) of the pastes were performed using a TGA850 Mettler Toledo thermobalance (temperature range: 35–500°C; heating rate: 10°- C·min ^{1} in an N_2 atmosphere. Samples were tested after 3 and 7 days.

3. Results and discussion

3.1. Chemical and physical characterization of OBA

The chemical composition of OBA is summarized in **Table 4.vii.1**. The main oxides of the ash are K_2O (32.16%) and CaO (27.77%), both significantly higher than previously reported (Cruz-Yusta et al., 2011). The sum of over 60% of these oxides suggests that OBA can be an important alkali source in AAMs. The OBA showed high alkalinity in water suspension with a value equal to 13.5 for an OBA:water ratio of 0.47. The mean particle diameter and 90%-passing diameter (d_{90}) values were 20.1 and 45.2 mm, respectively. XRD studies showed that the main crystalline phases are: portlandite ($Ca(OH)_2$), calcite ($CaCO_3$), anorthite ($CaAl_2Si_2O_8$) and kalicinite ($KHCO_3$). FESEM images are shown in **Fig.4.vii.1. Fig.4.vii.1a** presents the OBA before the milling process. At a lower magnification, highly irregular particles with size larger than 100 mm can be observed. When these particles are observed at a higher magnification, they appear to have a rough surface with signs of a sinterization event. **Fig.4.vii.1b** shows the OBA after the milling process. The particle size significantly reduced when compared to the original, and a more homogeneous particle distribution was observed, showing rough and smooth particle surfaces.

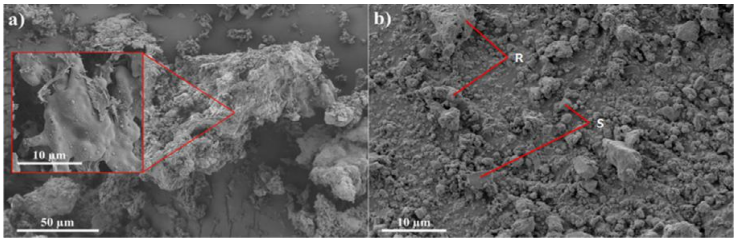

Fig.4.vii.1 *FESEM micrographs of: (a) original OBA; (b) OBA after the milling process (R: rough surface; S: smooth surface).*

3.2. Characterization of mortars and pastes

The compressive strength for M1, M2 and M3 mortars after 3 and 7 curing days is shown in **Fig.4.vii.2**. It is noticeable that for the M3 mixture, the system is 100% waste-based material. After 3 days of curing, the compressive strength for the control mortar with only water (M1) was 6.9 MPa, which corresponds to the self-hydraulic properties of the BFS (Pal et al., 2003)9. This value was significantly lower than those obtained for the other two mortars: M2 and M3 presented 12.7 MPa and 20.6 MPa, respectively. On the one hand, these results show that the alkaline activation of BFS improved the mechanical development when compared to a system with only water, as expected. On the other hand, the presence of OBA in the mixture enabled it to reach a compressive strength higher than that obtained in KOH alkali-activated mortar. Probably, the presence of both calcium and potassium from the OBA influenced positively the activation of BFS. Regarding 7-days cured mortars, M1 effectively maintained its compressive strength at 3 days, reaching 7.0 MPa. M2 and M3 showed a strength gain: the former mortar reached 16.9 MPa (33% gain with respect to the 3 days sample) and the latter presented 29.9 MPa (45% gain). It can be noticed that the presence of the OBA not only yielded the highest compressive strength, but also showed the best improvement in this curing interval.

Thermogravimetric analyses (DTG curves) for the M1, M2 and M3 pastes after 3 and 7 days of curing are shown in **Fig.4.vii.3**. In this test, three main peaks could be observed: similar results were reported by Rivera et al. (Rivera et al., 2016) for BFS activated by potassium hydroxide/silicate mixture. Peak 1 is related to dehydration of C-S-H gel (the main peak in all pastes). Peak 2 is associated with dehydration of C-A-S-H and (C,K)-A-S-H gels from the activated products. Peak 3 is only observed for the M2 and M3 pastes, and is related to the dehydration of the hydrotalcite (Abdel-Gawwad and Abd El-Aleem, 2015) (confirmed by XRD). No important difference between the DTG peaks for 3 and 7 days for all pastes was observed. Regarding the relative mass losses in the interval of 35–500 LC, after 3 days of curing the M2 paste presented the highest value (12.92%), followed by M3 (8.35%) and M1 (4.07%). The mass losses (a measure of the chemically combined water) showed significant increases from 3 to 7 days of curing because of the progress of the reaction. The corresponding mass losses for 7 days of curing were M2 = 15.51%, M3 = 10.82% and M1 = 4.52%. This behavior can be attributed to the formation of more cementing compounds from the reaction process. Curiously, the combined water for M2 is higher than that for M3, although the strength is opposite. This behavior may be due to two facts: on the one hand, the presence of more solid in the M3 mix (18.8% more) achieves a filler effect in the activated matrix. On the other hand, the presence of both potassium and calcium probably modifies the nature of the hydrates, making a stronger matrix.

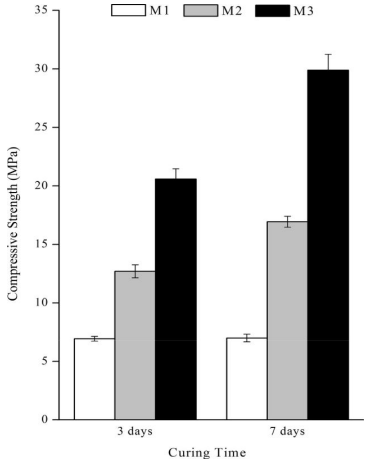

Fig.4.vii.2 *Compressive strength of mortars M1, M2 and M3 after 3 and 7 days of curing time at 65°C.*

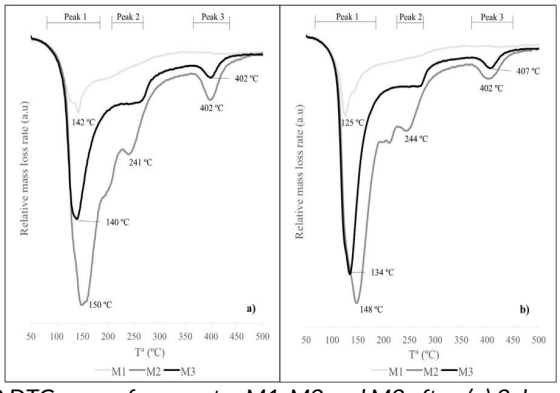

Fig.4.vii.3 *DTG curves from pastes M1, M2 and M3 after: (a) 3 days; (b) 7days of curing.*

4. Conclusions

OBA showed a high amount of calcium and potassium in its composition. In water suspension, OBA produces an alkaline medium. When the OBA was reacted with BFS, the ash influenced positively the compressive strength development of the mortars. After 3 and 7 days of curing time at 65 °C, this OBA + BFS mix showed better strength than the corresponding KOH-activated system, suggesting a synergic process in terms of the filler effect and chemical effect. The use of OBA opens an interesting new line in the

preparation of 100%-waste based AAMs. These results showed that new and better ecological and economical materials have been designed.

Acknowledgements

Thanks are given to Almazara Candela for providing the OBA sample and BIOMASA project (UPV).

References

Abdel-Gawwad, H.A., Abd El-Aleem, S., 2015. Effect of reactive magnesium oxide on properties of alkali activated slag geopolymer cement pastes. Ceram. - Silikaty 59, 37–47.

Bouzón, N., Payá, J., Borrachero, M. V., Soriano, L., Tashima, M.M., Monzó, J., 2014. Refluxed rice husk ash/NaOH suspension for preparing alkali activated binders. Mater. Lett. 115, 72–74. https://doi.org/10.1016/j.matlet.2013.10.001

Cabrera, M., Galvin, A.P., Agrela, F., Carvajal, M.D., Ayuso, J., 2014. Characterisation and technical feasibility of using biomass bottom ash for civil infrastructures. Constr. Build. Mater. 58, 234–244. https://doi.org/10.1016/j.conbuildmat.2014.01.087

Cruz-Yusta, M., Mármol, I., Morales, J., Sánchez, L., 2011. Use of olive biomass fly ash in the preparation of environmentally friendly mortars. Environ. Sci. Technol. 45, 6991–6996. https://doi.org/10.1021/es200968a

Mo, K.H., Alengaram, U.J., Jumaat, M.Z., Yap, S.P., Lee, S.C., 2016. Green concrete partially comprised of farming waste residues: A review. J. Clean. Prod. 117, 122–138. https://doi.org/10.1016/j.jclepro.2016.01.022

Moraes, J.C.B., Tashima, M.M., Akasaki, J.L., Melges, J.L.P., Monzó, J., Borrachero, M. V., Soriano, L., Payá, J., 2016. Increasing the sustainability of alkali-activated binders: The use of sugar cane straw ash (SCSA). Constr. Build. Mater. 124, 148–154. https://doi.org/10.1016/j.conbuildmat.2016.07.090

Pal, S.C., Mukherjee, A., Pathak, S.R., 2003. Investigation of hydraulic activity of ground granulated blast furnace slag in concrete. Cem. Concr. Res. 33, 1481–1486. https://doi.org/10.1016/S0008-8846(03)00062-0

Peys, A., Rahier, H., Pontikes, Y., 2016. Potassium-rich biomass ashes as activators in metakaolin-based inorganic polymers. Appl. Clay Sci. 119, 401–409. https://doi.org/10.1016/j.clay.2015.11.003

Rivera, O.G., Long, W.R., Weiss, C.A., Moser, R.D., Williams, B.A., Torres-Cancel, K., Gore, E.R., Allison, P.G., 2016. Effect of elevated temperature

on alkali-activated geopolymeric binders compared to portland cement-based binders. Cem. Concr. Res. 90, 43–51. https://doi.org/10.1016/j.cemconres.2016.09.013

Turner, L.K., Collins, F.G., 2013. Carbon dioxide equivalent (CO2-e) emissions: A comparison between geopolymer and OPC cement concrete. Constr. Build. Mater. 43, 125–130. https://doi.org/10.1016/j.conbuildmat.2013.01.023

Vassilev, S. V., Baxter, D., Andersen, L.K., Vassileva, C.G., 2010. An overview of the chemical composition of biomass. Fuel 89, 913–933. https://doi.org/10.1016/j.fuel.2009.10.022

viii. Olive-stone biomass ash (OBA): An alternative alkaline source for the blast furnace slag activation

AUTORES: Sayonara María de Moraes Pinheiro, Alba Font, Lourdes Soriano, Mauro M. Tashima, José Monzó, María Victoria Borrachero, Jordi Payá

REFERENCIA DE LA PUBLICACIÓN: Construction and Building Materials 178 (2018) 327-338
DOI: https://doi.org/10.1016/j.conbuildmat.2018.05.157

Factor de impacto/Cuartil (2018): 4.046/Q1	**Citas (excluyendo auto citas): 3**

OBJETIVOS PARCIALES ABORDADOS

MATERIALES	FABRICACIÓN
• **BAAM:** BFS + OBA (5-25% Ad) + H_2O • **BAAM:** BFS + OBA (15-35% Rp) + H_2O • **BAAM:** BFS + KOH(4-14M) + H_2O • **BAAM:** BFS + KOH(4-14M) + H_2O • **BAAM:** BFS + KOH(4M) + H_2O + KPH	• **CURADO:** TB • **Amasado con:** NM

PROCEDIMIENTO EXPERIMENTAL

CARACTERIZACIÓN DE MATERIAS PRIMAS	CARACTERIZACIÓN DE ESPECÍMENES
-	• Resistencia a la compresión (Rc) • Resistencia a la flexión (Rf) • TGA • FESEM Y EDS • XRD • MIP

RESULTADOS Y CONCLUSIONES MÁS RELEVANTES DE LA INVESTIGACIÓN

- Tanto para los sistemas en los que la OBA se adiciona como remplazo, como para los sistemas de adición, los resultados mecánicos de los BAAM fueron muy competitivos respecto a los obtenidos con el uso de activadores convencionales.
- Se estableció una equivalencia entre la concentración del reactivo químico (NaOH o KOH) en la disolución activadora y el porcentaje de remplazo de OBA para la activación de la BFS.
- Los resultados mecánicos, tras 7 días, más significativos fueron:

Material	Rc (MPa)	Rf (MPa)
BFS/OBA (20% Ad) + H_2O	34.7	6.9
BFS/OBA (25% Ad) + H_2O	38.4	7.0
BFS/OBA (20% Rp) + H_2O	26.0	6.5
BFS/OBA (25% Rp) + H_2O	29.4	6.3

- Las principales características microestructurales del efecto de la OBA en las pastas fueron la disminución del diámetro medio de los poros y la formación de fases zeolíticas.

Abstract: Alkali activated materials (AAM) are being investigated as an alternative binder that could be more eco-efficient than Portland cement. The effect of olive-stone biomass ash (OBA) on the activation of blast furnace slag (BFS) was studied. The mechanical behaviour of mortars in which OBA was replaced, or added to, BFS were compared to those found for BFS mortars activated with potassium hydroxide (KOH) and sodium hydroxide (NaOH) solutions in the range of 4–12 mol·kg^{-1}. The results showed the high efficiency of OBA as activating reagent because it provided similar, or higher, strengths when compared to the alkali hydroxide activating solutions. The microstructural characteristics of the new binding OBA/BFS systems were assessed by X-ray diffraction (XRD), thermogravimetric analysis (TGA), field emission scanning electron microscopy (FESEM) and mercury intrusion porosimetry (MIP). These systems showed lower mean pore diameter and scarcer formation of zeolite structures when compared to KOH/BFS systems. These promising results demonstrated the viability of the use of these type of ashes as activating reagents in AAM.

Keywords: Conservation, alkali activated material, blast furnace slag, olive-stone biomass ash, strength development

HIGHLIGHTS

- Olive-stone biomass ash (OBA) was successfully tested as activator.
- OBA has alkaline properties suitable for alkali activated materials (AAM).
- OBA was used as unique activator for blast furnace slag (BFS).
- The effectivity of OBA was higher than KOH and similar to NaOH.
- OBA reduces the consumption of commercial chemical reagents in AAM.

1. Introduction

Currently, cementing materials resulting from alkaline activation of alumino-silicate precursors are becoming a well-known alternative to Portland cement. They are overcoming the limitations of Portland cement in terms of mechanical and durability performance, and also minimize environmental impacts, such as CO_2 emissions and energy consumption (Turner and Collins, 2013)1. These materials are denominated as alkali-activated materials (AAM) or geopolymers (Davidovits, 2015; Pacheco-Torgal et al., 2014; Palomo et al., 2014).

In general, the raw materials used as source of alumino-silicates are blast furnace slag (BFS) (Fernández-Jiménez et al., 1999; Fernández-Jimenez and Puertas, 1997), metakaolin (Pelisser et al., 2013) or fly ash (Rattanasak and Chindaprasirt, 2009; Temuujin et al., 2010). In the last few years, some industrial and agricultural wastes have been investigated, and some of them have shown the ability for alkali-activated procedures in simple or combined systems, such as fluid catalytic cracking catalyst FCC residue (Tashima et al., 2012), ceramic waste (R. H. Geraldo et al., 2017; Reig et al., 2013), bottom coal

ash (Santa et al., 2013) and sugarcane waste-derived ash (Moraes et al., 2016), among others.

However, there are fewer examples in which wastes have been used in the preparation of the activating solution. This is a critical subject, because the environmental impact relates to its synthesis. The commercial reagents for preparing solutions used to activate the precursor are produced with natural raw materials and involve industrial processes with high energy costs and high CO_2 emission, especially the alkali silicates (Gao et al., 2017; Mellado et al., 2014).

In order to minimize this impact, several studies have been done (Bouzón et al., 2014; Gao et al., 2017; Rodrigo H Geraldo et al., 2017; Mejía et al., 2016, 2013; Mellado et al., 2014). Gao et al. (Gao et al., 2017) reported the use of nanosilica from olivine for preparing alkali activating reagents for the activation of slag-fly ash blends. In some cases, the goal was to supply soluble silicate by dissolution of the rice husk ash (Bouzón et al., 2014; Rodrigo H Geraldo et al., 2017; Mejía et al., 2016, 2013; Mellado et al., 2014). The reagent for producing the dissolution was commercial sodium hydroxide, and the results indicated the feasibility of its use. However, very few studies were reported in which AAM was prepared with raw materials (precursor and activating solution) and were derived exclusively from waste (100%-waste AAM).

Recently, an alkaline sodium hydroxide waste solution from an aluminium cleaning mould process was studied (Cristelo et al., 2019). In this study, the waste was used to supply the alkali activating solution on different precursors, and the results were promising for its use in the industry of geopolymers.

In this context, olive-stone biomass ash (OBA) comes up as a promising alkali source for preparation of AAMs. It has a significant amount of potassium and when mixed with BFS, showed promising properties, such as compressive and flexural strengths of the mortar (Font et al., 2017). Also, ashes from maize stalk and maize cob were used for activating metakaolin (Peys et al., 2016).

During the production of olive oil, two types of waste are generated, a liquid (waste water) and a solid phase (**Fig.4.viii.1)**. The liquid phase, "*alpechín*" (wastewater from olive oil mills), contains a large number of solid residues, oil, grease and polyphenols. It is a highly contaminant material (Junta de Andalucía, n.d.; M. L. Medeiros et al., 2016; Roig et al., 2006; Romero et al., 2017) because of its acidity and high chemical (DQO) and biochemical (DQO) oxygen demands. The solid waste (SW) phase is a paste formed by a mixture of pulp, bark, olive stone and residual oil, called "orujo", "alpeorujo", "orujillo" or "cake". This SW has a high concentration of organic matter, oil and grease, and is rich in calcium and potassium (Alburquerque et al., 2004; Vlyssides et al., 2004). It is a contaminant material, has a strong smell and high moisture content. It can be used as an energy resource, such as for biofuel, ani- mal feed and soil fertilizer (Caputo et al., 2003; Hanandeh, 2015; Roig et al., 2006)24,31,32.

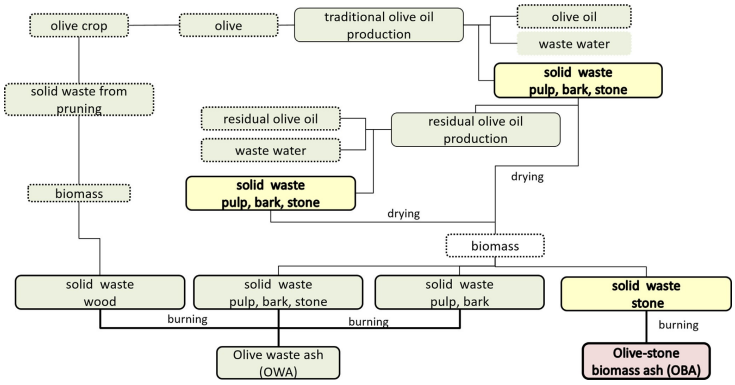

Fig.4.viii.1. Scheme of the production of olive oils, generation of wastes and their ashes by combustion.

The amount of the SW and its physical-chemical characteristics depend on the production process used for the oil extraction. It has been estimated that in 1000 kg of olive oil production, 1500–4000 kg of SW are generated. In addition to the type of process, changes in yield and contamination of the waste can occur (Alburquerque et al., 2004; Caputo et al., 2003; Nair. N.G and Markham, n.d.).

The world production of olive oil expected for 2016/2017 is estimated to be 2.7 Mt, and 92% will be produced in the Mediterranean area and 48.3% in Spain ("IOC-International Olive Oil Council, 2017, World Olive Oil Figures.," n.d.). Considering the average residue generation rate, where solid waste/olive oil = 2.5, it is possible to expect the generation of 4.9 Mt of SW in Spain.

To be used as a biofuel, the SW must be dried. In addition, the stone can be segregated to generate a by-product with a higher calorific value about 4490 kcal/kg (Vamvuka and Zografos, 2004). The combustion of these solid waste phases generates ashes (**Fig.4.viii.1**): a general olive waste ash (OWA) and a specific olive-stone biomass ash (OBA) (Junta de Andalucía, n.d.). The chemical characteristics of these ashes depend on many factors, such as SW composition, combustion temperature and the presence of contaminants (**Table 4.viii.1**). The estimated amount of ash generated in the burning process from dried SW is about 12% by mass (Al-Akhras et al., 2009).

The reuse of these ashes in the preparation of concrete and mortars has been widely reported. The studies with OWA were done with concrete and mortars, using it as a replacement material for Portland cement, fine filler material and sand (Al-Akhras et al., 2009; Al-Akhras and Abdulwahid, 2010; Al-Akhras, 2012; Eisa, 2014).

Specifically, Eisa (Eisa, 2014) found a reduction in the compressive and flexural strengths of concrete when OWA was used as a replacement for Portland cement. Al-Akhras et al. (Al-Akhras et al., 2009), obtained a more durable

material at high temperatures when OWA was used as a replacement for Portland cement. It was also more resistant to the alkali-silica reaction, when OWA was used as a replacement for sand (Al-Akhras, 2012). The authors explained the improvement in the performance of the material due to a possible pozzolanic and filler effects of OWA.

Al-Akhras and Abdulwahid (Al-Akhras and Abdulwahid, 2010) used OWA as a replacement for Portland cement and sand in mortars. The mortars they produced showed a decrease in the workability with the increase of OWA content. Also, they observed an increase in the compressive and flexural strengths when sand was replaced with OWA, and a decrease when Portland cement was replaced by it. Cruz-Yusta et al. (Cruz-Yusta et al., 2011) analyzed the effect of OWA as a replacement for Portland cement and as a filler material. The authors concluded that a replacement of up to 10% of Portland cement is feasible without major changes in strength, and showed a low pozzolanic activity of the material, as well as its filler effect.

The first study of OBA was carried out by Font et al. (Font et al., 2017). The ash was characterized and it showed a high amount of K_2O (32.16%) and CaO (27.77%). They also noted the high alkalinity in water suspension (pH = 13.5) and the presence of crystalline phases, such as portlandite, calcite, anorthite and kalicinite. These characteristics show that the material can be a potential source of alkalis in AAMs. In this first study, the potential of OBA in alkaline activation was assessed in BFS mortars and three types of mixtures (BFS/water, BFS/KOH and BFS/OBA). The results showed: a) the BFS was alkali activated by the OBA, b) the AAM matrix produced with OBA was stronger than the matrix produced with KOH and c) a filler effect in the matrix was observed.

To better understand of the behavior of OBA in AAM, this study analyzed the binary system composed by blast furnace slag (BFS) and olive-stone biomass ash (OBA) to evaluate the alkaline reactive potential of OBA. A comparison in mechanical behavior and microstructural parameters was carried out in order to assess the role of OBA, and the effect of the percentage of OBA, in the prepared BFS-based mixtures.

Table 4.viii.1
Reported chemical compositions for OWA and OBA.

Waste	SiO_2	CaO	Al_2O_3	Fe_2O_3	Na_2O	K_2O	MgO	P_2O_5	SO_3	LOI	REF
OWA-wood	2.70	52.30	1.40	2.10	0.10	1.50	2.70	1.50	2.60	32.06	
	8.10	32.80	1.60	0.70	2.90	19.90	2.40	8.50	2.10	20.90	(Vamvuka and Zografos, 2004)
	9.20	43.40	1.50	1.90	2.70	12.70	2.80	12.70	1.70	11.20	
	10.00	44.20	1.20	1.00	2.60	7.20	3.50	17.00	6.80	6.40	
	10.24	41.47	2.02	0.88	3.67	25.16	3.03	10.75	2.65	–	(Vassilev et al., 2010)
	11.84	54.82	2.60	1.38	0.16	9.26	4.36	3.40	–	11.73	(Cuenca et al., 2013)
OWA – bark	32.70	14.50	8.40	6.30	26.20	4.30	4.20	2.50	0.60	–	(Demirbas, 2004)
OWA – pulp, bark and stone	22.26	12.93	4.10	1.99	0.12	42.79	5.84	6.09	3.73	–	(Vassilev et al., 2010)
	33.00	18.14	16.66	6.50	2.50	11.20	10.00	–	2.93	3.52	(Cruz-Yusta et al., 2011)
OWA – pulp and bark	25.30	42.40	7.40	4.60	0.45	3.30	3.20	–	3.70	9.50	(Al-Akhras et al., 2009)
	25.80	42.90	8.50	5.70	0.25	0.33	3.20	–	3.80	9.50	(Al-Akhras and Abdulwahid, 2010)
	25.80	42.90	8.50	5.70	0.25	0.33	3.20	–	3.80	9.50	(Al - Akhras, 2012)
OBA – stone	31.47	13.66	6.45	6.97	27.43	1.77	4.48	33.33	1.98	–	
	21.40	33.00	4.40	7.90	0.60	2.70	3.70	2.30	4.40	18.70	
	10.70	22.00	2.70	1.70	3.40	24.70	3.00	14.70	3.50	13.30	(Vamvuka and Zografos, 2004)
	15.00	28.70	3.10	2.30	4.10	19.90	4.20	11.60	2.50	8.30	
	20.40	32.90	4.40	2.60	4.30	12.70	4.80	11.10	4.80	1.50	
	21.48	19.97	5.95	4.25	15.77	16.44	3.84	9.71	2.30	–	(Vassilev et al., 2010)
	5.33	27.77	0.70	3.45	0.78	32.12	5.13	2.68	1.67	18.90	(Font et al., 2017)

2. Materials and methods

2.1. Materials

The materials used in this experiment were blast furnace slag (BFS), olive-stone biomass ash (OBA), kephalite (KPH), potassium hydroxide (KOH) and sodium hydroxide (NaOH).

Blast furnace slag (BFS) was used as a precursor in all mixtures. It was supplied by Cementval (Puerto de Sagunto, Valencia, Spain). The particle size distribution is shown in **Fig.4.viii.2**. It had 26.0 μm mean particle diameter and its chemical composition is summarized in **Table 4.viii.2**.

Olive-stone biomass ash (OBA) was supplied by Almazara Candela – Elche, Spain. It was produced in the combustion of olive-stone to produce heat. The resulting ash was collected from the bottom of the furnace. The received sample was dried at 105 °C for 24 h and was immediately ground into a ball mill in order to homogenize the material, increase its fineness and improve its dissolution rate in water. It presented 27.4 μm mean particle diameter, and the particle size distribution is shown in **Fig.4.viii.2**. Its chemical composition is summarized in **Table 4.viii.2**. The XRD pattern showed the main crystalline phases (**Fig.4.viii.3**) as portlandite ($Ca(OH_2)$, PDF card 040733), calcite ($CaCO_3$, PDF card 050586), anorthite ($CaAl_2Si_2O_8$, PDF card 411486) and kalinicite ($KHCO_3$, PDF card 120292). Also, quartz (SiO_2, PDF card 331161), silvite (KCl, PDF card 411476) and gismondine ($CaAl_2Si_2O_8$ $4H_2O$, PDF card 200452) were detected. The size and shape of ground OBA particles are depicted in **Fig.4.viii.4**. In general, OBA particles were porous and irregular,

and some particles presented a smooth surface (these were identified as unburned olive-stone particles).

Kephalite (KPH) is a pure crystalline andalucite (Al_2SiO_5, 63% in Al_2O_3 and 37% in SiO_2 by weight) which is used as inert material because of its low solubility in an alkaline medium (the solubility in boiling 4M KOH solution for 4 h was less than 5%). The particle size distribution is shown in **Fig.4.viii.2**, and its mean particle diameter was 31.1 μm.

Commercial potassium hydroxide (KOH, 85% purity, pellets) and sodium hydroxide (NaOH, 98% purity, pellets) were supplied by Panreac S.A.

Table 4.viii.2
Chemical compositions for BFS and OBA.

Materials	Oxide composition (%)										
	SiO_2	CaO	Al_2O_3	Fe_2O_3	Na_2O	MgO	K_2O	P_2O_5	SO_3	others	LOI
BFS	30.53	40.15	10.55	1.29	0.87	7.43	0.57	0.26	1.93	0.89	5.53
OBA	5.33	27.77	0.70	3.45	0.78	5.13	32.16	2.68	1.67	0.95	18.90

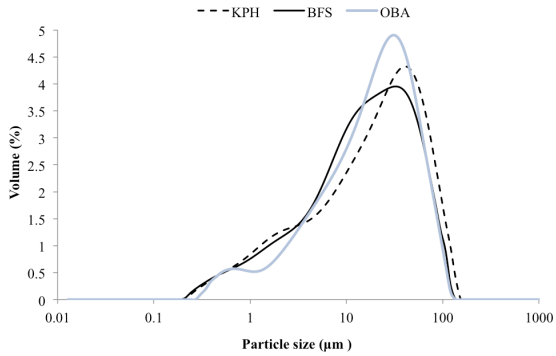

Fig.4.viii.2 *Particle size distribution curves for BFS, OBA and KPH.*

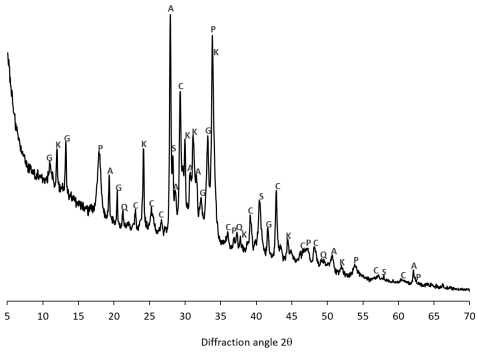

Fig.4.viii.3 *X-ray diffraction pattern of OBA (Key: P, portlandite; C, calcite; A, anorthite; K, kalinicite; Q, quartz; S, silvite; G, gismondine).*

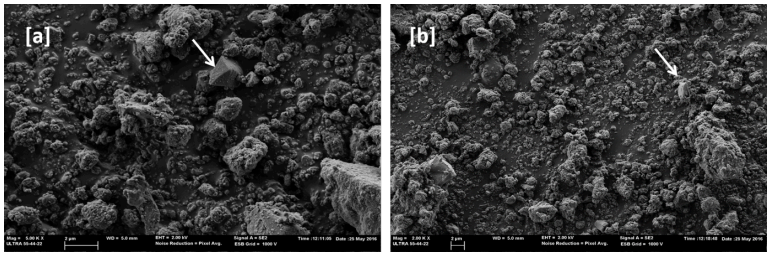

Fig.4.viii.4 *FESEM micrographs for OBA: a) 5000x; b) 2000x. Arrows indicate the presence of unburned olive-stone particles.*

2.2. Methods

The methodology applied to evaluate the reactive potential of OBA, as an alkaline source to activate BFS, included the analysis of mechanical properties and microstructural characteristics obtained in mortars and pastes. Alkali activated samples were produced with different mass ratios of BFS/OBA. The control mortars and pastes were produced with BFS/KOH, BFS/NaOH and BFS/ KOH + KPH.

Mortars were prepared with w/b=0.4 (water/binder, being the binder the quantity of BFS in control mortars) and a/b=3 (aggregate/binder) ratios. The fresh mixture was poured in three prismatic 40 x 40 x 160 mm^3 moulds and they were demoulded after 4 h in a thermal bath (65 °C). The specimens were cured for 7 days at 65 °C. Three values for flexural strength (Rf) and six values for compressive strength (Rc) were obtained for each mixture according to UNE 196-1 (AENOR, 2005).

Alkaline activation of BFS was assessed by a family of mortars produced with BFS/KOH and BFS/NaOH in different concentrations. These mortars were

noted as BFS/KOH-xM and BFS/NaOH-xM, where "x" is the molality (mol kg^{-1}) value of the alkaline solution (x = 4, 6, 8, 10, 12 and 14 mol kg^{-1}; the symbol M will be used in the manuscript for simplicity).

The filler effect was controlled by means of mortars produced with BFS/KOH + KPH. Two types of mortars with 4M KOH were synthetized, one with KPH 20% addition (Ad) respect to BFS and the other with 20% replacement (Rp) of the BFS. They were named as KPH-Ad20-4M and KPH-Rp20-4M, respectively.

BFS/OBA mortars were produced by blending both solids. An addition series (Ad) was prepared, where a given percentage of OBA was added by mass with respect to BFS content, and a replacement series (Rp) was prepared by the substitution by mass of BFS by OBA. They were named as OBA-Ady and OBA-Rpz respectively, where "y" is the addition content of OBA (y = 5, 10, 15, 20 and 25%) and "z" is the replacement by OBA (z = 15, 20, 25, 30 and 35%).

The pastes used in these analyses were prepared with w/b = 0.4 and were moulded in a plastic container, sealed and cured for 7 days at 65 °C. The microstructure of the hydrated products in the pastes was evaluated by: a) powder X-ray diffraction (XRD), carried out by a Bruker AXS D8 Advance, from 10° to 70° 2h, and with Cu Ka radiation at 40 kV and 20 mA; b) thermogravimetric analysis (TG/DTG), using a TGA850 Mettler Toledo thermobalance with a temperature range of 35–600 °C, heating rate of 10 °C min^{-1} in an N_2 atmosphere with 75 mL min^{-1} gas flow; c) field emission scanning electron microscopy (FESEM) by an ULTRA 55-ZEISS (the powdered sample of OBA was not covered by any material and the pastes were covered by carbon) and EDS with 6–8 mm work distance and extra high voltage of 20 kV; and d) mercury intrusion porosimetry (MIP) by means of an AutoPore IV 9500 by the Micromeritics Instrument Corporation, that measured pores in the range of 91.26 mm–5.5 nm.

For TG/DTG and XRD, 5 types of pastes were analyzed: P-BFS/KOH-xM (x = 4 and 8 M), P-OBA-Adx (x = 20 and 25%) and P-KPH-Ad20-4M. For FESEM and porosity studies, 4 types of pastes were analyzed: P-BFS/KOH-xM (x = 4, 8 M) and P-OBA-Adx (x = 10 and 25%).

3. Results and discussion

3.1. BFS activated by KOH and NaOH

The effect of KOH and NaOH solutions on the hydration of BFS was evaluated by the mechanical and microstructural performance of mortars and pastes. Samples were prepared by means of alkali activating solutions with different concentrations of KOH and NaOH. The mechanical properties evaluated in mortars included the compressive (Rc) and flexural (Rf) strengths. In **Table 3** the mechanical properties are summarized, while in **Figs.4.viii. 5 and 6** a

comparison of the compressive and flexural strengths of the mortars is shown respectively.

The KOH series showed a nonlinear behaviour with alkali concentration and a maximum Rc value was found for [KOH] equal to 8 M. For this mixture, the Rc value reached 25.56 MPa. The lowest values were found for [KOH] equal to 4 M and 14 M (in the 14–15 MPa range), whereas Rc values in the range 19–21 MPa were obtained for the rest of the KOH mortars. A similar trend was found for Rf, where the highest strength value of 3.90 MPa was obtained for [KOH] equal to 6 M.

The NaOH series showed similar behaviour to the KOH series. The Rc values increased for [NaOH] = 12 M and decreased for [NaOH] = 14 M. The maximum value was 31.11 MPa, and the lowest was 17.57 MPa. For Rf, the trend was the same, as it increased from 3.95 MPa for [NaOH] = 4 M to 6.05 MPa for [NaOH] = 12 M, and decreased to 5.12 MPa for [NaOH] = 14 M. In general, the strengths for the sodium series were slightly higher than for KOH series. Taking into account the chemical nature of OBA, which was richer in K2O than in Na2O, the systems prepared with OBA may be initially compared to those obtained with KOH, although comparisons will be done also to the NaOH series, to assess the equivalency among the ash and the commercial alkaline reagents.

Table 4.viii.3
Mechanical properties (compressive, Rc; flexural, Rf) of mortars cured for 7 days at 65ºC.

Mortars	Mechanical properties			
	Rc (MPa)		Rf (MPa)	
BFS/KOH-4M	14.55	±0.70	3.38	±0.15
BFS/KOH-6M	20.31	±0.32	3.90	±0.02
BFS/KOH-8M	25.56	±0.73	3.73	±0.53
BFS/KOH-10M	20.77	±0.64	2.32	±0.18
BFS/KOH-12M	19.31	±0.67	2.35	±0.14
BFS/KOH-14M	14.94	±0.66	1.79	±0.07
BFS/NaOH-4M	17.57	±0.59	3.95	±0.34
BFS/NaOH-6M	24.07	±0.38	5.64	±0.25
BFS/NaOH-8M	26.90	±0.67	5.82	±0.71
BFS/NaOH-10M	27.90	±0.64	4.35	±0.36
BFS/NaOH-12M	31.11	±1.46	6.06	±0.30
BFS/NaOH-14M	26.04	±0.79	5.12	±0.57
KPH-Ad20-4M	15.31	±0.60	3.80	±0.35
KPH-Rp20-4M	11.88	±0.54	3.41	±0.09
OBA-Rp15	16.27	±0.72	3.14	±0.05
OBA-Rp20	26.01	±0.81	6.47	±0.55
OBA-Rp25	29.42	±1.01	6.30	±0.16
OBA-Rp30	31.25	±1.00	6.04	±0.35
OBA-Rp35	27.81	±0.33	5.76	±0.16
OBA-Ad5	8.59	±0.25	2.64	±0.09
OBA-Ad10	16.13	±0.22	3.85	±0.23
OBA-Ad15	21.47	±0.61	3.47	±0.47
OBA-Ad20	34.74	±1.51	6.88	±0.62
OBA-Ad25	38.38	±1.29	7.01	±0.44

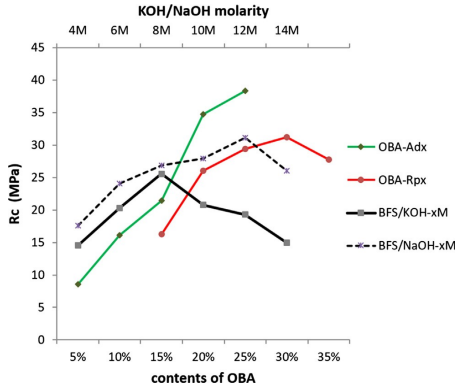

Fig.4.viii.5 *Compressive strength behavior of mortars.*

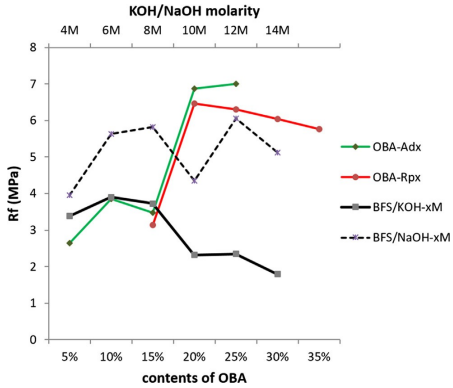

Fig.4.viii.6 *Flexural strength behavior of mortars.*

By means of the MIP data on the corresponding pastes (**Table 4.viii.4**) it was possible to observe the reduction in the porosity with the increase of the KOH concentration, from 47.16% (P-BFS/KOH-4M) to 23.74% (P-BFS/KOH-8M), as well as the reduction of mean pore diameter (from 48.2 nm to 22.9 nm). These characteristics con- firmed the refinement of the pore network, showing the increase in the compactness for P-BFS/KOH-8M, and consequently the higher mechanical strength (Chen et al., 2013).

Thermal analysis (TG/DTG) for the KOH family registered several mass loss events in the 35–600 °C range (**Table 4.viii.5 and Fig.4.viii.7**). The first one occurred around 140 °C and indicated the loss of combined water from the main hydrated products, C-S-H and (C,K)-S-H. The second event showed two peaks in the DTG curve at 200°C and in the 238–259 °C range, which were related to dehydration of C-A-S-H and (C,K)-A-S-H. The third peak, at about 390 °C, was associated to the presence of hydrotalcite. Similar results were

reported by other researchers (Abdel-Gawwad and Abd El-Aleem, 2015; Rattanasak and Chindaprasirt, 2009; Rivera et al., 2016). The total mass loss increased with the concentration of KOH, from 12.73% (P-BFS/ KOH-4M) to 20.78% (P-BFS/KOH-8M). This indicated that the amount of hydration products in P-BFS/KOH-8M were higher than in P-BFS/KOH-4M. This growth was expected, due to the increase of KOH content available to activate the BFS.

Table 4.viii.4
Mercury intrusion porosimetry data for P-BFS/KOH-xM and P-OBA-Adx pastes.

Description	Unit	P-BFS/KOH-4M	P-BFS/KOH-8M	P-OBA-Ad10	P-OBA-Ad25
Mean diameter pore	nm	48.20	22.92	16.74	11.87
Volume	cm^3/g	0.29	0.10	0.20	0.12
Surface area	m^2/g	4.11	6.43	17.42	18.35
Total porosity	%	47.16	23.74	42.85	29.67

Table 4.viii.5
Thermogravimetric data for selected alkali-activated pastes.

	Mass loss (ML, in %) in the temperature range (°C)			Total
Paste	0-200 (ML-1)	200-350 (ML-2)	350-600 (ML-3)	mass loss (%)
P-BFS/KOH-4M	6.11	4.41	2.21	12.73
P-BFS/KOH-8M	11.78	5	4	20.78
P-KPH-Ad20-4M	3.77	4.01	1.82	9.6
P-OBA-Ad20	5.52	3.3	2.49	11.31
P-OBA-Ad25	8.78	3.47	2.39	14.64

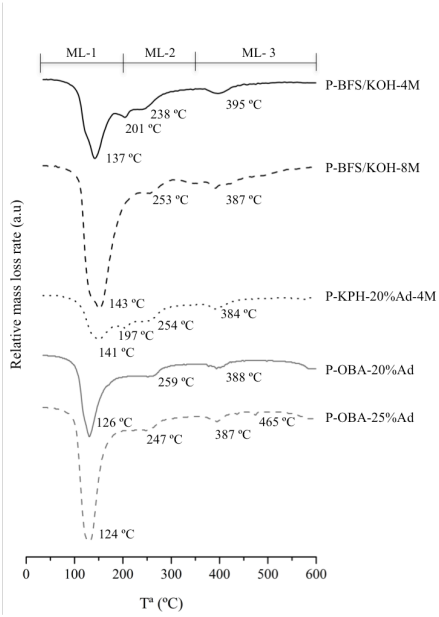

Fig.4.viii.7 *Selected DTG curves for pastes P-BFS/KOH-4M, P-BFS/KOH-8M, P-KPH-Ad20-4M, P-OBA-Ad20 and P-OBA-Ad25.*

The microstructure of hydrated products is shown in **Fig.4.viii.8(a) and (b)** for P-BFS/KOH-4M, and **Fig.4.viii.8(c) and (d)** for P-BFS/KOH- 8M. Both presented a dense matrix with microcrystals and amorphous rounded particles. Microcrystals in P-BFS/KOH-8M were more common, presenting a twined platelet-like microstructure (**Fig.4.viii.8(d)).** EDS analyses were carried out to compare the composition of the cementing gel in both pastes. Gels analysed in 4 M and 8 M pastes contained similar SiO_2 content (21.6 ± 2.1% vs 23.5 ± 2.3%), Al_2O_3 content (6.8 ± 0.8% vs 7.37 ± 1.4%) and CaO content (28.9 ± 2.1% vs 25.3 ± 7.9%). However, the K2O content was very different: 33.0 ± 3.6% for 4 M and 27.1 ± 1.7% for 8 M. The higher percentage for the gel formed in 4 M KOH paste suggested that less gel was formed, and the main part of the potassium was incorporated into the hydration products. In this way, a part of the BFS did not react, as suggested by the low value of mass loss in thermo-gravimetric analysis (**Table 4.viii.5**) and the weak strength development (**Table 4.viii.3**). In contrast, the higher KOH concentration for the P-BFS/KOH-8M system activated more BFS, producing more hydrates. That is why the potassium content in the formed gel was lower.

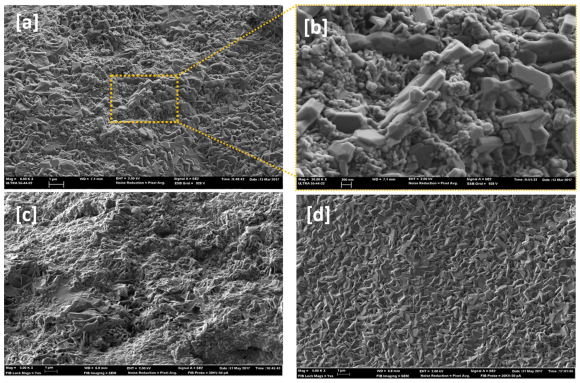

Fig.4.viii. 8 *FESEM micrographs of BFS pastes activated with KOH solution: a) General view for P-BFS/KOH-4M matrix; b) Detail from the above micrograph; c) General view for P- BFS/KOH-8M; d) microcrystals in P-BFS/KOH-8M.*

3.2. BFS activated by OBA

The effect of OBA on BFS reactivity was assessed by the mechanical strength and microstructure evolution for mortars and pastes produced with different contents of OBA (BFS replacement by OBA or OBA addition to BFS). **Table 4.viii.3** also summarizes the values of Rc and Rf strengths, and **Figs.4.viii. 5 and 6** show the behavior of the corresponding mortars cured at 65 °C for 7 days.

The replacement series, OBA-Rpz, also showed a nonlinear strength behavior with replacement percentage (**Figs.4.viii. 5 and 6**). Rc increased up to 30% of OBA content (Rc=31.25 MPa) and decreased for 35% (Rc=27.81 MPa). The minimum Rc value was found for 5% of OBA content (Rc=16.27 MPa). A similar trend was described for Rf development, in this case being 20% replacement the optimum (Rf=6.30 MPa). Despite the lower content in BFS for OBA replacement series, the strength development was good, and strength performance for z=20–35% was higher than that found for the KOH series. This means that the effectiveness of OBA as an activating reagent largely surpassed KOH. Most likely, the combined effect of potassium and calcium present in OBA makes BFS more reactive. The OBA replacement series had a similar trend to that observed for the NaOH series, and reached strengths that were comparable. Thus, the 12M NaOH and OBA-Rp30 systems reached optimum strengths (31.11 and 31.25 MPa respectively). Also, 6 M NaOH and OBA-Rp20 were similar. Fittings of compressive strength (Rc, in MPa) versus activation solution parameter (NaOH concentration: [NaOH]; or OBA replacement: [OBA-Rpz]) were calculated as follows by **Equations (1) and (2)**:

$$Rc = 11.592 * \mathrm{Ln}\,[NaOH] + 2.201 \quad (1)$$

$$Rc = 21.577 * Ln[OBA\text{-}Rpz] - 40.741 \quad (2)$$

From these equations, a relationship for equivalency between NaOH concentration and OBA replacement can be calculated (**Fig.4.viii.9**).

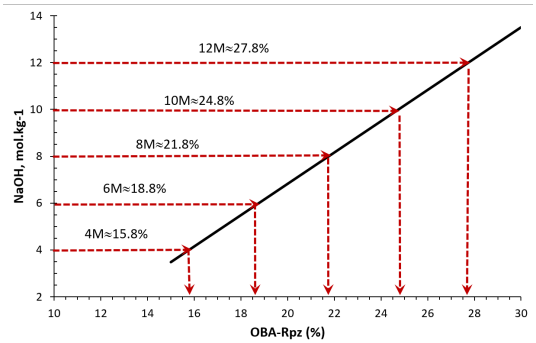

Fig.4.viii.9 *Equivalences between de NaOH concentration and % of OBA replacement, in BFS mortars.*

The addition series (BFS content was maintained constant and OBA was added in different percentages with respect to BFS), OBA-Ady, showed a continuously increasing strength up to 25% content of OBA (**Fig.4.viii. 5 and 6)**. The maximum values for Rc and Rf were found with 25% of OBA (Rc=38.38 MPa and Rf = 7.01 MPa), and the minimum values were found with 5% of OBA (Rc=8.59 MPa and Rf=2.64 MPa). Compressive strength depended linearly on the OBA addition (OBA-Ady), as shown in **Equation (4.viii.3)**

$$Rc = 1.564 * [OBA\text{-}Ady] + 0.405 \quad (4.viii.3)$$

Equivalency analysis for compressive strength revealed that Rc values using NaOH solutions (range from 17.57 to 31.11 MPa) were reached by using OBA addition percentages between 10.97% and 19.63 %, according to **Eq. (4.vii.3)**. The higher OBA addition percentage produced better mortars in terms of strength. Based on the reference family mortars activated with KOH and NaOH, it is clear that mortars produced with the addition of OBA, in amounts of 20% and 25%, presented compressive strength values higher than those developed by the reference series, which reached their maximums in 8M for KOH (Rc=25.56 MPa), and in 12M for NaOH (Rc=31.11 MPa).

The results of MIP tests (**Table 4.vii.4**) showed a significant reduction of porosity and mean pore diameter with the increase of OBA con- tents from 10 to 25%. Thus, P-OBA-Ad10 paste had 42.85% total porosity and P-OBA-Ad25 had 29.67%. This explained the large differences in strength (16.13 MPa vs. 38.38 MPa). Also, the lowest mean pore diameter value was found for P-OBA-Ad25 (11.9 nm). This means that the microstructure of the activated material

became more refined with increasing OBA addition, justifying the increase of mechanical strengths in the corresponding mortars.

Comparing the series P-BFS/KOH-x with P-OBA-Ady, a significant change in the total porosity was not observed (P-BFS/KOH-8M vs. P-OBA-Ad25, 23.74% vs 29.67%). However, the mechanical strengths of the corresponding mortars showed strong differences: BFS/KOH-8 M (Rc = 25.56 MPa, Rf = 5.81 MPa) and OBA-Ad25 (Rc = 38.38 MPa, Rf = 7.01 MPa).

The gain in strength for the OBA series could be attributed to the nature of the hydrated products. Also, the filler effect of the OBA may be taken into account: OBA was not dissolved totally in water, and consequently a filler effect (more fine particles in the mortar matrix) could play an additional role.

3.2.1. Analysis of the filler effect

The filler effect of the OBA was assessed considering the behaviour of the mechanical strengths of mortars produced with an inert material. Kephalite (KPH, andalucite) presented a similar fineness to OBA (**Fig.4.viii.2**). Two types of mortars, KPH-Ad20-4M (addition of 20% KPH by mass respect to BFS content, and activated with 4 M KOH solution) and KPH-Rp20-4M (replacement of 20% BFS by KPH, and activated with 4M KOH solution), were tested. The strength values are summarized in **Table 4.viii.3** and the behaviour depicted in **Fig.4.viii.10**. They were analysed the values for: a) replacement (BFS/KOH-4M, KPH-Rp20-4M, OBA-Rp20) and b) addition (BFS/KOH-4M, KPH-Ad20-4M, OBA-Ad-20). The replacement series showed that the inert-containing mortar yielded 11.88 MPa, which is slightly lower than the corresponding BFS/KOH sample (≈18% less strength). This means that KPH contributed as an inert material. The addition series showed that inert-containing mortar yielded 15.31 MPa, slightly higher than the corresponding BFS/KOH sample (≈5%). This behaviour suggests that, despite having the same BFS content and a larger quantity of fine particles, the filler contribution to strength development was practically negligible. Considering the filler effect as a function of the fineness (PDS), and the similarity of PDS curves for KPH and OBA (**Fig.4.viii.2**), it is suggested that the filler effect did not contribute significantly to the strength gain of the mortars produced with the OBA. The large strength gain observed when comparing the KOH activated sample and OBA activated sample in the replacing (≈79% gain) and addition (≈138% gain) tests is attributed to the contribution of OBA to the hydration of BFS.

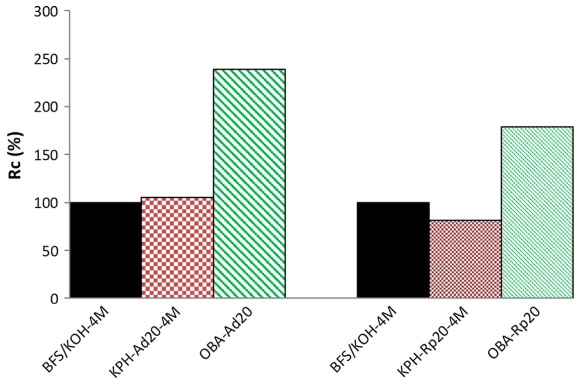

Fig.4.viii.10 *Filler effect assessment from compressive strength values.*

3.2.2. Hydration products in BFS/OBA activated systems

TG/DTG results for KPH and OBA pastes are shown in **Fig.4.viii.7** and **Table 4.viii.5**. The total mass loss for P-KPH-Ad20-4M was lower (≈25%) than that found for P-BFS/KOH-4M, which was attributed to the dilution effect produced with the addition of the inert material. The temperature DTG peaks were very similar, when comparing curves in **Fig.4.viii.7**.

DTG curves for OBA containing pastes showed a large peak at 124–126 °C, which indicated that the nature and amount of hydrates were slightly different than those observed in the KOH activated BFS-pastes. However, the total mass loss (**Table 4.viii.5**) for the OBA containing pastes was significantly lower than that found for KOH pastes. For example, P-BFS/KOH-8M showed 20.73% total mass loss, while P-OBA-Ad25 had only 14.71%. This behavior suggests that despite the lower amount of combined water, the mechanical properties and chemical nature of the hydrates formed in the activation of BFS in the presence of OBA is different than expected.

Results from XRD analyses on selected pastes are shown in **Fig.4.viii.11.** The differences between KOH and OBA activated pastes are clear. Both BFS pastes activated with KOH (4 M and 8 M) showed calcite, hydrotalcite ($Mg_6Al_2CO_3(OH)_{16}{\cdot}4H_2O$, PDF card 140191) and K-I zeolite ($K_2Al_2Si_2O_8$ $3.8H_2O$, PDF card 180988) as main crystalline products. Most likely, the calcite presence was because it was in the BFS composition; the rest of products were formed from the hydration processes. Additional zeolitic phases were formed in these KOH pastes. Potassium gismondine ($K_2AlSi_2O_8{\cdot}3H_2O$, PDF card 110188) was identified in the XRD pat- tern of 4M KOH activated paste and katoite ($Ca_3Al_2(SiO_4)(OH)_8$, PDF card 380368) was identified for the 8 M activated paste. Also, in this last paste, potassium carbonate hydrate ($K_2CO_3{\cdot}1.5H_2O$, PDF card 110655) was found, and its presence may be due to the carbonation of unreacted KOH.

OBA containing pastes (10 and 25% addition of OBA to BFS) also showed calcite as the main crystalline product in the XRD patterns, due to the presence of this phase in BFS and in OBA. However, the main crystalline compound formed under the activation by OBA was hydrotalcite. No presence of katoite and K-I zeolite was observed suggesting that evolution of zeolitic structures were not developed. This behaviour is in agreement with the better mechanical strength found for OBA containing systems. In the 10% and 25% OBA pastes, small amounts of fukalite ($Ca_4Si_2O_6(CO_3)(OH)_2$, PDF card 290308) and potassium carbonate hydrate, respectively, were found.

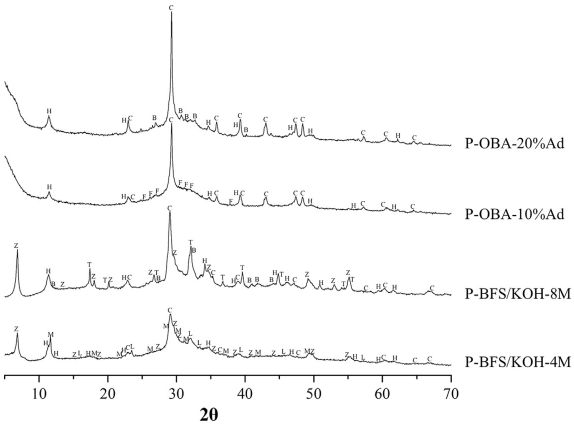

Fig.4.viii.11 *X-ray diffraction patterns for P-BFS/KOH-4M, P-BFS/KOH-8M, P-OBA-Ad10 and P-OBA-Ad25 (Key: C, calcite; Z, zeolite K-I, H, hydrotalcite; M, potassium gismondine; L, larnite; T, katoite; B, potassium carbonate hydrate; F, fukalite).*

The microstructure of the hydrated products in pastes was analysed by FESEM in **Fig.4.viii.12** (P-OBA-Ad10) and **Fig.4.viii.13** (P-OBA-Ad25). P-OBA-Ad25 presented a more compact microstructure than P- OBA-Ad10, and their microstructures were slightly different from the reference pastes (P-BFS/KOH-xM, see **Fig.4.viii.8**). Two different gels were observed in pastes with OBA: a dense one and a compact one. The morphology of the microcrystals (denser phases) was different that that observed for reference pastes, suggesting that these differences may be responsible of the different mechanical behavior of the corresponding mortars.

The mean chemical composition values were obtained by aver- aging 8–10 EDS data sets (see **Table 4.viii.6**). The SiO_2 content in OBA containing pastes (29.17 ± 3.39 for 10% OBA, 28.91 ± 1.61 for 25% OBA) was significantly higher than those found for KOH activated pastes. The same behavior was found for Al_2O_3 and CaO contents.

The CaO content was significantly high, reaching values from 34 to 41%, suggesting that calcium from OBA also reacted with the BFS. The K2O content was significantly lower, ranging less than a half of the percentage found in

KOH activated pastes. All these differences indicated that the activation of BFS was more complete in the presence of OBA.

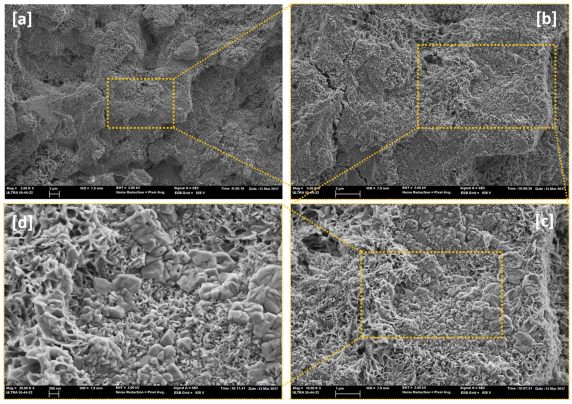

Fig. 4.viii.12 *FESEM micrographs of BFS pastes activated with 10% OBA (P-OBA-Ad10): a) general view, b) detail from the above micrograph, c) magnification of the above one, showing porous and dense particles and d) detailed view of the nature of the different formed gels.*

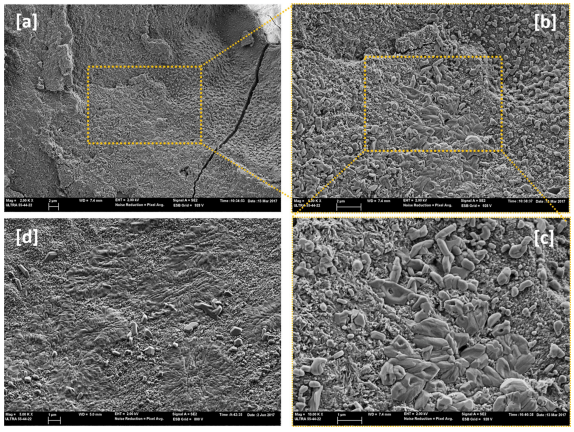

Fig. 4.viii.13 *FESEM micrographs of BFS pastes activated with 25% OBA (P-OBA-Ad25): a) general view, b) detail from the above micrograph, c) magnification of the above one, showing porous and dense particles and d) other views of the two types of gel.*

Table 4.viii.6
Chemical composition (EDS analysis) for studied pastes.

Oxide (% by mass)	P-BFS/KOH-4M	P-BFS/KOH-8M	P-OBA-Ad10%	P-OBA-Ad25%
Na2O	2.45 ± 0.59	1.64 ± 1.07	0.18 ± 0.37	0.60 ± 0.42
MgO	3.39 ± 0.79	4.15 ± 1.22	5.27 ± 0.64	7.47 ± 1.38
Al2O3	6.76 ± 0.80	7.37 ± 1.41	8.73 ± 1.09	9.61 ±1.11
SiO2	21.61 ± 2.14	23.50 ± 2.35	29.17 ± 3.39	28.91 ± 1.61
SO3	0.92 ± 1.14	5.27 ± 2.45	3.93 ± 1.20	4.07 ± 1.28
K2O	32.99 ± 3.64	27.16 ± 1.70	11.23 ± 2.64	14.91 ± 3.27
CaO	28.94 ± 2.08	25.28 ± 7.93	41.19 ± 3.03	34.04 ± 1.54

4. Conclusions

The ash obtained from the combustion of olive-stone biomass (OBA) was tested as an activator reagent for blast furnace slag (BFS), and compared to the effect of typical activating solutions of KOH and NaOH (in the range 4–14 mol·kg—1). The chemical com- position of OBA showed high percentages of K2O and CaO, which become interesting for preparing BFS activated systems. The effect of OBA on the strength development of BFS-based mortars was very significant for both partial replacement of BFS and addition to BFS. The compressive strength of mortars with 20–35% replacement of BFS by OBA yielded higher values than those obtained for BFS-KOH systems. An equivalency between NaOH concentration in the activating solution and OBA replacement in the activation of BFS was found (e.g., 4 M NaOH was equivalent to 15.8% OBA replacement and 8 M NaOH to 27.8% OBA replacement). The addition of 25% of OBA enabled reaching a value of 38 MPa in compressive strength. The effect of OBA on the microstructure was studied, and the main features to highlight were the reduction in the mean pore diameter in the BFS activated paste and the very limited formation of zeolitic phases.

This study demonstrated the viability of using OBA in the activation of BFS and the reduction in the consumption of commercial chemical reagents for AAM preparation. This allows a more sustainable AAM.

Acknowledgements

The authors are grateful to CAPES for the scholarship. Thanks are also given to Electron Microscopy Service of the Universitat Politècnica de València, the GeocelPlus-UPV project and Almazara Candela – Elche, Spain.

References

Abdel-Gawwad, H.A., Abd El-Aleem, S., 2015. Effect of reactive magnesium oxide on properties of alkali activated slag geopolymer cement pastes. Ceram. - Silikaty 59, 37–47.

AENOR, 2005. UNE-EN 196-1, Methods of Testing Cement – Part 1: Determination of Strength.

Al-Akhras, N.M., Abdulwahid, M.Y., 2010. Utilisation of olive waste ash in mortar mixes. Struct. Concr. 11, 221–228. https://doi.org/https://doi.org/10.1680/ stco.2010.11.4.221.

Al-Akhras, N.M., Al-Akhras, K.M., Attom, M.F., 2009. Performance of olive waste ash concrete exposed to elevated temperatures. Fire Saf. J. 44, 370–375. https://doi.org/https://doi.org/10.1016/j.firesaf.2008.08.006

Al-Akhras, N.M., 2012. Performance of olive waste ash concrete exposed to

alkali-silica reaction. Struct. Concr. 13, 221–226. https://doi.org/https://doi.org/10.1002/suco.201100058

Alburquerque, J.A., Gonzálvez, J., García, D., Cegarra, J., 2004. Agrochemical characterisation of "alperujo", a solid by-product of the two-phase centrifugation method for olive oil extraction. Bioresour. Technol. 91, 195–200. https://doi.org/https://doi.org/10.1016/S0960-8524(03)00177-9

Bouzón, N., Payá, J., Borrachero, M. V., Soriano, L., Tashima, M.M., Monzó, J., 2014. Refluxed rice husk ash/NaOH suspension for preparing alkali activated binders. Mater. Lett. 115, 72–74. https://doi.org/10.1016/j.matlet.2013.10.001

Caputo, A.C., Scacchia, F., Pelagagge, P.M., 2003. Disposal of by-products in olive oil industry: waste-to-energy solutions. Appl. Therm. Eng. 23, 197–214. https://doi.org/https://doi.org/10.1016/S1359-4311(02)00173-4

Chen, X., Wu, S., Zhou, J., 2013. Influence of porosity on compressive and tensile strength of cement mortar. Constr. Build. Mater. 40, 869–874. https://doi.org/https://doi.org/10.1016/j.conbuildmat.2012.11.072

Cristelo, N., Fernández-Jiménez, A., Castro, F., Fernandes, L., Tavares, P., 2019. Sustainable alkaline activation of fly ash, aluminium anodising sludge and glass powder blends with a recycled alkaline cleaning solution. Constr. Build. Mater. 204, 609–620. https://doi.org/10.1016/j.conbuildmat.2019.01.226

Cruz-Yusta, M., Mármol, I., Morales, J., Sánchez, L., 2011. Use of olive biomass fly ash in the preparation of environmentally friendly mortars. Environ. Sci. Technol. 45, 6991–6996. https://doi.org/10.1021/es200968a

Cuenca, J., Rodríguez, J., Martín-Morales, M., Sánchez-Roldán, Z., Zamorano, M., 2013. Effects of olive residue biomass fly ash as filler in self-compacting concrete. Constr. Build. Mater. 40, 702–709. https://doi.org/https://doi.org/10.1016/j.conbuildmat.2012.09.101

Davidovits, J., 2015. Geoplymer Chemistry & Applications 4th ed. Institut Géopolymère. https://doi.org/10.1017/S0022278X04254441

Demirbas, A., 2004. Combustion characteristics of different biomass fuels. Prog. Energy Combust. Sci. 30, 219–230. https://doi.org/https://doi.org/10.1016/j.pecs.2003.10.004

Eisa, A., 2014. Properties of Concrete Incorporating Recycled Post-Consumer Environmental Wastes. Int. J. Concr. Struct. Mater. 8, 251–258. https://doi.org/https://doi.org/10.1007/s40069-013-0065-9

Fernández-Jiménez, A., Palomo, J.G., Puertas, F., 1999. Alkali-activated slag mortars: Mechanical strength behaviour. Cem. Concr. Res. https://doi.org/10.1016/S0008-8846(99)00154-4

Fernández-Jimenez, A., Puertas, F., 1997. Influence of the activator concentration on the kinetics of the alkaline activation process of a blastfurnace slag. Mater. Constr. 1997, 31–42. https://doi.org/10.3989/mc.1997.v47.i246.505

Font, A., Soriano, L., Moraes, J.C.B., Tashima, M.M., Monzó, J., Borrachero, M.V., Payá, J., 2017. A 100% waste-based alkali-activated material by using olive-stone biomass ash (OBA) and blast furnace slag (BFS). Mater. Lett. 203. https://doi.org/10.1016/j.matlet.2017.05.129

Gao, X., Yu, Q.L., Lazaro, A., Brouwers, H.J.H., 2017. Investigation on a green olivine nano-silica source based activator in alkali activated slag-fly ash blends: Reaction kinetics, gel structure and carbon footprint. Cem. Concr. Res. 100, 129–139. https://doi.org/10.1016/j.cemconres.2017.06.007

Geraldo, Rodrigo H, Fernandes, L.F.R., Camarini, G., 2017. Water treatment sludge and rice husk ash to sustainable geopolymer production. J. Clean. Prod. 149, 146–155. https://doi.org/https://doi.org/10.1016/j.jclepro.2017.02.076

Geraldo, R. H., Ouellet-Plamondon, C.M., Muianga, E.A.D., Camarini, G., 2017. Alkali-activated binder containing wastes: A study with rice husk ash and red ceramic. Ceramica 63, 44–51. https://doi.org/10.1590/0366-69132017633652057

Hanandeh, A. El, 2015. Energy recovery alternatives for the sustainable management of olive oil industry waste in Australia: life cycle assessment. J. Clean. Prod. 91, 78–88. https://doi.org/https://doi.org/10.1016/j.jclepro.2014.12.005

IOC-International Olive Oil Council, 2017, World Olive Oil Figures. [WWW Document], n.d.

Junta de Andalucía, n.d. Potencial energético de los subproductos de la industria olivarera en Andalucía, Secretaría General del Medio Rural y la Producción Ecológica, 2010. [WWW Document]. URL http://ws128.juntadeandalucia.es/agriculturaypesca/portal/export/sites/%0D%0A%0D%0Adefault/comun/galerias/galeriaDescargas/cap/servicio-estadisticas/Estudios-e-informes/desarrollo-rural-sost/IND_OLIVAR_V1_CC.pdf.%0D%0A

M. L. Medeiros, R., Villa, F., F. Silva, D., R. C. Luciana, J., 2016. Destinação e

Reaproveitamento de Subprodutos da Extração Olivícola. A Rev. Sci. Agrar. Parana. 15, 100–108. https://doi.org/http://dx.doi.org/10.18188/1983-1471/sap.v15n2p100-108

Mejía, J.M., Mejía De Gutiérrez, R., Montes, C., 2016. Rice husk ash and spent diatomaceous earth as a source of silica to fabricate a geopolymeric binary binder. J. Clean. Prod. 118, 133–139. https://doi.org/10.1016/j.jclepro.2016.01.057

Mejía, J.M., Mejía de Gutiérrez, R., Puertas, F., 2013. Ceniza de cascarilla de arroz como fuente de sílice en sistemas cementicios de ceniza volante y escoria activados alcalinamente. Mater. Construcción 63, 361–375. https://doi.org/10.3989/mc.2013.04712

Mellado, A., Catalán, C., Bouzón, N., Borrachero, M. V., Monzó, J.M., Payá, J., 2014. Carbon footprint of geopolymeric mortar: study of the contribution of the alkaline activating solution and assessment of an alternative route. RSC Adv. 4, 23846–23852. https://doi.org/10.1039/C4RA03375B

Moraes, J.C.B., Tashima, M.M., Akasaki, J.L., Melges, J.L.P., Monzó, J., Borrachero, M. V., Soriano, L., Payá, J., 2016. Increasing the sustainability of alkali-activated binders: The use of sugar cane straw ash (SCSA). Constr. Build. Mater. 124, 148–154. https://doi.org/10.1016/j.conbuildmat.2016.07.090

Nair. N.G, Markham, J., n.d. Recycling Solid Waste from the Olive Oil Extraction, Rural Industries Research and Development Corporation – Australian Government, 2008 [WWW Document]. URL https://agrifutures.infoservices.com.au/downloads/08-16

Pacheco-Torgal, F., Labrincha, J.A., Leonelli, C., Palomo, A., Chindaprasirt, P., 2014. Handbook of Alkali-Activated Cements, Mortars and Concretes. Elsevier. https://doi.org/https://doi.org/10.1016/C2013-0-16511-7

Palomo, A., Krivenko, P., Garcia-Lodeiro, I., Kavalerova, E., Maltseva, O., Fernández-Jiménez, A., 2014. A review on alkaline activation: new analytical perspectives. Mater. Construcción 64, e022. https://doi.org/10.3989/mc.2014.00314

Pelisser, F., Guerrino, E.L., Menger, M., Michel, M.D., Labrincha, J.A., 2013. Micromechanical characterization of metakaolin-based geopolymers. Constr. Build. Mater. 49, 547–553. https://doi.org/10.1016/j.conbuildmat.2013.08.081

Peys, A., Rahier, H., Pontikes, Y., 2016. Potassium-rich biomass ashes as activators in metakaolin-based inorganic polymers. Appl. Clay Sci. 119,

401–409. https://doi.org/10.1016/j.clay.2015.11.003

Rattanasak, U., Chindaprasirt, P., 2009. Influence of NaOH solution on the synthesis of fly ash geopolymer. Miner. Eng. 22, 1073–1078. https://doi.org/https://doi.org/10.1016/j.mineng.2009.03.022

Reig, L., Tashima, M.M., Borrachero, M. V, Monzó, J., Cheeseman, C.R., Payá, J., 2013. Properties and microstructure of alkali-activated red clay brick waste. Constr. Build. Mater. 43, 98–106. https://doi.org/https://doi.org/10.1016/j.conbuildmat.2013.01.031

Rivera, O.G., Long, W.R., Weiss, C.A., Moser, R.D., Williams, B.A., Torres-Cancel, K., Gore, E.R., Allison, P.G., 2016. Effect of elevated temperature on alkali-activated geopolymeric binders compared to portland cement-based binders. Cem. Concr. Res. 90, 43–51. https://doi.org/10.1016/j.cemconres.2016.09.013

Roig, A., Cayuela, M.L., Sánchez-Monedero, M.A., 2006. An overview on olive mill wastes and their valorisation methods. Waste Manag. 26, 960–969. https://doi.org/https://doi.org/10.1016/j.wasman.2005.07.024

Romero, E., Quirantes, M., Nogales, R., 2017. Characterization of biomass ashes produced at different temperatures from olive-oil-industry and greenhouse vegetable wastes. Fuel 208, 1–9. https://doi.org/https://doi.org/10.1016/j.fuel.2017.06.133

Santa, R.A.A.B., Bernardin, A.M., Riella, H.G., Kuhnen, N.C., 2013. Geopolymer synthetized from bottom coal ash and calcined paper sludge. J. Clean. Prod. 57, 302–307. https://doi.org/https://doi.org/10.1016/j.jclepro.2013.05.017

Tashima, M.M., Akasaki, J.L., Castaldelli, V.N., Soriano, L., Monzó, J., Payá, J., Borrachero, M. V., 2012. New geopolymeric binder based on fluid catalytic cracking catalyst residue (FCC). Mater. Lett. 80, 50–52. https://doi.org/10.1016/j.matlet.2012.04.051

Temuujin, J., van Riessen, A., MacKenzie, K.J.D., 2010. Preparation and characterisation of fly ash based geopolymer mortars. Constr. Build. Mater. 24, 1906–1910. https://doi.org/https://doi.org/10.1016/j.conbuildmat.2010.04.012

Turner, L.K., Collins, F.G., 2013. Carbon dioxide equivalent (CO2-e) emissions: A comparison between geopolymer and OPC cement concrete. Constr. Build. Mater. 43, 125–130. https://doi.org/10.1016/j.conbuildmat.2013.01.023

Vamvuka, D., Zografos, D., 2004. Predicting the behaviour of ash from agricultural wastes during combustion. Fuel 83, 2051–2057.

https://doi.org/https://doi.org/10.1016/j.fuel.2004.04.012

Vassilev, S. V., Baxter, D., Andersen, L.K., Vassileva, C.G., 2010. An overview of the chemical composition of biomass. Fuel 89, 913–933. https://doi.org/10.1016/j.fuel.2009.10.022

Vlyssides, A.G., Loizides, M., Karlis, P.K., 2004. Integrated strategic approach for reusing olive oil extraction by-products. J. Clean. Prod. 12, 603–611. https://doi.org/https://doi.org/10.1016/S0959-6526(03)00078-7

ix. Design and properties of 100% waste-based ternary alkali-activated mortars: blast furnace slag, olive-stone biomass ash and rice husk ash.

AUTORES: Alba Font, Lourdes Soriano, Sayonara María de Moraes Pinheiro, Mauro M. Tashima, José Monzó, María Victoria Borrachero, Jordi Payá

REFERENCIA DE LA PUBLICACIÓN: Journal of Cleaner Production 243 (2020) 118568
DOI: https://doi.org/10.1016/j.jclepro.2019.118568

Factor de impacto/Cuartil (2018): 6.395/Q1	**Citas (excluyendo auto citas): -**

OBJETIVOS PARCIALES ABORDADOS

MATERIALES	FABRICACIÓN
• **TAAM:** BFS + OBA (15-25% Ad) + RHA + H_2O • **TAAM:** BFS + OBA (20%Ad/20%Rp) + RHA + H_2O	• **CURADO:** TB, TA y CM • **Amasado con:** NM

PROCEDIMIENTO EXPERIMENTAL

CARACTERIZACIÓN DE MATERIAS PRIMAS	CARACTERIZACIÓN DE ESPECÍMENES
-	• Resistencia a la compresión (Rc) • Resistencia a la flexión (Rf) • TGA • FESEM Y EDS • XRD • MIP

RESULTADOS Y CONCLUSIONES MÁS RELEVANTES DE LA INVESTIGACIÓN

- La combinación de la RHA como fuente de sílice con la OBA como fuente de potasio para la activación alcalina de BFS mejoró notablemente los resultados respecto a los sistemas binarios previamente estudiados (los BAAM).
- Los TAAM en los que la relación OBA/BFS se modifica manteniendo constante la dosificación de RHA evolucionaron mecánicamente en función del porcentaje de OBA adicionado:

Material	Rc (MPa)	Rf (MPa)
	7días-TB	
BFS/OBA(15% Ad)/RHA + H_2O	38.1	7.2
BFS/OBA(20% Ad)/RHA + H_2O	52.6	8.5
BFS/OBA(25% Ad)/RHA + H_2O	58.4	9.2

- Respecto a las condiciones de curado, se observó una rápida reacción en TB, mientras que a TA la formación de geles y de una matriz estable se prolonga en el tiempo. Con el CM no se observan ventajas.

Material	Rc (MPa)	Rf (MPa)
BFS/OBA(20% Ad)/RHA + H_2O - TB	52.6	8.5
BFS/OBA(20% Ad)/RHA + H_2O - TA	26.9	3.8
BFS/OBA(20% Ad)/RHA+ H_2O - CM	28.3	5.7

- Los TAAM en los que la OBA se incluye como adición y sustitución (**BFS/OBA (20%Ad/20%Rp)/RHA + H_2O**) resultaron con muy buen rendimiento. En ellos se optimizó el efecto químico y mecánico de la OBA en las matrices cementicias. Se obtuvo resultados mecánicos de **46 MPa a los 28 días y 67 MPa a los 90 días** de curado a TA.

Abstract: Alkali-activated cements (AACs) technology is being widely investigated as a replacement for ordinary Portland cement (OPC) for environmental benefits. Blast furnace slag (BFS) is one of the most well-known precursors used in AACs, having comparable properties to those of traditional OPC-based materials. AACs require alkali solutions, which are commonly based on a combination of sodium or potassium hydroxides with sodium or potassium silicates in high concentration. These alkali solutions represent the use of chemical reagents, and thus can have major environmental, health and economic impacts. Olive-stone (also known as olive pits) biomass ash (OBA) is a residue mainly composed of calcium and potassium oxides. Rice husk ash (RHA) is a rich silica residue from the combustion of rice husk. The combination of both residues can produce a good activating reagent for BFS-based AACs. In the present work, 100% waste-based ternary alkali-activated mortars (TAAM) based on BFS activated by OBA and RHA were developed. The mortars were assessed in terms of their dosage, curing treatment and time evolution. Finally, an eco-friendly 100% waste-based TAAM with 67.39 ± 0.44 MPa after 90 days of curing at 20ºC is obtained and a complete microstructural characterization shows a dense and compact matrix with binding gel products labelled as C(K)-S(A)-H and C(K)-S-H.

Keywords: Alkali-activated cement, blast furnace slag, olive-stone biomass ash, rice husk ash, ternary binder.

Abbreviations:
AACs: Alkali-activated cements
BAAMs: Binary alkali-activated mortars
TAAMs: Ternary alkali-activated mortars
TAAPs: Ternary alkali-activated cements
BFS: Blast furnace slag
OBA: Olive-stone biomass ash
RHA: Rice husk ash

HIGHLIGHTS:

- 100 % waste-based ternary alkali-activated mortars were successfully developed.
- Blast furnace slag (BFS) was activated by means a mixture of biomass derived ashes.
- Biomass derived ashes (from Olive-stone, OBA, and from rice husk ash, RHA) were employed.
- The ternary BFS/OBA/RHA systems yielded mortars with strength in the range 40 – 70 MPa.

1. Introduction

The relationship between climate change and human activity is evident. In the last century, global warming has been the reason for great natural catastrophes. Greenhouse gas emissions, especially from burning fossil fuels, are the main causes of this global warming.

The cement industry is responsible for 5–8% of the anthropogenic CO_2 emissions around the world (Andrew, 2018; Turner and Collins, 2013) and, according to some estimates, it could reach 12–23% in 2050 ("World busines council for sustainable development," n.d.). The use of alternative fuels, biomass and supplementary materials in the construction industry does not seem sufficient to reduce the CO_2 emissions: thus, taking into account the binder content and the associated CO_2 emissions of concrete respect to developed strength, Yang et al (2015) concluded that the value of the CO_2 emission intensity decreased strongly when the replacement level of clinker by supplementary cementing materials was increased up to 15–20%, and higher replacement values represented a large decrease on compressive strength beyond decreased CO_2 emission intensity. Hence, studies and investigations focusing on new ecological and sustainable materials are crucial to reduce environmental problems associated with this massive industry.

Nowadays, one of the great challenges in the construction industry focuses on the use of alkali-activated cements (AACs) or geopolymers. These binders can be produced without Portland cement. They are composed of two main components: an aluminosilicate material (named "precursor", usually derived from waste materials) and an alkaline activating solution (Shirley and Black, 2011). The alkaline activating solution (usually composed of alkali hydroxides, such as NaOH or KOH, and alkali silicates) allows the dissolution of the precursor and its subsequent polymerization in order to form the different structures responsible for the mechanical AACs performance.

According to the literature, the CO_2 emissions associated with the AACs production can be 55–75% lower than those obtained for Portland cement. Most of these emissions are produced by the activating solution, especially when sodium or potassium silicates are employed. Concretely, the 70–90% of total emissions from AACs production are associated to the activating solution (Mellado et al., 2014; Passuello et al., 2017; Yang et al., 2013).

For this reason, the replacement of commercial products by environmentally friendly activating solutions could achieve a significant reduction in the CO_2 emissions associated with AACs. In recent years, researchers have been making efforts to replace synthetic (commercial chemicals) alkaline silicates by alternative silica sources. In such case, the alkaline solution is composed of NaOH/KOH solution and an amorphous silica source. The main silica sources are rice husk ash (RHA), diatomaceous earth residues (DE), glass waste, sugar cane straw ash (SCSA) and silica fume (SF), among others (Font et al., 2018; Payá et al., 2017).

Several studies have been reported on the use of rice husk ash (RHA) as a source of silica (Bernal et al., 2015; Bouzón et al., 2014; Mejía et al., 2013). Bouzón et al. (2014) prepared mixtures of RHA, water and sodium hydroxide and they applied a reflux process (between 15 and 240 minutes) to achieve the alternative activating solution. The activation of the fluid catalytic cracking catalyst residue (FCC) with this alternative solution achieved mortars with 41 MPa compressive strength in only one day of curing at 65ºC. These values resulted similar than the obtained by the control FCC samples activated with an equivalent mixture of NaOH and waterglass.

Mejía et al. (2016) studied two alternative sources of silica (RHA and DE) in metakaolin/fly ash (MK/FA) mixtures and they demonstrated that the strength of systems with the alternative silicate achieved 50% lower compressive strength than the commercial sodium silicate.

Torres-Carrasco and Puertas (2015) described a similar preparation to obtain the activating solution. They mixed waste glass and NaOH for 6 hours at 80 ± 2 ° C and then the mixture was filtered. The filtered activating reagent was combined in different proportions with fly ash (FA) as precursor. The solutions based on NaOH 10M + waterglass and NaOH 10M + waste glass were compared: mortars activated with the alternative alkali solution system yielded, after 28 days of curing, similar compressive strength than in the case where commercial waterglass was employed.

Tchakouté et al. (2016) studied MK geopolymers with different activating systems by reacting NaOH with RHA or waste glass. They prepared the activator at 100ºC for 2 hours. After this time, the dissolution was filtered and the liquid was stored for one week before use. The presence of calcium in the sodium silicate derived from waste glass enhances the depolymerization of metakaolin particles and the results are slightly better than those obtained using sodium silicate from RHA.

Sugar cane straw ash (SCSA) can also be used as a silica source. Moraes et al. (2018) prepared different activating solutions by means of a thermal bottle and fabricated mortars using blast furnace slag as precursor. The authors analysed the influence of the time of reaction inside the thermal bottle and the influence of the SiO_2/Na_2O ratio (ε). The results demonstrated that the compressive strength values obtained were similar to those reached for RHA and less than the mixtures with the commercial reagent.

In the last few years, greener alternative alkaline activators have been investigated. In these cases, a total absence of commercial chemical reagents is achieved. Two types of activators have been reported: materials from industrial processes and those from agro-industrial processes. The wastes from industrial processes are rich in sodium compounds and the agro-industrial wastes usually contain potassium compounds. One example of industrial waste is Bayer liquor, which is produced form industrial manufacture of alumina in the Bayer process. Van Riessen et al. (2013) used this waste in mixtures with FA, and concluded that the mortars with this waste

had similar strength to the reference mortar. Hu et al. (2018) investigated the use of red mud, another toxic residue from the Bayer process, as a partial precursor in fly ash geopolymers activated with sodium hydroxide and sodium silicate. The authors concluded that the high alkalinity of the red mud improve the geopolymerization but additional NaOH and waterglass was needed to achieve optimum compressive strength development. Recently, the reusing of red mud after their use in a flue gas desulfurization process (FGD) (Nie et al., 2019) as alternative activator was investigated. The activation of class C fly ash based mortars was assessed obtaining 30.3 MPa when the sulphate rich red mud (RMD) was employed as alkali source. With the use of RMD, 25% increase in strength was obtained compared to the geopolymer prepared with the original red mud. Another waste studied is the caustic solution waste from the industrial cleaning process of aluminium. This residue was used as activator in mixtures with FA (Fernández-Jiménez et al., 2017; Shirley and Black, 2011): a compressive strength similar to that obtained by mixtures activated with 8M NaOH was achieved.

Cheah et al. (2015) studied a high calcium wood ash (HCWA) obtained from the use of wood ash biomass. The resulting ash had CaO as a principal oxide (61%) and a smaller proportion of K_2O (12%). Different ratios of HCWA/FA were prepared and mixed with water. The mixtures achieved near to 18 MPa and the main reaction product was a potassium aluminosilicate hydrate (K-A-S-H) gel. Other hydration products formed in this reaction were tobermorite and hydrated gehlenite.

In the group of agro-industrial wastes, different biomass ashes were studied. Peys et al. (2016) studied rich potassium biomass ashes. The authors prepared geopolymers with metakaolin (MK) as precursor and biomass ashes as alkaline activator. Maize salt and maize cob ashes reached around pH=13 after mixing with water and yielded the best mechanical behaviour (30 MPa) after 2 days of curing at 80ºC.

Recently, Font et al. (2017) employed olive-stone (also known as olive pits) biomass ash (OBA) in mixtures with blast furnace slag (BFS) and compared these with mixtures with only water and with a 4M KOH solution. After 3 and 7 days of curing at 65ºC, the mixtures with OBA showed the best mechanical behaviour. At 7 days of curing, the mortar with OBA yielded a compressive strength of 30 MPa. The study of OBA as activator was extended with more percentages of substitution/addition in mortars with BFS by de Moraes Pinheiro et al. (2018). The mortars with the replacement of BFS by OBA yielded more than 20% higher compressive strength than the BFS-KOH systems. A compressive strength of 38 MPa was achieved when OBA was used as mineral addition (25%) for a BFS AAC system. The authors reported a comparison of OBA and Kephalite (inert mineral addition) in order to distinguish the filler effect versus the chemical reaction of geopolymerization. The study concluded that the filler effect due the presence of OBA was negligible in terms of the mechanical behaviour.

In the present work, new 100% waste-based ternary alkali-activated mortars (TAAMs) are designed and investigated, where no commercial reagents need to be employed. An alternative potassium silicate solution based on a mixture of olive-stone biomass ash (OBA), rice husk ash (RHA) and water is developed for blast furnace slag (BFS) activation and the mechanical and microstructural properties of these alkali-activated materials are assessed.

2. Experimental procedure

2.1. Materials

The raw materials used in this work were an industrial by-product, blast furnace slag (BFS), and two agro-industrial residues: olive-stone (or olive pits) biomass ash (OBA) and rice husk ash (RHA).

BFS was used as a precursor in all mixtures. It was supplied by Cementval (Puerto de Sagunto, Valencia, Spain) and it has a 26.0 μm mean particle diameter (D[4,3]) and 17.3 μm median particle diameter (D50) after being ground in a ball mill. The olive stone biomass ash (OBA) was supplied by Almazara Candela (olive-oil company, Elche, Spain), where the resulting ash from the olive- stone combustion was collected from the bottom of the furnace. For employing the OBA in the alkali-activated system, it was necessary to grind it in a ball mill, resulting in a powder with a D[4,3] = 27.3 μm and D50 = 20.8μm (de Moraes Pinheiro et al., 2018). The rice husk ash (RHA) was supplied by DACSA S.A. (Tabernes Blanques, Spain). For the use of this ash as an alternative silica source in the activating solution, it was ground in a ball mill, resulting in a D[4,3] = 20.3 μm and D50 = 10.5μm.

The chemical compositions (XRF) of these three raw materials are summarized in **Table 4.ix.1** (Bouzón et al., 2014; de Moraes Pinheiro et al., 2018). The BFS is mainly composed of calcium oxide (40.15%) and silica (30.53%). The chemical analysis corroborated the alkaline nature of OBA, potassium (32.12%) and calcium (27.77%) oxides being the main components. Finally, for RHA it can be seen that the main composition is silica (85.58%).

Table 4.ix.1
Chemical composition (XRF) of the raw materials.

Material	Oxide composition (wt%)										
	SiO_2	CaO	Al_2O_3	Fe_2O_3	Na_2O	MgO	K_2O	P_2O_5	SO_3	Others	LOI*
BFS	30.53	40.15	10.55	1.29	0.87	7.43	0.57	0.26	1.93	0.89	5.53
OBA	5.33	27.77	0.70	3.45	0.78	5.13	32.12	2.68	1.67	0.95	18.90
RHA	85.58	1.83	0.25	0.21	-	0.50	3.39	0.67	0.26	0.32	6.99

*Loss on ignition

2.2. Methods

The methodology applied for ternary systems (TAAMs) composed of BFS/OBA/RHA comprised the analysis of the mechanical properties and microstructural characteristics obtained in mortars and pastes. It is well known that the mechanical behaviour of alkali-activated BFS depends on the

slag specific surface, curing temperature, activator concentration, and the nature of the alkaline activator (Wang et al., 1995). Thus, the study is divided into two main steps with two sub-studies for each step.

The amount of RHA was constant in the two steps (step 1 and step 2) and the difference between steps was the OBA/BFS mass ratio: i) in step 1, the OBA was used as addition (A) with respect to the precursor (OBA addition system); and ii) in step 2, the OBA was used as both an addition (A) and a replacement (R) with respect to the precursor (OBA addition plus replacement system).

The samples of TAAMs in step 1 were assessed in terms of their OBA addition content (sub-study 1.1) and curing temperature (sub-study 1.2). The TAAMs developed in step 2 were assessed in terms of the curing process (sub-study 2.1) and curing time (sub-study 2.2). The samples are named as follows:

- Sub-study 1.1: xA-B, where "x" is the % of OBA addition ("A") in mass respect the BFS. "B" is referring to the curing treatment (B – 65ºC,).
- Sub-study 1.2: 20A-y, where "y" is the curing treatment (B – 65ºC; C – 20ºC/100% RH; and M = 24h B + 6d C).
- Sub-study 2.1: 20A/20R-y, where OBA is used as addition (A) and replacement material (R) and "y" is the curing treatment as the previous step (sub-study 1.2).
- Sub-study 2.2: 20A/20R-Cz, where all samples were cured at room temperature (C – 20ºC/100% RH) and z is the test time evaluation (3, 7, 28, 60 and 90 days).

The designed mixes and the acronyms employed are summarized in **Table 4.ix.2**.

The alkaline solutions were prepared 24 hours before the preparation of mortars, by means of sealed plastic bottles to improve the dissolution rate of the particles of both ashes. The corresponding OBA quantity (addition or addition/replacement) was dry mixed with RHA followed by the addition of water. The plastic bottles were sealed with a cap and kept in a thermal bath (65ºC). For the first 6 hours, the bottles were manually shaken for one minute per hour, and were then left without agitation until the mortar was prepared. After this, the water suspensions were left at room temperature for one hour. Manufacture of the mortars consisted of mixing the precursor (BFS) with the corresponding activating solution for 60 seconds, and then addition of the sand to the obtained paste and stirring of the mixture for 180 seconds.

Table 4.ix.2
TAAMs designed and studied distributed in each work step, with dosages by mass.

		Sample	Alkaline activator			Precursor	Precursor /sand
			H_2O (g)	OBA (g)	RHA (g)	BFS (g)	
Step 1	Sub-study 1.1	15A-B		67.5			
		20A-B		90.0			
		25A-B		112.5		450.0	1/3
	Sub-study 1.2	20A-B					
		20A-C		90.0			
		20A-M					
Step 2	Sub-study 2.1	20A/20R-B	202.5		40.0		
		20A/20R-C					
		20A/20R-M					
	Sub-study 2.2	20A/20R-C3		180.0		360.0	1/3.75
		20A/20R-C7					
		20A/20R-C28					
		20A/20R-C60					
		20A/20R-C90					

The fresh mixtures were moulded and vibrated in three prismatic samples with dimensions of 40x40x160 mm^3, and the following sequence was carried out, depending on the curing treatment:

- B: mix, stored for 24 hours at 65ºC, demolded and stored at 65ºC until the corresponding age of mechanical test.
- C: mix, stored for 48 hours at 20ºC/100% RH, demolded and stored at 20ºC/100% RH until age of mechanical test.
- M: mix, stored for 24 hours at 65ºC, demolded and stored at 20ºC/100% RH until age of mechanical test.

For the sub-studies 1.1, 1.2 and 2.1 the curing time was 7 days, and for the sub-study 2.2 the samples were tested after 3, 7, 28, 60 and 90 days.

Three values for the flexural strength (R_f) and six values for the compressive strength (R_c) were obtained according to UNE 196-1 for each mixture.

A microstructural study was carried out after 28 days of curing of the TAAMs in sub-study 2.2 (20A/20R-C28 sample) using field emission scanning electron microscopy (FESEM) and mercury intrusion porosimetry (MIP) techniques. Finally, equivalent pastes (TAAPs) were tested by thermogravimetric analysis (TGA), powder X-ray diffraction (XRD), FESEM and MIP. TGA was carried out by means of a TGA850 Mettler Toledo thermobalance instrument in N_2 atmosphere (75 mL·min^{-1} gas flow), with temperature range 35–500ºC and heating rate 10ºC·min^{-1}. For testing, samples of dry paste powder (heated for 30 min at 65ºC) were placed in aluminium crucibles with sealed lids, which had a micro-hole. The mass loss and derivative curves (DTG) were obtained from the thermogravimetric curves (TG). The XRD patterns were acquired by a Bruker AXS D8 Advanced with 40 kV, 20 mA and Bragg's angle (2θ) in the 5–70º ranges. To take the FESEM images, a ZEISS Supra 55 was used, with the samples coated with carbon. An extra high tension of 20 kV and 6–8 mm of working distance were selected for the energy dispersive X-ray spectroscopy (EDS). The MIP test was carried out by means of an AutoPore IV 9500 from

Micrometrics Instrument Corporation that measured pores in the 91.26 µm to 5.5 nm range.

3. Results and discussion

3.1. Step 1: OBA addition systems

3.1.1. Sub-study 1.1: Effect of OBA addition content

Three TAAMs (BFS+RHA+OBA) were prepared using different percentages of OBA addition (15, 20 and 25% by mass of BFS). The specimens were cured at 65°C for 7 days (B curing method). As can be seen in **Fig.4.ix.1.a**, the specimens yielded compressive strength values that increased with the OBA percentage addition, from 15% to 25%. The mechanical behaviour for the 20A-B (20% addition) sample was 38% better than the 15A-B sample. When the percentage of OBA addition was incremented by 5% (25A-B), the compressive strength increased by only 11%. The flexural strength was 7.2 ± 0.1 MPa for 15A-B, 8.5 ± 0.2 MPa for 20A-B, and 9.2 ± 0.1 MPa for 25A-B. These values represent a progressive increment of 18% and 8%, respectively.

In a previous work, binary alkali-activated mortars (BAAMs) of BFS activated by only OBA addition were investigated and compressive strength values of 21.5 ± 0.6, 34.7 ± 1.5 and 38.4 ± 1.3 MPa for 15%, 20% and 25% respectively of OBA addition were obtained after 7 days of curing at 65°C (de Moraes Pinheiro et al., 2018). With respect to these results, in the present work, with RHA as the silica source in the activating solution, the compressive strength increased by 77.5% in the 15% OBA addition samples, 51% in the 20% OBA addition samples and 52% in the 25% OBA addition samples. The use of RHA combined with OBA allows the dissolution of silica from the RHA, and the activation of BFS is more effective than with only OBA. The combination of 15% OBA with RHA (15A-B samples) yielded the same mechanical mortar behaviour as when only 25% OBA addition was employed (38.1 ± 0.2 MPa in TAAM with 15% OBA and 38.4 ± 1.3 MPa in BAAM) by using the same curing treatment (7 days at 65°C).

Additionally, by comparison with the mechanical results for the binary systems obtained by de Moraes Pinheiro et al. (2018), the BAAM samples presented an increment of 61% and 10% with the 5% progressive increment of OBA addition (from 15 to 25%). The ternary samples produced in this work yielded a similar increment in the mechanical development, maintaining a constant amount of RHA, which revealed that the amount of potassium from OBA has a great influence on the BFS activated system. This behaviour could be attributed to the silica solubilisation from RHA, which is enhanced with increment of the OBA addition.

In general, the specimens in sub-study 1.1 (15A-B, 20A-B and 25A-B samples) have a very good mechanical behaviour, surpassing strengths reported for BAAMs (de Moraes Pinheiro et al. (2018). It is notable that the mechanical evolution from the 15% to 20% addition was higher than from the 20% to 25%

addition. Potassium solubilisation from OBA is more difficult as the amount of OBA increases for a fixed quantity of water. 20% OBA addition is suggested as the optimal for the TAAM system. Additionally, when 25% of OBA was employed, some difficulty was found with compacting because of poor workability. In this respect, with 5% OBA or less, the 20A-B sample yielded good characteristics in the fresh state.

3.1.2. Sub-study 1.2: Effect of curing temperature

The aim of sub-study 1.2 was to assess the effect of the curing temperature in the TAAMs previously selected (20A-B system). The curing temperature is an important factor for both BFS alkali-activated products formation and the physical and microstructural properties of the resultant materials (Fernández-Jiménez et al., 1999). The use of a high calcium precursor, such as BFS, allows a stable matrix at lower curing temperatures than the low calcium precursors (silica-alumina based precursor) (Lee and Lee, 2013).

As can be seen in **Fig.4.ix.1.b**, at a 65ºC curing temperature (curing method B) a higher compressive strength was reached after 7 days of curing (52.6 ± 0.4 MPa for the 20A-B sample). With the same percentage of OBA addition, when the curing treatment was carried out at 20ºC with 100% RH (curing method C, 20A-C sample), the mechanical behaviour result was 49% lower than the one observed for 20A-B. The same behaviour was observed for the flexural strength, which yielded 8.5 ± 0.2 MPa for samples cured for 7 days at 65ºC (20A-B systems) and 3.8 ± 0.3 MPa for the samples cured at 20ºC (20A-C systems). These results suggested a lower reaction rate in the short term due to the low curing temperature. The BFS activation with OBA/RHA requires a high curing temperature for fast binding gel formation with a consequent increase in strength.

The 20A-M sample (mixed curing method: 24 hours at 65ºC and 6 days at 20ºC) achieved similar mechanical behaviour to the 20A-C, reaching 2 MPa more in compressive strength when a previous 24 h treatment at 65ºC was applied (26.9 ± 0.3 MPa for 20A-C sample and 28.3 ± 0.9 MPa for 20A-M sample) and the same growth of 2 MPa for flexural strength (3.8 ± 0.3 MPa for 20A-C sample and 5.7 ± 0.9 MPa for 20A-M sample). This behaviour suggested that for good development of the binding structure, longer curing periods will be required or alternatively a high curing temperature should be used.

In a previous work reported, in which OBA was used as a potassium source, three systems were compared: BFA/H_2O, BFS/KOH (4 molar in KOH) and BFS/OBA (18% addition) (Font et al., 2017). The samples were cured at 65ºC, yielding after 3/7 days compressive strengths of 6.9 MPa/7.0 MPa, 12.7 MPa/16.9 MPa and 20.6 MPa/29.9 MPa, respectively. With the addition of just 2% more OBA and its combination with RHA for BFS activation, a significant strength increase was reached with the same curing treatment (20A-B sample).

The authors who developed alkali-activated systems with a total replacement of commercial chemical reagent obtained the following conclusions: i) Peys et al. (2016) prepared maize cob ash/MK alkali-activated systems, obtaining 30 MPa after 2 days of curing at 80ºC; ii) Van Riessen et al. (2013) used Bayer liquor for FA activation and after a mixed curing treatment (24 h at 70ºC and 27 days at room temperature) the systems yielded 43 MPa; and iii) Cheah et al. (2015) developed FA alkali-activated mortars by using wood ash (HCWA) which yielded 18 MPa after 90 days at 28ºC.

Compared with these reports, the proposed TAAMs cured at room temperature (20A-C samples) have competitive mechanical performance: the strength was lower than that obtained after curing at 65ºC (method B). However, we assume a very good behaviour when a green material is trying to develop, avoiding the high temperature treatment (curing) which has high-energy consumptions and environmental impacts.

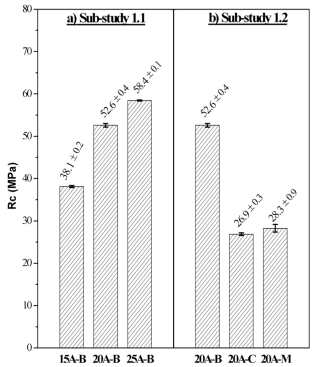

Fig.4.ix.1 *Compressive strength of mortars for Step 1 after 7 days of curing: a) sub-study 1.1 (B method: curing at 65ºC); b) sub-study 1.2 (curing in different conditions; B: curing at 65ºC; C: curing at 20ºC/100% RH; and M : curing 24h method "B" + 6days method "C").*

3.2. Step 2: OBA addition plus replacement systems

In order to increase the reactivity of the system, a second study (Step 2) was proposed: in this case, the OBA/BFS ratio was changed, maintaining a constant amount of RHA (see **Table 4.ix.2**). In the previous study (Step 1, sub-study 1.2: OBA addition) the OBA/BFS ratio was 20/100, because OBA was added as 20% by mass of BFS. In this section, an additional part of the BFS was replaced (20% by mass), the OBA/BFS ratio thus being equal to 40/80. With this proposal, an increase in the alkalinity was achieved in order to enhance the solubilisation of the RHA and the reaction rate of the hydration process.

3.2.1. Sub-study 2.1: Effect of curing temperature

In this sub-study, the comparison was based on the effect of the curing temperature of the samples: methods B (65ºC, 7 days), C (20ºC, 7 days) and M (65ºC, 24 hours plus 20ºC 6 days).

The mechanical behaviour of the specimens is shown in **Fig.4.ix.2.**

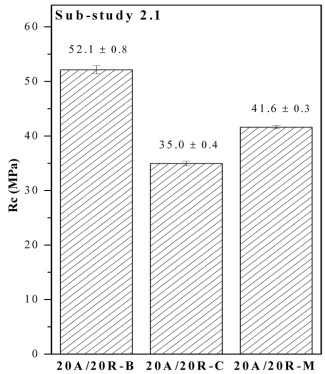

Fig.4.ix.2 *Compressive strength of mortars developed in step 2: sub-study 2.1 specimens after 7 days of curing and different curing conditions.(Method B: curing at 65ºC; Method C: curing at 20ºC/100% RH; and Method M : curing 24h method "B" + 6days method "C").*

The samples cured in the thermal bath at 65ºC for 7 days (20A/20R-B sample) yielded 52.1 ± 0.8 MPa of compressive strength after 7 days and, compared with the 20A-B sample (from the previous sub-study 1.2), no significant difference is observed (20A-B yielded 52.6 ± 0.4 MPa). These 20A/20R-B systems achieved 5.1 ± 0.1 MPa of flexural strength (3 MPa less than the 20A-B sample). The potassium increment from the OBA in the specimens does not have a relevant effect on the mechanical strength development when the high-temperature curing treatment is employed.

On the other hand, the mortar cured at 20ºC (20A/20R-C sample) yielded 35.0 ± 0.4 MPa of compressive strength, 23% higher with respect to the system with OBA addition (20A-C sample). This enhancement in strength is achieved with low BFS content in the mix and the better behaviour observed for the 20A/20R-C sample is attributed to the greater ability to dissolve silica from the RHA due to the higher alkalinity of the medium with respect to the 20A-C system. Qureshi and Ghosh (2013) affirmed that the compressive strength in blast furnace slag pastes cured at room temperature increases from 3 to 28 days with the increase in alkali content (%K_2O) from 4% to 8%, while keeping the water to slag ratio and silica content constant. However, the authors found a compressive strength reduction after 28 days when the K_2O percentage increased from 8% to 10%. The value of flexural strength obtained for this system was 4.6 ± 0.6 MPa, which represents an increment of 1 MPa compared with the OBA addition systems (20A-C).

Finally, for the 20A/20R-M sample, when a combined curing method was carried out (24 hours at 65°C and 6 days at 20°C), the compressive strength was 41.6 ± 0.3 MPa, representing an increase of 45% compared with the OBA addition sample (20A-M sample). This behaviour demonstrated that the increase in the alkalinity has an important role in the development of strength at an early age, causing an important production of cementing phase. In the case of the flexural strength, for the 20A/20R-M systems this was slightly lower than that obtained for the 20A-M sample, yielding 1.2 MPa less (4.6 ± 0.6 MPa for the 20A/20R-M).

As previously discussed in sub-study 1.2, a lower reaction rate of the geopolymerization process and the formation of the amorphous binding gel are probably influenced by the low temperature (20°C) of the curing treatment during the early ages of the specimens. In these proposed addition/replacement series, higher silica dissolution from the RHA is possible with increase of the potassium content from the OBA.

3.2.2. Sub-study 2.2: Time evolution of strength of mortars cured at 20°C

In the last study of the TAAM system, the time evolution of the samples cured at 20°C/ 100% RH was assessed. The mechanical tests were carried out for the mortars after 3, 7, 28, 60 and 90 days.

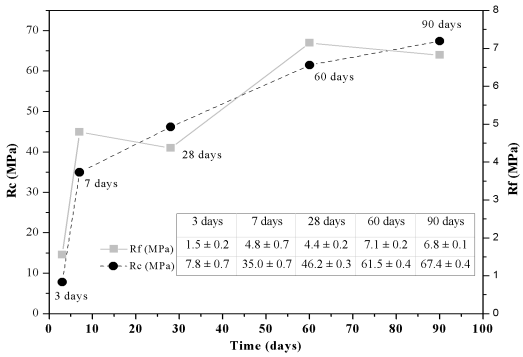

Fig.4.ix.3. *Flexural (R_f) and compressive (R_c) strength development of mortars cured at 20°C (Step 2: sub-study 2.2 specimens).*

As can be seen in **Fig.4.ix.3**, an evident progressive increase in compressive strength from 7.8 ± 0.7 MPa to 67.4 ± 0.4 MPa was developed by the ternary system samples between 3 and 90 days respectively (approximately nine times more in strength). When geopolymers are cured at room temperature conditions, in the early curing time the precursor particles start to slowly dissolve into the activating solution. As the dissolution continues, the dissolved precursor species rearrange themselves and gradually polymerize. Consequently, by this curing treatment, the time to present a large geopolymerization is extended. Recently, Pereira et al. (2015) presented an

evolution from 5.7 MPa to 46.2 MPa in compressive strength for 3 to 90 curing days in mortars based on BFS activated by KOH 8M alkali solution. The same strength evolution over time is observed when alternative alkali solutions are investigated: Luukkonen et al. (2018) presented BFS binders activated by RHA as the silica source and NaOH, obtaining a compressive strength evolution from 18 MPa at 3 days to 39/40 MPa at 90 days. BFS mortars activated by microsilica/NaOH activating solution presented a similar behaviour.

The change in the flexural strength between 3 to 90 days was 5.3 MPa. After 7 days of curing 4.8 ± 0.7 MPa were achieved. These values are slightly lower than the values obtained by de Moraes Pinheiro et al. (2018) in the BAAM (BFS activated with 20% OBA addition systems), which yielded 6.8 ± 0.6 MPa after 7 days of curing. Therefore, the value obtained in the present investigation for the TAAM was higher than those obtained by these authors in the control systems of BFS activated with KOH in 4 and 8 molar ratios (3.4 ± 0.2 MPa and 3.7 ± 0.5 MPa respectively after 7 days of curing).

From the results of the present investigation, it is possible to confirm the effectiveness of the BFS activation by using OBA (in the addition plus replacement combination) and RHA, in room temperature conditions with the curing time. The strength reached (67.4 MPa) at 90 days at 20ºC was significantly higher than that for more extreme conditions (65ºC for 7 days, 52.1 MPa), which suggested that the development of binding gel is much more effective in mild conditions. In order to confirm this point, 20A/20R-B sample was cured (three prismatic specimens) in a thermal bath at 65ºC for 14 days, finding that the compressive strength did not vary respect to 7 days curing time (49.8±1.2 MPa vs 52.1±0.8 MPa). The high-temperature curing treatment reached a limit with fast gel formation, but with the low-temperature treatment a better strength contribution of the formed gel can be observed. With the curing time, at room temperature conditions, evolution of the reaction will favour the condensation of silicates and the gel formation in the TAAM matrix and a stable material will form. This behaviour suggested that the development for long-curing ages was very favourable when room curing is carried out.

In this work it may be highlighted that after 28 days the mechanical behaviour was similar to that obtained for the TAAM cured at high temperature after 7 days in the previous sub-study 2.1 (20A/20R-B sample). Furthermore, for 20A/20R-C28 specimens the strength was 46.2 ± 0.3 MPa, a higher result than that obtained for the same curing time in previous investigations where KOH was employed as the alkaline activator and the samples required a pre-curing treatment at high temperature. Thus, Tippayasam et al. (2016) recently presented metakaolin-based geopolymers activated by 10M KOH and a K_2SiO_3/KOH mass ratio of 1.5 that yielded 30.3 MPa after 24 h at 40ºC and 27 days at 25ºC. The BFS-based mortars activated by using KOH reagent in 8M yielded 35.5 MPa after 24 h at 25ºC, 7 h at 65ºC and storage at room temperature until 28 days (Pereira et al., 2015). The use of RHA as an alternative silica source mixed with NaOH for the activation of BFS-based geopolymers was carried out by Moraes et al. (2018) obtaining 59.7 MPa after

28 curing days at 20ºC. The investigation showed values of 54.9 MPa when SCSA was employed as a silica source under the same conditions. All these comparisons show that the activation of BFS by a mixture of OBA and RHA led to very good mechanical performance for the medium and long terms.

3.3. Microstructural characterization of TAAMs

XRD patterns of the TAAPs from sub-study 2.2 (pastes) are presented in **Fig.4.ix.4**. A baseline deviation of the Bragg's angle in the range from 25° to 40° was observed in all cases. This baseline deviation is characteristic of geopolymerized BFS pastes, as was shown by several authors (Moraes et al., 2017; Pereira et al., 2015), and it is attributed to the gel formation. The same characteristic peaks for 20A/20R-C pastes were identified for all analysed curing ages. The main crystalline peaks of calcite ($CaCO_3$, PDFcard 050586), quartz (SiO_2, PDFcard 331161) and hydrotalcite ($Mg_6Al_2CO_3(OH)_{16}$, PDFcard 411428) were observed. Additionally, some minor peaks corresponding to arcanite (K_2SO_4, PDFcard 050613), hydroxyapatite ($Ca_5(PO_4)_3(OH)$, PDFcard 090432) and cristobalite (SiO_2, PDFcard 391425) were identified. Seeing the chemical composition of the raw materials (**Table 4.ix.1**), it is possible to deduce that the presence of calcite as well as the crystalline quartz phases suggest the unreacted BFS and OBA particles and is probably because it did not react in the activating process (Moraes et al., 2017). Beltrán et al. (2016) identified the peaks of arcanite in the XRD spectrum of the biomass bottom ash from the olive pruning waste after combustion at 403ºC. The presence of arcanite may be attributed to a combination of some OBA compounds: K2O (32.12% by weight) and SO_3 (1.67% by weight). When the BFS has more than 5% by weight of MgO, the hydrotalcite peak is commonly observed as a part of the main reaction products (Adesanya et al., 2018). Thus, as is shown in **Table 4.ix.1**, the BFS used in the present investigation has 7.43% by weight of MgO. The hydrotalcite was previously identified in pastes of BFS activated with OBA by Font et al. (2017). Finally the cristobalite peaks can be attributed to the RHA (Luukkonen et al., 2018).

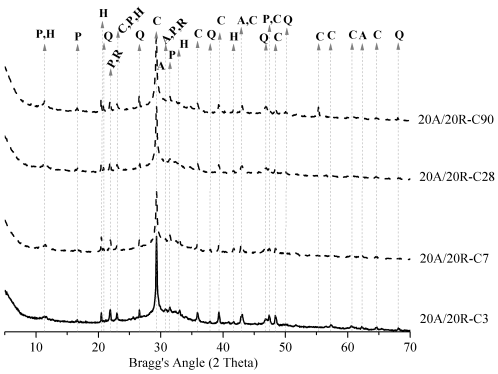

Fig.4.ix.4 *XRD patterns of TAAPs from sub-study 2.2 (Key: Q = quartz; R = cristobalite; C = calcite; A = arcanite; P = hydroxyapatite; H = hydrotalcite).*

Derivate thermogravimetric curves (DTG) for the TAAPs from sub-study 2.2 are shown in **Fig.4.ix.5**. The literature shows DTG analysis for BFS pastes with the distribution of mass losses in characteristic peaks which appear in the following temperature ranges: i) between 110–140°C corresponding to the loss of combined water from the main hydrated products C-S-H and (C-x)-S-H (with x = Na (in sodium-activated systems) or K (in potassium-activated systems)); ii) between 140–200°C related to the dehydration of (C-x)-A-S-H (normally in the range between 140–155°C) and C-A-S-H (in the range from 180 to 200°C); and iii) at about 390°C, which is commonly related with the dehydration of hydrotalcite (de Moraes Pinheiro et al., 2018; Moraes et al., 2018; Rivera et al., 2016). The thermogravimetric analysis carried out by Font et al. (2017)showed the first two characteristic peaks in pastes of BFS/water related to i) and ii) above-mentioned mass losses and the presence of the DTG peak related to the hydrotalcite in pastes of BFS/KOH 4M and BFS/OBA (18% addition). Pereira et al. (2015) found only one characteristic peak between 145–170°C in BFS pastes activated by NaOH solution, corresponding to dehydration of the reaction gels formed.

In the DTG curves obtained for the TAAPs, it can be noticed that a very similar DTG characteristic peak was found when comparing the curves (**Fig.4.ix.5**). In general terms, the DTG curves for the TAAPs showed only one large DTG peak at the temperature range between 128–140°C. The mass losses corresponding to the different decomposition/dehydration of C-A-S-H and (C-K)-A-S-H were produced together in the same temperature range. These results may be due to the formation of gels with a different nature yielding a stronger matrix by the addition of a silica source in the system (from RHA) and its combination with a higher amount of potassium and calcium from OBA. Although the corresponding hydrotalcite peak was identified in the XRD patterns of the pastes, in the DTG curves it was difficult to observe: a small deviation was perceived in the range 380–420°C.

Furthermore, as indicated in **Fig.4.ix.5**, the total mass losses (35–500°C) increased from 3 to 90 days of curing, suggesting that the quantity of hydrated compounds was increasing during the curing of the pastes.

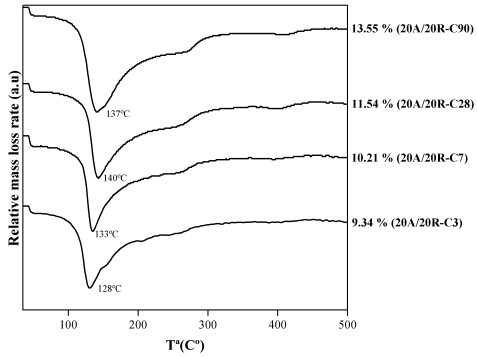

Fig.4.ix.5 *DTG curves of TAAPs from sub-study 2.2 (20°C curing). Percentages on the right indicate the total mass loss in the 35–500°C range.*

By comparing the results of the total mass losses from the TGA and the TAAMs mechanical behaviour discussed above (**Fig.4.ix.3**) in sub-study 2.2, a sample evolution with age can be observed in both cases: mass loss as well as compressive strength increased with curing time. With the progress of the BFS alkaline activation, more hydrated products are formed and consequently the mortars developed better compressive strength behaviour. Between 3 and 90 days there is an increase of ≈ 88.5% in compressive strength and ≈ 30.8% in total mass loss. A linear relationship between the compressive strength and the mass loss was obtained (**Fig.4.ix.6**).

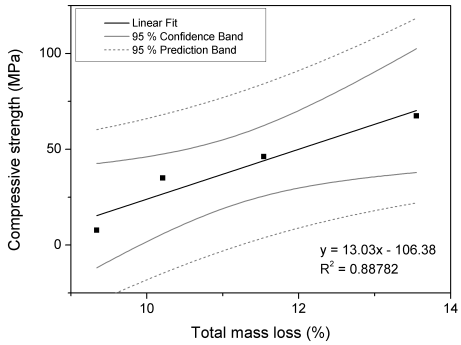

Fig.4.ix.6 *Linear fit model between compressive strength and thermogravimetric mass loss for 20A/20R-C sample (curing ages: 3, 7, 28 and 90 days).*

A similar linear relationship between the compressive strength and the thermogravimetric mass loss with the curing time was obtained by Moraes et al. (2018) in pastes of BFS and BFS with SCSA in 25% replacement, activated by NaOH or NaOH/commercial waterglass solutions. The results obtained for 20A/20R-C pastes suggested that, with the OBA/RHA blending for BFS activation, it is possible to obtain the synthesis of the traditional gel forms for slag.

The MIP curves of the 20A/20R TAAM and TAAP cured for 28 days are shown in **Fig.4.ix.7**, where the accumulated distribution of the intruded Hg volume per gram of material is represented as a function of the pore size diameter. Inserted in these graphs are tables with the porosimetry parameters obtained for TAAM and TAAP of 20/20R-C28 samples. In the curves, vertical lines mark the pore structure differentiation into gel pores, capillary pores and air voids, according to the authors (Aligizaki, 2006; Neville, 1982).

For the TAAM sample, the total porosity was 12.48%, of which 40.60% correspond to gel pores, 56.65% correspond to capillary pores and the remaining 2.75% correspond to air voids. In the case of the paste (TAAP), as expected, the total porosity was higher than the mortar one (21.22%) due to the absence of sand in the sample, and consequently the volume of paste analysed was higher. In the TAAP sample, 39.00% of the porosity corresponds to the gel pores, 59.88% to the capillary pores and 1.12% to the air voids. It can be seen that the proportions of the different kinds of pores for mortar and paste were equivalent. de Moraes Pinheiro et al. (2018) affirmed that the increment of the OBA addition in the BFS pastes causes a reduction of total porosity, which was correlated with the compressive strength increment in mortars. The pastes based on BFS/OBA systems resulted in a total porosity of 42.85% when 10% of OBA was added and of 29.16% when 25% of OBA was added. In the present work the TAAP resulted in a lower total porosity because of the higher total OBA employed (40%, which is equivalent to 20% addition plus 20% substitution) and the chemical effect of RHA dissolution and reaction towards BFS.

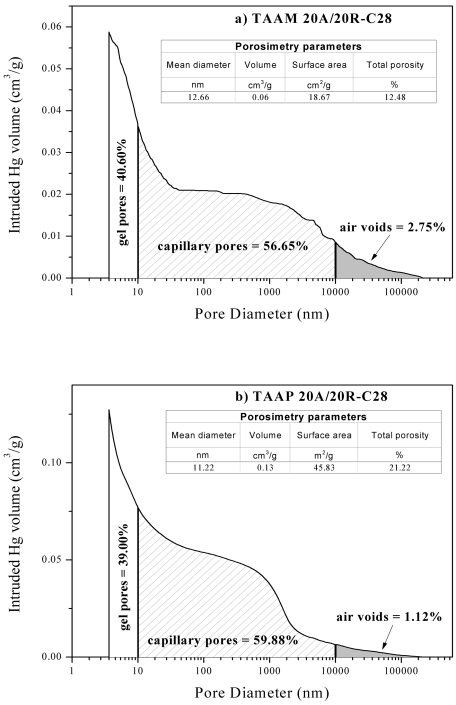

Fig.4.ix.7. *Results from MIP for: a) 20A/20R-C28 mortar (TAAM); b) 20A/20R-C28 paste (TAAP).*

FESEM micrographs of the TAAP after 28 days at 20°C (20A/20R-C28 sample) are shown in **Figs.4.ix. 8 and 9**. In the selected micrographs the most representative topography and gel particles and their details can be observed. As can be appreciated, the paste matrix presented three different particle morphologies in terms of shape.

The first micrograph (**Fig.4.ix.8a**) shows an overview of the paste surface with a dense and compact topography without large pores. In the previous investigation of binary pastes based on BFS/OBA, a highly porous surface was observed (de Moraes Pinheiro et al., 2018). The incorporation of RHA in the ternary systems allows the reduction of the matrix micro-porosity by the silicates reaction forming inter-clustered gels. Two main structures can be distinguished in this micrograph as shown in **Figs.4.ix. 8b and 8c**:

i) A particle of BFS appears in the centre of Fig. 8a and the first detail shown in **Fig.4.ix. 8b** corresponds to hydration products (0.1–0.5 μm in size) formed on the BFS particles. The EDS analysis yielded MgO = 3.1 ± 1.3%, Al_2O_3 = 5.3 ± 1.7%, SiO_2 = 16.1 ± 3.8%, K_2O = 20.1 ± 4.7% and CaO = 53.1 ± 6.3% as principal

oxides. The presence of MgO can be attributed to the BFS. The gel can be identified as C(K)-S(A)-H.

ii) The second detail of the micrograph (**Fig.4.ix.8c**) corresponds to a different crystallization pattern where the matrix is less dense than the other zone (**Fig.4.ix.8b**) and no magnesium or aluminium were in the chemical composition determined by EDS. The EDS analysis of the zone yielded a lower amount of silica (6.2 ± 0.9%) and CaO (42.9 ± 3.3%) and a higher amount of K_2O (48.3 ± 3.5%). The gel can be labelled as C(K)-S-H. A similar morphology of the particles was found by de Moraes Pinheiro et al. (2018) in pastes of BFS/OBA binary systems.

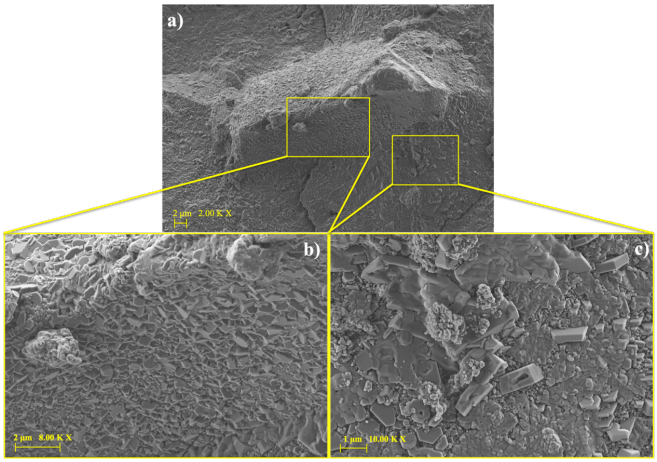

Fig.4.ix.8 *FESEM micrographs of pastes from sub-study 2.2 samples cured for 28 days at 20°C (20A/20R-C28 paste): a) general view in 2000x magnification; b) detail of the one characteristic zone from the above micrograph in 8000x magnification; and c) detail of the other characteristic zone from micrograph a) in 10000x magnification.*

In the other micrograph (**Fig.4.ix.9**) thinner and more isolated microcrystals can be observed in the dense matrix of the material. These microcrystals have flat flake morphology, as shown in the detail of the zone where they are located (**Fig.4.ix.9b**). In other investigations, these characteristic formations were attributed to the formation of Mg-Al-CO_3-hydrotalcite microcrystals (Liao et al., 2012). As discussed above, in the XRD section, the patterns of the 20A/20R-C28 paste presented hydrotalcite peaks.

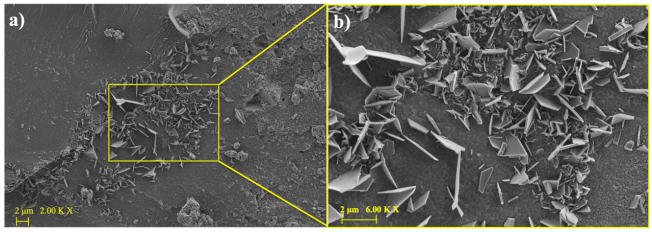

Fig.4.ix.9. *FESEM micrographs of pastes from sub-study 2.2 samples cured for 28 days at 20ºC (20A/20R-C28 paste): a) general view in 2000x magnification; b) detail of the microcrystals from the above micrograph in 6000x magnification.*

4. Conclusions

The main conclusion from the present investigation is the successful development of new ternary alkali-activated systems that are 100% waste based on: blast furnace slag (BFS), olive-stone biomass ash (OBA) and rice husk ash (RHA).

Respect the mechanical test on TAAMs, the following statements can be done:

- The ternary alkali-activated mortars (TAAM), where the OBA/BFS ratio was changed while keeping the amount of RHA constant, showed an enhanced strength development when the OBA proportion in the BFS weight addition was increased from 15% to 25%.

- Focusing the study on the TAAMs' behaviour with respect to different curing conditions, the high temperature (65ºC) produced a fast reaction in the binder gel formation. The combined curing method (65ºC for 24 hours plus 20ºC for 6 days) does not produce remarkable differences in the mechanical behaviour of the TAAMs. A 20ºC curing temperature produced the hydration products gently and consequently the mechanical strength development is slower.

- The use of OBA as addition plus the replacement of BFS by OBA (where the OBA/BFS ratio was increased from 0.25 to 0.5) made it possible to obtain excellent strength development, especially for mortars cured at 20ºC. For the TAAMs with 0.5 OBA/BFS ratio, very good performance of the mortars was produced after 28 and 90 days of curing: 46 and 67 MPa were reached respectively. It is highlighted that these values were significantly better than those previously obtained for binary alkali-activated systems of BFS/OBA, suggesting that the RHA

has an important role in the development of these alternative materials.

From the microstructural characterization of BFS/OBA/RHA system with 0.5 OBA/BFS ratio, the following is concluded:

- The reaction of the OBA with the RHA dissolved part of the potassium and the silica, forming potassium silicate. This potassium silicate enhanced the alkali activation of the BFS. The microstructural results demonstrated that a large amount of gel was formed during the curing of the ternary BFS/OBA/RHA system.

- In XRD patterns of the ternary pastes (TAAP), the main crystalline peaks of calcite, quartz and hydrotalcite were identified and some minor peaks corresponding to arcanite, hydroxyapatite and cristobalite were also identified.

- The DTG curves showed a large peak corresponding to the decomposition/dehydration of C(K)-S-H and (C(K)-S(A)-H gels together. The combination of silica from RHA and potassium from OBA allows a strong gel matrix development.

- The corresponding hydrotalcite peak identified in the XRD patterns was difficult to observe in DTG curves.

- For TAAM, the total porosity was 12.48 % and for TAAP was 21.22 %. The main type of pores found in both samples (TAAM and TAAP) was the capillary pore.

- The FESEM micrographs showed an important dense matrix with the presence of two types of microcrystals. The EDS results demonstrated that a large amount of gel was formed during the curing of the ternary pastes. Two types of gel were identified, one of them containing mainly Ca/K/Si/Al (C(K)-S(A)-H gel) and the other containing Ca/K/Si (C(K)-S-H gel).

As final conclusion, the mixing of OBA and RHA is an interesting proposal for increasing the alkali activation rate of BFS.

Acknowledgements

The authors gratefully acknowledge the GeocelPlus-UPV project, Almazara Candela – Elche, Spain and DACSA S.A. - Tabernes Blanques, Spain. Thanks are also given to the Electron Microscopy Service of the Universitat Politècnica de València.

References

Adesanya, E., Ohenoja, K., Luukkonen, T., Kinnunen, P., Illikainen, M., 2018. One-part geopolymer cement from slag and pretreated paper sludge. J. Clean. Prod. https://doi.org/10.1016/j.jclepro.2018.03.007

Aligizaki, K.K., 2006. Pore structure of cement-based materials, First. ed. Taylor & Francis, Canada and USA.

Andrew, R.M., 2018. Global CO 2 emissions from cement production. Earth Syst. Sci. Data 10, 2213–2239.

Beltrán, M.G., Barbudo, A., Agrela, F., Jiménez, J.R., De Brito, J., 2016. Mechanical performance of bedding mortars made with olive biomass bottom ash. Constr. Build. Mater. https://doi.org/10.1016/j.conbuildmat.2016.02.065

Bernal, S.A., Rodríguez, E.D., Mejía de Gutiérrez, R., Provis, J.L., 2015. Performance at high temperature of alkali-activated slag pastes produced with silica fume and rice husk ash based activators. Mater. Construcción 65, e049. https://doi.org/10.3989/mc.2015.03114

Bouzón, N., Payá, J., Borrachero, M. V., Soriano, L., Tashima, M.M., Monzó, J., 2014. Refluxed rice husk ash/NaOH suspension for preparing alkali activated binders. Mater. Lett. 115, 72–74. https://doi.org/10.1016/j.matlet.2013.10.001

Cheah, C.B., Part, W.K., Ramli, M., 2015. The hybridizations of coal fly ash and wood ash for the fabrication of low alkalinity geopolymer load bearing block cured at ambient temperature. Constr. Build. Mater. 88, 41–55. https://doi.org/10.1016/j.conbuildmat.2015.04.020

de Moraes Pinheiro, S.M., Font, A., Soriano, L., Tashima, M.M., Monzó, J., Borrachero, M.V., Payá, J., 2018. Olive-stone biomass ash (OBA): An alternative alkaline source for the blast furnace slag activation. Constr. Build. Mater. https://doi.org/10.1016/j.conbuildmat.2018.05.157

Fernández-Jiménez, A., Cristelo, N., Miranda, T., Palomo, Á., 2017. Sustainable alkali activated materials: Precursor and activator derived from industrial wastes. J. Clean. Prod. 162, 1200–1209. https://doi.org/10.1016/j.jclepro.2017.06.151

Fernández-Jiménez, A., Palomo, J.G., Puertas, F., 1999. Alkali-activated slag mortars: Mechanical strength behaviour. Cem. Concr. Res. https://doi.org/10.1016/S0008-8846(99)00154-4

Font, A., Soriano, L., Moraes, J.C.B., Tashima, M.M., Monzó, J., Borrachero, M.V., Payá, J., 2017. A 100% waste-based alkali-activated material by

using olive-stone biomass ash (OBA) and blast furnace slag (BFS). Mater. Lett. 203. https://doi.org/10.1016/j.matlet.2017.05.129

Font, A., Soriano, L., Reig, L., Tashima, M.M., Borrachero, M. V., Monzó, J., Payá, J., 2018. Use of residual diatomaceous earth as a silica source in geopolymer production. Mater. Lett. 223, 10–13. https://doi.org/10.1016/j.matlet.2018.04.010

Hu, W., Nie, Q., Huang, B., Shu, X., He, Q., 2018. Mechanical and microstructural characterization of geopolymers derived from red mud and fly ashes. J. Clean. Prod. 186, 799–806. https://doi.org/10.1016/j.jclepro.2018.03.086

Lee, N.K., Lee, H.K., 2013. Setting and mechanical properties of alkali-activated fly ash/slag concrete manufactured at room temperature. Constr. Build. Mater. https://doi.org/10.1016/j.conbuildmat.2013.05.107

Liao, L., Zhao, N., Xia, Z., 2012. Hydrothermal synthesis of Mg-Al layered double hydroxides (LDHs) from natural brucite and Al(OH) 3. Mater. Res. Bull. 47, 3897–3901. https://doi.org/10.1016/j.materresbull.2012.07.007

Luukkonen, T., Abdollahnejad, Z., Yliniemi, J., Kinnunen, P., Illikainen, M., 2018. Comparison of alkali and silica sources in one-part alkali-activated blast furnace slag mortar. J. Clean. Prod. 187, 171–179. https://doi.org/10.1016/j.jclepro.2018.03.202

Mejía, J.M., Mejía De Gutiérrez, R., Montes, C., 2016. Rice husk ash and spent diatomaceous earth as a source of silica to fabricate a geopolymeric binary binder. J. Clean. Prod. 118, 133–139. https://doi.org/10.1016/j.jclepro.2016.01.057

Mejía, J.M., Mejía de Gutiérrez, R., Puertas, F., 2013. Ceniza de cascarilla de arroz como fuente de sílice en sistemas cementicios de ceniza volante y escoria activados alcalinamente. Mater. Construcción 63, 361–375. https://doi.org/10.3989/mc.2013.04712

Mellado, A., Catalán, C., Bouzón, N., Borrachero, M. V., Monzó, J.M., Payá, J., 2014. Carbon footprint of geopolymeric mortar: study of the contribution of the alkaline activating solution and assessment of an alternative route. RSC Adv. 4, 23846–23852. https://doi.org/10.1039/C4RA03375B

Moraes, J.C.B., Font, A., Soriano, L., Akasaki, J.L., Tashima, M.M., Monzó, J., Borrachero, M.V., Payá, J., 2018. New use of sugar cane straw ash in alkali-activated materials: A silica source for the preparation of the alkaline activator. Constr. Build. Mater. 171.

https://doi.org/10.1016/j.conbuildmat.2018.03.230

Moraes, J.C.B., Tashima, M.M., Akasaki, J.L., Melges, J.L.P., Monzó, J., Borrachero, M. V., Soriano, L., Payá, J., 2017. Effect of sugar cane straw ash (SCSA) as solid precursor and the alkaline activator composition on alkali-activated binders based on blast furnace slag (BFS). Constr. Build. Mater. 144, 214–224. https://doi.org/10.1016/j.conbuildmat.2017.03.166

Neville, A.M., 1982. Properties of concrete, Fifth. ed, Journal of General Microbiology. Pearson Education Limited, England. https://doi.org/10.4135/9781412975704.n88

Nie, Q., Hu, W., Huang, B., Shu, X., He, Q., 2019. Synergistic utilization of red mud for flue-gas desulfurization and fly ash-based geopolymer preparation. J. Hazard. Mater. 369, 503–511. https://doi.org/10.1016/j.jhazmat.2019.02.059

Passuello, A., Rodríguez, E.D., Hirt, E., Longhi, M., Bernal, S.A., Provis, J.L., Kirchheim, A.P., 2017. Evaluation of the potential improvement in the environmental footprint of geopolymers using waste-derived activators. J. Clean. Prod. 166, 680–689. https://doi.org/10.1016/j.jclepro.2017.08.007

Payá, J., Monzó, J., Borrachero, M.V., Soriano, L., Akasaki, J.L., Tashima, M.M., 2017. New inorganic binders containing ashes from agricultural wastes, Sustainable and Nonconventional Construction Materials using Inorganic Bonded Fiber Composites. https://doi.org/10.1016/B978-0-08-102001-2.00006-1

Pereira, A., Akasaki, J.L., Melges, J.L.P., Tashima, M.M., Soriano, L., Borrachero, M. V., Monzó, J., Payá, J., 2015. Mechanical and durability properties of alkali-activated mortar based on sugarcane bagasse ash and blast furnace slag. Ceram. Int. 41, 13012–13024. https://doi.org/10.1016/j.ceramint.2015.07.001

Peys, A., Rahier, H., Pontikes, Y., 2016. Potassium-rich biomass ashes as activators in metakaolin-based inorganic polymers. Appl. Clay Sci. 119, 401–409. https://doi.org/10.1016/j.clay.2015.11.003

Qureshi, M.N., Ghosh, S., 2013. Effect of Alkali Content on Strength and Microstructure of GGBFS Paste. Glob. J. Res. Eng. Civ. Struct. Eng. 13, 11–20.

Rivera, O.G., Long, W.R., Weiss, C.A., Moser, R.D., Williams, B.A., Torres-Cancel, K., Gore, E.R., Allison, P.G., 2016. Effect of elevated temperature on alkali-activated geopolymeric binders compared to portland cement-based binders. Cem. Concr. Res. 90, 43–51.

https://doi.org/10.1016/j.cemconres.2016.09.013

Shirley, R., Black, L., 2011. Alkali activated solidification/stabilisation of air pollution control residues and co-fired pulverised fuel ash. J. Hazard. Mater. 194, 232–242. https://doi.org/10.1016/j.jhazmat.2011.07.100

Tchakouté, H.K., Rüscher, C.H., Kong, S., Kamseu, E., Leonelli, C., 2016. Geopolymer binders from metakaolin using sodium waterglass from waste glass and rice husk ash as alternative activators: A comparative study. Constr. Build. Mater. 114, 276–289. https://doi.org/10.1016/j.conbuildmat.2016.03.184

Tippayasam, C., Balyore, P., Thavorniti, P., Kamseu, E., Leonelli, C., Chindaprasirt, P., Chaysuwan, D., 2016. Potassium alkali concentration and heat treatment affected metakaolin-based geopolymer. Constr. Build. Mater. https://doi.org/10.1016/j.conbuildmat.2015.11.027

Torres-Carrasco, M., Puertas, F., 2015. Waste glass in the geopolymer preparation. Mechanical and microstructural characterisation. J. Clean. Prod. 90, 397–408. https://doi.org/10.1016/j.jclepro.2014.11.074

Turner, L.K., Collins, F.G., 2013. Carbon dioxide equivalent (CO2-e) emissions: A comparison between geopolymer and OPC cement concrete. Constr. Build. Mater. 43, 125–130. https://doi.org/10.1016/j.conbuildmat.2013.01.023

Van Riessen, A., Jamieson, E., Kealley, C.S., Hart, R.D., Williams, R.P., 2013. Bayer-geopolymers: An exploration of synergy between the alumina and geopolymer industries. Cem. Concr. Compos. 41, 29–33. https://doi.org/10.1016/j.cemconcomp.2013.04.010

Wang, S.-D., Pu, X.-C., Scrivener, K.L., Pratt, P.L., 1995. Alkali-activated slag cement and concrete: a review of properties and problems. Adv. Cem. Res. 7, 93–102. https://doi.org/10.1680/adcr.1995.7.27.93

World busines council for sustainable development [WWW Document], n.d. URL https://www.wbcsd.org/Sector-Projects/Cement-Sustainability-Initiative/News/Cement-technology-roadmap-shows-how-the-path-to-achieve-CO2-reductions-up-to-24-by-2050 (accessed 6.11.19).

Yang, K.H., Song, J.K., Song, K. Il, 2013. Assessment of CO 2 reduction of alkali-activated concrete. J. Clean. Prod. 39, 265–272. https://doi.org/10.1016/j.jclepro.2012.08.001

4.3.2 Hormigones Eco-celulares "one part" (ECC-OP)

Finalmente se presenta en esta **última etapa** experimental la publicación correspondiente a la culminación del objetivo general de la investigación llevada a cabo objeto de esta Tesis Doctoral:

x. Step-by-step development of one-part eco-cellular concretes (ECC-OP) for precast industry: functional features and life cycle assessment (LCA)

AUTORES: Alba Font, Lourdes Soriano, Mauro M. Tashima, José Monzó, María Victoria Borrachero, Jordi Payá

REFERENCIA DE LA PUBLICACIÓN: Enviado a Journal Of Cleaner Production (En revisión)

Factor de impacto/Cuartil (2018): 6. 395/Q1	**Citas (excluyendo auto citas):** -

OBJETIVOS PARCIALES ABORDADOS

MATERIALES	FABRICACIÓN
• **TCC:** OPC + H_2O + A • **AACC:** BFS + [WG+NaOH+H_2O] + A • **AACC:** BFS + [WG+NaOH+H_2O] + A_R • **ECC:** BFS + [RHA+NaOH+H_2O] + A_R • **ECC-OP**: [BFS/OBA/RHA] + H_2O + A_R	• **CO-M:** BFS + A_R + RHA + OBA = BRm-RO • **CURADO:** TA • **Amasado con:** PD

PROCEDIMIENTO EXPERIMENTAL

CARACTERIZACIÓN DE MATERIAS PRIMAS	CARACTERIZACIÓN DE ESPECÍMENES
-	• Densidad natural (D_N) • Resistencia mecánica (Rc) • Ensayos hídricos (D_{AP}) • Conductividad térmica (KD2-Pro) (λ) • Análisis del ciclo de vida (LCA)

RESULTADOS Y CONCLUSIONES MÁS RELEVANTES DE LA INVESTIGACIÓN

- Los materiales se ensayan y comparan con los requisitos establecidos por la normativa europea de piezas prefabricadas de fábrica para albañilería (UNE-EN 771-4).
- Además, con el fin de demostrar su aplicabilidad a nivel global, se compara con los requisitos establecidos por el Instituto Americano del Hormigón (ACI) en la comisión 523R de hormigón prefabricado.

Material	D_{AP} (kg/m³)	D_N (kg/m³)	Rc (MPa)	λ (W/mK)	GWP–100 (CO_2eq/m³)
TCC	617	618	6.5	0.180	526.0
AACC aireados con A	635	583	6.1	0.130	385.9
AACC con BFSRm	681	674	7.1	0.280	283.2
ECC	616	691	5.6	0.220	181.3
ECC-OP	660	704	6.3	0.200	19.2

- Se cumple lo establecido en la normativa europea para su aplicación en la industria de los prefabricados.
- Se consigue desarrollar un material a base de un 100 % residuos que cumple las expectativas de consumo de energía en la fabricación casi nula.
- Los nuevos ECC-OP tienen un GWP-100 de 19.2 kgCO_2eq por cada metro cúbico de material fabricado. Este valor supone una reducción del 96 % respecto a los sistemas tradicionales (TCC).

Abstract: This paper focuses on investigating greener alternatives of cellular concrete technology to fulfil current searches for a shift to circular economy. A novel one-part eco-cellular concrete (ECC-OP) was developed and studied. The one-part alkali activated materials (AAM-OP) and new alkali-activated cellular concrete (AACC) technologies were combined to develop greener alternatives of cellular concrete production. The progressive steps from traditional cellular concrete (TCC) based on ordinary Portland cement (OPC) and commercial aluminium powder (A) to a 100% waste-based cellular concrete are presented. Blast furnace slag (BFS) was the precursor, RHA was employed as the silica source, olive stone biomass ash (OBA) was the alkali source and recycled aluminium foil (A_R) was employed as an aerating agent. The functional features of the materials were studied and compared to those established by the European standard and the American Concrete Institute (ACI) Committee 523 guides. The new ECC-OP with a bulk density, compressive strength and thermal conductivity that respectively equal 660 kg/m^3, 6.3 MPa and 0.20 W/mK was obtained. Finally, a cradle-to-gate life cycle assessment (ACV) was made, where the industrial process of a masonry unit manufacture was raised by using each studied material. A 96% reduction in the kgCO_2eq per m^3 of material was reached with the new proposed ECC-OP compared to TCC manufacturing.

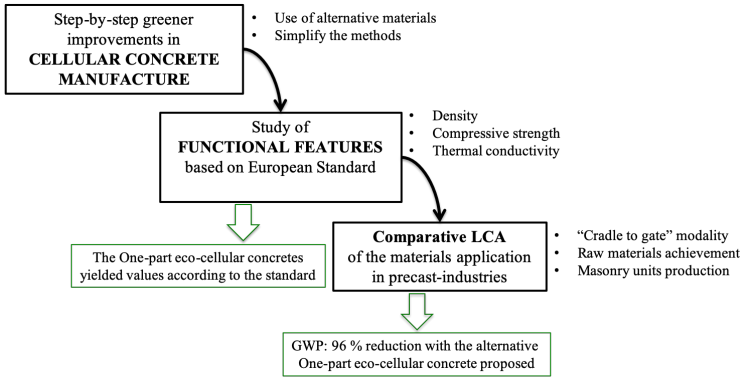

GRAPHYCAL ABSTRACT (4.x)

Keywords: One-part alkali-activated material, cellular concrete, life cycle assessment, CO_2 emissions, blast furnace slag, biomass ash.

Abbreviations:
TCC: Traditional cellular concrete
AACC: Alkali-activated cellular concrete
ECC: Eco-cellular concrete
ECC-OP: One-part eco-cellular concrete
OPC: Ordinary Portland Cement
BFS: Blast furnace slag
OBA: Olive stone biomass ash
RHA: Rice husk ash
A: Commercial aluminium powder
A_R: Recycled aluminium foil
LCA: Life cycle assessment
GWP: Global Warming Potential relative to CO_2
100-GWP: 100-year GWP time horizon

HIGHLIGHTS:

- *A new one-part eco-cellular concrete (ECC-OP) was developed*
- *ECC-OP based on blast furnace slag was composed of 100% residue*
- *One-part manufacturing consists in the singly mix of co-milled waste with water*
- *Functional ECC-OP features fulfil precast industry European/American standards*
- *The new ECC-OP has a 96% less 100-year GWP than traditional cellular concrete*

1. Introduction

Today the concrete industry needs a greener and economic evolution in both raw materials and the manufacturing method. Concrete is the most employed construction material in the world (Colangelo et al., 2018; Van Den Heede and De Belie, 2012). In the European Union (EU), buildings have a strong socio-economic impact by having 40% energy demands, 36% CO_2 emissions, 50% non-renewable raw materials and 35% waste (Novais et al., 2019; Zabalza Bribián et al., 2011). Consequently, the search for a circular economy system is growing for its industrial application (Funfación Conama - Grupo de trabajo GT-6, 2018; Hogeling and Derjanecz, 2018; Schroeder et al., 2018). In recent years, global institutions have opted for the precast construction concept and the responsible use of waste, materials, soil, water, air and power sources (Dahmen et al., 2018).

Traditional cellular concretes (TCC) are low-density insulating materials whose importance is increasing by reducing the volume of material requirements and their suitability in precast industry applications (Chica and Alzate, 2019; Hajimohammadi et al., 2017; Mak et al., 2008; Pytlik and Saxena, 1992). The typical relation among the natural density (wet weight/volume), compressive strength and thermal conductivity of autoclaved cellular concretes to their application in pre-cast construction elements (in structural and non-structural elements) is shown in **Table 4.x.1**.

Table 4.x.1.
Relationship between the physical characteristics of the cellular concretes commonly described by authors. Adapted from Dolton and Hannah (Dolton and Hannah, 2006).

Density (kg/m^3)	Compressive strength (MPa)	Thermal conductivity (W/mK)
600	1.98	0.097
550	1.51	0.092
500	1.14	0.086
450	0.84	0.080
400	0.71	0.075

Precast cellular concrete is presented as an interest alternative to develop a greener construction activity. Notwithstanding, environmental issues are commonly linked with TCC components and their manufacture process: i) the main component is ordinary Portland cement (OPC), which is well-known for its major environmental impacts (considerable use of energy and non-renewable raw materials, and around 8% of the world's anthropogenic CO_2 emissions) (Luukkonen et al., 2018a); ii) commercial aluminium powder (A) was the most employed aerating agent, and its achievement and manufacture involve serious environmental issues (Alba Font et al., 2017); iii) the curing treatment of TCC is currently carried out in autoclaves under high temperature and pressure conditions. Thus strong enviro-economic impacts are associated (Esmaily and Nuranian, 2012; Keawpapasson et al., 2014).

Greener alternatives have been studied in recent years by applying alkali-activated material (AAM) (high-calcium hydraulic precursors) and geopolymer (low-calcium aluminosilicate precursors) technologies in alternative cellular

concrete manufacturing, commonly known as the new alkali-activated cellular concretes (AACC) (Hajimohammadi et al., 2017; He et al., 2019; Yang et al., 2014) and geopolymer cellular concretes (GCC), respectively (Bai and Colombo, 2018; Alba Font et al., 2017; Hassan et al., 2018; Novais et al., 2016; Xuan et al., 2019). These systems are characterised by being prepared to avoid autoclave treatment: cellular systems with low density and appropriate compressive strength may be achieved under soft curing conditions. Blast furnace slag (BFS) was employed as a precursor in AACC and A was used as an aerating agent (Esmaily and Nuranian, 2012). The synthesised AACC were cured at 70°C, 78°C and 87°C to achieve density and compressive strength of 953 kg/m^3 and 3.7 MPa after 28 days, respectively. Font et al. developed GCCs based on fluid catalytic cracking catalyst residue (FCC), which was aerated with recycled aluminium foil (Alba Font et al., 2017). The new GCC specimens yielded 600-700 kg/m^3, 2.5-3.5 MPa and 0.581 W/mK after 7 curing days at room temperature.

The most recent research into low CO_2 materials (AAM and geopolymers) has focused on searching for 100% waste-based materials by replacing the required commercial chemical reagents: high alkali hydroxides (NaOH or KOH) and sodium or potassium silicate sources (Choo et al., 2016; de Moraes Pinheiro et al., 2018; Peys et al., 2016). In cellular concrete technology, this concern has been recently introduced. Kamseu et al. manufactured AACC aerated with A by employing rice husk ash or volcanic ash (RHA or VPA) combined with metakaolin activated with a highly concentrated NaOH (8 M) solution (Kamseu et al., 2015). Samples were cured at room temperature for 7 days, and yielded a total porosity exceeding 50%. RHA was also employed (as a silica source) combined with KOH in the alkali-activating reagent preparation for FA-based cellular concretes (Ziegler et al., 2016). The designed samples were aerated by adding A within the 0.05-0.3% range and were cured for 24 h at 50°C before being stored at room temperature until 60 days. GCCs, aerated with 0.2% of A, had an apparent porosity within the 54–63% range and compressive strength within the 2–2.5 MPa range. The use of RHA as a silica source in preparing the alkali-activating reagent in the FCC-based GCCs and BFS-based AACCs systems was firstly introduced by Font et al. (Font et al., 2018). These authors compared TCCs to the GCCs and AACCs activated with: NaOH/sodium silicate aqueous solution; ii) NaOH/RHA aqueous suspension (for this option, the resulting cellular concrete was called new eco-cellular concretes, ECC). In the new ECC systems, the employed aerating agent was recycled aluminium foil, added before the milling treatment of the precursors. The resulting new ECC specimens had ranges of 782–611 kg/m^3 for density, 3.2–4.6 MPa for compressive strength and 0.113/0.224 W/mK for thermal conductivity after 28 curing days at room temperature, which allowed the reduction of 74-78% of CO_2 emissions *versus* TCC when FCC or BFS was used as a precursor. Stoleriu et al. presented materials based on BFS partially replaced with waste glass powder activated by an NaOH solution, where high porosity was induced by thermal treatment at 900–1,000°C for 30-60 minutes (Stoleriu et al., 2019).

Olive stone biomass ash (OBA) has been quite recently introduced as a KOH replacement for BFS activation (de Moraes Pinheiro et al., 2018; A. Font et al., 2017). A 100% waste-based material based on new ternary BFS/OBA/RHA systems has been developed with good properties and a high environmental improvement potential (Font et al., 2020).

For pre-cast applications in the concrete industry, the development of one-part AAM has been potentially studied to avoid technical disadvantages while preparing the alkali activator solution (difficulties because large amounts are handled given its corrosiveness and viscosity) (Luukkonen et al., 2018b; Ma et al., 2019; Sturm et al., 2016). These one-part materials consist in a unique solid phase formed by a precursor and alkali source mix, which only needs water as the liquid phase, and is similar to using OPC. Recently, Luukkonen et al. published a review about this initiative to search for close-to-the-market projects of alternative low-carbon materials (Luukkonen et al., 2018a). To the best of our knowledge, there are no published research works that combine the innovations of one-part concretes and ECC technologies.

The aim of the present research was to study and compare the new ECC-OP to be applied to precast-industries as masonry units. Five different typologies of cellular concretes were designed and studied for which step-by-step greener improvements were introduced from TCC to the one-part 100% waste-based eco-cellular concrete production. A study about the functional features of the materials obtained in each step was carried out and compared with the values set by the European standard and by the American Concrete Institute (ACI) Committee 523 guides (AENOR, 2016a; Babbitt et al., 2014). The application of the compared cellular concretes as a masonry unit was assessed and a comparative cradle-to-gate modality life cycle assessment (LCA) was carried out, where the contribution of the new one-part ECC to circular economy was evaluated.

2. Experimental procedure

In this research, the step-by-step development of one-part eco-cellular concrete (ECC) is presented. In **Fig.4.x.1**, the outline of the followed procedure is shown and the used samples/acronyms are explained.

In this diagram (**Fig.4.x.1**), the compared samples are boxed and the directional black arrow indicates the steps of the introduced improvements. The negative factors are plotted as red arrows and the positive ones as green arrows. The direction of the arrows shows if the factor was introduced or removed in the following alternative cellular concrete.

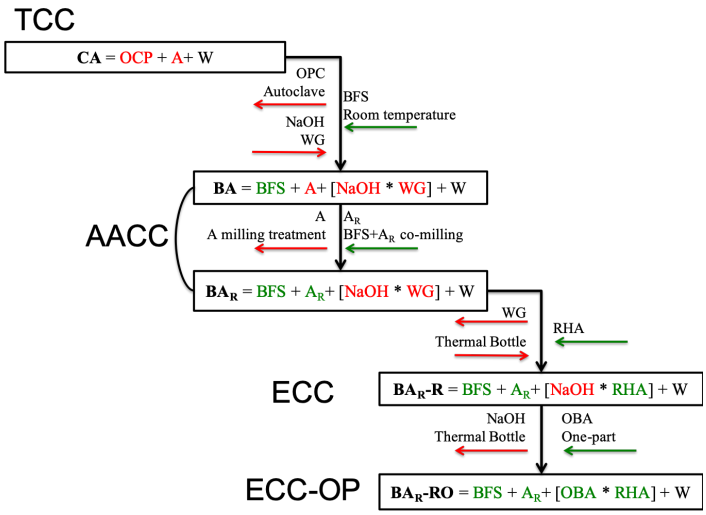

Fig.4.x.1. *Outline of the step-by-step improvement introduced into cellular concrete (The negative factors are plotted as red arrows and the positive ones as green arrows).*

List of acronyms:

CA: Traditional cellular concrete (TCC) based on ordinary Portland cement (OPC) and water (W), aerated with commercial aluminium powder (A)

BA: Alkali-activated cellular concrete (AACC) based on blast furnace slag (BFS) activated with a sodium hydroxide/sodium silicate (NaOH/WG) solution, aerated with commercial aluminium powder (A)

BA_R: Alkali-activated cellular concrete (AACC) based on blast furnace slag (BFS) activated with a sodium hydroxide/sodium silicate (NaOH/WG) solution, aerated with recycled aluminium foil (A_R)

BA_R-R: Eco-cellular concrete (ECC) based on blast furnace slag (BFS) activated with a sodium hydroxide/rice husk ash (NaOH/RHA) suspension, aerated with recycled aluminium foil (A_R)

BA_R-RO: One-part eco-cellular concrete (ECC-OP) based on blast furnace slag (BFS) activated with olive-stone biomass ash/rice husk ash (OBA/RHA), aerated with recycled aluminium foil (AR) in which all the solid raw materials are co-milled and then blended with water (W).

2.1. *Materials*

Ordinary Portland cement (OPC: CEM I-52.5R) was supplied by Lafarge S.A (Puerto de Sagunto, Valencia, Spain), blast furnace slag (BFS) was acquired from Cementval S.A (Puerto de Sagunto, Valencia, Spain) as large granules. Olive stone biomass ash (OBA) was supplied by Almazara Candela (olive oil company, Elche, Spain). Rice husk ash (RHA) was supplied by DACSA S.A. (Tabernes Blanques, Valencia, Spain). The chemical compositions of these four materials were determined by X-Ray fluorescence (XRF, Magic Pro Spectrometer-Philips) and are summarised in **Table 4.x.2**.

Table 4.x.2.
Chemical composition (XRF) of the raw materials (w%).

Material	Oxide composition (wt%)										
	SiO_2	CaO	Al_2O_3	Fe_2O_3	Na_2O	MgO	K_2O	P_2O_5	SO_3	Others	LOI*
OPC	20.80	65.60	4.60	4.80	0.07	1.20	1.00	-	1.70	-	0.23
BFS	30.53	40.15	10.55	1.29	0.87	7.43	0.57	0.26	1.93	0.89	5.53
RHA	85.58	1.83	0.25	0.21	-	0.5	3.39	0.67	0.26	0.32	6.99
OBA	5.33	27.77	0.70	3.45	0.78	5.13	32.12	2.68	1.67	1.47	18.90

*Loss on ignition

Commercial aluminium powder (A) was acquired from Schlenk Metallic Pigments GmbH and the recycled aluminium foil (A_R) was supplied by the Department of Agricultural Forest Ecosystems at the Universitat Politècnica de València (Valencia, Spain).

A milling treatment of the raw materials was required to manufacture alternative cellular concretes. A 1-litre capacity ball mill model Gabrielli Mill-2, with 98 alumina balls, was employed in all cases (except for RHA). The BFS used in the BA system was milled for 30 minutes and BFS+A_R was co-milled in the BA_R system. The RHA used in BA_R-R activation was singly pre-milled in an industrial grinder for 4 h (Bouzón et al., 2014). Finally, for the BA_R-RO samples, BFS, A_R, RHA and OBA were co-milled for 30 minutes and the obtained powder was employed as a single raw material in the ECC mix (one-part). The mean particle diameter (D_m) and particle size parameters (d(0.1) μm, d(0.5) μm and d(0.9) μm) were obtained with a Malvern Mastersizer 2000 laser granulometer in water suspension, and are summarised in **Table 4.x.3**.

Table 4.x.3.
Mean particle diameter (D_m) and particle size parameters (d(0.1) μm, d(0.5) μm and d(0.9) μm) of the solid materials employed in cellular concretes.

MATERIAL	D_m (μm)	PARAMETERS		
		d(0.1)μm	d(0.5)μm	d(0.9)μm
BFS	28.8	2.8	19.7	68.9
BFS/A_R	29.3	2.8	19.9	70.2
RHA	20.3	2.5	10.5	41.2
BFS/A_R/RHA/OBA	25.1	1.2	14.5	66.4

The chemical reagents used for the alkali-activated solution preparation in AACCs (samples BA and BA_R) were sodium silicate (WG, 8 wt% Na_2O, 28 wt% SiO_2 and 64 wt% H_2O) and sodium hydroxide pellets (NaOH, 98% purity), both

supplied by Merck-Spain.

2.1. Methods

2.2.1. Cellular concretes manufacturing

In this research, the volume of cellular concrete manufacturing was selected to obtain the material required to fill moulds for the functional features test (see the following section "2.2.2 Functional features"). For each batch, eight 1000-cm^3 cubes and six 64-cm^3 cubes were prepared.

The calculated dose for each sample is shown in **Table 4.x.4**. During the mixing procedure, the solid phase indicated the raw materials introduced as solid powders and the liquid phase corresponded to the added single materials (water in CA and BA_R-RO samples) or to the combined ones in aqueous medium (NaOH+WG alkali solution in BA and BA_R or alternative OBA/RHA alkali suspension in BA_R-R).

Table 4.x.4.
Doses (per mass) of the manufactured cellular concretes.

Sample	Solid phase	Liquid phase
CA	OPC: 7000.0 g A: 14.0 g	W: 3150.0 g
BA	BFS: 7000.0 g A: 14.0 g	W: 840.0 g NaOH: 426.8 g WG: 1968.8 g
BA_R	BFS: 7000.0 g A_R: 14.0 g	
BA_R-R	BFS: 7000.0 g A_R: 14.0 g	W: 3150.0 g NaOH: 945.0 g RHA: 918.8 g
BA_R-RO	BFS: 5600.0 g A_R: 16.8 g RHA: 716.7 g OBA: 2800 g	W: 3500.0 g

For samples CA, BA, BA_R and BA_R-R, the liquid phase doses were determined according to previous works and experimental procedures (Font et al., 2018). For the new ECC-OP (BA_R-RO sample), the dose was determined based on the combination of previous ternary alkali-activated systems (BFS/RHA/OBA) with the addition of A_R (Font et al., 2020). In this case, the water/solid ratio was selected by comparing several experimental parameters: the consistency of fresh pastes must be appropriate for developing a porous structure to avoid gas leaks through the matrix and to maximise gas entrapments in the matrix. Mixing was carried out by a power drill, model AEG SBE705RE, connected to a paint mixer. The manufacturing procedure was divided into three stages, as shown in **Table 4.x.5**.

Table 4.x.5.
Stages of the procedure carried out to manufacture each cellular concrete.

	PRE-MANUFACTURE	MANUFACTURE	POST-MANUFACTURE
CA	-	-**OPC/A** dry mix -**OPC/A** + **W** (180 s)	-24h (48h for BA_R-RO) RT[5] -Cut out the expanded free surface with a saw blade and demoulding. -RT until testing.
BA	-BFS grinding. -AS preparation[1]	-**BFS/A** dry mix -**AS** stirring (30 s) -**BFS/A+ AS** (180 s)	
BA_R	-BFS /A_R Co-milling -AS[1] preparation[2]	-**AS** stirring (30 s) -**BFS/A_R** + **AS** (180 s)	
BA_R-R	-BFS /A_R Co-milling -AAS[3] preparation[4]	-**AAS** stirring (30 s) -**BFS/A_R** + **AAS** (180 s)	
BA_R-RO	-BFS/A_R/RHA/OBA Co-milling	-**BFS/A_R/RHA/OBA** + **W**(180 s)	

[1]AS = alkali solution
[2]AS preparation: remained in a plastic beaker sealed with plastic film until room temperature was reached
[3]AAS = alternative alkali dissolution
[4]AAS preparation: NaOH pellets were dissolved in water by rising the temperature. Then RHA was added to the hot solution and mixed for 1 minute. The alternative alkali suspension was stored at 65°C for 24 h to improve the silica solubilisation from RHA.
[5]RT = room temperature (23°C/100% RH)

2.2.2. Functional features

The analysed functional features were density, compressive strength and thermal conductivity, according to the guidelines of Standard UNE EN 771-4: "*Specifications for masonry units-part 4: autoclaved aerated concrete masonry units*" (AENOR, 2016a) and compared to the ACI Committee 523.2-R96: "*Guide for Precast Cellular Concrete*" (Babbitt et al., 2014). The functional features tests were carried out after 28 curing days at room temperature (23°C/100 RH).

A. DENSITY: Six specimens (4 x 4 x 4 cm^3) were employed to analyse the bulk and dry densities based on Standard UNE EN 772-13: *"Methods of test for masonry units-part 13: determination of net and gross dry density of masonry units (except for natural stone)"*(AENOR, 2001). Hydric tests were carried out as follows:
   1. Dry weight (W_d) determination: specimens drying at 105±5 °C until constant mass (24 h with a change in weight under 0.2%).
   2. Absolute volume (or net volume) (V_n) of specimens obtained by hydrostatic balance means according to the specifications in UNE-EN 772-13 and by applying **Equation (4.x.1)**:

$$V_n = \frac{W_a - W_w}{\rho_w} \ (m^3) \qquad (4.x.1)$$

Where:
V_n = Absolute volume (m^3).
W_a = Air weight of specimens (conditioning 2 h after the curing treatment under laboratory conditions) (kg).
W_w = Weight submerged in water (kg).
ρ_w = Water density (kg/m^3).

3. Absolute density (ρ_n) (or net density) calculation by **Equation (4.x.2)**, as follows:

$$\rho_n = \frac{W_d}{(V_n - V_v)} \left(\frac{kg}{m^3}\right) \quad (4.x.2)$$

Where:
ρ_n = Dry density (kg/m^3).
W_d = Dry weight (kg).
V_n = Absolute volume (m^3).
V_v = Void volume (V_v = V_g - V_n, being V_g = gross volume), (m^3).

4. Bulk density (ρ_b) (or gross density) calculation by using **Equation (4.x.3)** as follows:

$$\rho_b = \frac{W_d}{(V_g - V_v)} \left(\frac{kg}{m^3}\right) \quad (4.x.3)$$

Where:
ρ_b = Bulk density (kg/m^3).
W_d = Dry weight (kg).
V_g = Gross volume (m^3).
V_v = Void volume (m^3).

B. COMPRESSIVE STRENGTH: Four specimens (10 x 10 x 10 cm^3) were tested for the compressive strength (R_c) assessment, and the average and standard deviations were calculated. Standard UNE EN 772-1: "*Methods of test for masonry units-part 1: determination of compressive strength*"(AENOR, 2016b), was followed and a universal testing INSTRON 3282 machine was employed. The required loading rate (0.05 MPa per second) was adjusted at a displacement rate of 1 mm per minute. Samples were weighed before testing and natural density (ρ) was determined as the mass per unit volume.

C. THERMAL CONDUCTIVITY: Four samples (10 x 10 x 10 cm^3) were employed for thermal conductivity (λ) determinations according to Standard UNE EN 1745: *"Masonry and masonry products - methods for determining thermal properties"*(AENOR, 2013). For the test, a KD2-Pro handheld device (Decagon Devices Inc.) was used with a thick single RK-1 sensor (length x diameter = 6 cm x 0.39 cm). The measurement method was the transient line source, based on the dual needle probe system following ASTM D5534-08 (ASTM International, 2008) and IEEE 442-1981(IEEE STANDARDS ASSOCIATION, 1981). To accommodate the

sensor, five distributed pilot holes (length x diameter = 6 cm x 0.4 cm) were drilled on the specimen surface.

D.

2.2.3. Live cycle assessment (LCA)

The cradle-to-gate modality of the LCA was selected to limit the study coverage by following Standard ISO 14040 and the Intergovernmental Panel on Climate Change 2006 (IPCC) specifications (IPCC, 2006). The manufacture of 1 m^3 of each proposed cellular concrete was analysed and compared (TCC, AACC, ECC and ECC-OP systems) in terms of their 100-years Global Warming Potential time horizon (100-GWP) associated with their materials and procedures. 100-GWP is a measure of how much heat the emissions of 1 ton of greenhouse gases will be trapped over a 100-year period in relation to the emissions of 1 ton of carbon dioxide (CO_2). Calculations were done from the extracted raw materials to their industrial block manufacturing, and before their distribution. **Fig.4.x.2** shows a correlational framework of the selected flows and processes from the studied "cradle-to-gate LCA" for manufacturing the masonry units of each material.

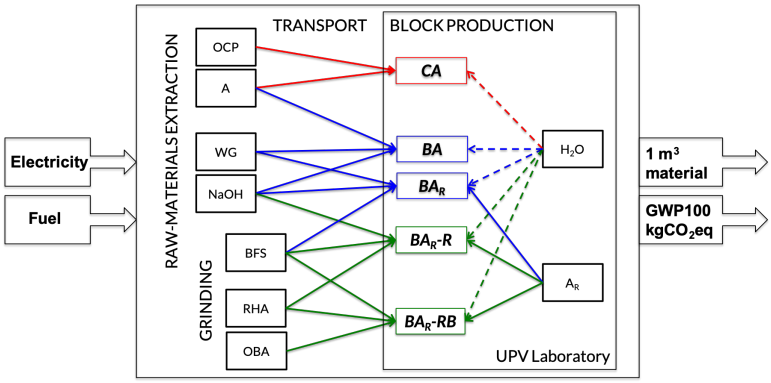

Fig. 4.x.2: *Overview of the selected flows and processes in the cradle-to-gate LCA carried out to compare the industrial pre-cast blocks manufacturing with CA, BA, BA_R, BA_R-R and BA_R-RB.*

The following considerations were taken for the LCA calculations:

- The industrial manufacturing of masonry units was selected, with dimensions 20x62.5x25 cm^3 and a density of 550 kg/m^3, by comparing the use of CA, BA, BA_R, BA_R-R and BA_R-RO. The 1 m^3 dose of each material was theoretically calculated with which 32 precast blocks could be manufactured. The European emission factors of manufacturingf and equipment of this process are standardized in Ecoinvent 3.3. The curing treatment was not considered because the ambient temperature was selected for comparing the five cellular

concretes. To reference the factory's location, the laboratory in the Universitat Politècnica de València (UPV) was selected.

- The proportion of the different materials was obtained using a thermogravimetric analysis (TGA) following the methodology introduced by Font et al. (Font et al., 2018). The TGA was carried out with a TGA 850 Mettler Toledo thermobalance within the 35-600°C temperature range, in an N_2 atmosphere, and dry samples were placed inside aluminium crucibles with a micro-hole in their sealed lids. The weight loss obtained in the derivate thermogravimetric curves (DTG) was from the combined water. The constant range between the total solid weight and solid phases (precursor and from the alkali solution, Na_2O and SiO_2) in the cellular concretes was employed to obtain the doses of the theoretical samples for the LCA.

- BFS was considered a subproduct as suggested by Van Der Heede and De Belie (Van Den Heede and De Belie, 2012) and Chen et al.(Chen et al., 2018). Their secondary production includes treatment and refurbishment after metal collection: solidification (granulated BFS) and grinding (BFS). Ase RHA and OBA were wastes, their extraction was not considered, but their necessary conditioning pre-treatment was taken into account to be employed in cellular concrete manufacturing.

- The milling treatment of all the alternative raw materials was considered and was carried out the same as the milling treatment for OPC (equipment and energy demands) in the Cementval S.A industrial plant (Puerto de Sagunto, Spain).

- The used transport references were: Diesel truck, EURO4, ≤ 7.5t and mixed transport (urban/interurban). Distances were selected from the raw-materials extraction emplacements to the UPV laboratory as the sum of the lorry's return trips (British Standards Institution, 2011) (see **Table 4.x.5**). If two raw materials came from the same company, only one transport unit was considered (with length taken as only the sum of the two raw materials without it exceeding the lorry's capacity).

- In the production unit for BA_R-R, the alkali suspension preparation was included in the calculations by considering the more extreme situation: two electric resistances of 1 kW operating for 24 h to keep water at 65°C (by assuming that the water in the bath was hot at the time the alkali solution was being prepared).

The software employed to perform the analysis was OpenLCA 1.7.2 with a combination of live-cycle inventory (LCI) databases from Ecoinvent 3.3 Open LCA Nexus (Ecoinvent Association, 2019; Moreno-Ruiz E. et al., 2019). **Table**

4.x.6 provides the employed LCI and the corresponding environmental impact factors (IP) for each unity, as well as transport distances (km).

Table 4.x.6.
Employed LCI, environmental impact factors (IP) for each unity and transport distances (km).

		IP	LCI	Distance[1]
Raw materials	OPC	0.907 $kgCO_2$ * kg	Ecoinvent	53.8 km
	BFS	0.0192 $kgCO_2$ * kg	Ecoinvent	53.4 km
	A	15.601 $kgCO_2$ * kg	Ecoinvent	710 km
	A_R	0	-	0 km
	NaOH	1.120 $kgCO_2$ * kg	SigmaPro	732 km
	WG	1.213 $kgCO_2$ * kg	SigmaPro	
	RHA	0	-	53.4 km
	OBA	0	-	
H_2O		4.288 x 10^{-4} $kgCO_2$ * kg	Ecoinvent	0 km
Transport		0.126 $kgCO_2$ * km	(IDAE, 2019)	
Grinding	Power	35.4 kWh * ton	LabIngSos	
Production	Energy[2]	0.272 $kgCO_2$ * kWh	(CNMC, 2018)	
	Thermal bath[3]	0.272 $kgCO_2$* 2 kW * 24 h		
	Manufacture	0.138$kgCO_2$ * block	Ecoinvent	

[1] Sum of return lorry routes from the extraction emplacement to the UPV laboratory.
[2] National Energy Mix (2018)
[3] In the BA_R-R alkali solution preparation: two electrical resistances working for 24 h.

3. Results and discussion

3.1. Functional features

European standard in UNE-EN UNE EN 771-4 sets a maximum bulk density of 1,000 kg/m^3 and a minimum compressive strength of 1.5 MPa for autoclaved aerated concrete masonry unit applications. The reference values set by the ACI Committee 523.2-R96, "*Guide for Precast Cellular Concrete*", are a maximum bulk density of 800 kg/m^3 and a minimum compressive strength of 2.07 MPa for applications to floor, roof and wall units. In both of them, the obtained thermal conductivity values should not vary by more than 5% of the proposed ones.

Table 4.x.7 provides the results of the hydric (absolute density (ρ_n) and bulk density (ρ_b)) and physical/mechanical (natural density (ρ) and compressive strength (R_c)) tests.

Table 4.x.7.
Results of the hydric and mechanical tests for the studied cellular concretes after 28 days.

Sample	Hydric tests		Mechanical tests	
	ρ_n (kg/m^3)	ρ_b (kg/m^3)	ρ (kg/m^3)	R_c (MPa)
CA	661 ± 6	617 ± 9	618 ± 2	6.5 ± 0.4
BA	770 ± 1	635 ± 3	583 ± 4	6.1 ± 0.2
BA_R	778 ± 7	681 ± 8	674 ± 4	7.1 ± 0.2
BA_R-R	794 ± 8	616 ± 2	691 ± 4	5.6 ± 0.3
BA_R-RO	713 ± 1	660 ± 8	704 ± 4	6.3 ± 0.1

As expected, the bulk density and compressive strength values of the CA samples (TCC) fell well within the mandated requirements of UNE EN 771-4 and the ACI Committee 523.2-R96. The TCC systems yielded 617 kg/m^3 for bulk density and 618 kg/m^3 as natural density with 6.5 MPa after 28 curing days under ambient conditions.

In general, the studied alternative cellular concretes yielded similar absolute and bulk densities to the TCC ones. In the first step of the greener improvements in cellular concretes (BA sample), when the alkali-activated slag replaced the use of OPC, the obtained values of absolute and bulk densities were slightly higher than for the TCC mix (CA), 14% for ρ_n and 3% for ρ_b. In the second step (the second AACC system), when commercial A was replaced with recycled foil (BA_R sample), the increase in ρ_n and ρ_b was 14% and 8%, respectively. The next improvement introduced into the systems gave way to the first ECC (BA_R-R), in which the silica source resulted from using RHA. This sample achieved an absolute density that was 17% higher than the TCC samples, but bulk density was similar (617 kg/m^3 for the CA sample vs. 616 kg/m^3 for the alternative BA_R-R sample). Finally, the ECC-OP made from 100% residues (BA_R-RO sample) achieved an absolute density that was 7% higher and a bulk density that was 6% higher than the control TCC.

Regarding the natural density and compressive strength of the alternative cellular concretes, when the alkali-activated technology was introduced (AACC systems) and the material was aerated by A, the BA sample yielded 583 kg/m^3 and 6.1 MPa after 28 curing days at room temperature. Similar systems with alkali-activated slag aerated with commercial aluminium powder have been studied by Esmaily and Nuranian, who presented 1,227 kg/m^3 and <1 MPa at curing regime temperatures for 14 h (Esmaily and Nuranian, 2012). When the second step was introduced and the aluminium powder source was replaced with recycled foil (the BA_R sample), natural density was higher (674 kg/m^3) and compressive strength increased by 1 MPa (compared to the previous AACC system, the BA sample).

The ECC system (the BA_R-R sample) yielded 691 kg/m^3 and 5.6 MPa. The introduction of RHA as a silica source into the replacement of sodium silicate allowed the natural density range to be maintained, but compressive strength slightly decreased (BA_R-R vs BA_R). In previous research works, the same systems were developed and compared, and the only difference was the water/binder (w/b) ratio (Font et al., 2018): i) for the previous AACC (BFS + A_R + ordinary alkali solution (WG + NaOH + W)), the w/b ratio was 0.35 (the w/b ratio herein was 0.30); ii) in the previous ECC (BFS + A_R + alternative alkali solution (RHA + NaOH + W)), the w/b ratio was 0.45 (the w/b employed was 0.40 herein). These previous results showed that density increased from 474 kg/m^3 to 611 kg/m^3 when commercial waterglass was replaced with RHA, and compressive strength also increased from 2.6 MPa to 4.6 MPa after 28 curing days at room temperature. A lower w/b ratio allowed an increase in viscosity, which was enough to void/system development with a stable matrix yielding higher density (but < 1,000 kg/m^3) and greater compressive strength. This influence was much stronger for the AACC systems than for the GCC ones.

Finally, the one-part eco-cellular concrete (BA_R-RO) sample, where sodium silicate was replaced with OBA, yielded 704 kg/m^3 and 6.3 MPa. The first 100% waste-based one-part eco-cellular concrete increased density by less than 100 kg/m^3 and merely decreased 0.1 MPa compared to the TCC manufactured under the same conditions.

To analyse the evolution of the natural density and compressive strength achieved with the step-by-step greener improvements, a relative coefficient can be obtained by taking the TCC system values as a reference:

$$\varphi_d = {}^{\rho_A}/_{\rho_r} \quad (4.x.4)$$

Where:
φ_d = Density relative coefficient
ρ_A = Natural density of the selected alternative cellular concrete (kg/m^3)
ρ_r = Natural density of the reference cellular concrete (the CA sample) (kg/m^3)

$$\varphi_R = {}^{R_A}/_{R_r} \quad (4.x.5)$$

Where:
φ_R = Compressive strength relative coefficient
R_A = Compressive strength of the selected alternative cellular concrete (MPa)
R_r = Compressive strength of the reference cellular concrete (the CA sample) (MPa)

The coefficients near the unity indicated a close relation between the materials (alternative with reference cellular concretes). When the values exceeded the unity, the property of the alternative cellular concrete was higher than the reference. When the value went below the unity, the property of the alternative cellular concrete was lower than the reference.

Relative factor ω, obtained by the ratio between the relative coefficients of the natural density and compressive strength, can be obtained with these relative values:

$$\omega = \varphi_d / \varphi_R \quad (4.x.6)$$

Where:
ω = Relative factor between density and compressive strength
φ_d = Density relative coefficient
φ_R = Compressive strength relative coefficient

In this case, relative factor (ω) equalled the unity, which indicated that the material presented an equal relationship between density and compressive strength as CA.

Fig.4.x.3 shows the obtained coefficients (φ_d and φ_R) and the relative factor (ω) for the alternative cellular concretes.

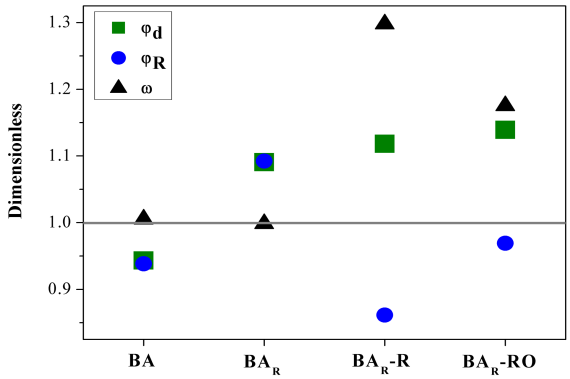

Fig. 4.x.3: *The relative coefficients of density (φ_d) and compressive strength (φ_R)) and relative factor (ω) for the alternative cellular concretes*

As observed, both coefficients were below the unit line for the BA sample, which indicates that the density and the compressive strength values are less than those of the CA samples. The overlapping of coefficients φ_d and φ_R indicates the direct linear relation between density and compressive. For the BA_R sample, where alternative aluminium was employed as an aerating agent, the φ_d and φ_R values were above the unit line.

When RHA was employed as a silica source (BA_R-R sample), the coefficients were above the unit line for density and below it for compressive strength, which indicates an inverse relation of the obtained properties vs. the control (CA). The same behaviour was observed for the proposed ECC-OP, where OBA was employed as an alkali source to avoid chemical reagents: the BA_R-RO sample allowed greater mechanical behaviour to be achieved with less commitment to density.

When observing the resultant relative factor for the two AACC samples (BA and BA_R), which were on the unit line in the graph, it was established that the relation between the two properties was similar to the control one. With the ECC samples (BA_R-R and BA_R-RO), the relation between the properties when comparing it to the control was greater than the unit, and the new BA_R-RO relative factor came nearest to the unit. This reveals that with a determined

compressive strength value, the ECC-OP system aerating effect was less than for the ECC system. As alkalinity provided by OBA in the systems, it was is less than that provided by NaOH, the reaction rate and, consequently, hydrogen generation were lower for the ECC-OP systems.

It is highlighted that the standard specification was substantially exceeded by all the alternative developed cellular concretes, as shown in **Fig.4.x.4**. In bulk density terms (**Fig.4.x.4b**), the improvement of BA_R-RO can be established as a lower percentage in relation to: i) UNE EN 771-4 (1,000 kg/m^3) with 34%; and ii) the ACI Committee 523.2-R96 (800 kg/m^3) with 18%. For compressive strength (**Fig.4.x.4b**), the improvement for BA_R-RO was represented by an increased percentage as follows in relation to: i) UNE EN 771-4 (1.5 MPa) with 320% (an increase of 4.8 MPa); and ii) the ACI Committee 523.2-R96 (2.07 MPa) with 204% (an increase of 4.2 MPa).

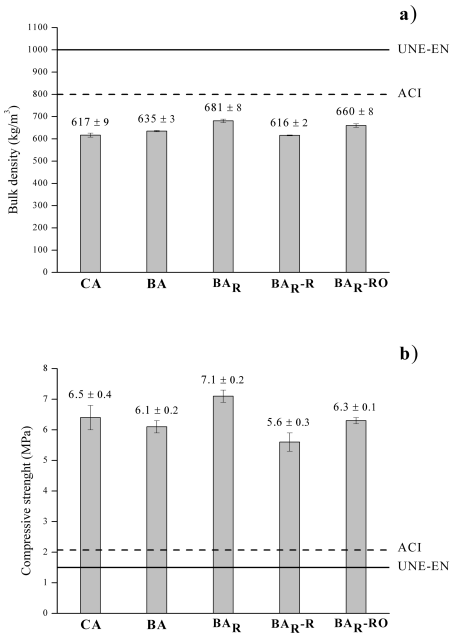

Fig.4.x.4: *a) Bulk densities obtained after 28 days and the lines of the maximum limited values by standards UNE-EN and ACI; b) compressive strength after 28 days and the lines of the minimum limited values by standards UNE-EN and ACI.*

According to the catalogue of building elements established by the Technical Building Code (CTE) (Ministerio de Fomento - Gobierno de España, 2018), autoclaved aerated concrete masonry units should meet thermal property requirements according to their bulk density. These ratios are proposed to fulfil general design requirements in habitability demands, and in energy efficiency and energy saving plan terms. The same ratio between bulk density

and required thermal conductivity is proposed by ACI committee 523.2R-96 (Babbitt et al., 2014).

The maximum thermal conductivity value and its dependence on bulk density (CTE and ACI requirements) are shown in **Table 4.x.8**, which were compared to the experimental values obtained for the studied cellular concretes.

Table 4.x.8.
Thermal conductivity of the analysed cellular concretes: values obtained in the study and the CTE/ACI requirements based on bulk density.

Sample	Obtained values		CTE		ACI	
	ρ_b (kg/m^3)	λ (W/mK)	ρ_b (kg/m^3)	λ (W/mK)	ρ_b (kg/m^3)	λ (W/mK)
CA	617 ± 9	0.18 ± 0.01	600	0.18	640	0.20
BA	635 ± 3	0.13 ± 0.02	600	0.18	640	0.20
BA$_R$	681 ± 8	0.28 ± 0.07	700	0.20	640	0.20
BA$_R$-R	616 ± 2	0.22 ± 0.01	600	0.18	640	0.20
BA$_R$-RO	660 ± 8	0.20 ± 0.01	700	0.20	640	0.20

As observed, the required insulation values were achieved by TCC (the CA sample), and also by the resulting material in the first step towards greener improvements (when the alkali-activated technology was applied), namely the BA sample (the first AACC system). The thermal conductivity of the BA (0.13 W/mK) sample was lower than it was for the CA sample (0.18 W/mK), which indicates greater insulation properties. When addressing the second step, and the commercial aluminium powder was replaced with recycled foil milled by the precursor (the BA$_R$ sample), thermal conductivity (0.28 W/mK) was higher than that required by the standards UNE-EN (0.20 W/mK) and by ACI (0.18 W/mK). This second AACC system was the less insulating one of all the studied materials. When RHA was used as a silica source (ECC, the BA$_R$-R sample) the thermal insulation properties were enhanced (λ = 0.22 W/mK), but this was not enough to fulfil the standards. The BA$_R$-RO sample (the ECC-OP system) yielded a thermal conductivity value within the limits of both standards (0.20 W/mK), which indicates enhanced improvement in the material's thermal insulation properties when adopting 100% greener alternatives in the dose.

3.1. Live cycle assessment (LCA)

Table 4.x.9 shows the TGA results for the different assessed pastes and the calculated proportions of the materials for the LCA. These proportions allowed 1 m^3 to be obtained for each proposed material to manufacture 32 pre-cast blocks with a density of 550 kg/m^3.

Table 4.x.9.
The total weight loss (TWL %) obtained in the TGA test and the theoretical calculated proportion (in mass) for manufacturing 1m³ (32 pre-cast blocks) for each cellular concrete.

Sample	TWL %	Solid phase (kg)	Liquid phase (kg)
CA	17.57	OPC: 453.3 (69 %)[1] A: 0.9 (1 %)	W: 204.0 (30 %)
BA	13.45	BFS: 414.5 (68 %) A: 0.8 (1 %)	W: 49.7 (3 %) NaOH: 25.3 (8 %) WG: 116.6 (20 %)
BA_R	13.60	BFS: 413.8 (68 %) A_R: 0.8 (1 %)	W: 49.5 (3 %) NaOH: 25.2 (8 %) WG: 116.4 (20 %)
BA_R-R	12.60	BFS: 393.1 (58 %) A_R: 0.8 (1 %)	W: 177.0 (26 %) NaOH: 53.1 (8 %) RHA: 51.6 (7 %)
BA_R-RO	11.50	BFS: 323.8 (44 %) A_R: 1.2 (1 %) RHA: 41.4 (5 %) OBA: 161.9 (22 %)	W: 202.4 (28 %)

[1] In brackets: percentage representing the raw material vs. the total proportion of cellular concrete.

The resulting matrices of the $kgCO_2eq$ from the different flows and the total 100-GWP for the CA, BA, BA_R, BA_R-R and BA_R-RO cellular concrete systems are plotted from **Fig.4.x.5** to **Fig.4.x.9**, respectively.

The raw materials extraction had the strongest impact on CA utilisation and represents 81% of the total emissions. In the TCC material, OPC had the strongest influence on dose (69%) but its influence was stronger on the total 100-GWP (96%) compared to the other materials (A and W). The pre-treatment of the raw materials (grinding) was not included because it was carried out on both the primary OPC and primary A industrial procurements (extraction). Despite the low dose of A in the CA manufacturing (0.2% of the OPC weight, which represents a 0.13% dose of the total CA components), its extraction substantially impacted the LCA (14% of the total 100-GWP). Transport activity led to 18% of the total 100-GWP. Thus, the distance from the company which supplied the UPV laboratory with A was the longest (see **Table 4.x.6**): the A in this flow was the most influential greenhouse gas producer (93%). The production of $1m^3$ (standardised European equipment and block manufacture procedures) had the least influence on the total environmental impact (1% of the total 100-GWP).

The masonry unit manufacturing performed by the TCC system technology yielded a 100-GWP of 526 $kgCO_2eq$. This value was slightly higher than that presented by Yang et al (Yang et al., 2014), who indicated a 1 m^3 production of 500-kg/m^3 OPC-based foamed concrete that yielded 412 $kgCO_2eq$. Those authors considered only the go-trip in the transport flows and the material's lower density. Thus, their lower OPC dose could cause this reduction. Dahmen et al (Dahmen et al., 2018) recently assessed the life cycle of OPC-based masonry blocks and obtained 216 $kgCO_2eq$ by using 1,840-kg/m^3 materials. However, these blocks had a 66% higher volume than the cellular concrete herein analysed, where OPC was only 11% of the concrete dose in this manufacturing.

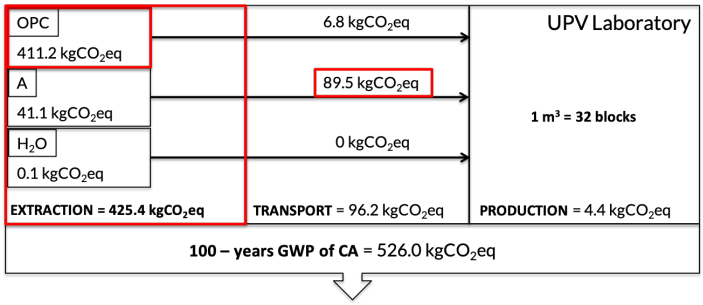

Fig. 4.x.5: *The 100-GWP impacts associated with each unitary flow and the production of 1m³ of CA (in red, the unit or subunit with the strongest influence).*

With the first step environmental improvement (the BA samples), the influence of raw materials extraction dropped by 56% and represented 49% of the total 100-GWP. The highest dose material was BFS, but WG was the most influential component on environmental impact emissions. Relative to the dose total materials, the proportion of BFS was 68 % and the proportion of WG was 20 %, however, in terms of 100-years GWP, the influence of BFS was merely 4 % and the influence of WG was 74 %. The key role of WG on the AAM environmental impact is commonly found (Mellado et al., 2014; Moraes et al., 2018; Puertas and Torres-Carrasco, 2014). As the influence of BFS grinding was introduced into the LCA calculations in that step, the improvement compared with OPC extraction offset emissions (the sum of BFS extraction and grinding was 55% lower than it was for OPC production). Transport flow was higher than the CA sample because the needed commercial chemical activators (WG and NaOH) and this influenced negatively in the total GWP improvements. For manufacturing BA blocks, the influence of transport was 49% because total emissions were the main cause from transporting the required chemical reagents and A (49% and 47%, respectively). The production process of the masonry units was maintained constant as it was the same for both materials and continued to be the lowest flow.

The masonry unit manufacturing done with the BA cellular concretes (the AACCs technology) yielded 386 $kgCO_2eq$ of the total 100-GWP. This value was 27% lower than the CA material. When considering the drastic reduction in the material volume of required material when using cellular concretes, and the good performance of previously studied functional requirements, the results in the ACV of BA can be compared with the traditional systems found in the bibliography. Robayo-salazar et al. (Robayo-salazar et al., 2018) compared the GWP of compounds of natural pozzolan/BFS in 70/30 proportions with the OPC ones to find a 45% reduction in total emissions. The works published about BFS-cellular concretes Yang et al. present reductions up to 85% compared to OPC cellular concretes (Yang et al., 2014). As explained above, those authors only considered one transport trip and the considered doses were lower than those analysed in the present work.

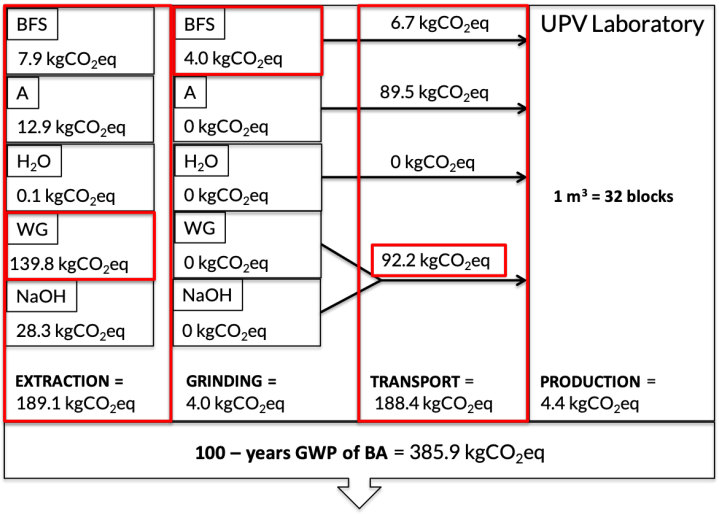

Fig.4.x.6: *The 100-GWP impacts associated with each unitary flow and a total production of 1m³ of BA (in red, the unit or subunit with the strongest influence).*

By replacing commercial A with recycled foil (the BA_R material), a total 27% 100-GWP improvement was achieved. However, the most marked decrease was found in transport flow (47% lower than BA) as A_R was not considered because it was obtained directly from the UPV laboratories. Material extraction decreased by 7%, and grinding and production flows remained constant.

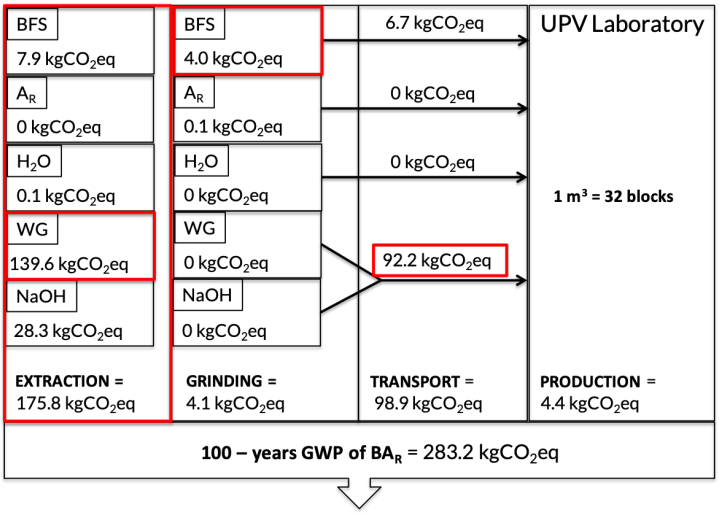

Fig.4.x.7: *The 100-GWP impacts associated with each unitary flow and a total production of 1m³ of BA_R (in red, the unit or subunit with the strongest influence).*

The ECC system (when using RHA as a silica source) allowed a 36% improvement in the 100-GWP compared to the BA_R sample and one of 66% vs. CA. Mellado et al. (Mellado et al., 2014) found that CO_2 emissions reduced by 50% when WG was replaced with RHA in the alkali activator dissolution for FCC-based mortars manufacturing. The improvement in the material herein developed allows an 80% reduction in the material's volume. By using BA_R-R, the emissions due to material extraction reduced by 62%. The strongest influence was NaOH, whose production released 59% of the total extraction flow. Transport flow was the same $kgCO_2eq$ as the previous AACC system because the transport of NaOH had to still be considered. The introduction of RHA involved an increase in GWP for the raw materials pre-treatment requirements (grinding, 7% more than BA_R). Pre-cast block production required a 24-hour storage of the RHA/NaOH/water alkali solution, and the production flow increased by 60% at 24 h. With the use of BA_R-R the production flow was 10.9 $kgCO_2eq$ versus the other studied materials with 4.4 $kgCO_2eq$. However, the total 100-GWP lowered thanks to the reduction in the other flows.

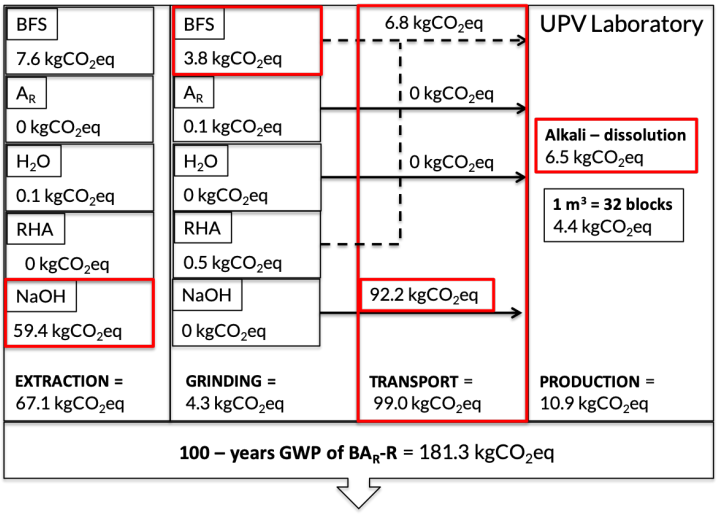

Fig.4.x.8: *The 100-GWP impacts associated with each unitary flow and to a total production of 1m³ of BA_R-R (in red, the unit or subunit with the strongest influence).*

Finally, with the one-part eco-cellular concrete, the total 100-GWP was 19 $kgCO_2eq$. The use of OBA as an alkali source allowed 100% waste-based material to be obtained, which was positively reflected by the environmental impact. It should be highlighted that the four processes had a proportional environmental impact with no flow with more than 10 $kgCO_2eq$ (30% of total emissions).

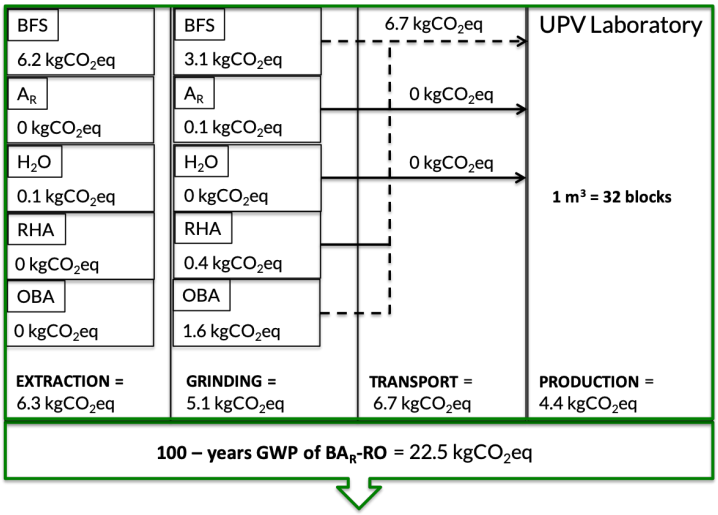

Fig.4.x.9: *The 100-GWP impacts associated with each unitary flow and a total production of 1m³ of BA_R-RO (in red, the unit or subunit with the strongest influence).*

Figure 4.x.10 shows the percentages of progressive decreases in the total 100-GWP achieved with each step-by-step greener improved material. The drawings inside each material-cloud show the influence of the different flows on the total 100-GWP. The new one-part 100% waste-based material, namely the ECC-OP system, yielded a total 96% reduction compared to TCC based on OPC (CA).

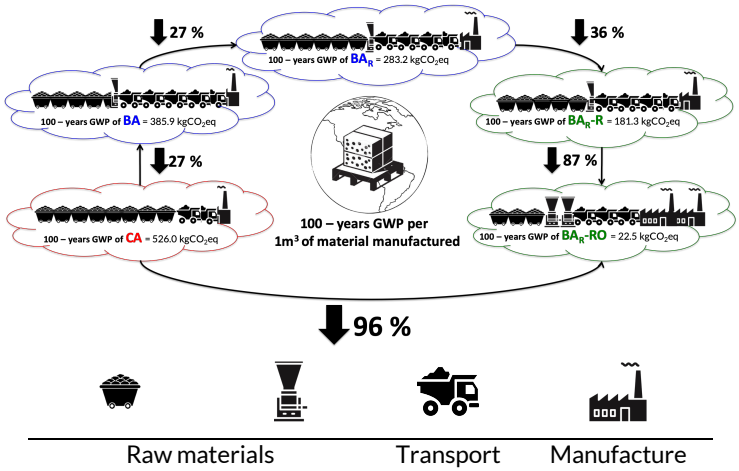

Fig.4.x.10: *Overview of total 100-GWP per 1m^3 of material manufactured and its progressive decreases with each step-by-step greener improvement introduced in the materials and manufacture.*

4. Conclusions

The study of step-by-step greener improvements in the manufacturing of cellular concretes was successfully implemented.

The proposed alternative cellular concretes (the AACC, ECC and ECC-OP systems), yielded similar absolute and bulk densities to TCC. In the last step, a new one-part eco-cellular concrete was developed with only an increase in density of 100 kg/m^3 compared to CA, but compressive strength was similar to the traditional system.

This research presents an evaluation of functional features in line with European and American standards to apply cellular concrete to precast masonry units manufacturing:

- All the alternative developed cellular concretes well exceeded the obtained bulk density and compressive strength

- For thermal conductivity, the required minimum value depends on the material's bulk density. Compared with standard specifications (CTE and ACI), the application of alkali activation technology (BA) yielded values that complied with those specified, but with the introduction of recycled foil (second step, the BA$_R$ sample), as well as the silica-based residue (third step, the BA$_R$-R sample), the materials'

thermal requirements were not met. Finally, the new 100% waste-based one-part eco-cellular concrete (ECC-OP) met the standard, and displayed a major eco-efficiency improvement for the alternative cellular concretes.

The LCA done with the step-by-step greener improvements in the materials showed a progressive reduction in the 100-GWP ($kgCO_2eq$) compared to TCCs: 27% for BA, 46% for BA_R, 66% for BA_R-R and 96% for BA_R-RO.

This research shows the possible utilisation of the new ECC in precast masonry unit manufacturing. Its functional features comply with standards' specifications and its manufacturing by combining 100% waste-based and "one-part" technology concepts, which involves near-zero energy use and scarce greenhouse gas emissions.

Acknowledgements

The authors gratefully acknowledge the GeocelPlus-UPV Project, Almazara Candela – Elche, Spain and DACSA S.A. - Tabernes Blanques, Spain and Cementval – Puerto de Sagunto, Spain.

References

AENOR, 2016a. UNE-EN 771-4:2011+A1: Especificaciones de piezas para fábrica de albañilería Parte4: Bloques de horigón celular curado en autoclave.

AENOR, 2016b. UNE-EN 772-1:2011+A1: Métodos de ensayo de piezas para fábrica de albañilería. Parte 1: Determinación de la resistencia a compresión.

AENOR, 2013. UNE-EN 1745: Fábrica de albañilería y componentes para fábrica. Métodos para determinar las propiedades térmicas.

AENOR, 2001. UNE-EN 772-13: Métodos de ensayo de piezas para fábrica de albañilería. Parte 13: Determinación de la densidad absoluta seca y de la densidad aparente seca de piezas para fábrica de albañilería (excepto piedra natural) 9.

ASTM International, 2008. ASTM D5334 - 14 Standard Test Method for Determination of Thermal Conductivity of Soil and Soft Rock by Thermal Needle Probe Procedure [WWW Document].

Babbitt, F., Barnett, R.E., Cornelius, M.L., Dye, B.T., Liotti, D.L., Schmidt, S.B., Tanner, J.E., Valentini, S.C., 2014. ACI 523.3R-14 Guide for Cellular Concretes above 50 lb/ft3 (800 kg/m3).

Bai, C., Colombo, P., 2018. Processing , properties and applications of highly

porous geopolymers : A review. Ceram. Int. 44, 16103–16118. https://doi.org/10.1016/j.ceramint.2018.05.219

Bouzón, N., Payá, J., Borrachero, M. V., Soriano, L., Tashima, M.M., Monzó, J., 2014. Refluxed rice husk ash/NaOH suspension for preparing alkali activated binders. Mater. Lett. 115, 72–74. https://doi.org/10.1016/j.matlet.2013.10.001

British Standards Institution, 2011. PAS 2050:2011 Specification for the assessment of the life cycle greenhouse gas emissions of goods and services. London.

Chen, Y., Ko, M., Chang, J., Lin, C., 2018. Recycling of desulfurization slag for the production of autoclaved aerated concrete. Constr. Build. Mater. 158, 132–140. https://doi.org/10.1016/j.conbuildmat.2017.09.195

Chica, L., Alzate, A., 2019. Cellular concrete review: New trends for application in construction. Constr. Build. Mater. 200, 637–647. https://doi.org/10.1016/j.conbuildmat.2018.12.136

Choo, H., Lim, S., Lee, W., Lee, C., 2016. Compressive strength of one-part alkali activated fly ash using red mud as alkali supplier. Constr. Build. Mater. 125, 21–28. https://doi.org/10.1016/j.conbuildmat.2016.08.015

CNMC, 2018. Sede electrónica - Listado de Informes de Etiquetado de Electricidad [WWW Document]. Com. Nac. los Mercados y la Competencia. URL https://gdo.cnmc.es/CNE/resumenGdo.do?anio=2018 (accessed 8.21.19).

Colangelo, F., Forcina, A., Farina, I., Petrillo, A., 2018. Life Cycle Assessment (LCA) of Different Kinds of Concrete Containing Waste for Sustainable Construction. Buildings 8, 70. https://doi.org/10.3390/buildings8050070

Dahmen, J., Kim, J., Ouellet-Plamondon, C.M., 2018. Life cycle assessment of emergent masonry blocks. J. Clean. Prod. 171, 1622–1637. https://doi.org/10.1016/j.jclepro.2017.10.044

de Moraes Pinheiro, S.M., Font, A., Soriano, L., Tashima, M.M., Monzó, J., Borrachero, M.V., Payá, J., 2018. Olive-stone biomass ash (OBA): An alternative alkaline source for the blast furnace slag activation. Constr. Build. Mater. https://doi.org/10.1016/j.conbuildmat.2018.05.157

Dolton, B., Hannah, C., 2006. Cellular Concrete : Engineering and Technological Advancement for Construction in Cold Climates 1–11.

Ecoinvent Association, 2019. Ecoinvent database version 3 [WWW

Document]. URL https://www.ecoinvent.org/database/database.html (accessed 8.14.19).

Esmaily, H., Nuranian, H., 2012. Non-autoclaved high strength cellular concrete from alkali activated slag. Constr. Build. Mater. 26, 200–206. https://doi.org/10.1016/j.conbuildmat.2011.06.010

Font, A., Borrachero, M.V., Soriano, L., Monzó, J., Mellado, A., Payá, J., 2018. New eco-cellular concretes: Sustainable and energy-efficient materials. Green Chem. https://doi.org/10.1039/c8gc02066c

Font, Alba, Borrachero, M.V., Soriano, L., Monzó, J., Payá, J., 2017. Geopolymer eco-cellular concrete (GECC) based on fluid catalytic cracking catalyst residue (FCC) with addition of recycled aluminium foil powder. J. Clean. Prod. 168, 1120–1131. https://doi.org/10.1016/j.jclepro.2017.09.110

Font, A., Soriano, L., de Moraes Pinheiro, S.M., Tashima, M.M., Monzó, J., Borrachero, M.V., Payá, J., 2020. Design and properties of 100% waste-based ternary alkali-activated mortars: Blast furnace slag, olive-stone biomass ash and rice husk ash. J. Clean. Prod. 243. https://doi.org/10.1016/j.jclepro.2019.118568

Font, A., Soriano, L., Moraes, J.C.B., Tashima, M.M., Monzó, J., Borrachero, M.V., Payá, J., 2017. A 100% waste-based alkali-activated material by using olive-stone biomass ash (OBA) and blast furnace slag (BFS). Mater. Lett. 203. https://doi.org/10.1016/j.matlet.2017.05.129

Funfación Conama - Grupo de trabajo GT-6, 2018. Economía circular en el sector de la construcción. Congr. Nac. del Medio Ambient. 2018.

Hajimohammadi, A., Ngo, T., Mendis, P., Kashani, A., van Deventer, J.S.J., 2017. Alkali activated slag foams: The effect of the alkali reaction on foam characteristics. J. Clean. Prod. 147, 330–339. https://doi.org/10.1016/j.jclepro.2017.01.134

Hassan, H.S., Abdel-Gawwad, H.A., García, S.R.V., Israde-Alcántara, I., 2018. Fabrication and characterization of thermally-insulating coconut ash-based geopolymer foam. Waste Manag. 80, 235–240. https://doi.org/10.1016/j.wasman.2018.09.022

He, Juan, Gao, Q., Song, X., Bu, X., He, Junhong, 2019. Effect of foaming agent on physical and mechanical properties of alkali-activated slag foamed concrete. Constr. Build. Mater. 226, 280–287. https://doi.org/10.1016/j.conbuildmat.2019.07.302

Hogeling, J., Derjanecz, A., 2018. The 2nd recast of the Energy Performance of Buildings Directive (EPBD). Sustain. Dev. 1–30.

IDAE, 2019. Base de datos - Consumo y Emisiones de CO2 en Vehículos Nuevos [WWW Document]. Inst. para la Divers. y Ahorr. la Energía - Gob. España. URL https://www.idae.es/bases-de-datosherramientas (accessed 8.10.19).

IEEE STANDARDS ASSOCIATION, 1981. IEEE 442-1981 - IEEE Guide for Soil Thermal Resistivity Measurements [WWW Document].

IPCC, 2006. Introducción a las Directrices de 2006 1–13.

Kamseu, E., Ngouloure, Z.N.M., Ali, B.N., Zekeng, S., Melo, U.C., Rossignol, S., Leonelli, C., 2015. Cumulative pore volume, pore size distribution and phases percolation in porous inorganic polymer composites: Relation microstructure and effective thermal conductivity. Energy Build. 88, 45–56. https://doi.org/10.1016/j.enbuild.2014.11.066

Keawpapasson, P., Tippayasam, C., Ruangjan, S., Thavorniti, P., Panyathanmaporn, T., Fontaine, A., Leonelli, C., Chayasuwan, D., 2014. Metakaolin-Based Porous Geopolymer with Aluminium Powder. Key Eng. Mater. 608, 132–138. https://doi.org/10.4028/www.scientific.net/KEM.608.132

Luukkonen, T., Abdollahnejad, Z., Yliniemi, J., Kinnunen, P., Illikainen, M., 2018a. One-part alkali-activated materials: A review. Cem. Concr. Res. https://doi.org/10.1016/j.cemconres.2017.10.001

Luukkonen, T., Abdollahnejad, Z., Yliniemi, J., Kinnunen, P., Illikainen, M., 2018b. Comparison of alkali and silica sources in one-part alkali-activated blast furnace slag mortar. J. Clean. Prod. 187, 171–179. https://doi.org/10.1016/j.jclepro.2018.03.202

Ma, C., Zhao, B., Guo, S., Long, G., Xie, Y., 2019. Properties and characterization of green one-part geopolymer activated by composite activators. J. Clean. Prod. 220, 188–199. https://doi.org/10.1016/j.jclepro.2019.02.159

Mak, S., Seo, S., Ambrose, M., Gesthuizen, L., 2008. Sustainable Housing using lightweight cellular concrete. Proc. World Conf. SB08 314–321.

Mellado, A., Catalán, C., Bouzón, N., Borrachero, M. V., Monzó, J.M., Payá, J., 2014. Carbon footprint of geopolymeric mortar: study of the contribution of the alkaline activating solution and assessment of an alternative route. RSC Adv. 4, 23846–23852. https://doi.org/10.1039/C4RA03375B

Ministerio de Fomento - Gobierno de España, 2018. CTE-HE. Código Técnico de la Edificación. Basic document HE (Energy saving). June 68.

Moraes, J.C.B., Font, A., Soriano, L., Akasaki, J.L., Tashima, M.M., Monzó, J., Borrachero, M.V., Payá, J., 2018. New use of sugar cane straw ash in alkali-activated materials: A silica source for the preparation of the alkaline activator. Constr. Build. Mater. 171. https://doi.org/10.1016/j.conbuildmat.2018.03.230

Moreno-Ruiz E., Valsasina L., FitzGerald D., Brunner F., Symeonidis A., Bourgault G., G., W., 2019. Documentation of changes implemented in ecoinvent database v3.6.

Novais, R.M., Buruberri, L.H., Seabra, M.P., Bajare, D., Labrincha, J.A., 2016. Novel porous fly ash-containing geopolymers for pH buffering applications. J. Clean. Prod. 124, 395–404. https://doi.org/10.1016/j.jclepro.2016.02.114

Novais, R.M., Senff, L., Carvalheiras, J., Seabra, M.P., Pullar, R.C., Labrincha, J.A., 2019. Sustainable and efficient cork - inorganic polymer composites_ An innovative and eco-friendly approach to produce ultra-lightweight and low thermal conductivity materials. Cem. Concr. Compos. 97, 107–117. https://doi.org/10.1016/j.cemconcomp.2018.12.024

Peys, A., Rahier, H., Pontikes, Y., 2016. Potassium-rich biomass ashes as activators in metakaolin-based inorganic polymers. Appl. Clay Sci. 119, 401–409. https://doi.org/10.1016/j.clay.2015.11.003

Puertas, F., Torres-Carrasco, M., 2014. Use of glass waste as an activator in the preparation of alkali-activated slag. Mechanical strength and paste characterisation. Cem. Concr. Res. 57, 95–104. https://doi.org/10.1016/j.cemconres.2013.12.005

Pytlik, E.C., Saxena, J., 1992. Autoclaved Cellular Concrete: the Building Material for the 21St Century. Proc. 3rd RILEM Int. Symp. Autoclaved Aerated Concr. 18.

Robayo-salazar, R.A., Robayo-salazar, R., Mejía-arcila, J., Mejía, R., Gutiérrez, D., Martínez, E., 2018. Life cycle assessment (LCA) of an alkali-activated binary concrete based on natural volcanic pozzolan : A comparative analysis to OPC concrete Life cycle assessment (LCA) of an alkali-activated binary concrete based on natural volcanic pozzolan : A co. Constr. Build. Mater. 176, 103–111. https://doi.org/10.1016/j.conbuildmat.2018.05.017

Schroeder, P., Anggraeni, K., Weber, U., 2018. The Relevance of Circular Economy Practices to the Sustainable Development Goals: Circular Economy and SDGs. J. Ind. Ecol. https://doi.org/10.1111/jiec.12732

Stoleriu, S., Vlasceanu, I.N., Dima, C., Badanoiu, A.I., Voicu, G., 2019. Alkali

activated materials based on glass waste and slag for thermal and acoustic insulation. Mater. Construcción 69, 194. https://doi.org/10.3989/mc.2019.08518

Sturm, P., Gluth, G.J.G., Brouwers, H.J.H., Kühne, H.C., 2016. Synthesizing one-part geopolymers from rice husk ash. Constr. Build. Mater. 124, 961–966. https://doi.org/10.1016/j.conbuildmat.2016.08.017

Van Den Heede, P., De Belie, N., 2012. Environmental impact and life cycle assessment (LCA) of traditional and "green" concretes: Literature review and theoretical calculations. Cem. Concr. Compos. 34, 431–442. https://doi.org/10.1016/j.cemconcomp.2012.01.004

Xuan, D., Tang, P., Poon, C.S., 2019. MSWIBA-based cellular alkali-activated concrete incorporating waste glass powder. Cem. Concr. Compos. 95, 128–136. https://doi.org/10.1016/j.cemconcomp.2018.10.018

Yang, K.H., Lee, K.H., Song, J.K., Gong, M.H., 2014. Properties and sustainability of alkali-activated slag foamed concrete. J. Clean. Prod. 68, 226–233. https://doi.org/10.1016/j.jclepro.2013.12.068

Zabalza Bribián, I., Valero Capilla, A., Aranda Usón, A., 2011. Life cycle assessment of building materials: Comparative analysis of energy and environmental impacts and evaluation of the eco-efficiency improvement potential. Build. Environ. 46, 1133–1140. https://doi.org/10.1016/j.buildenv.2010.12.002

Ziegler, D., Formia, A., Tulliani, J.M., Palmero, P., 2016. Environmentally-friendly dense and porous geopolymers using fly ash and rice husk ash as raw materials. Materials (Basel). 9. https://doi.org/10.3390/ma9060466

CAPÍTULO V: CONCLUSIONES Y LÍNEAS DE INVESTIGACIÓN FUTURAS

CONTENIDO

5 CONCLUSIONES Y LÍNEAS DE INVESTIGACIÓN FUTURAS

En el trabajo de investigación se ha llevado a cabo una metodología "paso a paso" basada en la introducción progresiva de mejoras medioambientales y ecológicas en un material de construcción tradicional: el hormigón celular. El objetivo general ha sido diseñar un nuevo material, de aplicación en el sector de los prefabricados, de acuerdo con: por una parte, los criterios normativos de diseño y, por otra parte, los horizontes (económico y medioambiental) hacia los que se están enfocando los procesos industriales. Para ello, se han planteado una serie de objetivos específicos de acuerdo con los cuales se ha estructurado el presente documento (ver Capítulo 2).

En el Capítulo 4 se ha expuesto cada uno de los pasos de mejora dentro de la correspondiente etapa de investigación y se ha dado a conocer las conclusiones específicas de cada uno de las publicaciones que dan cabida a la presente Tesis Doctoral.

A continuación, se exponen las conclusiones generales más relevantes y se propone una serie de líneas de investigación que se considera necesario abordar para, con las bases obtenidas en el presente trabajo, llegar a una caracterización completa del material y necesaria para su aplicación industrial.

5.1 CONCLUSIONES

Las conclusiones generales más relevantes a las que se ha llegado en la investigación según los objetivos específicos son las siguientes:

En primer lugar, se ha investigado los hormigones celulares geopoliméricos (**GCC**) y los hormigones celulares de activación alcalina (**AACC**), correspondiente a la ***Fase 1*** **-** ***Etapa*** **1** de la investigación:

- Se ha obtenido sistemas muy competitivos mediante la tecnología de los hormigones celulares en matrices geopoliméricas (empleando como precursor el catalizador gastado de craqueo catalítico) así como en matrices de activación alcalina (empleando como precursor la escoria de alto horno). Las condiciones de elevada basicidad y temperatura del medio favorecen la reacción de aireación (oxidación del aluminio en polvo y generación de hidrógeno) y la configuración de una estructura alveolar estable de las pastas.
- Además, se han aplicado de manera efectiva los métodos de aireación alternativa (aluminio residual (A_R), peróxido de hidrógeno (H_2O_2) y sub-productos de escorias salinas (PG)), tanto en GCC como en AACC, comprobándose que la reactividad en ambos medios resulta mayor que en el caso de los hormigones celulares tradicionales (TCC).
- La combinación del efecto químico (aireación) con el mecánico (espumado) mediante la adición aluminio en polvo y lauril sulfato de

sodio respectivamente, en la fabricación de GCC y AACC también se ha llevado a cabo con buenos resultados. Esta tipología puede ser una alternativa interesante ante determinadas situaciones constructivas "in-situ" en las que se requiera de una reacción mas controlable. Los resultados mejoran con respecto a los sistemas tradicionales (TCC) así como a los sistemas en los que únicamente se emplea el reactivo espumante.

- Finalmente, cabe destacar que se ha conseguido mejorar de manera notable la ecología del material mediante dos aspectos introducidos en la fabricación tanto de los GCC como de los AACC:
    - Por una parte, se ha mejorado significativamente el proceso de fabricación de los materiales mediante la co-molienda (**Co-M**) de los precursores con los agentes aireantes alternativos, tanto el A_R como el PG. Los resultados obtenidos mejoran la reacción de aireación, aportando estabilidad a la matriz y resultando una estructura porosa homogénea.
    - Por otra parte, se ha optimizado cada uno de los materiales con la finalidad de obtener matrices estables mediante un procedimiento de curado a temperatura ambiente (**TA**), obviando el proceso de autoclave necesario en los TCC.

Seguidamente, se ha investigado los nuevos hormigones eco-celulares (**ECC**), correspondiente a la ***Fase 1 - Etapa* 2:**

- La aplicación del uso de cáscara de arroz (RHA) como fuente de sílice para la activación de los sistemas, en la fabricación de hormigones celulares alternativos, ha resultado con muy buenos resultados.
- Los nuevos ECC permiten obviar el empleo de silicato sódico (WG), y permiten disminuir la huella de carbono en un 74 % mediante el empleo de $FCCR_m$ y en un 78 % mediante el empleo de $BFSR_m$.
- El análisis de la red porosa de los AACC, GCC y los ECC ha permitido establecer relaciones entre las características funcionales de los materiales y su configuración interna. Se ha demostrado que un sistema de poros homogéneo, con tamaños similares y sin interconexiones, favorece a la estabilidad de la matriz: densidad más baja sin comprometer la resistencia a la compresión y mayor aislamiento térmico. Este punto es fundamental para estudios futuros que permitan predecir el comportamiento de los materiales en función de su dosificación.

En el siguiente paso del trabajo, se introduce el empleo de la ceniza de hueso de oliva (OBA) como impulsor del medio básico en la activación alcalina (***Fase 2***):

En esta fase, la **primera etapa (*Fase 2 - Etapa 3*)** ha consistido en la fabricación de materiales de activación alcalina binarios (BAAM) y ternarios (TAAM), demostrándose:

- Con el estudio de los BAAM basados en BFS/OBA se obtuvieron sistemas muy competitivos con respecto al empleo de los activadores químicos tradicionales.
- Cuando se aplica el uso de OBA y RHA para activar las matrices de activación alcalina de BFS se mejoran de manera notable los resultados (sistemas TAAM). El mayor rendimiento se obtiene cuando la OBA se incluye en los sistemas como adición (en combinación con RHA para la preparación de la disolución) y sustitución de la BFS: sistemas **BFS/OBA (20%Ad/20%Rp)/RHA + H_2O.**
- El curado a TA de los TAAM presenta resultados muy buenos, aunque su consecución es más lenta que en el caso del curado a altas temperaturas (TB)

Finalmente, en la **última etapa (*Fase 2 - Etapa 4*)** del trabajo se puede afirmar que ha aplicado con muy buenos resultados la combinación de la tecnología de los TAAM con el proceso de fabricación "one-part" para el desarrollo de los **ECC-OP.**

En la Tabla 5.1 se sintetiza la comparativa entre los hormigones celulares alternativos desarrollados en la presente investigación y las características funcionales (densidad, resistencia a compresión y conductividad térmica) obtenidas tras 7 o 28 días de curado a temperatura ambiente. Los valores se presentan en relación con las exigencias de la normativa europea para piezas prefabricadas de fábrica para albañilería (UNE-EN 771-4) y el código técnico de la edificación (CTE).

Tabla 5.1

Síntesis comparativa de los resultados obtenidos y las exigencias normativas.

		Fase sólida	Fase líquida	D_{AP} (kg/m^3)		Rc (MPa)		λ (W/mK)[2]	
					UNE		UNE		CTE
ETAPA 1	GCC	$FCCR_m$	WG/NaOH/ H_2O	797	1000	6.5	1.5	0.08	0.21
		FCC	H_2O_2 WG/NaOH/H_2O	812[1]		3.0		0.24	0.21
		FCC/SLS/A	WG/NaOH/H_2O	1143[1]		6.9		-	-
	AACC	$FCCPG_m$	WG/NaOH/H_2O	753		6.8		0.31	0.21
		$BFSR_m$	WG/NaOH/H_2O	681		7.1		0.28	0.20
		BFS	H_2O_2 WG/NaOH/H_2O	711[1]		3.8		0.19	0.20
		BFS/SLS/A	WG/NaOH/H_2O	1046[1]		8.6		-	-
		$BFSPG_m$	WG/NaOH/H_2O	602		7.5		0.16	0.18
ETAPA 2	ECC	$FCCR_m$	RHA/NaOH/H_2O	740		3.2		0.11	
		$BFSR_m$		616		5.6		0.22	0.18
ETAPA 4	ECC-OP	BRm-RO	H_2O	660		6.3		0.20	0.20

[1]Datos a los 7 días de curado.

[2]Los requisitos de conductividad térmica se establecen en función de la densidad aparente del material.

Como conclusión general de la Tesis doctoral se puede enunciar lo siguiente:

Se ha demostrado la posibilidad de fabricar un material celular mediante el uso únicamente de materiales residuales y aplicando una tecnología de fabricación de consumo energético casi-nulo. Los nuevos **ECC-OP** cumplen con los requerimientos funcionales establecidos en la normativa europea para la fabricación de piezas prefabricadas de hormigón celular y permiten reducir el potencial de calentamiento global (GWP-100) en un 96 % respecto a los hormigones celulares tradicionales.

El trabajo de investigación desarrollado sirve de precedente, demuestra y sienta las bases de un nuevo material ligero y aislante con el que se puede avanzar hacia el concepto de economía inteligente en el sector de la construcción mediante su aplicación en la industria de los prefabricados.

5.2 PROPUESTAS PARA LA CONTINUIDAD EXPERIMENTAL DE LA INVESTIGACIÓN

A partir de las conclusiones a las que se ha llegado mediante el presente trabajo de investigación, se propone el desarrollo de los siguientes estudios:

- En la actualidad se están llevando a cabo investigaciones que demuestran el buen rendimiento de otras materias primas residuales en la fabricación de BAAM, así como TAAM. Precursores como ceniza paja de caña de azúcar, bagazo de caña de azúcar, lodos de depuradora, biomasa procedente de ceniza de hoja de bamboo, residuos de construcción y demolición, así como activadores alternativos a base de polvo de vidrio, tierra de diatomeas o biomasa de ceniza de cáscara de almendra, por ejemplo. La aplicación de estos sistemas en la fabricación de hormigones celulares permitiría optimizar estos materiales para su aplicación en determinadas situaciones constructivas y en determinadas zonas.
- Búsqueda de posibles materias primas residuales que, por su composición química, tengan la doble función en las matrices celulares como precursoras y/o activadoras y como agentes de aireación.
- En vistas a una fabricación industrializada del material sería necesario llevar a cabo ensayos destinados a estudiar la reacción de aireación con la finalidad de establecer parámetros que permitan dosificar el material en función de las características funcionales requeridas.
- La aplicación real en construcción del material requiere de la caracterización del mismo mediante ensayos complementarios a los funcionales: durabilidad, resistencia al fuego, aislamiento acústico y comportamiento ante la humedad.
- Fabricación de piezas de dimensionamiento real que se ensayen de acuerdo con lo establecido en la normativa. En este sentido se debe ampliar el estudio ante lo contemplado en los siguientes documentos de referencia:
    - DAU (Documento de adecuación al uso).
    - CTE (Código técnico de la edificación): DB SE-F (Seguridad Estructural Fábrica), DB SE-AE (Acciones en la Edificación), DB SI (Seguridad en caso de Incendio), DB HS (Salubridad), DB HE (Ahorro de Energía) y DB HR (Protección frente al Ruido).
    - UNE – EN 771 – 4: Bloques de hormigón celular curado en autoclave.
    - NCSE O2: Norma de construcción sismorresistente.
    - Eurocódigo 8: Disposiciones para el proyecto de estructuras sismorresistentes.
    - Eurocódigo 6: Proyectos de estructuras de fábrica.
    - Directiva 2018/844 relativa a la eficiencia energética de los edificios.

- Desarrollo de un estudio económico del producto en lo que a las piezas de fábrica a base de ECC-OP se refiere: costes materiales y productivos.
- Fabricación de prototipos constructivos con las piezas de fábrica de ECC-OP, que permitan:
    - Ensayos físicos del conjunto: comportamiento funcional, control del confort térmico, características acústicas, durabilidad y resistencia al fuego.
    - Establecimiento de pautas de dimensionamiento estructural.
    - Estudios medioambientales y de sostenibilidad: análisis del ciclo de vida (ACV), evaluación de higiene y salud.
    - Desarrollo de un estudio económico completo desde los materiales constituyentes hasta la construcción del prototipo y su posterior uso.
    - Establecimiento de pautas de construcción y adecuación de la normativa aplicable.